**Université catholique de Louvain**
Ecole polytechnique de Louvain
Institut de Mécanique, Matériaux et Génie Civil

# Experimental and numerical investigation of a two-stage downdraft biomass gasification process

Benjamin Berger

August 2018

**Composition du jury:**
Pr. T. Pardoen (UCL, président)
Pr. H. Jeanmart (UCL, promoteur)
Pr. J. de Wilde (UCL)
Dr. JM. Seynhaeve (UCL)
Pr. S. Salvador (IMT Mines Albi-Carmaux, France)
Pr. J. Porteiro (Université de Vigo, Espagne)

Thèse présentée en vue de l'obtention du grade de docteur en sciences de l'ingénieur

2018

Benjamin Berger

*A la mémoire de Bonne maman et Bon papa.*

# Contents

# Remerciements

Cette thèse fut pour moi une magnifique opportunité d'apprendre énormément de choses, non seulement sur le plan technique mais également sur le plan humain. Je tiens donc à remercier chaque personne qui a pu rendre cette thèse possible, à commencer par mon promoteur Hervé Jeanmart. Je le remercie pour sa présence, ses conseils, sa persévérance et le fait d'avoir toujours cru en moi, même dans les moments où je doutais. Je n'oublierai pas les discussions, toujours intéressantes, sur tous types de sujets et j'attends avec impatience nos futurs échanges.

Je tiens également à remercier les membres de mon comité d'encadrement : Jean-Marie Seynhaeve, pour ses conseils précieux sur l'incertitude de mesure et Juray de Wilde pour ses remarques et son regard extérieur sur mon sujet. Je remercie également Sylvain Salvador, Jacobo Porteiro et Thomas Pardoen, les membres de mon jury, pour les questions et remarques qui m'ont permis d'améliorer le manuscrit de ma thèse.

Cette thèse a été constituée d'une partie expérimentale conséquente. Je n'aurais pu venir à bout de celle-ci sans l'équipe de techniciens. Les moments passés au laboratoire restent parmi les meilleurs de cette thèse. Je remercie : Julien Vervotte, toujours volontaire et qui m'a tellement appris sur la mécanique ; Frank Hesbois, d'une curiosité exemplaire avec qui j'ai passé des heures à chercher comment fonctionnaient certains (trop) vieux appareils ; François Vercheval, dont l'expérience et les idées sont une réelle mine d'or et enfin Yan Liu, toujours disponible pour réaliser les (trop) nombreuses modifications de LabVIEW® que je réclamais.

J'ai aussi pu bénéficier d'une aide précieuse de collègues partageant des thématiques proches dans la réalisation de cette thèse. Je remercie tout particulièrement : Véronique Dias pour son soutien sans faille, son don naturel pour le karaoké et son aide sur la partie cinétique chimique de cette thèse ; Amel Hemidi, avec qui j'ai eu la chance de partager le bureau, de nombreux fou-rires mais aussi beaucoup de conseils techniques ; Francesco Contino, qui fut mon encadrant avant de devenir un collègue et un ami, toujours disponible pour discuter et me guider ; Julien Blondeau, chanteur portugais à ses heures perdues, dont la thèse fut mon livre de chevet et avec qui les discussions (philosophiques ou non) étaient toujours enrichissantes ; Maxime Pochet, qui a accepté de relire certains chapitres de ma thèse ; Gauthier Limpens pour son aide dans la manipulation de maillages et Elise Dupont pour ses relectures et les discussions sur l'exploitation des diverses ressources d'énergie renouvelable.

Cette thèse fut réalisée en partie en collaboration avec la société Xylowatt s.a. que je remercie chaleureusement et en particulier : Alexandre Bacq, qui m'a tout appris sur le pilotage d'un gazogène ; Michaël Haube, pour les discussions très intéressantes sur les unités industrielles et Frédéric Bourgois, dont la connaissance des gazogènes m'impressionne encore aujourd'hui.

Le pôle TFL fut comme une seconde maison durant cette thèse, l'ambiance qui y régnait m'a permis de passer des années inoubliables, je remercie donc chaleureusement tous ses membres actuels et passés. Un merci tout particulier à Isabelle Hennau pour son support sans faille. Egalement, je tiens à remercier chronologiquement le groupe de chercheurs dits "Les Furieux", à savoir : Yves Marichal aka "9 fois, je te jure" ; Nicolas Bourgeois aka "Le bolchévique" ; Pierre Schroyen aka "Prends une patate" ; Olivier "La pinaille" Thiry ; Maud "Mamoens" Moens ; Haddy "Le professeur" Mbuyi Katshiashia et Philippe Parmentier aka "Il faut lire la doc". Je remercie aussi le groupe de chercheurs qui succéda au premier avec le nom original "Les Jeunes Furieux" : PGDDG, TG, Billou, Caro, Gaut'ch, Victor, Max et Elise. Je remercie également tous les membres de l'équipe pédagogique avec lesquels j'ai eu le plaisir de collaborer et en particulier : Grégoire Winckelmans, Philippe Vortex-Chatelain, Yann Bartosiewicz et Matthieu Duponcheel.

Je tiens également à remercier les étudiants que j'ai encadrés lors de leurs travaux de fin d'étude sur la gazéification, certains d'entre eux sont d'ailleurs cités dans le présent manuscrit. Je les remercie pour leur sérieux, leur investissement et leur intérêt pour le domaine de recherche.

Un merci particulier à toute l'équipe de l'ECAM qui m'a accueilli en son sein depuis deux ans, tant la direction, qui a bien voulu adapter mon emploi du temps afin de pouvoir assurer mes tâches pédagogiques en parallèle de ma fin de thèse, que mes collègues, très compréhensifs qui m'ont aidé au quotidien afin de pouvoir mener à bien ces deux projets simultanément. Un merci tout particulier à l'équipe du Projet Intégrateur à savoir Nathalie Bauche, Nathalie Siebert, Cédric Marchand et Pierre Mathieu.

Je tiens également à remercier tous mes proches, ma famille ainsi que mes amis pour leur soutien indéfectible et quotidien. Je les remercie tout particulièrement pour les années à me demander "Et alors cette thèse, ça avance ?", cette petite phrase que tout thésard adore.

Enfin, je tiens à remercier la personne sans qui cette thèse n'aurait pu aboutir, pour les heures passées à me soutenir malgré ma mauvaise humeur, pour avoir cru en moi dans les moments où je n'y croyais plus, pour avoir assurer à la maison quand je n'en avais pas le temps ou le courage, mon épouse, Typhanie Maurer. Je remercie également notre adorable fils Nathan qui a été très compréhensif et s'est toujours montré patient lorsque son papa devait avancer dans sa rédaction.

A toutes les personnes que je n'ai pas pu citer par faute d'espace rédactionnel ainsi qu'au lecteur courageux : Merci également.

# Abstract

The amount of tar in the producer gas is the main drawback for the industrial development of biomass gasification facilities. Recently, successful designs, based on the two-stage concept from the Asian Institute of Technology (AIT) and the Danish Technical University (DTU), have been developed for small-scale applications. In such facilities, very low tar levels are achieved.

The present work focuses on a two-stage technology presenting a physical separation between the pyrolysis and the oxidation/reduction zones. The air is injected in two separate inlets like on the AIT design with part of the air being injected at the pyrolysis level and part being used for the oxidation. The main evolution is the physical separation of the pyrolysis and oxidation/reduction zones as in the DTU design. It allows an independent control of the pyrolysis and the tar oxidation and cracking in a gaseous zone.

This thesis presents the experimental results obtained on a research gasification plant with a thermal power of 200 kW. The influence of several parameters on the performances of the process have been investigated, among them : the air ratio, the bed heights and porous medium injection in the pyrolysis zone. Aside from those results, the use of gasifying agents other than air in order to modify the characteristics of the producer gas is also discussed.

This study also presents experiments on the influence of different biomass feedstocks since the future of gasification may reside in energy recovery from wastes. The experiments performed with waste biomass highlighted the importance of the pyrolysis zone in the gasification process. Further experimental investigations were performed on the pyrolysis zone using natural wood.

In parallel, a model combining a wood particle model (based on the work of Julien Blondeau) with a 2D axisymmetric reactive simulation of the pyrolysis zone was developed using ANSYS Fluent®. The model can help to predict the influence of the feedstock on the tar level at the end of the pyrolysis zone that can be linked to the tar level at the outlet of the gasifier.

# Nomenclature

**Abbreviations**

| | |
|---|---|
| $AIT$ | Asian Institute of Technology |
| $CHP$ | Combined heat and power |
| $DPM$ | Discrete Particle Model |
| $DTU$ | Danmarks Tekniske Universitet - Technical University of Denmark |
| $ECN$ | Energy research Center of the Netherlands |
| $ER$ | Equivalence Ratio |
| $FID$ | Flame Ionisation Detector |
| $GC$ | Gas Chromatography |
| $HCCI$ | Homogeneous Charge Compression Ignition (refers to engines) |
| $M\&EB$ | Mass and Energy Balance |
| $RPM$ | Representative Particle Model |
| $SI$ | Spark Ignition (refers to engines) |
| $SV$ | Superficial velocity |
| $TCD$ | Thermal Conductivity Detector |
| $TGP$ | Test Gasification Plant |
| $UDF$ | User Defined Function (Fluent) |
| $WWTP$ | Waste Water Treatment Plant |

**Greek letters**

| | |
|---|---|
| $\alpha$ | Air ratio for two-stage gasification (ratio between primary and total air injection) [-] |
| $\epsilon$ | Emissivity [-] |
| $\eta$ | Conversion factor [-] |
| $\hat{\rho}$ | Intrinsic density [kg $m^{-3}$] |
| $\mu$ | Viscosity [Pa s] |
| $\omega$ | Mass source term [kg $m^{-3}$ $s^{-1}$] |
| $\omega_h$ | Heat source term [W $m^{-3}$] |
| $\rho$ | Apparent density [kg $m^{-3}$] |
| $\sigma$ | Stefan-Boltzmann constant [W $m^{-2}$ $K^{-4}$] |
| $\upsilon$ | Volume [$m^3$] |
| $\varepsilon$ | Porosity [-] |

**Symbols**

| | |
|---|---|
| $\Delta h$ | Heat of reaction [J $kg^{-1}$] |
| $A$ | Arrhenius pre-exponential factor [*] / Area [$m^2$] |
| $c$ | Heat capacity [J $kg^{-1}$ $K^{-1}$] |
| $E$ | Arrhenius activation energy [J $mol^{-1}$] |
| $h$ | Heat convection coefficient [W $m^{-2}$ $K^{-1}$] |
| $K$ | Kinetic constant [*] |
| $k$ | Heat conductivity [W $m^{-1}$ $K^{-1}$] |
| $L$ | Length scale [m] |
| $M_m$ | Molar weight [kg $mol^{-1}$] |
| $p$ | Pressure [Pa] |
| $P_{th}$ | Themal power [kW] |

| | |
|---|---|
| $q$ | Heat flux [W $m^{-2}$] |
| $R$ | Ideal gas constant [J $mol^{-1}$ $K^{-1}$] |
| $R^*$ | Specific ideal gas constant [J $kg^{-1}$ $K^{-1}$] |
| $SGR$ | Specific Gasification Rate [$kg/h.m^2$] |
| $SV$ | Superficial velocity [$m/s$] |
| $T$ | Temperature [K] |
| $t$ | Time [s] |
| $u$ | Bulk velocity [m $s^{-1}$] |
| $V$ | Volume [$m^3$] |
| $y$ | Mass fraction [-] |

# Introduction

Biomass is seen by many as one of the largest energy resources after solar and wind energies. Devries et al. estimate that the potential of biomass is equivalent to the one of the wind energy sector while solar energy presents a much higher potential in their scenarios [1, 2]. Estimated at 150 EJ/y by van Swaaij et al., it could represent 30% of the present world consumption [3]. The challenge for biomass resides in its diversity. Biomass can take many shapes and forms, has different origins, composition and is a largely distributed energy. Biomass is a raw energy vector and there are many options to harness it. The main conversion paths to heat and electricity are either chemical or biological. They are represented in Figure 1.

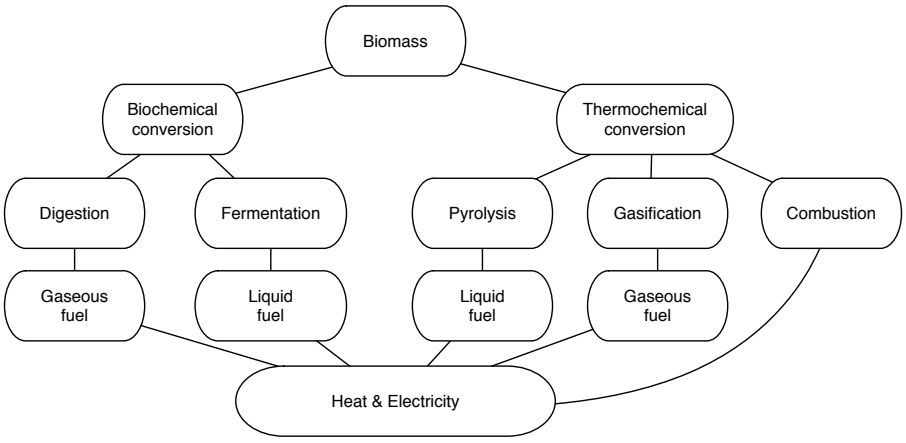


***Figure 1*** *– Biomass conversion routes.*

Gasification has been used for 200 years for heat and electricity production [4]. Historically, gasification was developed to convert coal into a gaseous fuel. In the past decades, interest for biomass gasification has grown for Combined

Heat and Power (CHP) and power generation applications. The objective of gasification is to propose a solution to the various shapes and compositions that the solid biomass can take by converting it into more convenient gaseous fuels. These fuels are easier to transport (e.g. through pipelines), store (e.g. in storage tanks) and/or use (e.g. through gas burners). The result of the gasification process is a fuel gas called either producer gas, synthetic gas or syngas. Historically, the name syngas is a contraction of synthesis gas, the name given to the $H_2$ rich gas produced by some gasification processes and suitable for the synthesis of many different fuels and by-products [4].

Biomass gasification is a process consisting of four steps:

- Drying
- Pyrolysis
- Oxidation and thermal cracking
- Reduction (also called gasification)

There is a discussion about the drying step of the process. Depending on the author, it is sometimes included in the pyrolysis step. Indeed, drying is not a chemical reaction and there is always a minimum drying step immediately preceding the pyrolysis.

As the aim of the process is to produce a gas, all other components, solid or liquid at process reference temperature, are considered as impurities. The liquid part of these impurities is called tar. Before describing the process and the gasifier designs, it is important to clearly define what tar is. Indeed, tars are the major point of interest in the choice of a gasification technology. They are thus described in the first section of this chapter. After defining tars, this chapter presents the different gasification technologies in the second section. It ends with the presentation of several applications in the last section.

## Tars in gasification

The main drawback of the development of industrial gasification facilities is the presence of tars in the syngas. Tars are a fraction of the pyrolysis gases (produced by the thermal cracking of biomass) that are found at the outlet of the gasifier. As tars are liquid at reference process temperature, their uncontrolled condensation could cause problems such as pipes clogging and requires to remove them or prevent their condensation. Depending on the application, tar could be considered as harmless for the process but even for these applications (e.g. direct combustion of hot syngas) it could lead to problems during transitory phases or unsteady running conditions. Tars treatment is thus still seen as the main technical barrier of all gasification technologies [5] as it represents high maintenance and investment costs.

Tars are a product of the pyrolysis step which is the thermal cracking of biomass. Pyrolysis also produces char (carbon skeleton with traces of other elements) and light gases. It is difficult to precisely define tars since their composition and chemical affinity vary greatly and depend on the conditions in which they were emitted and the biomass particles they come from. Milne defines them as: "The organics, produced under thermal or partial-oxidation regimes (gasification) of any organic material, are called tars and are generally assumed to be largely aromatic" [6]. Their effect on the process depends on their concentration and the conditions in which they are used such a generic definition is not sufficient.

Since it is too complex and not necessarily useful to define them by their composition, another way of differentiating them could be their influence on the process. Tar formation depends on serveral factors [5] [1]:

- Temperature
- Gasifying agent
- Equivalence ratio
- Residence time
- Presence of catalysts

[1] List modified by the author

- Dynamic effects like the temperature profile
- Shape and size of biomass

Twenty years ago, the scientific community agreed that a standard measurement method and a definition of tars was required. The "TAR PROTOCOL" is the resulting measurement method [7] even though the definition of tars is still subject to discussion and at this point is given as "organic contaminants (tars) are the hydrocarbon species in the biomass fuel gas, in particular those which can cause damage to the engine or turbine or will incur an unacceptable level of maintenance"[8]. This definition emphasises the fact that some organic compounds that could have been considered as tars under other definitions are acceptable if they do not have a negative impact on the process. For example, another proposition was to define tars as "hydrocarbons with molecular weight higher than benzene" [9] which qualifies phenol as tar even though it does not cause problem in many processes as its volatility is higher than that of water and it has good combustion characteristics.

There are two ways to quantify tars. One method is based on the direct measurement of the concentration of tars in the syngas by collecting and measuring them (e.g. the TAR PROTOCOL) and the other one is based on the measurement of the temperature of condensation of tars in the syngas.

The first method consists in collecting the tars but it does not necessarily consider the composition of the tars. It can consider the total amount of tars measured as an image of the quality of the syngas. Ignoring the composition of the tars neglects the fact that some tars will cause more problems than others. Even if the standardised TAR PROTOCOL allows to measure both composition and concentration (for each component), its application remains complex and requires heavy equipment to identify all the species. A gravimetric analysis of the tars sampled through the TAR PROTOCOL can be implemented to determine the total amount of tars without determining its composition, hence reducing the complexity of the measurement. It consists in measuring the mass collected in the impinger bottles of the TAR PROTOCOL without further analysis. Nevertheless, in order to avoid the addition of a complete TAR PROTOCOL sampling line, the easiest way to realise a gravimetric test is to condense the tars on a cold filter. The mass off the filter is measured

before the test and after drying at 105 $[°C]$ in order to evaporate the water condensed on the filter during the test. The gas flow going through the filter during the test is measured in order to retrieve the tar content.

The second method combines concentration and composition measurements. The tar dew point is defined by ECN [10] as the temperature at which tars will start to condense at constant pressure. Rabou et al. [10] defines the tar dew point as the temperature for which the partial pressure of tars is equal to the saturation pressure of tars ($p_{tar} = p_{sv,tar}(T)$). It can thus be expressed as a function of the concentration of each single tar compound from the saturation of steam in the gas with the formula:

$$\begin{aligned} p_{tar} &= p_{sv,i}(T) \\ R\ 273\frac{1}{p_N}\frac{\frac{m_i}{V_N}}{M_{m,i}}\frac{T}{273} &= p_{sv,i}(T) \\ 22400\frac{C_i}{M_{m,i}}\frac{T}{273}\frac{1}{p_{sv,i}(T)} &= 1 \end{aligned}$$

where $T$ is the absolute temperature in $[K]$, $C$ is the tar content of the species $i$ in $[g/Nm^3]$, $M_{m,i}$ is the molar mass of the species $i$ in $[kg/mol]$, and $p_{sv}(T)$ is the saturated vapour pressure at temperature $T$ in $[mbar]$.

As shown in the above equation, the dew point combines the effects of concentration (through the tar content $C_i$) and composition (through the molar mass $M_{m,i}$ of the species). It is possible to calculate the tar dew point of a gas containing a mixture of tars by applying the above equation for each tar contained in the mixture. The tar dew point will thus be the highest temperature obtained for the calculations of all compounds. If all the concentrations are the same, the heavier compounds will have a higher influence on the dew point as their saturated pressure is lower, giving them a tar dew point higher than the lighter one. This means that they cannot be neglected in the calculation, even if their fraction is significantly lower. Hence both types and quantities must be considered to capture the complexity of this phenomenon.

An online calculator model is proposed on the Energy research Center of the Netherlands (ECN) website (www.thersites.nl). The estimated or measured tar dew point can then be compared directly with the lowest temperature observed in the process to know if condensation will occur and if preventive treatment is required.

Rabou et al. [10] propose a measurement method of the tar dew point based on a laser reflexion on a heated mirror. The mirror temperature is decreased until reflexion measurement is disturbed. The temperature at which the condensation is observed is thus the dew point. The only disadvantage in comparison to the Tar Protocol is that concentration and composition are taken into account together and cannot be differentiated.

In addition to these methods, it is interesting to note that some researchers are working on a third method consisting in online tar measurement systems with a reduced analysis time. For example, in 2016, Neubauer et al. proposed a system based on laser mass-spectrometry [11]. The development of such measurement tools could help monitor the performances of a gasification process.

| Technology | Average tar concentration in the syngas [g/Nm$^3$] |
|---|---|
| Fluidised bed gasifier | 1 - 30 |
| Updraft gasifier | 10 - 150 |
| Downdraft gasifier | 0.01 - 6 |

***Table 1*** *– Average tar content in the producer gas for different gasification technologies. Source: Basu [12].*

Depending on the gasification technology used, the measured tar content can vary greatly as shown in Table 1 from Basu [12]. These differences come from changes in the sequential order of the reaction steps for each process.

The condensation of tars is thus critical for the gasification technologies and their applications. The types and amount of tars depend on the process and determine their behaviour in the gasification facilities. The next section details the three main gasification process designs. It exposes their differences and describes the sequential order of the reactions within each process that lead to different gas compositions and the associated tar contents.

## Gasification technologies

The gasification technologies can be divided into four categories [13]:

- Quasi-non-moving or self-moving-feedstock (e.g. fixed bed reactors)
- Mechanically-moved feedstock (e.g. heated screw conveyors)
- Fluidically-moved feedstock (e.g. fluidised bed reactor)
- Other particular reactors (rare and not discussed in this work)

The fixed beds and the fluidised beds are the most commonly used designs for industrial gasification facilities.

The first category can be divided into two subgroups based on the directions of the solid and gas flows. In the fixed-bed updraft technologies, the solid and gas particles flow in opposite directions. The solid goes from top to bottom while the gas goes from bottom to top. For this reason, these gasifiers are also called counter-current. In the downdraft technologies, also called co-current, the gas and solid particles have the same direction, usually from top to bottom.

There is no example of a technology using mechanically-moved feedstock for an entire gasification reactor. There are examples of processes using heated screw conveyors for the pyrolysis part of the process however it is always combined with another type of reactor (updraft or downdraft). For this reason, they do not represent a category of gasification reactor hence they will not be discussed as such in this thesis even though mechanically-moved bed will be included in the description of some updraft and downdraft technologies.

For fluidised beds, there is no such classification based on the sequential order of the reactions as the mixing inside the reactor makes it difficult to establish an ordered reaction scheme. All the reactions occur simultaneously in the reactor [12] and reactive zones limits cannot be established clearly. Hence, their properties are between updraft and downdraft gasification. For this reason, downdraft and updraft gasifiers are described in the first and second parts of this section before ending with the introduction of fluidised bed gasification in the third part of this section.

## Updraft technology

In updraft gasifiers, the reactions encountered by the biomass are successively drying, pyrolysis, gasification and finally oxidation [14, 15] as shown in Figure 2. As the gases go through the process in an opposite direction, the sequential order of the reactions is logically reversed for the gas. The last reactions encountered by the gas are thus pyrolysis and drying. The tars released by the pyrolysis are partially condensed on the fresh biomass and partially entrained by the gas. As the water released from the solid fuel drying does not go through the other steps of the process, updraft gasifiers can operate with high water content biomass.

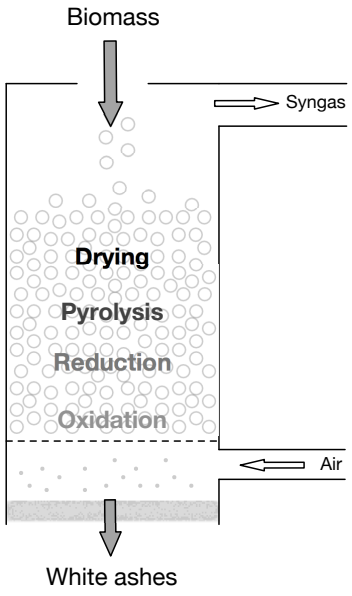


***Figure 2*** *– Illustration of the updraft technology.*

For the same reasons, updraft gasifiers are known to produce a gas containing a high level of tars (approx. 50 $g/Nm^3$) and a high water content. The producer gas is thus only suitable for direct combustion since condensation of the tars, which in this case represent a fair share of the total mass, would occur otherwise. The gas must be maintained at high temperature (above $350[°C]$) and requires specific boilers or burners. The objective is to use the gas inside a steam cycle in order to produce electricity as the gas from updraft gasification requires too much treatment to be used into gas turbines or IC engines.

The minimal power requirement for such applications is quite high due to the efficiency of the steam cycle decreasing with size [16].

The advantage of this design is the high temperature in the oxidation zone at the bottom of the gasifier. The char present at the bottom is char that did not react in the previous zone (reduction zone), hence it is the least reactive char of the process. The direct oxidation of the char with air burns the majority of this less reactive char. This allows a high conversion of the carbon found in biomass to gaseous carbonated compounds. The ratio of the carbon found in the syngas on the carbon found in the biomass is called the carbon conversion rate or carbon conversion efficiency. Note that the unconverted carbon is found in the ashes. A high carbon conversion efficiency translates into the production of white ashes (carbon free ashes) at the bottom of the gasifier [17] for updraft gasifiers. The oxidation temperature can be controlled if needed via the addition of steam or the injection of air with a high moisture content. Another advantage is the low dust (solide particles entrained by the flow) content of the syngas. As they are produced at the bottom of the gasifier, the whole solid particles bed is acting as a granular filter for these solid particles. Finally, updraft gasifiers can also be scaled up more easily than downdraft ones [13]. It is explained by the fact that the air injection is made in the gaseous phase below the grid supporting the biomass bed hence presenting no air distribution problem. Hence the biomass bed is more stable and less channeling problems appear.

## Downdraft technology

As said in the introduction, tars are the main drawback of the gasification technologies due to the treatment they require. It is even more important when it comes to small-scale power generation. For small power CHP applications, where a heavy gas treatment cannot be tolerated due to high investment and operational costs, downdraft gasification is the best solution. Downdraft gasifiers produce, thanks to their design, a low tar content syngas (around 2 $g/Nm^3$) that can be used into IC engines to produce electricity, even at a small-scale. It makes them suitable for decentralised electricity production near a biomass source, thus reducing transport costs and allowing electricity production in rural areas.

The sequential order of the reactions in a downdraft gasifier is the following: drying, pyrolysis, oxidation and reduction as illustrated in Figure 3. Downdraft gasifier are “tar killers" by design. In downdraft technologies, the tars produced by the pyrolysis are forced to go through the high temperature oxidation zone where they are cracked and partially oxidised. The tars still present in the syngas at the outlet of the reactor are thus residue from the pyrolysis. They should normally be cracked or oxidised inside the oxidation and reduction zones hence their presence at the outlet of the reactor is an image of the imperfections of the process. Tar contents are thus very low for downdraft gasifiers.

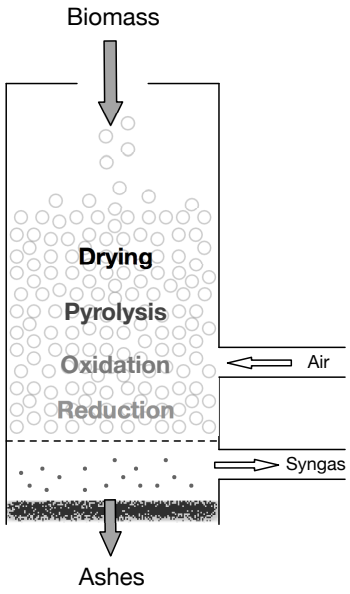


***Figure 3*** *– Illustration of the downdraft technology.*

The first drawback of this technology is that the carbon at the bottom of the reduction zone cannot be fully converted in opposition to the high carbon conversion efficiency of updraft gasifiers. The carbon at the bottom of the reduction zone is not sufficiently reactive to convert into gas due to the conditions in this zone (temperature of approximatively 700 $[^{\circ}C]$) since reduction reactions are endothermal. It leads to ashes with high carbon content in downdraft gasifiers and thus lower the carbon conversion efficiency in comparison to updraft technology.

The second drawback is the difficulty to increase the power of downdraft gasifiers due to the air injection in the porous medium. Injecting into porous medium complexifies the mixing of air and pyrolysis gases as air has difficulties to reach the center of the reactor. The pressure drops create inhomogeneous distribution of air even when it is injected at multiple points on the perimeter. This inhomogeneities worsen when the size of the reactor increases [18].

The porous medium induces a third drawback: a high pressure drop. These phenomena can go as far as the clogging of the reactor. These effects are difficult to predict due to the process the solid particles in the bed are going through and the stratification that can appear in the reactor [19]. Sharma et al. [20] observed that the pressure drops are inversely correlated with the particle size (that varies through the reactor due to the chemical reactions). Their study indicates that accumulation of ashes must be avoided to maintain a stable level of pressure drops and thus a constant flow of gas at the outlet of the gasifier.

Pressure drops are critical because they regulate the flow of gas inside the gasifier hence they influence the air injection system. There are two options for admitting the air into a downdraft gasifier: pushing the air inside or extracting the syngas at the outlet of the cleaning system. Extracting the syngas at the outlet of the reactor is not an option because of the temperature of the gas and the impurities it contains.

The first option is to blow the air inside the gasifier. The gasifier will then be slightly pressurised in comparison to the ambiant conditions and every leak will result in gas going out to the atmosphere. As gasifiers are exposed to large temperature variations, they can be subject to the apparition of leaks. When working with carbon monoxide, the risk of intoxication is high. Nonetheless this can be easily controlled and prevented as carbon monoxide, present in all the stages of the process, can be detected easily and in small concentrations with detectors that are well-known and widespread.

The second solution is to extract the syngas outside of the gasifier. The gasifier pressure will then be slightly below the atmospheric pressure. Every leak will then translate into air going into the system. This can present major risks

in some parts of the system where an explosive atmosphere and a very high temperature could be reached. The advantage is that for the intake of biomass, no special attention is required and some designs are even called "open-top", meaning air can penetrate in the system through the biomass feeding system. The control on the air inlet in this type of gasifier is less precise, usually leading to low quality syngas due to a lack of control.

The first option is preferred in a lot of cases, even with the increased cost due to leakage monitoring, safety and complex biomass feeding system.

A last drawback of downdraft gasifiers (partially shared with fluidised bed ones) is that the water emitted during the drying step goes through all the reactive zone, decreasing the temperature in each reaction zone thus having a negative impact on the gas production. Drying the biomass before injection in the gasifier should thus always be considered for downdraft gasification. Moreover, it is not a real drawback as low temperature heat is one of the by-products of the process and it can be used for drying. This increases the chemical conversion rate (hence the electricity conversion rate in case of CHP and power plants) and is thus often more valuable than any other use of this heat.

### Fluidised bed technology

In fluidised bed gasifiers, the feedstock is chopped into small pieces prior to insertion into the reactor and mixed with a hot bed material that can be inert or have a catalytic effect. The bed material has a great thermal inertia and the high mixing allows a very good temperature homogeneity in the whole bed. An homogeneity (in the radial direction) of this quality cannot be achieved in updraft and downdraft gasifiers where temperature gradients appear in the reaction beds.

As mentioned before, the tar content of fluidised beds is between the contents of the updraft and the downdraft technologies. According to Bocci, fluidised beds have a tar content of approximately 10 $g/Nm^3$ without the use of catalysts [15]. Due to the mixing, the small particle size and the attrition of the particles including the bed material, the dust content entrained by the flow of the syngas is higher than in both fixed bed technologies [13]. The gas treatment thus requires special attention to solid particles removal.

The homogenous conditions created by the mixing allows fluidised bed to be suitable for high power gasification plants. The complexity added by the circulation of bed material and its treatment (separation of ashes, bed material, additives, etc.) is compensated by the power scale advantage. The circulating bed also allows the addition of catalysts than can improve tar cracking or carbon conversion which is really difficult to do in other technologies without the addition of a specific equipment. Unfortunately, the complexity and high tar content (in comparison to downdraft technologies) generally forbid them to be considered for small-scale applications.

### Comparison between the three technologies

When comparing the HHV of the syngas produced by the three different technologies, the conclusion is that the gas energy content is similar for all technologies using air as a gasifying agent. Table 2 shows typical compositions for the main compounds found in the syngas produced by the three different processes using natural wood as feedstock.

| Technology | CO [%] | $H_2$ [%] | $CH_4$ [%] | $CO_2$ [%] | $N_2$ [%] | HHV [kJ/Nm$^3$] |
|---|---|---|---|---|---|---|
| Fluid bed gasifier | 14 | 9 | 7 | 20 | 50 | 5400 |
| Updraft gasifier | 24 | 11 | 3 | 9 | 53 | 5500 |
| Downdraft gasifier | 21 | 17 | 1 | 13 | 48 | 5700 |

***Table 2*** *– Performances comparison between different gasification technologies. Source: Basu [12].*

The differences between the processes are thus not based on the energy content or the energy conversion efficiency but on the composition of the gas at the outlet of the reactor. The composition is important for the applications aimed at, e.g. direct combustion, power generation or fuel synthesis. The use of syngas is another element of classification and is discussed in the next section.

## The use of syngas

The large variety of technologies proposed for gasification leads to a great flexibility of the process and allows it to fulfill the needs of a large number of

applications. As seen before, the gasification technologies can be divided into categories and subcategories following the sequential order of the reactions and the solid and gaseous flows (e.g. their respective direction) through the process. Another way to categorise gasification technologies is by the requirements of the application.

For instance, the requirements could be on the characteristics of the fuel produced by the process. These characteristics are for example: the composition, the HHV or the hydrogen content. In fact, as the interest for alternatives to conventional fuel grows, the interest for syngas as a product is growing too [4]. The producer gas is in those cases considered for its chemical compounds and not for its potential as a heat source. Its composition can be modified to fit the application by changing the gasifying agent. For example, oxygen enriched air or steam gasification increases the yields of hydrogen and carbon monoxide. A syngas with a higher carbon monoxide and hydrogen content is for example more suitable for Fischer Tropsch processes to produce biofuels. A syngas containing less nitrogen also presents a higher LHV, making it more suitable for methane substitution into boilers. This would be useful in some particular industries like glass factory or brickyard were the temperature of the flame (linked to the LHV of the fuel) is critical to the process.

Another classification can thus be made based on the fuel characteristics. As mentioned before, the fuel characteristics vary greatly with the gasifying agent. The most commonly used gasifying agents are:

- Air
- Oxygen enriched air (from 20.95 to 100 % oxygen)
- Air and steam
- Oxygen enriched air and steam
- Hydrogen and air
- Carbon dioxide
- Hot flue gases associated with air
- Recycled syngas associated with air

Table 3 shows that the syngas HHV obtained from downdraft gasification can double depending on the gasifying agents used.

| Technology | CO [%] | $H_2$ [%] | $CH_4$ [%] | $CO_2$ [%] | $N_2$ [%] | HHV [kJ/Nm$^3$] |
|---|---|---|---|---|---|---|
| Air blown Downdraft Gasifier | 21 | 17 | 1 | 13 | 48 | 5700 |
| Oxygen blown Downdraft Gasifier | 48 | 32 | 2 | 15 | 3 | 10400 |
| Oxygen/Steam blown Downdraft Gasifier | 39 | 29 | 6 | 24.5 | 3 | 11200 |

***Table 3*** *– Performances comparison between different gasifying agents. Sources: Basu [12] and Brown [4].*

Another constraint on the process choice is the available feedstock. As the energy market is changing, the approach of energy production evolves. People are trying, on the one hand, to find ways to produce clean energy and, on the other hand, to valorise non-conventional biomass considered as waste such as, sludge from Waste Water Treatment Plant (WWTP), straw or rice husks. Waste gasification potential is estimated by Groeneveld as high as half of the current crude oil production [21]. Moreover, the price of wood is starting to raise and the need for cheaper feedstock is increasing to keep gasification energy production cost competitive on an financial point of view. A lot of people are thus investigating gasification of new feedstocks in gasifiers. In the end, the influence of the biomass composition on the technology choice is, in a way, limited. In fact, when a technology fits the available feedstock, it is often due to the fact that the considered feedstocks presents characteristics close to the feedstocks for which the technology was designed. The comparison between similar technologies using different feedstocks can therefore be made with a good reliability considering the feedstock characteristics are often more similar than expected.

## Objectives of this thesis

The research presented in this thesis is aimed at small-scale cogeneration technologies using Internal Combustion (IC) engines for power generation. Engine manufacturers requirements demand less than 2 $mg/Nm^3$ of tars with the gas at the engine inlet [22], translating into huge operation and maintenance costs on gasifiers that produce syngas with a high tar content. The low tar content design makes downdraft gasifiers the best fit for the use into internal combustion gas engines. The first downdraft gasification technologies produced gas with tar contents as low as 1 to 2 $g/Nm^3$. Unfortunately it still leads to high maintenance and operational costs, reducing the economical interests for small scale downdraft gasification plants.

In the 2000s, a Belgian company named Xylowatt, a spin-off of the Université catholique de Louvain, developed a two-stage fixed bed downdraft technology to reach a tar content lower than the existing technologies. The research presented in this document investigates their innovative fixed-bed two-stage downdraft gasification technology that reduces the tar content to level as low as $50mg/Nm^3$ on industrial reactors.

The objective of the present work is to investigate Xylowatt's technology and its potential applications. The first chapter of the present document is thus focused on technologies adapted to small-scale CHP and electricity production in order to compare them to the investigated technology. After the state of the art, this thesis presents research on Xylowatt's technology. The first part of the research focused on the characterisation of the technology and the optimisation of three of its parameters: the ratio of the two stages of air injection, the residence time in the pyrolysis zone and the disposition of the air injection in the pyrolysis zone.

The second objective is to test the suitability of the technology to other types of biomass (i.e. waste biomass) and to other gasifying agents (i.e. oxygen enriched air). In these investigation, the role of the pyrolysis zone appeared as critical and this lead to the definition of a third objective: increase the knowledge on the pyrolysis operating conditions both experimentally and numerically.

In order to detail the research covered by this thesis, it is divided into six chapters. The first chapter focuses on air gasification of biomass, discussing different technologies of gasification suitable for decentralised production and their application to gasification of feedstocks that differ from wood. As mentioned before, the gasification technologies are flexible and can be modified to best fit the specificities of different types of biomass even though these modifications are often limited (e.g. downdraft gasifier will never be able to gasify high water content feedstock).

The second chapter focuses on gasifying agents that differ from air and their effect on syngas composition. It describes how they were introduced into gasification processes and why some of them are more suitable than others for small-scale power generation. It also presents technologies aimed at the gasification of wastes.

The third chapter describes the technology used during this thesis and details the specificities of the experimental setup used to lead this research on one particular two-stage downdraft gasification process. The results are thus particular to this technology even though some of the results could benefit to other technologies.

The fourth chapter presents the results of our experimental investigations on two-stage downdraft fixed bed gasification using air as gasifying agent. It starts with reference tests of the experimental setup using natural wood as feedstock. It then presents the investigations on the influence of the three parameters cited before and ends by presenting results of the use of other types of biomass in Xylowatt's technology.

The fifth and sixth chapters focus on the experimental and numerical characterisation of the pyrolysis zone of the gasifier. Gasification reactors are often considered as a whole and some research are aiming at particular step of the process like the continuous fixed bed reactor from the CIRAD laboratory [23].

# Chapter 1

# Air gasification technologies

This chapter describes the development of gasification technologies using air as a gasifying agent. It is divided into four sections. The first and second sections briefly describe recent development in updraft and fluidised bed gasification technologies to compete with downdraft gasification in the small scale power range. As mentioned in the introduction, these two types of gasifier are generally more adapted to medium and large scale facilities due to their higher production of tars. Recent studies try to decrease this production for smaller scale applications.

The third section describes downdraft gasification technologies which is the main focus of this thesis. Their basic design is more suitable for decentralised energy utilisation. It describes the evolution of the technology from a tar content of 1 or 2 $g/Nm^3$ to 0.05 $g/Nm^3$.

The last section presents what could be the future of biomass gasification: waste gasification. This section gives a small overview of technologies that could help develop the potential of waste as a source of energy.

## 1.1 Updraft Gasification technologies

Updraft gasification technologies are simple and reliable and therefore this technology is the most widespread one. Updraft gasifiers are the oldest form of gasification reactors. Their main drawback is, as mentioned before and even

more than for other gasification technology, their tar production (around 50 $g/Nm^3$ according to [6]). This is due to the fact that from a gas point of view, the last reaction encountered are pyrolysis and drying as illustrated in Figure 1.1. This is the technology producing the highest tar content, requiring a heavy gas cleaning system before use into engines [14]. This problem can be avoided by immediate combustion of the hot syngas [24]. This could be done for example in small scale co-combustion boilers [25]. The problem is then the conversion of heat to electricity with a sufficient efficiency.

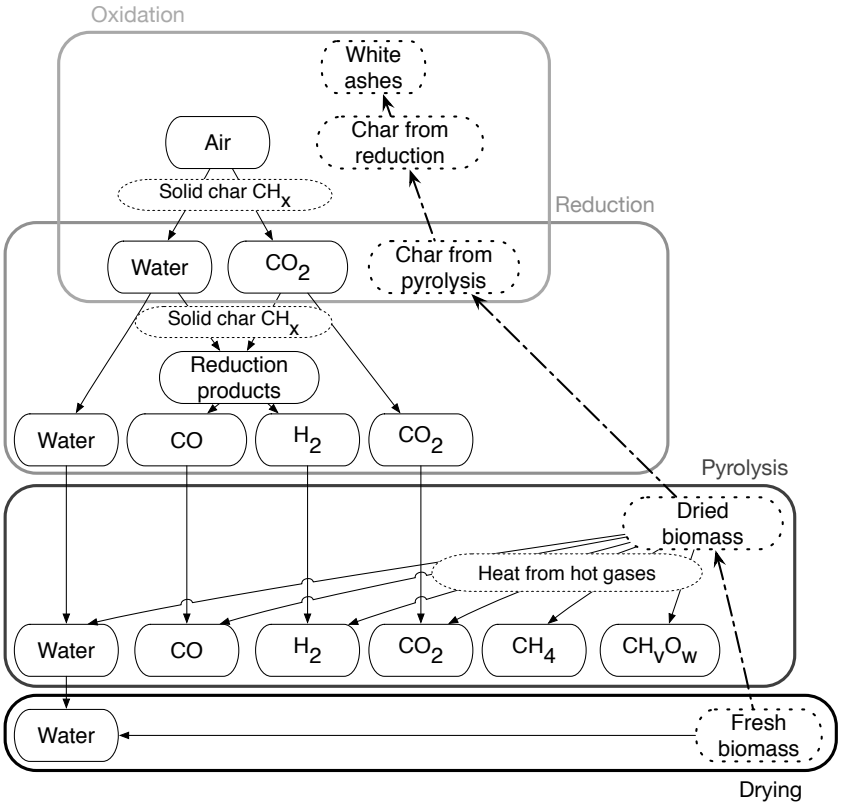


***Figure 1.1*** *– Simplified biomass reaction scheme inside an updraft gasifier from the gas point of view. The reaction scheme of the solid is illustrated in dotted line and goes from the bottom to the top of the illustration.*

To decrease the tar content, two types of measures can be applied: on the gasification process (primary methods) or on the cleaning system (secondary methods). Secondary measures have been investigated to increase the tar cracking through the use of catalysts [26]. As said before, catalysts can not be injected

into the updraft gasifier which is why it is considered as a secondary method for updraft gasification.

Some research was published in 2016 on design modifications to reduce the tar content at the outlet of the gasifier (primary method) [27]. Taylor et al. propose a design with a bottom biomass feeding system [28] and a two-stage air injection system, leading to a modification in the sequential order of the reactions as shown in Figure 1.2. This type of technology allowed Pedroso et al. to reduce the tar content to a level as low as 21 $mg/Nm^3$ while achieving an HHV of 6,05 $MJ/Nm^3$ [29] using poplar woodchips as feedstock. The advantage of this design is also to reduce fouling and slagging on the grate encountered in classical updraft gasifier. Even if the melting point of the ashes is low, the temperature in this zone is lower than in usual updraft gasifiers and boilers, avoiding to reach the melting point of ashes, removing the need of additives like limestone (which is known for increasing their melting point).

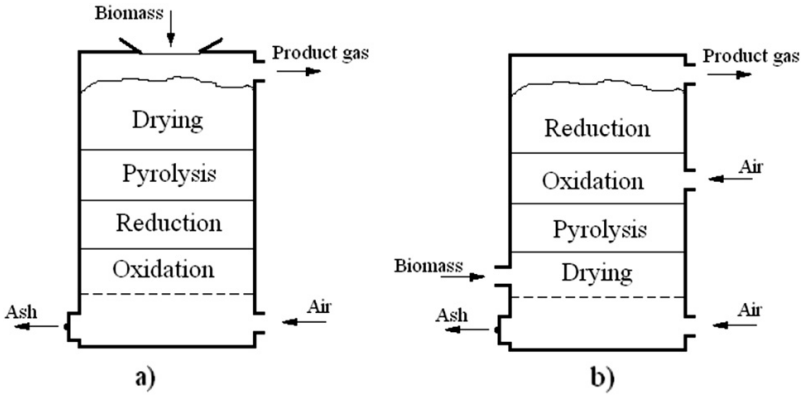


***Figure 1.2*** *– Typical updraft design on the left (a) and innovative two-stage updraft design on the right (b)[29].*

A syngas presenting such quality could qualify for the use in small CHP plants and this technology will thus be included in our comparison of the different technologies suitable for small CHP plants. Note that changing the sequential order of reactions changes the philosophy of the gasification process and it is not purely updraft gasification anymore. The sequential order of reactions is closer to a downdraft reactor but the design keeps some advantages of the updraft gasification. These advantages are the low pressure drops due to the

fluidisation of the particles bed by the gas and the high carbon conversion efficiency.

Table 1.1 summarises the main characteristics of two innovative updraft technologies and compares them to the performances of the latest two-stage fixed bed downdraft technology presented in this thesis (referenced here as T.G.P.). It also presents the ratio between the biomass consumption and a specific area of the gasifier for the three technologies. This ratio is called the Specific Gasification Rate (SGR) and is expressed in $[kg/h.m^2]$. For throat-type downdraft reactors similar to the Imbert gasifier design [30], the smallest section crossed by the biomass is called the hearth and the SGR is thus sometimes referred as "hearth load". SGR can be defined as:

$$SGR = \frac{\dot{m}_b}{S} \quad [kg/h.m^2],$$

where $\dot{m}_b$ is the mass flow rate in $[kg/h]$ and $S$ the surface in $[m^2]$.

| Gasifier Technology | P [$kW_{th}$] | CO | $H_2$ | $CH_4$ | $CO_2$ | LHV [$kJ/Nm^3$] | SGR [$kg/h.m^2$] | Tar [$mg/Nm^3$] |
|---|---|---|---|---|---|---|---|---|
| Bottom feed updraft (US) [28] | 1800 -2400 | 34.04 | 3.45 | 4.83 | / | 6404 | 24.25 | / |
| Bottom feed updraft (JAP) [29] | 48 | 28.9 | 7.07 | 4.69 | 19 | 6050 | 445.9 | / |
| T.G.P. [31] | 100 -150 | 22 | 20 | 0.8 | 12 | 5500 | 141 | 10 - 50 |

***Table 1.1*** *– Performances comparison between new updraft and two-stage downdraft gasifiers design.*

As shown by Table 1.1, the SGR can vary greatly between technologies even though the typical values found in the literature are in the range from 100 to 250 $[kg/h.m^2]$ for classical fixed-bed gasification technologies. The SGR links the power to dimensions of the reactor.

## 1.2 Fluidised bed Gasification technologies

Even if they produce less tars than updraft gasifiers, fluidised beds are usually not adapted for small scale applications. In fact, they still produce syngas with a relatively high tar content (around 10 $g/Nm^3$ according to [6]) and the highest dust content in comparison to updraft and downdraft technologies due to the conditioning of the biomass. It translates in the need for a heavier cleaning system not well suited for small scale reactors.

Another problem can come from the high residence time at high temperature in the reactive zones that could lead to fusion of low-softening mineral matter content biomasses [13]. More recently, a new three stage gasification design aimed at small and medium scale gasification appeared [32]. This concept (illustrated by Figure 1.3) reduces the tar content from 31 $[g/Nm^3]$ to 0.01 $[g/Nm^3]$and increases the carbon conversion efficiency from 59% to 98% (less carbon found in the residual char and more carbon in the gas) [32].

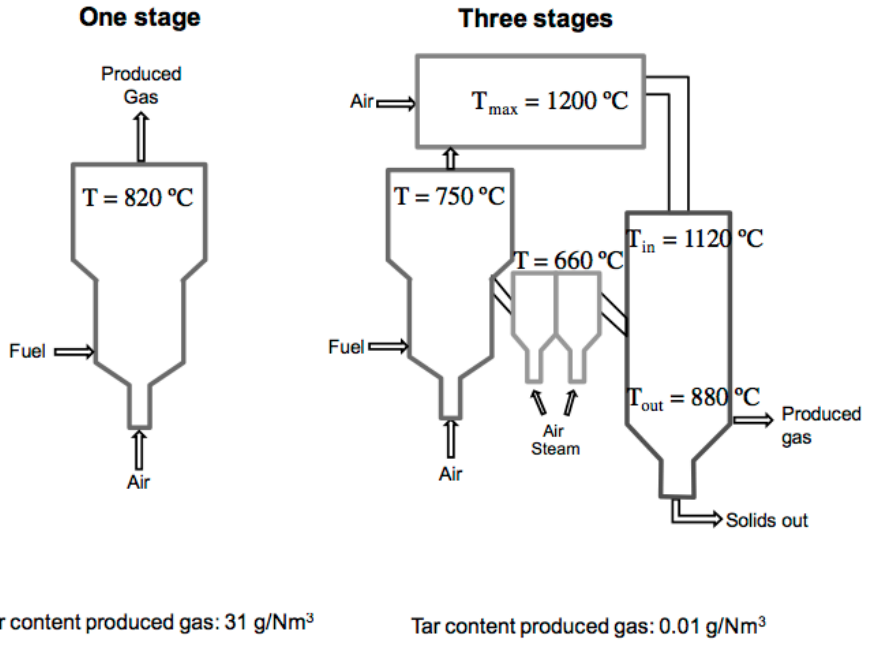


***Figure 1.3*** *– Typical fluidised bed gasifier design on the left and three stage fluidised bed gasifier design on the right [32].*

The idea behind this design is similar to what is seen in recent downdraft gasification technologies. The concept in fixed bed technologies (both downdraft and updraft) is to separate the reaction zones and the solid and gaseous flows. The estimated tar content is as low as 10 $mg/Nm^3$ and is thus also suitable for small scale applications.

One of the advantages of the fluidised bed is to allow the addition of catalysts in the bed material, reducing the temperatures required for thermal cracking of the tars.

Recently, the UNIQUE concept proposed a new approach of integrated gas cleaning system [33] as shown in Figure 1.4. The tars and particulate in the syngas are usually removed at the outlet of the gasifier, reducing the syngas temperature and therefore decreasing the tar conversion efficiency. Integrating the gas cleaning into the gasifier allows to reduce heat losses, plant space and equipment. It also increases the thermal efficiency and avoids particle entrainment. This type of process makes it suitable for small and medium scale power generation as the potential tar reduction is high. Heidenrich et al. announce an efficiency of 95% for the tar removal [33].

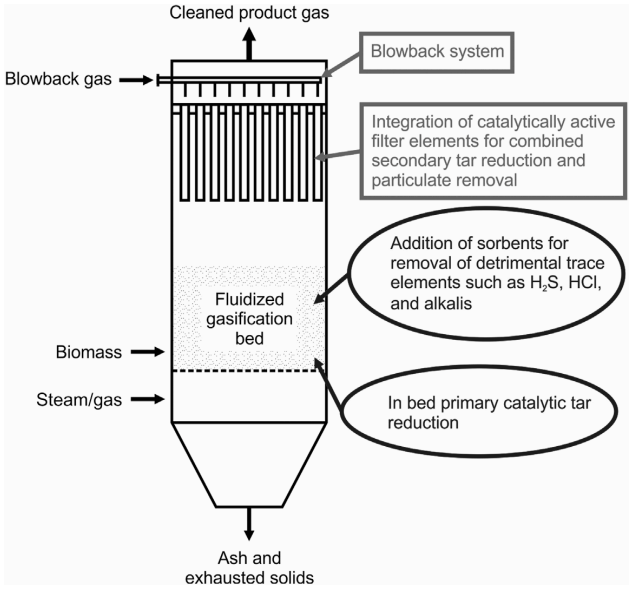


***Figure 1.4*** *– Scheme of the UNIQUE gasifier concept [34].*

Finally, if the goal is to produce a certain type of gas, the addition of a catalyst could also allow to change the composition of the producer gas to fit the application. It could bring an added value to the process like for the Unifhy project (UNIque gasifier for the production of pure HYdrogen) that uses a gasifier to produce hydrogen [34].

## 1.3 Downdraft Gasification technologies

As mentioned before, tar reduction methods are divided into two categories: primary methods that try to reduce the tar content of the syngas at the outlet of the gasifier and secondary methods that improve the efficiency of the tar removal technologies in the gas cleaning system of the gasification unit [17].

This thesis focuses on primary measures that try to modify the downdraft gasifier design to decrease the tar content before the outlet of the gasifier. The most critical reaction for downdraft gasification is usually pyrolysis. Pyrolysis has effects on the whole process as it is the first to occur in downdraft gasifier as shown in Figure 1.5 that presents a summary of the reactions inside downdraft gasifiers.

Pyrolysis is also probably the most complex reaction due to the number of products involved. As written in the introduction, pyrolysis is the thermal cracking of biomass, producing gas (part condensable, called tars, part non condensable) and char. In a downdraft gasifier using air as a gasifying agent, this thermal cracking occurs before the oxidation zone that produces the heat required for the pyrolysis.

Tar content is thus the main characteristic that allows to evaluate the syngas quality but it is not the only one. Another parameter is the LHV of the syngas. LHV is directly linked to the applications that the syngas can be used in. In engines, it determines the power available for a specific engine size, load and volumetric efficiency. In boilers, it determines the maximal temperature of the flame. Classical downdraft gasifiers produce what is called low LHV syngas with approximately 4-6 $MJ/Nm^3$ [14]. The low power density of this kind of gas translates into low temperature flames and engines with larger displacement for the same power output.

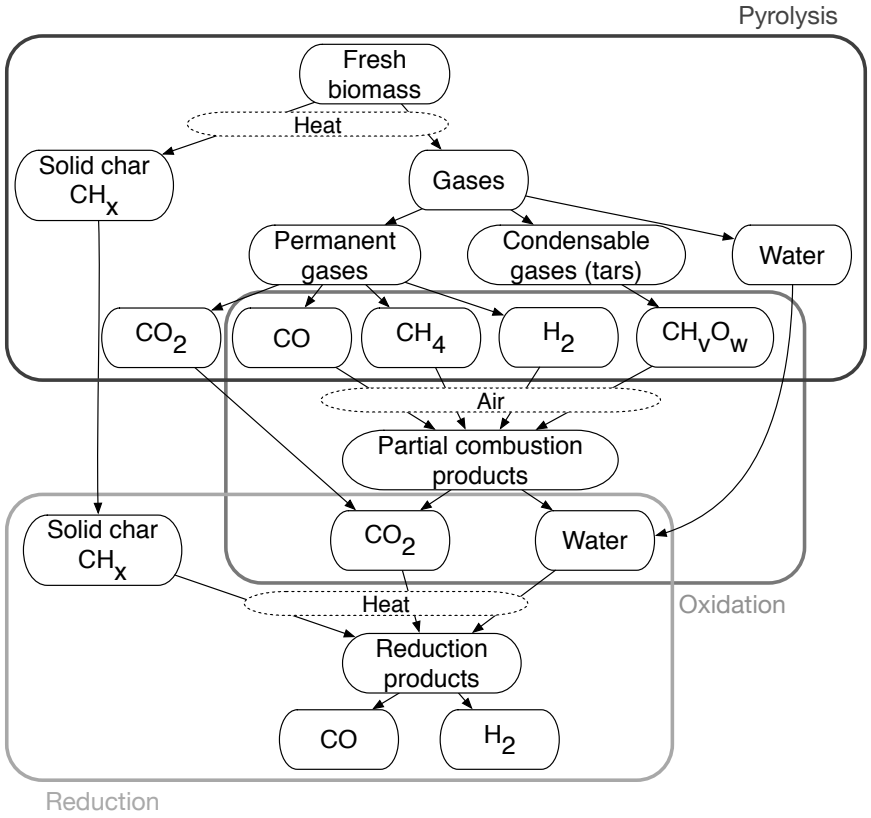


***Figure 1.5*** *– Simplified biomass reaction scheme inside a downdraft gasifier.*

In 1996, The Asian Institute of Technology (AIT) published a paper [35] presenting a gasifier design reducing the amount of tars by dividing the air injection into two zones. A first air injection is made above the oxidation zone to partially combust pyrolysis gases and thus increase the size of the high temperature zone hence increasing the size of the pyrolysis zone as shown in Figure 1.6.

This primary air injection also allows the control of the oxidative pyrolysis zone independently in opposition to the one-stage design where it is dependent from the oxidation zone. The secondary air injection is made in the oxidation zone. This new gasifier design introduced a new parameter: the ratio between the flow of air injected in the primary injection (pyrolysis zone) and the total flow of air injected in the gasifier (pyrolysis and oxidation zones). This ratio is called the air ratio ($\alpha$) and it can be defined as:

$$\textit{Air Ratio} \triangleq \alpha = \frac{\text{Air injected at the primary injection}}{\text{Air injected at the primary \& secondary injections}}.$$

Regarding its definition, the air ratio should stands in an interval $]0, 1[$ but it is generally fixed between 0.2 and 0.5.

Another important parameter is the ratio of the total amount of oxygen injected on the oxygen required for a complete stoichiometric combustion of the feedstock tested. This second ratio is frequently used in combustion and is called the Equivalence Ratio (ER or $\lambda$). It can be defined as:

$$\textit{Equivalence Ratio} = ER = \lambda \triangleq \frac{\text{Oxygen injected}}{\text{Stoichiometric oxygen}}.$$

These parameters are complementary and both are required in order to characterise the reactors using multi-stage technologies.

The gasifier from Bui et al. has two air injections but it presents an overall ER similar to the ones met in single-stage gasifiers. In gasification, in opposition to combustion, ER is always be lower than 1. Practically, ER belongs to the interval between 0.19 and 0.43 [37].

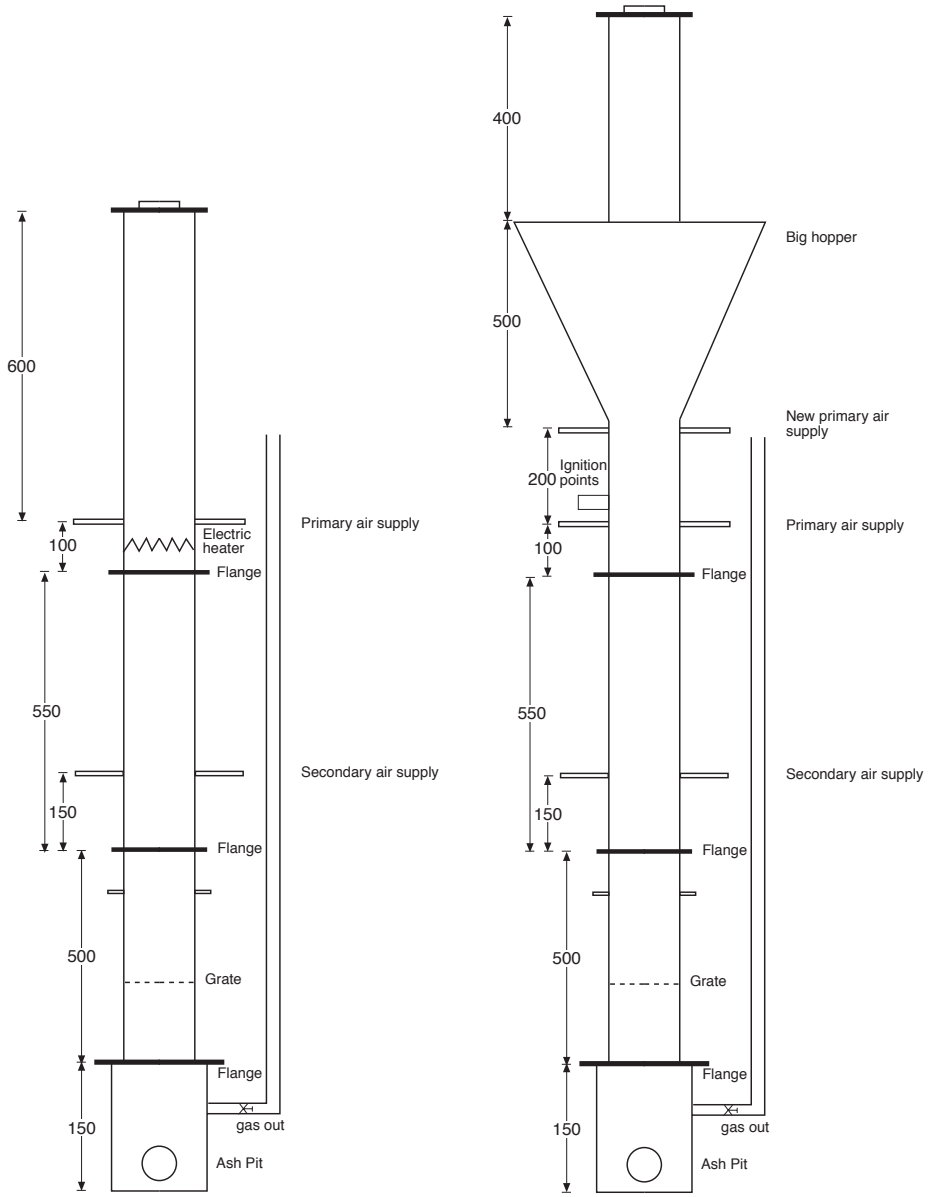


***Figure 1.6*** *– AIT Gasifier two-stage air injection design with (right) and without (left) the addition of a third air supply before the primary air supply of pyrolysis used only to start the gasifier [36].*

With this two-stage injection, Bui et al. can achieve the production of syngas with a tar content as low as 50 $[mg/Nm^3]$ which is an important step forward in the tar reduction from primary measures [35]. However, the LHV obtained for the syngas was below 5 $[MJ/Nm^3]$ mainly due to a low hydrogen content. The power, measured as the volumetric LHV of the syngas at the outlet of the gasifier multiplied by the volumetric flow in $[Nm^3]$, was 30 $[kW]$.

In 1999, the AIT team modified the design to add a third air injection in the pyrolysis zone, above the primary air supply for the start-up as shown in Figure 1.6. To avoid high tar content during transitional states (e.g. for the start-up), they used to add charcoal above the primary air injection but they replaced it with an additionnal air injection above the primary one. They achieved a tar content ranging from 19 to 34 $mg/Nm^3$. Thanks to the addition of a buffer tank where the gas stagnated and tars were collected, they could even reach a tar content as low as 9.24 $mg/Nm^3$ [36] but this could be considered as a primary filtering measure.

In their paper from 1999, Bhattacharya et al. studied the influence of the air ratio, the power, the moisture content and the wood species [36]. Moisture content is as told before, a disadvantage for downdraft gasification. In fact, the high moisture content translate into a higher hydrogen content. Unfortunately, the carbon monoxyde content and the overall LHV are lower due to the temperature decrease in each reaction zone caused by the presence of additional water steam. The water gas shift reaction ($CO + H_2O \Leftrightarrow H_2 + CO_2$) should be favoured at low temperature and thus helped by the presence of water reducing the temperature and having a positive effect on the equilibrium of the reaction. The problem is that, in fact, the equivalent water content is already more than enough to get a reaction that promotes the production of $H_2$ and the temperature decrease has a negative impact on the kinetics of the reactions that exceeds the positive impact on equilibrium. Adding more water has thus a negative influence on the LHV of the produced gas.

Additionally to this observation, Bhattacharya et al. [36] highlight the interesting fact that the influence of the type of wood on the process is not significant. In their research, they note that it was only significant at low power and they emit the hypothesis that it is due to the slightly different moisture contents

between the two species. The difference of moisture content can be neglected at high power but it has more importance at low power where moisture variations induce larger temperature differences.

In 2000, the Technical University of Denmark (DTU) published a paper presenting a primary method based on the separation of the reaction zones [38]. Their gasifier, called Viking, uses a heated screw worm to dry and pyrolyse biomass to allow an independent control of the pyrolysis. After the screw worm, the reactor presents a zone free of solid particles. This gaseous zone is where the oxidation takes place, above the reduction bed as shown in Figure 1.7. This design combines a mechanically moved feedstock for pyrolysis with a fixed bed for reduction. This design is the first one to present a discontinuity in the solid flow, allowing to free space for a gaseous oxidation zone.

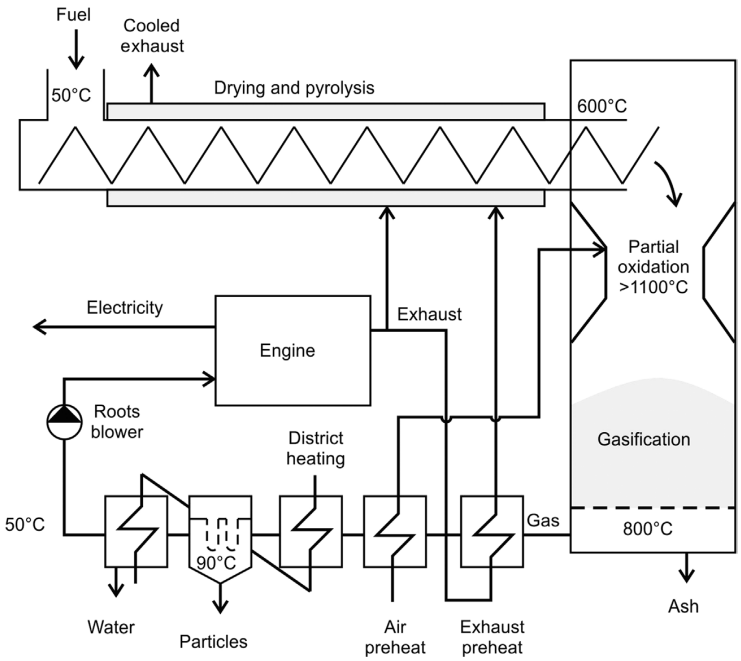


***Figure 1.7*** – *The Viking Gasifier [38].*

The first Viking gasifier has a thermal power of 100 $[kW]$. The gasifying agent is a mixture of air and steam at high temperature. This feature of the gasifier shall be discussed in the next section for this regard. Nevertheless, the specific innovation in the solid flow management lead to important modifications for

air gasifier designs that justify its introduction in this chapter. The results seemed promising with tar content of $10 - 40 mg/Nm^3$. During experimental test, they could accidentally observe the role of the charcoal bed in the tar cracking. A bypass inside the reduction bed occurred during one experience and the gas showed a significant increase in the tar content to $1 g/Nm^3$. The gaseous oxidation zone alone is thus not enough to explain the tar content below $40 mg/Nm^3$, this bypass highlighted the importance of the catalyst characteristics of the charcoal bed for the tar cracking.

In 2001, AIT [39] presented a new design of an hybrid gasifier using three air supplies and one charcoal injection (presented in Figure 1.8) to help gasify a non-conventionnal type of biomass: coconut shells. Even if they are not usual biomass, coconut shells have a composition and moisture content close to natural wood. Bhattacharya et al. could achieve a tar content ranging between 28 and 83 $mg/Nm^3$ (depending on the three injection flows) and a LHV increased to values as high as 5.3 $MJ/Nm^3$ [39].

The previous design only used the third air injection for startup but the new version uses it permanently. The charcoal is necessary to reach high temperature in the oxidation zone but can be reduced with an optimised air supply.

They implement a three stage technology and study the influence of primary, secondary and tertiary air injection. Primary and secondary air injections are there for pyrolysis while tertiary air injection is aimed at oxidation. An interesting phenomenon can be observed when too much air is injected in the secondary air injection. When the air injected in this secondary inlet is too high, the temperature increases and the zone acts like an oxidation zone. The tar levels then start to increase. This can be explained by the fact that the gasifier is then working as a two-stage one (as in previous experiments).

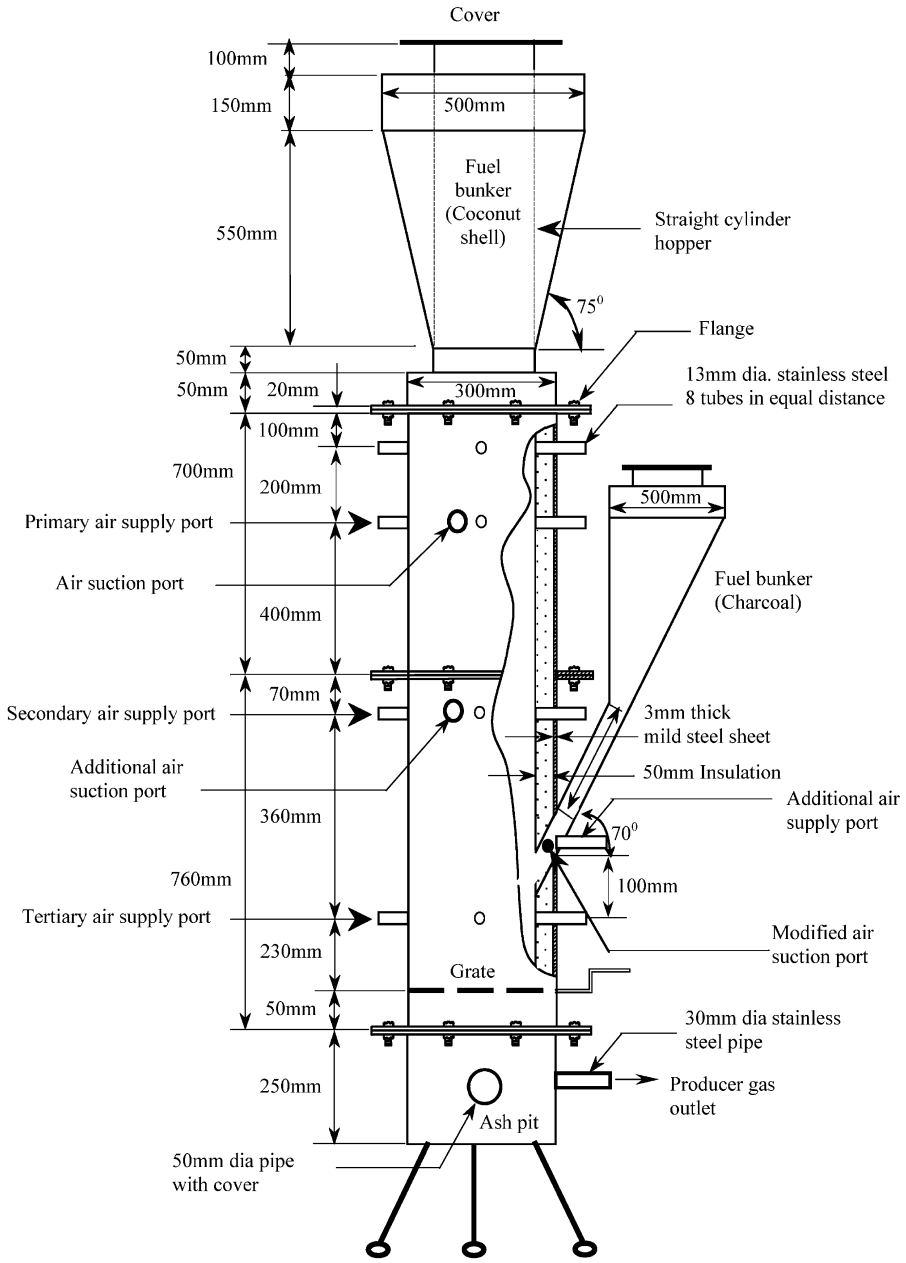


***Figure 1.8*** – *The AIT Multi-stage Gasifier aimed at gasifying coconut shells [39].*

Barrio et al. [40] presented a multi-stage gasifier with three stages of air inlets based on Bhattacharya design but at a smaller lab scale. Results show an interesting LHV of 5.3 to 5.7 $[MJ/Nm^3]$ but a really high tar content of 3 $[g/Nm^3]$ on all tests. It may be due to the small size of the gasifier: reduced size sometimes translates into an increased porosity of the bed, reducing the residence time of the gas and allowing preferential paths on the external part of the reactor. Reduced size also induces higher relative heat losses.

In 2005, TK Energi, a company from Denmark, presented a design similar to the Viking. They used air as a gasifying agent. The electrical power output was approximately 50 $kW_e$ [41, 42]. The tar content was announced between 1 and 20 mg/Nm$^3$. Figure 1.9 presents an industrial plant built by TK Energy. They installed industrial plants going from 200 kW$_{th}$ to 2.3 MW$_{th}$.

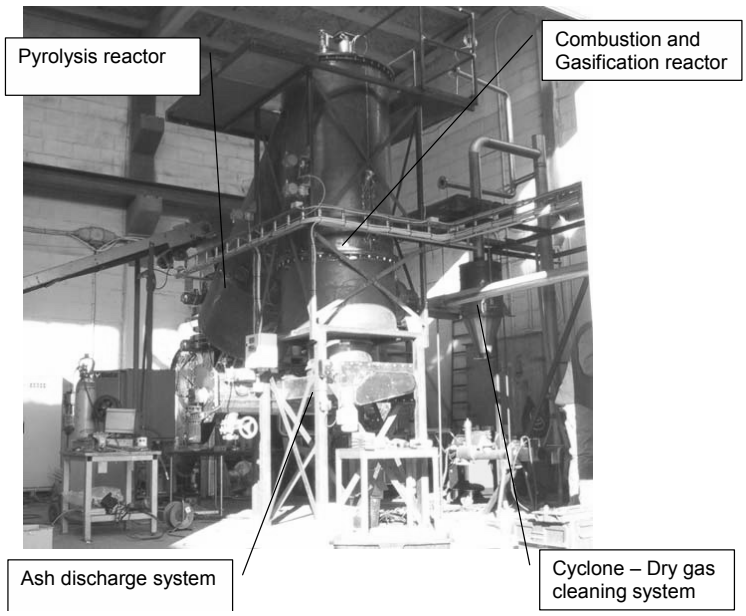


***Figure 1.9*** *– TK Energi Gasification plant (125kW$_e$) [42].*

In 2008, a team from Vienna university published their research on a pilot gasifier of 125 $kW_{th}$ [43]. Kramreiter et al. approach is different since they proposed to combine the downdraft and updraft technologies with an air injection in the oxidation zone, as on a single-stage gasifier, and a second one below the reduction zone, as shown in Figure 1.10. The sequential order of the

reactions is therefore a combination of downdraft and updraft ones. It did not increase the quality of the pyrolysis and thus the tar content but it increased the carbon conversion rate. This type of combination was previously tested at UCL but not published, the temperature in the oxidation zone was really difficult to stabilise.

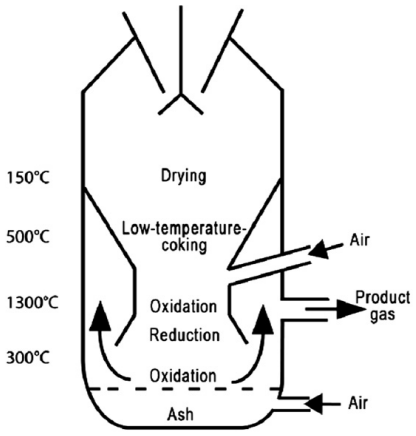


***Figure 1.10*** *– Illustration of the Austrian gasifier design from Kramreiter [43].*

The combination of updraft and downdraft would be even more interesting if it was combined with a two-stage downdraft gasifier. The resulting gasifier would then have 3 air injections, 2 for the downdraft part and 1 for the updraft part. The two-stage principle would be complex to implement on this type of technology as it presents a two-layer envelope inside the reactor as shown in Figure 1.11.

In the presented form, this innovating design from Kramreiter combining single-stage downdraft and updraft technologies produces a gas presenting a LHV of 6.3 $MJ/Nm^3$ [43]. Unfortunately, the gas tar content was fluctuating in a range going from 200 to 2000 $mg/Nm^3$ which is higher than regular two-stage downdraft technologies. The aim of Kramreiter et al. study was to build a 2 $MW_{th}$ gasification plant. Their cleaning system also rises interest with its original combination of water and rapemethylester (RME or biodiesel) in a single cleaning system. The water has one goal: to avoid RME cracking at the high gas outlet temperature (650°C). The advantage is that RME is hydrophobic with a density different than water and is therefore easily separated in a

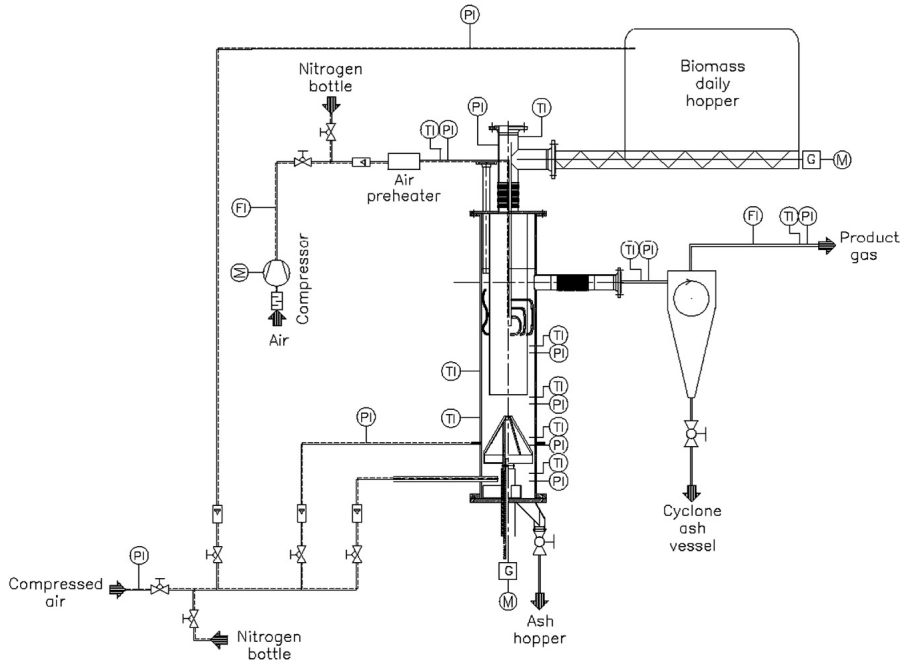


***Figure 1.11*** *– Austrian gasifier P&ID from Kramreiter [43].*

sedimentation tank. The residues collected by the cleaning system (dust and char) are found at the interface of the sedimentation tank and can be collected and transferred back into the fixed bed gasifier. In comparison to the LHV of the gas produced in the pilot plant, the LHV of the gas from industrial plants was very close but the tar content they observed was higher with values going from 1200 to 2000 mg/Nm$^3$.

In 2011, a team from Brazil [44] tested a design (illustrated by Figure 1.12) similar to the one from Bhattacharya et al. with two-air supplies in porous medium without discontinuity. The power of the gasifier tested is 50 kW$_{th}$. They focus on the influence of the air ratio. Martinez et al.[44] experimented air ratios between 0.28 and 0.44. This means that when one unit of air is injected at the primary injection, approximately 2.5 to 1.25 units of air is injected at the secondary injection. On the $ER$ point of view, the ER measured ($\approx 0.47$) is really high for air gasification (usually $\approx 0.30 - 0.35$). The gas yield is constant and between 2.6 and 2.8 $[Nm^3/kg_{dry\ biomass}]$. The LHV achieved is 4500 $[kJ/Nm^3]$ for single-stage and 4600 $[kJ/Nm^3]$ for two-stage operations. This is probably due to the high ER in the two-stage gasification configuration

since the authors published another study in 2014 showing a maximum LHV of 5250 $[kJ/Nm^3]$ but with an ER of approximately 0.42 at the same power [45]. The gas composition shows a decrease of more than 5% in nitrogen content without changing the gasifying agent meaning that less air was injected in the gasifier. They obtained a low tar content ranging between 54 and 172 $[mg/Nm^3]$ with this configuration.

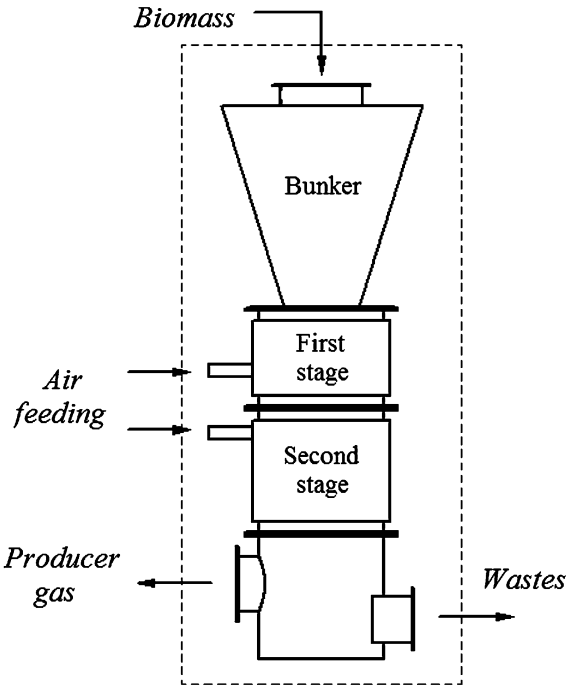


***Figure 1.12*** *– Brazilian gasifier based on the two-stage principle [44].*

In 2011, a research team from Korea [46] published a paper on a single-stage gasifier producing a gas with a LHV of 4600 $[kJ/Nm^3]$ which is quite high for single-stage technology. The drawback is the tar content that goes from 3.9 to 4.4 $[g/Nm^3]$ meaning the treatment to use into IC engine would require too much efforts.

In 2012, a team from China implemented the two-stage design from Bhattacharya et al. and improved it by pre-heating the air through a double enveloppe gasifier [47], hence reducing the amount of air required for the pyrolysis

zone. Their solution presents an ER of 0.28 which directly translates into less nitrogen in the syngas, explaining the increased LHV of the resulting syngas in comparison to Bhattacharya et al. design. The air injections are still made in porous medium which shall lead to relatively high tar content, unfortunately there was no information available on tar measurement. Their pilot of 190 $kW_e$ presents a maximal gas LHV of 5250 $[kJ/Nm^3]$ and an average LHV of 4700 $[kJ/Nm^3]$ [47].

In 2013, an Indian team [48] presented a two-stage gasifier design similar to the Chinese one with pre-heated air injection (shown in Figure 1.13). The difference is a special ash pit system that allows low tar and dust content in the produced syngas. Thanks to this addition, they could remove wet scrubbers from the gas cleaning system. With this ash pit, the reduction bed plays the role of a granular filter, reducing the cleaning equipment required. The maximum LHV achieved is 5300 $[kJ/Nm^3]$ (average 4700 $[kJ/Nm^3]$) and the tar content goes from 17 to 90 $[mg/Nm^3]$. The equivalence ratio used is 0.27.

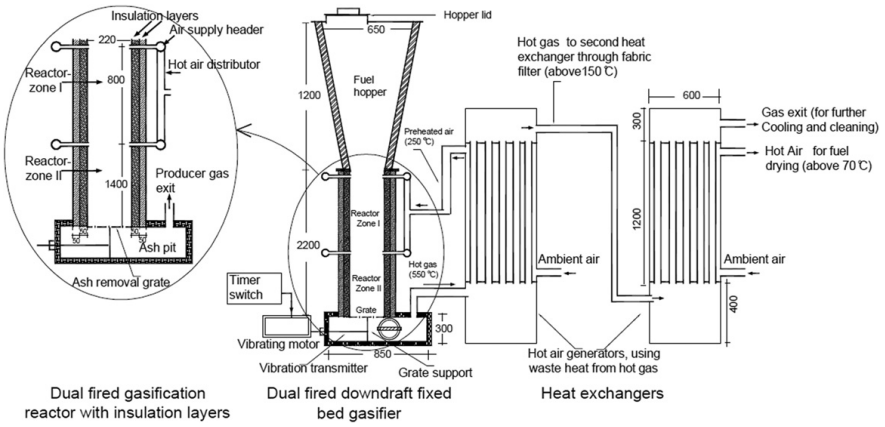


***Figure 1.13*** *– Indian gasifier presenting an innovative ash pit [48].*

Table 1.2 summarises the different characteristics of the downdraft technologies presented in this section. It compares them to the gasifier used in this study and referenced under the name TGP at the bottom of the table. Table 1.2 illustrates that there is a compromise between a high LHV and a low tar content. There is clearly a potential interest for a gasifier presenting those type of performances. Moreover, this particular gasifier also shows the highest

| Gasifier | Power [$kW_{th}$] | CO % | $H_2$ % | $CH_4$ % | $CO_2$ % | LHV [$kJ/Nm^3$] | Tar [$mg/Nm^3$] | SGR [$kg/h.m^2$] |
|---|---|---|---|---|---|---|---|---|
| Asian IT [36] | 25 | 21 | 14 | / | 15 | / | 19 - 34 | 546 |
| Asian IT [39] | 25 | 23 | 15 | 3 | 15 | 5300 | / | 546 |
| Trondheim [40] | 40 | 26.4 | 17.2 | 1.4 | 8.8 | 5700 | / | 239 |
| TK Energi [41] | 200 | / | / | / | / | / | 20 | / |
| Vienna [43] | 125 | 26 | 15 | 3 | 10 | 6000 | $\geq$ 800 | 625 |
| Brazil [44] | 50 | 19 | 16 | 0.9 | / | 4500 | / | 200 |
| Korea [46] | 150 | 20 | 18 | 3 | 15 | 4600 | 3900 | / |
| Nanjing [47] | $\pm$ 600 | 17 | 16 | 2.3 | 14 | 5250 | / | 60 |
| Brazil [45] | 50 | 21 | 18 | 2 | / | 5250 | 55 | 200 |
| India [48] | 10-125 | 20.5 | 21.3 | 1.1 | 10.7 | 5300 | 17 - 90 | 2000 |
| TGP [31] | 150 | 22 | 20 | 0.8 | 12 | 5500 | 10 - 50 | 142 |

***Table 1.2*** *– Summary of the performances of the gasifiers presented in this section, TGP being the reference name for the gasifier used in this thesis.*

concentration of hydrogen which could be interesting from a poly-generation point of view. Note that the comparison between the tar contents is difficult as definition and measurement of tars may vary between the research teams. For example, Galindo et al. [45] use the tar protocol while Bhattacharya et al. use cooled ceramic filter that cannot measure light hydrocarbon like benzene because they required a drying at 105 [$°C$].

It can also be observed on Table 1.2 that methane, even if desirable from a LHV point of view is also linked to a higher tar content. Methane synthesis requires severe conditions that are not met in low pressure gasifiers. It is thus the main residue of pyrolysis gases and it goes with light hydrocarbons and all the unwanted tar species from pyrolysis.

## 1.4 Waste gasification

Waste disposal has become a major concern in the last decades due to the environmental impact of the traditional routes and due to regulation changes. For example, sludge from Waste Water Treatment Plant (WWTP) is excluded from direct landfill disposal and is expected to be excluded from the use as soil amendment [49].

For such wastes, the solution is usually incineration but the pollutants they contain require special gas treatment and incinerators use very high ER in order to ensure total destruction of wastes, hence decreasing the thermal efficiency. Gasification can thus propose an alternative since it is more efficient, can be used at small scale near the waste production (therefore reducing transport) and pollutant can be treated in the syngas and not in the exhaust gases (smaller volume to treat and higher concentrations reduce the costs of treatment).

The challenge of these wastes resides usually in two different aspects that can differ from wood characteristics. The first one is the ash content and the second one is their thermal characteristics.

Natural wood ash content is approximately 1% when some waste can present ash content up to 40% [50]. On that regard, one of the most difficult biomass to treat is rice husk due to its high ash content (≈16-23%), its relatively low melting point ($\approx 1440\ [°C]$) caused by the high percentage of silica in the ashes ($\approx 95\%$) and its mechanical characteristics (high volume of ashes) [51]. Nevertheless, a study shows that gasification is the most suitable option for rice husk valorisation in Ecuador [52] and rice husk presents a huge feedstock around the world as it is produced in 75 countries [51].

Another waste presenting a huge feedstock and with no other use than incineration is sewage sludge from waste water treatment plants (WWTPs). It also presents a high ash content (between 20 to 40%) and thermal characteristics (e.g. thermal conductivity inside sludge particles) that can vary greatly depending on the drying process of the sludge. One solution to avoid the problems induced by ashes is to mix the sewage sludge with a low ash content feedstock like wood, hence reducing the overall ash content and the risk of clinkering and slagging [53]. Mixing the sludge with wood also reduces the influence of the thermal characteristics of the sludge. Dogru et al. [53] obtained a syngas presenting a tar content between 1 and 2 $g/Nm^3$ from sewage sludge used in single-stage downdraft technology. These results are similar to wood gasification for the same technology. The syngas obtained presents a LHV of 4 $MJ/Nm^3$ which is already great regarding the LHV of the sludge (approx. 12 $MJ/kg$) much lower than natural wood (approx. 18 $MJ/kg$).

A team from Latvia [54] presented a work on a small scale gasifier with a very simple design using co-gasification of pellets made of wood and straw. The interest for the mixing is to decrease the overall ash content and increase the melting point. Their gasifier works by batches and the process is started using propane. Pellets presents another challenge: their density is much higher than wood chips and the heating phenomenon (ruled by the internal heat conductivity) is thus slower inside pellets than wood particles. This gasifier is a lab-scale experiment presenting a simple design as shown in Figure 1.14.

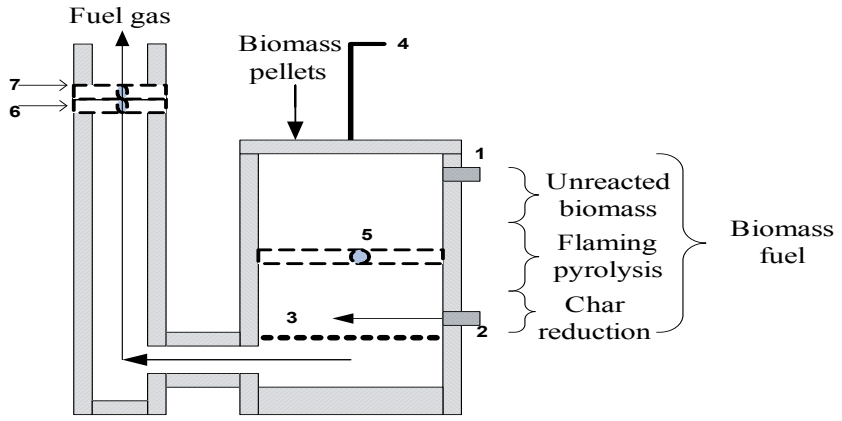


***Figure 1.14*** *– Latvia gasifier [54] presenting a propane injection located at position 2 on the schematic.*

Another interesting feedstock is plastic wastes. There are three ways to treat plastic wastes: mechanical recycling, feedstock or chemical recycling and energy recovery [55]. Mechanical recycling, if available, is of course the best option: it is cheap, simple and sustainable. Feedstock or chemical recycling can convert plastic into useful basic chemicals or convenient fuel. It can be considered to be more sustainable than energy recovery if the chemical compounds can be reused for other purposes. Gasification can be considered as chemical recycling since producer can either be used to produce electricity or synthesise chemical products as said in the introduction.

A Korean team [55] developed a gasifier to gasify a mix of plastic wastes, its design is presented in Figure 1.15. The research is only lab-scale and uses a fluidised bed associated with screw drivers heated with water for pyrolysis.

It is thus combining concepts from downdraft gasifiers (i.e. the Viking [38]) with fluidised bed. The LHV achieved is incredibly high for air gasification at a maximum of 14.5 $[MJ/Nm^3]$ [55]. The value of the LHV is high but the LHV of plastics used is 41.5 $[MJ/kg]$ which is approximately twice higher than wood LHV. The gas presents high percentage of hydrogen and methane that could be interesting for product synthesis. The tar content reached is below 5 $[mg/Nm^3]$ but is it also due to the good pyrolysis of plastics and cannot be compared to wood gasification.

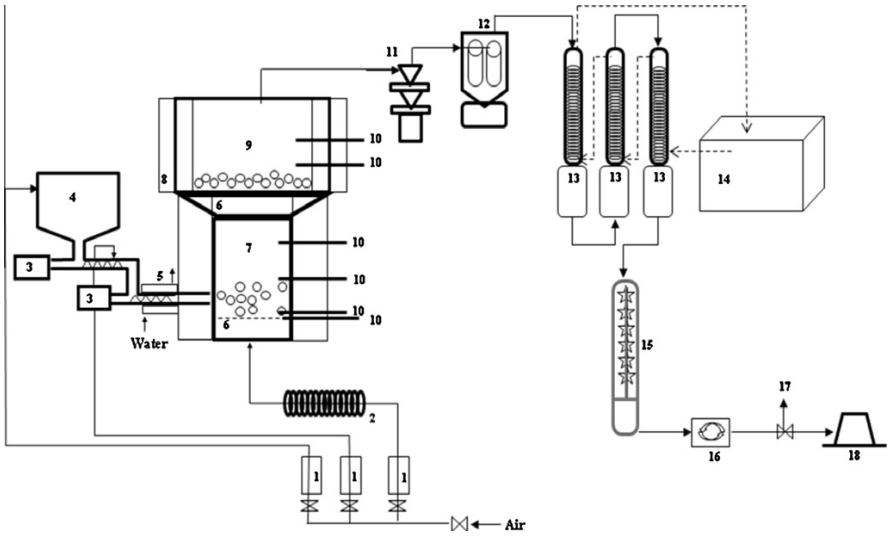


***Figure 1.15*** *– Korean gasifier using plastic wastes as feedstock [55] and using screw drivers heated (position 3) with water for pyrolysis.*

Table 1.3 summarises the different characteristics of the waste gasification technologies presented in this section. It compares them to the gasifier used in this study (when gasifying creosoted wood) and referenced under the name TGP at the bottom of the table.

| Gasifier | P $[kW_{th}]$ | CO [%] | $H_2$ [%] | $CH_4$ [%] | $CO_2$ [%] | LHV $[kJ/Nm^3]$ | HHV $[kJ/Nm^3]$ | Tar $[mg/Nm^3]$ |
|---|---|---|---|---|---|---|---|---|
| Niu et al. [56] MSW | $< 1$ | 30 | 8 | 10 | 40 | 8200 | / | / |
| Seoul [57] Sewage sludge | $\leq 1$ | 6.5 | 9.6 | 6.2 | 14.1 | 7310 | / | 5.85 |
| Korea [55] Plastic waste | $< 1$ | 8 | 21 | 16 | 4 | 14000 | / | / |
| T.G.P. Creosoted wood | 150 | 22 | 20 | 0.8 | 12 | 5500 | / | 10 - 50 |

***Table 1.3*** *– Performances comparison between different types of wastes used in different gasifier technologies.*

## 1.5 Chapter summary

This chapter presented the different gasification technologies and their main advantages and drawbacks. Depending on the applications, there is generally a possibility to find a gasification technology that fits the requirements (biomass type, moisture content, use, etc), even for some biomass that are hard to treat like wastes. The focus of this thesis is on small CHP using IC engines. Therefore, the downdraft fixed bed gasification technologies are the best fit thanks to the low tar content found in the syngas. The next chapter presents another aspect of the gasification technologies, the use of an alternative gasifying agent.

# Chapter 2

# Alternative gasifying agents

Air is the most common gasifying agent met in gasification technologies. It is cheap, available everywhere and does not require special installations. The problem with air is that when it comes to a specific technology, the composition is often the same and the high nitrogen content in the resulting gas decreases the LHV by dilution. In order to change the resulting gas composition, it can be interesting to change the gasifying agent to obtain a different synthesis gas more suitable for a specific application. Some agents can also displace the chemical equilibrium in place in the process and lead to better conversion efficiencies. For these reasons, alternative gasifying agents can be justified even if they always come with increased costs.

When considering alternative gasifying agents to improve the gasification process or to increase the syngas LHV, the first agent that comes to mind may be oxygen enriched air as it requires few modifications of the process for a huge impact on the gas composition thanks to the removal of inert gases.

Another well-known agent is steam. As mentioned before, syngas is now seen not only as a mean but also as a product itself. In this regard, its properties (composition for cogeneration, LHV for methane substitution) are more important than when it is only considered as a gaseous fuel to be used in CHP, engines or boilers. The steam gasification presents a high hydrogen yield which is becoming really attractive for renewable fuel production. The problem of steam gasification is the energy cost linked to the production of the required steam (i.e. at high temperature).

One solution to reduce this cost is to inject low temperature steam mixed with air in order to realise a partial combustion of pyrolysis gases like in classic air-driven processes. This solution is thus intermediate between the air gasification and the steam gasification. Another approach is to inject steam in air gasification process to reduce the amount of inert gases. These two approaches are not equivalent as the proportions of air and steam differ greatly. The consequences is that they lead to slightly different propositions for steam and air use as gasifying agents. Moreover, for the same reasons that oxygen enriched air is interesting to replace air gasification, oxygen enriched air is also interesting for air steam gasification.

The last alternative to air is the addition of hot flue gases coming from the combustion of air and fuel in the process. It is not completely an alternative gasifying agent as the idea is not to replace all the air by hot combustion gases but only a part of it. Indeed, some researchers propose [54] to help the heating of some endothermic parts of the process by injecting a mixture of air and fuel to maintain and stabilise the process. This fuel can either come from an external source or be produced by the process though a recycling loop of the producer gas.

In order to assess the potential of alternative gasifying agents, basic equilibrium models can predict the theoretical syngas composition accurately. This chapter thus starts by describing the chemistry behind downdraft gasification in order to detail the equilibrium model used to evaluate the interest of other gasifying agents.

The second section then describes the use of oxygen enriched air, its effects on the syngas composition and the conversion efficiency of the process.

The third section discusses the use of steam and its combination with air. It also presents results of the use of enriched air and steam which tries to combine the advantage of two alternative gasifying agents into one process.

This chapter ends by describing the addition of gaseous fuel inside gasifications processes.

## 2.1 Chemistry of downdraft gasification

The gasification process is complex, however, downdraft gasification can be reduced to a series of reactions that are: drying - pyrolysis - oxidation - reduction. In order to increase the knowledge on gasification, complex models have been developed to reduce the tar content and improve the carbon conversion.

When looking at the numbers, tars, even if their impact on maintenance costs is huge, represent a really small amount of mass and energy in the balance of the system and can thus be neglected in simplified reaction schemes. Moreover, at least 98% of the mass in the process stands in less than ten compounds that are: $N_2$, CO, $CH_4$, $H_2$, $CO_2$, $H_2O$ and Ashes (made of carbon and minerals). Even if capturing complexity of the gasification process is important for the development of the technology, a simple equilibrium modelling considering only these main compounds can help understand the basic principles of downdraft gasification and the impact of the use of specific gasification agents.

Equilibrium models can help to predict the ideal case gasification by taking assumptions that help to simplify the problem [58]. The only parts considered into equilibrium models are the gas phase reaction and the carbon conversion inside the reactor. The equilibrium model is based on the assumption that all the reactions occurring in the reduction bed are at thermodynamic equilibrium. This assumption is never met in experimental or industrial reactors but the trends shown in equilibrium models can generally be transposed to experiments. The drying, pyrolysis and oxidation parts are neglected and the reactor is seen as a black box where all the elements and the energy are mixed. Another assumption is a complete consumption of the oxygen during the oxidation step which presents a good agreement with experimental data.

A simple approach can be made considering the energy balance of the whole gasifier as one reactor where all the selected species interact through a limited number of equilibrium reactions. The energy input is the sum of the sensible enthalpy and the enthalpy of formation of the air and the biomass. The equilibrium is determined by several iterations on the temperature of the equilibrium. It starts with a given temperature (based on experimental data or assumptions) to calculate the composition of the produced gas based on the equilibrium constants at the given temperature. It then calculates the forma-

tion enthalpy of all the compounds and subtracts it from the energy input. The difference obtained is thus the sensible enthalpy of the gas and it allows to determine the temperature at which the compounds should be to close the energy balance. This new output temperature is then used to calculate a new composition based on the equilibrium constants at this temperature and the new composition is then again used to determine a temperature that closes the energy balance. The iterative calculation stops when the temperature difference between two iteration steps is considered sufficiently small (parameter fixed by the user). The variables of the problem are thus the species considered.

The inputs of the model are the following:

- Wood elemental composition in terms of C, H and O
- Wood moisture content
- Air content (expressed through the equivalence ratio), composed only of $O_2$ and $N_2$
- The LHV of wood is either given or calculated based on the composition

For the model, the elements in the producer gas are limited to seven compounds that are:

- CO
- $CO_2$
- $H_2O$
- $H_2$
- $CH_4$
- $N_2$
- Ashes, considered as pure carbon ($C_s$)

Other compounds like light hydrocarbons or tars found in syngas are neglected in order to simplify the model. Note that there is no oxygen in the outlet gas thanks to the assumption of complete consumption of oxygen.

There are thus 7 variables from the composition, to which can be added the temperature of the resulting syngas, making a total of 8 variables in the system. Eight equations are thus required to solve it. The first equation was previously discussed, it is the conservation of energy. A second series of equations comes from the elemental balance that can be made on C, O, H and N, representing 4 equations.

The last 3 equations required to close the system come from the reactions in the reduction zone which are truly the gasification reactions. The three reactions considered in this work are:

- The shift reaction: $CO + H_2O \leftrightarrow CO_2 + H_2$
- The Boudouard reaction: $C_s + CO_2 \leftrightarrow 2CO$
- The methanation reaction: $C_s + 2H_2 \leftrightarrow CH_4$

These reactions are equilibrium reactions. The resulting concentrations can be calculated thanks to the equilibrium constant that expresses a ratio between the chemical activities of the products and the chemical activities of the reactants. The equilibrium constant is temperature dependant, this means that when the temperature changes, the equilibrium is displaced in one direction or in the opposite. The equilibrium constants of these three reactions as a function of temperature are derived from JANAF tables [59]. Their evolution with temperature are represented in Figure 2.1. When the value is high, it means that the reaction is displaced on the right side of the equation. For example, the shift reaction produces more hydrogen and less carbon monoxyde at low temperature.

The model can be used to investigate the effect of the biomass moisture content on the gas composition or air enrichment.

Figure 2.2 presents the gas composition of the producer gas as a function of the moisture content of the biomass. The trends shown in Figure 2.2 are in good agreement with the ones presented by Sharma et al. [60].

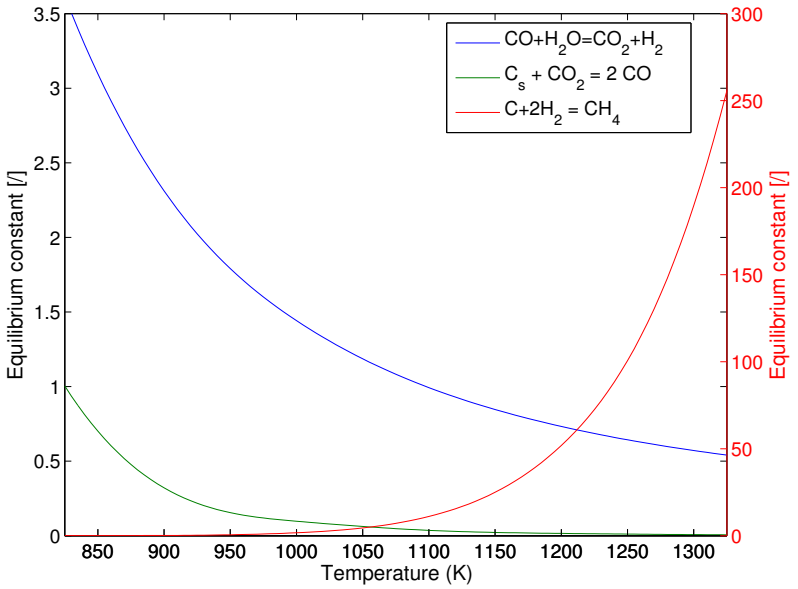


***Figure 2.1*** *– Evolution of the equilibrium constants with the temperature for the shift reaction (value on left axis), the Boudouard reaction (value on left axis) and the methanation reaction (value right axis).*

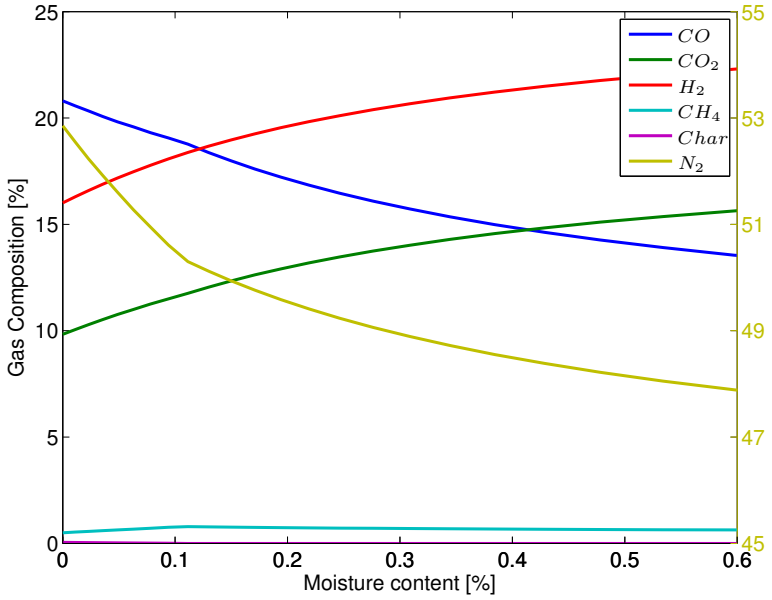


***Figure 2.2*** *– Dry gas molar fraction predicted by the equilibrium model as a function of the moisture content of biomass.*

Figure 2.2 shows that the hydrogen and carbon dioxide content increases with moisture content while carbon monoxide decreases with the moisture content. The methane level is quite stable while the nitrogen content decreases due to the presence of more species in the dry syngas. Hence, there is an interest to have a high water content in the reaction zone as it promotes the production of hydrogen in the process as shown previously in other studies ([61],[58]). This can be the case with high moisture content biomass but it comes with the disadvantage that the water evaporation reduces the temperature in the reactive zones which cancels the benefit of the presence of water as pointed out by Schuster et al. [61]. Hence the addition of steam at high temperature could be interesting for hydrogen production. Moreover, a pure steam gasification produces a syngas without nitrogen, increasing its LHV and the hydrogen content, making the hydrogen recovery easier. Steam gasification thus presents a high potential as long as the costs of steam production are balanced by the benefits of steam addition.

The main component of the synthesis gas predicted by the model is nitrogen. As nitrogen is non combustible, it acts as a diluent in the gases through the whole process reducing the temperature in each reaction zone. Figure 2.3 shows the composition of the syngas predicted by the model for pure oxygen gasification with an ER of 0.2. Removing it directly increases the energy density of the gas. However, it also increases the temperature in the process, displacing all the equilibriums, resulting in a better conversion efficiency. The produced syngas presents a composition that is not equivalent to the syngas composition without nitrogen. Its composition is better as it presents a higher $CO$ to $CO_2$ ratio. The LHV is thus even higher than syngas from air gasification after nitrogen removal. Moreover, the char content in the bottom ashes is lower due to a higher temperature reached without nitrogen.

For all the reasons exposed, changing gasifying agent presents interests. The most simple to understand is air enrichment which is described in the next section.

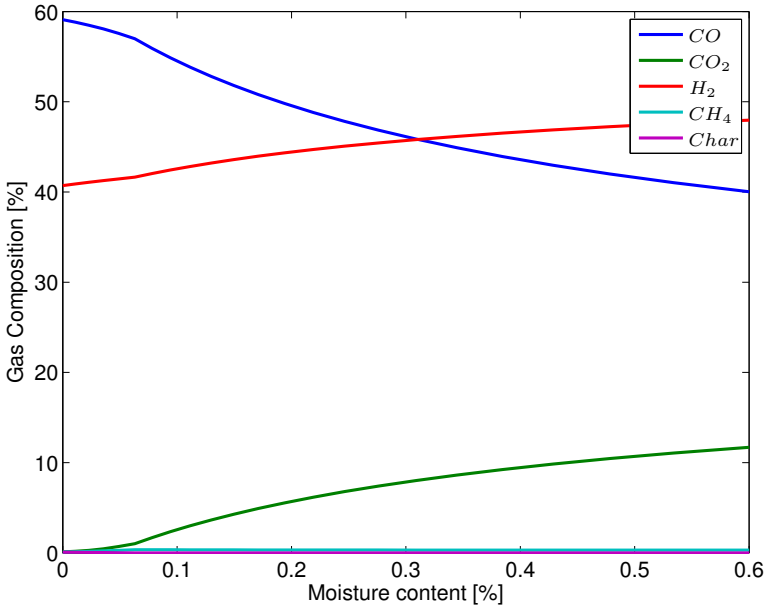


***Figure 2.3*** *– Dry gas molar fraction predicted by the equilibrium model as a function of the moisture content ($\%_{mass,drybasis}$) of biomass for pure oxygen gasification.*

## 2.2 Oxygen enriched air gasification

Oxygen enriched air gasification could increase the value of syngas as a product. Removing nitrogen increases the LHV of the gas turning it from a low heating value gas to a medium heating value gas. Pure oxygen syngas is, for example, better suited to synthesis of transport fuels and commodity chemicals due to the absence of nitrogen [62]. Removing nitrogen also decreases the dilution of syngas flame, translating into higher flame temperatures that are wanted for methane substitution into boilers. For example, a high flame temperature is essential for applications in the glass industry. In these cases, the additional costs of oxygen production are compensated by the higher syngas quality or simply by allowing the use of syngas for special applications.

Oxygen enrichment of the gasifying air has also other benefits than the removal of nitrogen in the producer gas. The lower nitrogen content induces a higher temperature in each reaction zones, accelerating some reactions and displacing the chemical equilibriums, leading to an increased energetic efficiency [63] and carbon conversion [56].

Another advantage of oxygen gasification is the reduction of the pressure losses through the solid particle beds due to the reduced volumetric flows. As the pressure drops in the porous media are a limiting factor for a power increase, oxygen gasification could translate into an increase of the flow of gas for the same section of the gasifier. This means than the power of the gasifier would increase with the use of oxygen.

## 2.3 Air and steam gasification

In 2006, DTU presented results showing the Viking gasifier (75 $kW_{th}$) could produce a gas with a LHV as high as 6 $MJ/Nm^3$ [64]. This LHV is really high in comparison to other two-stage technologies and is not only due to the innovative gaseous phase combustion. There are two reason to this high LHV. The first one is due to the pyrolysis and the second one is the steam injection. Sadly, there are no numbers on the external energy input made for pyrolysis and steam heating so it cannot be compared with traditional two-stage air gasifiers. Externally heated pyrolysis also allows a lower equivalence ratio in comparison to pure air gasification technologies, reducing the amount of nitrogen in the syngas. External heating and steam gasification combined allows the Viking gasifier to produce a gas containing 51.5 % of combustible gases, 20% of CO and 29.5 % of nitrogen while air downdraft gasifiers usually presents 45-50% of nitrogen therefore decreasing the LHV of the producer gas. The Viking was successfully tested on 400 hours and then monitored during 75h [65]. During these tests, the gasifier was successfully connected to an engine using syngas during 50 hours.

In 2010, two teams from Thailand and Canada joined their forces to build a multi-stage gasifier, presented in Figure 2.4, mixing air and steam as gasifying agents to produce hydrogen rich syngas [66]. The power of the gasifier during the tests goes from approximately 20 to 35 $kW_{th}$. Jarungthammachote et al. [66] compare the performances of air gasification and air and steam gasification. With air, the HHV achieved is 5200 $kJ/Nm^3$ with a minimal tar content of 90 mg/$Nm^3$. Unfortunately, steam injection, while allowing a higher hydrogen content, increases tar levels. The amount of CO + $H_2$ increases with steam injection to a maximum of 36%.

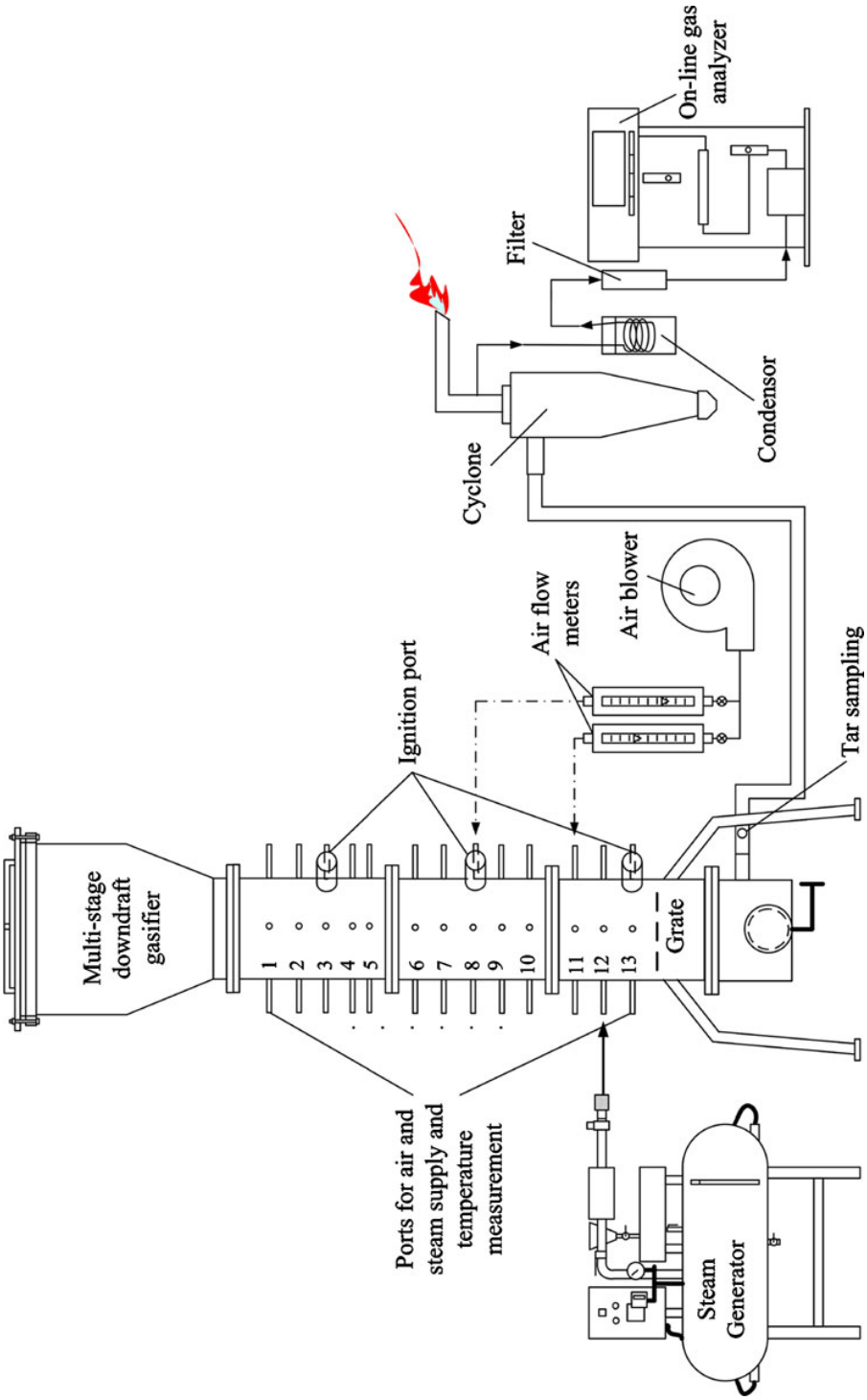


***Figure 2.4*** *– Schematic diagram of Jarungthammachote et al.[66].*

The gasifiers presented in these two papers [67, 66] used steam injection to enhance the conversion performances and achieve a higher LHV to use syngas into IC engines. As mentioned before, syngas is now seen as a product and interests for steam gasification are now more complex. Steam gasification increases the LHV and conversion by increasing the hydrogen yield. It is thus seen as a route to hydrogen production. Hydrogen is considered as a major fuel for our future and researchers are trying to find renewable ways to produce it. Steam reforming after gasification could help produce a gas that contains more hydrogen and would be easier to treat than air gasification. For example, Zhang et al. [67] obtained syngas containing 30% hydrogen with their catalytic reforming process. The syngas they have before reforming comes from air gasification and contains only 8% of hydrogen. This solution can be used to increase the content of hydrogen from air blown gasifiers even though it cannot compete with primary methods of steam gasification. In fact, the content obtained by Zhang et al. is low in comparison to the 54% hydrogen content obtained by Acharya et al. [68] with pure steam gasification.

## 2.4 Oxygen enriched air and steam gasification

As seen before, steam addition to air gasification can, in some cases, increase the LHV of the syngas and the production of hydrogen. While increasing the LHV and quality of the syngas and the efficiency of the process, oxygen gasification can present a high reactivity and problematic temperature at high oxygen concentration. Combining steam and oxygen can allow the control of the reactivity of the process [69]. Huynh et al. used a bubbling bed to show that $H_2/CO$ ratio increases with $O_2/biomass$ ratio which is interesting considering this ratio is important for Fischer-Tropsch processes.

In 2012, Huynh et al. showed that steam can actually be used to control peak temperature and increase the hydrogen content [69]. They also propose to replace nitrogen by carbon dioxide considering it is easier to remove it into a cleaning process. Carbon dioxide could come from flue gases and be used as oxygen dilettante instead of steam with lower costs of production. The presence of carbon dioxide is opposite to steam, meaning that it influences the water gas shift reaction in the inverse direction, producing more carbon monoxide and decreasing the hydrogen content.

## 2.5 Syngas recycling

In 2011, a research team from Thailand [70] proposed a design (presented in Figure 2.5) where the air at the inlet of the pyrolysis zone is mixed with producer gas. This idea came from some observations of instability of the reactive front inside the pyrolysis zone.

In some experiments, Jaojaruek et al. reported that the pyrolysis zone moved down and merged with the oxidation zone leading to a one-stage gasifier operation conditions [70]. They compare the results of single stage, two stage and two stage with gas mixing gasification on a lab scale gasifier.

The power is approximately 25 $kW_{th}$ and the air ratios tested go from 0 (single stage) to 0.5 (same amount of air in each air injection). The advantage of the syngas injection is the ability to reduce the air ratio of the gasification therefore increasing the LHV. Their gasifier produces a gas with an HHV of 6500 kJ/Nm$^3$with a lowest tar content of 44 mg/Nm$^3$.

Table 2.1 summarises the different characteristics of the gasification technologies using alternative gasifying agents presented in this section.

| Gasifier | P $[kW_{th}]$ | CO [%] | $H_2$ [%] | $CH_4$ [%] | $CO_2$ [%] | LHV $[kJ/Nm^3]$ | HHV $[kJ/Nm^3]$ | Tar $[mg/Nm^3]$ | SGR $[kg/h.m^2]$ |
|---|---|---|---|---|---|---|---|---|---|
| Niu et al. [56] Oxygen | $< 1$ | 30 | 8 | 10 | 40 | 8200 | / | / | / |
| DTU [64] Air & steam | 75 | 16 | 33 | 2.5 | 20 | 6000 | / | / | 238 |
| Thaïland [66] Air & steam | 25 | 22 | 21 | 1.6 | 14 | / | 5200 | 90 | 47 |
| Thaïland [70] Air & syngas | 25 | 20 | 21 | 3 | 14 | / | 6500 | 90 | 47 |

***Table 2.1*** *– Performances comparison between different types of gasifying agents used in different gasifier technologies.*

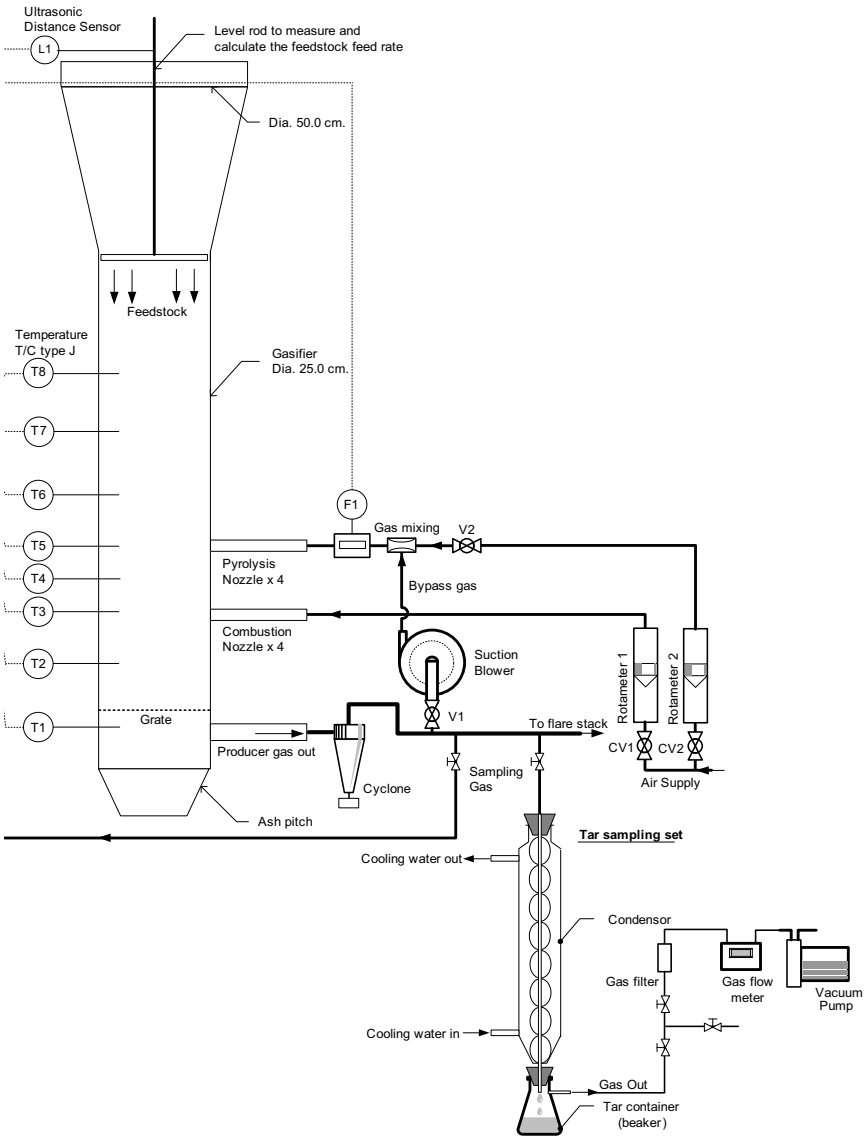


***Figure 2.5*** *– Schematic diagram of the gasifier developed by Jaojaruek et al.[70].*

## 2.6 Chapter summary

This chapter presented the interest for the use of alternative gasifying agent. The use of a gasifying agent different than air is often associated with increased investment and operational costs but the additional benefits can surpass the cost. For example, it allows the use of gasification for application where syngas from air-gasification does not meet the fuel requirements in terms of LHV. Research in this field still has a long way to go and seems promising when combining different agents as seen with oxygen enriched air gasification moderated with steam. The use of oxygen-enriched air is quiet simple to put in place and presents therefore a large interests for the scientific community. It will thus be investigated further in this thesis.

# Chapter 3

# Two-stage downdraft fixed bed gasification technology

Previous chapters presented state of the art technologies and applications of gasification with their advantages and disadvantages. This chapter presents the two-stage downdraft gasification technology developed by Xylowatt to address typical issues met in downdraft technologies. This design combines the advantages of the two-stage technologies developed by Battacharya et al. [36] and DTU [65] presented in the previous chapter.

The first section of this chapter describes the particularities introduced by the NOTAR® downdraft technology.

The second section of this chapter details the experimental setup installed at the Université catholique de Louvain and used for the experimental campaigns. It describes the reactor itself, its gas cleaning system and its instrumentation.

## 3.1 The NOTAR® technology

As seen in the introduction, the main drawback for downdraft technologies as for all gasification technologies is the tar content. As a reminder, downdraft gasification is by design the gasification process with the lowest tar content. The low tar content is due to the fact that the tars produced during pyrolysis

are forced to go through the high temperature oxidation zone were they are cracked and oxidised. The reduction bed after the oxidation zone also acts as a catalyst in the tar thermal cracking as observed on DTU gasifier [38].

Despite this design, the tar content still induces high investment and maintenance costs. These tars are due to several imperfections of the process: inhomogeneity of the oxidation zone, by-passes in the particles bed, or incomplete pyrolysis, to name a few.

The major source of tars is the inhomogeneity of the oxidation zone. In single-stage gasifiers, the oxidation zone is a porous medium. It increases the difficulty to obtain an homogeneous air distribution in this zone.

Moreover, as seen in the introduction, even with several injection points and a controlled blower for the air inlet, the porous medium injection forbid high power gasification plants for single-stage technologies. The power is linked to the diameter of the gasifier. Even if the range of specific gasification rates (SGR) found in literature and presented in the introduction is wide, a lot of them point to the same range of values (between 50 and 300 $[kg/m^2h]$). If the SGR is limited for a technology, increasing the power can thus only be made by increasing the diameter.

An increased diameter complexifies the air injection into porous medium leading to concepts with air injection at the center of the hearth, increasing costs of construction and making maintenance more difficult. Seynhaeve et al.[18] presented a numerical and experimental study to illustrate the complexity of porous medium injection with nozzles at the hearth of the reactor as illustrated in Figure 3.1. These concepts do not go further than the laboratory stage. In order to avoid costly injection systems, another solution is to inject air inside a gaseous zone.

Xylowatt developed a two-stage technology that avoided this porous medium air injection like in the "Viking" two-stage downdraft gasifier [38]. This technology is called the NOTAR® reactor and is illustrated in Figure 3.2. The idea is to decrease the tar content and develop a technology more suitable for higher power scale (up to 1 $MW_e$).

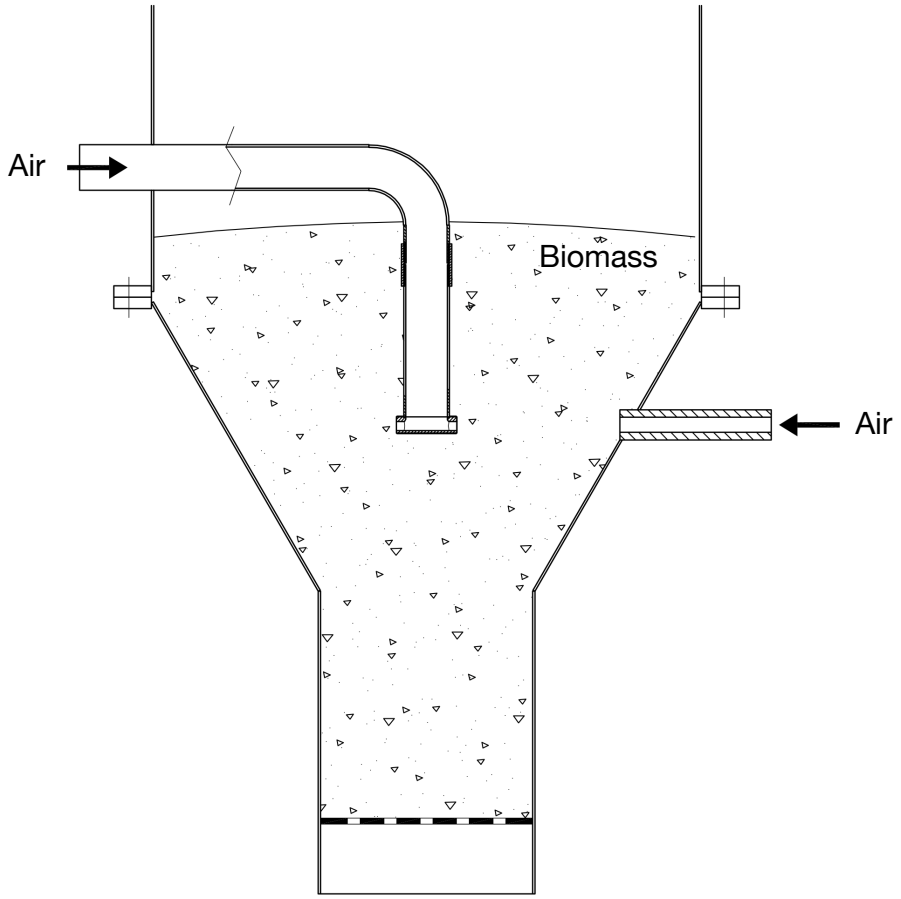


***Figure 3.1*** *– Illustration of one concept with additional air injection at the center of the reactor for high-power single-stage downdraft technology.*

The gasifier developed by Xylowatt presents a physical separation between the pyrolysis and the oxidation zones, freeing up some space in the biomass bed. This gaseous zone is where the oxidation occurs, replacing the injection of air into a porous medium by gaseous phase injection. It increases the homogeneity of the oxidation zone by offering a better mixing of the gases. This design improves the oxidation and cracking of the pyrolysis gases.

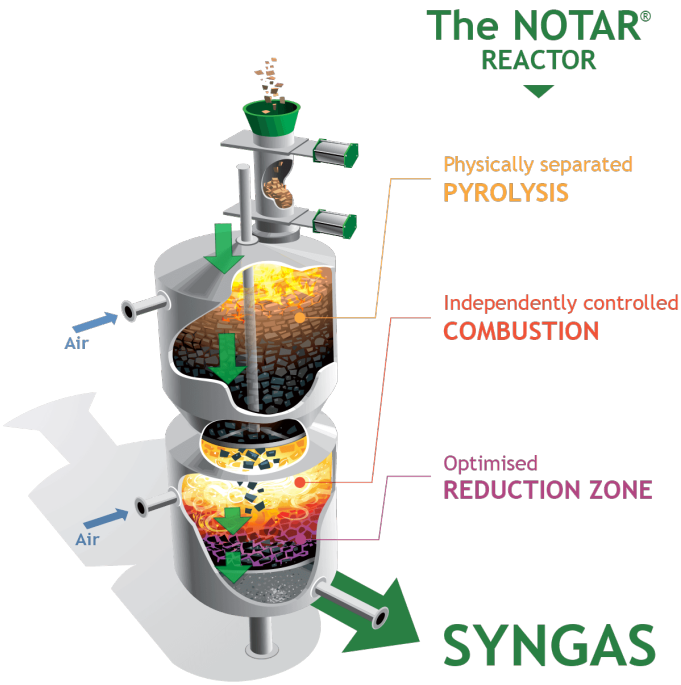


***Figure 3.2*** *– Illustration of the NOTAR® technology from Xylowatt.* (source: Xylowatt)

In Xylowatt's technology, the biomass particles fall freely through the oxidation zone thanks to gravity, leading to really small residence time at high temperature in the oxidising atmosphere. As a consequence, the char going out of the pyrolysis zone goes through this zone without reacting and keeps its reactivity for the reduction reactions. This small residence time is also an advantage when it comes to high ash content biomass that presents a low fusion point. In fact, when the char particles reach the reduction bed, they quickly cool down due to the highly endothermic reduction reactions occurring in the char bed. This small time in the high temperature oxidation zone forbids the inorganic matter inside the biomass particles to reach their melting point temperature.

Figure 3.3 illustrates the concept of the NOTAR®, it presents:

- the biomass and primary air inputs at the top of the reactor, above the particle bed,
- the physical separation between the pyrolysis and oxidation zone with a mechanism to transfer solid particles from the pyrolysis zone to the reduction bed,
- the secondary air input in the gaseous phase oxidation zone, above the reduction bed,
- the particles falling though the oxidation zone on the biomass bed,
- the ashes passing through the grid that supports the reduction bed.

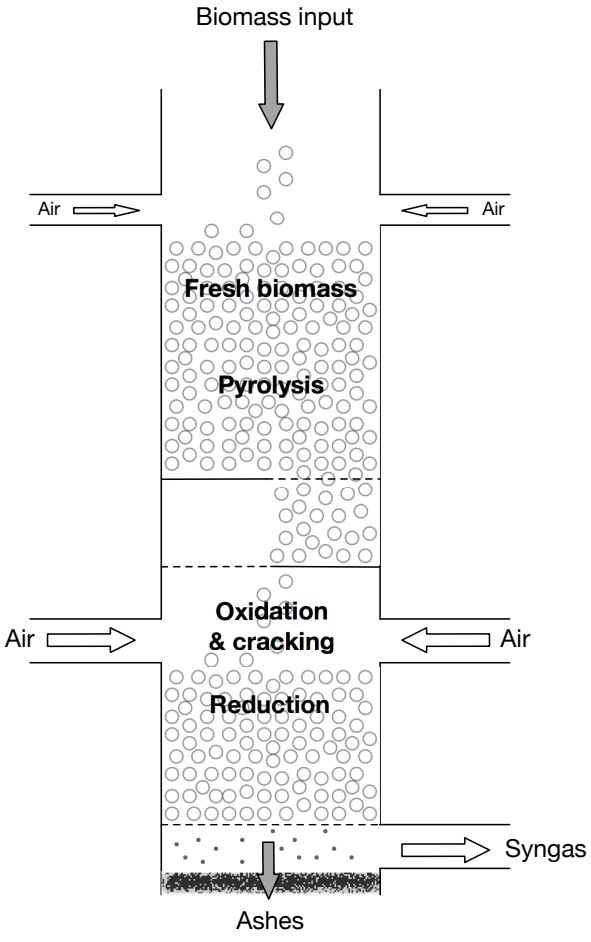


***Figure 3.3*** *– Illustration of the two-stage downdraft NOTAR® technology.*

The physical separation added to the gasifier modifies the approach of the first step of the process, i.e. the pyrolysis. In the Viking concept from DTU[38], the pyrolysis is realised thanks to a screw worm with external heating. This external heat can be taken, at least partially, on heat from engine flue gases or syngas at the outlet of the reactor. Unfortunately, the conductive heat transfer through the external walls of the screw worm limits the power of the gasifier. In the NOTAR® technology, the physical separation strongly reduces the heat transfer from the oxidation zone to the pyrolysis zone (main source of heat for the pyrolysis in single-stage technologies).

The heat required for the pyrolysis has to be transferred to the biomass particles by another mean. The choice is to have an internal production of heat by partial combustion of the pyrolysis gases thanks to a primary air injection as seen on some other two-stage gasifiers, for example the one used by Bhattacharya et al [36]. The heat is transferred by convective transfer from the gases to the biomass particles. This allow better scaling-up of the whole unit since the heat addition is evenly thoughout the whole section of the reactor. In the case of single-stage technologies, the distribution is uneven and in the case of the Viking, it is only made at the external wall with conductive heating, limiting the scaling-up potential of both technologies.

The modification of the heat source for the pyrolysis has the advantage that the temperature in this zone can be controlled independently with the primary air injection. The pyrolysis temperature is thus no longer depending on the air injected in the oxidation zone, hereby called the secondary air injection.

In a single-stage gasifier, the heat required for pyrolysis comes from the combustion mainly through conductive transfer through the biomass particles from the oxidation zone through the pyrolysis zone. The gas flow is going in the opposite direction (from pyrolysis to oxidation) forbidding a convective transfer between the two zones. As wood beds have a low heat conductivity [71], the conductive heat transfer is limited. The bed conductivity being fixed by physical properties, the only way to increase the heat transfer to the pyrolysis zone is to increase the temperature difference between the zones by increasing the oxidation zone temperature. An increase of the air flow injected in the oxidation zone allows to reach higher temperatures in this zone. The problem is that

this leads to an increase of the biomass consumption thus increasing the solid mass flow of the whole process. The speed of the solid particles is thus higher and this requires an even higher heat flux for the pyrolysis zone. Trying to solve the first problem creates a new one and the process operating conditions are not improved. In single stage technologies, the heat flux to the pyrolysis zone is thus directly dependent on the design parameters of the gasifier and the biomass properties without any possible adjustment. This means that the design parameters need to fit the characteristics of the biomass without flexibility. An independent control of the pyrolysis zone seen on two-stage technologies solves this problem. In two-stage technologies, if the biomass requires increased pyrolysis temperature in comparison to the reference biomass of the process, it can be adjusted without changing the geometry of the reactor by adapting the air ratio. It allows to control the heat flux, resulting in more flexibility on the feedstocks suitable for the gasifier.

The development of this technology introduced new parameters like, for example, the air ratio defining the distribution of air between the primary and the secondary injections or the bed heights determining the residence times in the different reactions. There was an interest to investigate these parameters and the need of a specific gasifier to investigate them. This is the reason the Test Gasification Plant (T.G.P.) was developed. It is described in the next section.

## 3.2 Test Gasification plant

The Test Gasification Plant is a complete gasification plant aimed at research on two-stage gasification. It can be considered as a complete plant since it includes all the parts of an industrial gasifier plant. These parts are the following:

- an automated biomass feeding system,
- a two-stage downdraft fixed bed gasifier,
- a gas cleaning and conditioning system,
- a gas engine and a flare.

Figure 3.4 presents a more detailed illustration of the components of the Test Gasification Plant including the ash container, the ash extraction worm drive,

the NOTAR® gasification reactor, the fine ashes collector, the condenser, the wet cyclone, the granular filter and the flare.

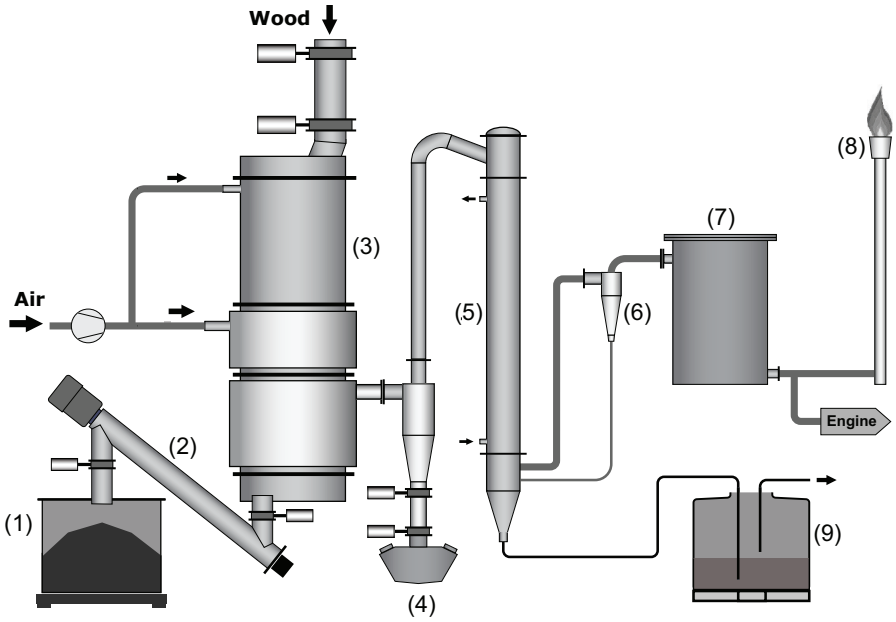


***Figure 3.4*** *– Illustration of the components of TGP. (1) Ash container, (2) Ash extraction worm drive, (3) NOTAR® gasification reactor, (4) Fine ashes collector, (5) Condenser, (6) Wet cyclone, (7) Granular filter and (8) Flare.*

The spatial arrangement of the reactor and the cleaning system of TGP is also illustrated thanks to a 3D visualisation in Figure 3.5.

The four different parts of the plant are described in the next subsections, starting with the core of the process: the gasification reactor itself. The gas conditioning unit or gas cleaning system are then detailed before ending the section with the presentation of the gas applications.

### 3.2.1 Gasification reactor

The gasifier is a scale down of Xylowatt NOTAR® gasifier with additional flexibility aimed at research. The reactor presents two physical zones and three reaction zones like a regular one, as presented in Figure 3.2. The difference is its ability to be modified. For example, the bed height in each physical zone can be easily adapted to study residence time influence on syngas quality.

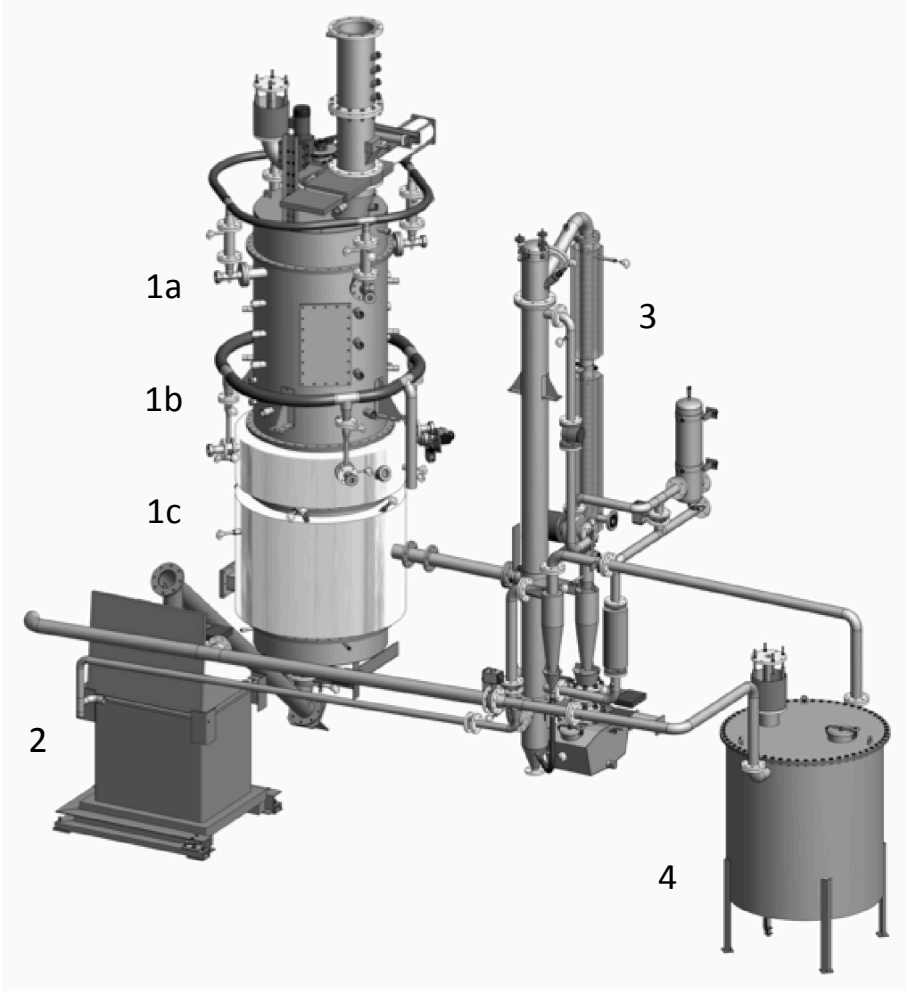


***Figure 3.5*** *– 3D view of the T.G.P., 1 - the gasification reactor (a-pyrolysis zone, b-oxidation zone & c-reduction zone), 2 - ash extraction system, 3 - gas conditioning unit and 4 - final filter.*

Another particularity is that the air injection in the pyrolysis zone (primary air injection) can be moved upward and downward to investigate the influence of porous medium or gaseous injection in this zone. The gasifier can also use other gasifying agents like oxygen enriched air with a complete oxygen piping independent from air distribution. It has also been designed to allow gas recirculation but this has not been implemented yet.

In this experimental setup, the inner diameter of the gasifier is constant along the whole height (no hearth required for two-stage gasifiers) and is 600 $[mm]$. The total height of the gasifier is approximately 3 $[m]$ and is as said before divided into 3 reaction zones. The height of a reaction zone determines the residence time of solid particles inside this zone once the power is fixed. The maximum power for air gasification is approximately 200 $[kW]$ on syngas LHV (normalised gas flow * syngas volume LHV) which puts it between the laboratory and industrial scales (approximately 900 $[kW]$ on syngas LHV for the smallest industrial models). The advantage is that the results obtained on the experimental pilot can be quickly translated into improvements on industrial gasifiers.

Figure 3.6 presents the dimensions of the different reaction zones. The height of the particle beds are regulated with level measurements and thus oscillate around an average position. The oxidation zone, which is defined on one side by the physical separation and on the other side by the reduction bed is thus not fixed either. Nevertheless, in this section, the theoretical level positions and bed sizes are considered when discussing the design of the reactor. The height of the pyrolysis zone can be modified from 525 to 1050 $[mm]$. This represents a residence time at nominal power (thus the smallest residence times) between 2700 and 5400 [s] or between 45 or 90 minutes. The maximal size of the bed is actually twice the one met on industrial gasifiers (2700 [s] of residence time in industrial applications). This flexible design allowed to investigate the influence of increased residence time on wood chips gasification in comparison to industrial gasifiers. It also allowed to test feedstocks requiring an increased residence time in the pyrolysis zone due to their physical properties (e.g. sewage sludge). The height of the oxidation zone is 550 $[mm]$. The reduction bed height is 950 $[mm]$ which is equivalent to a residence time of more than 5000 $[s]$ or 85 minutes.

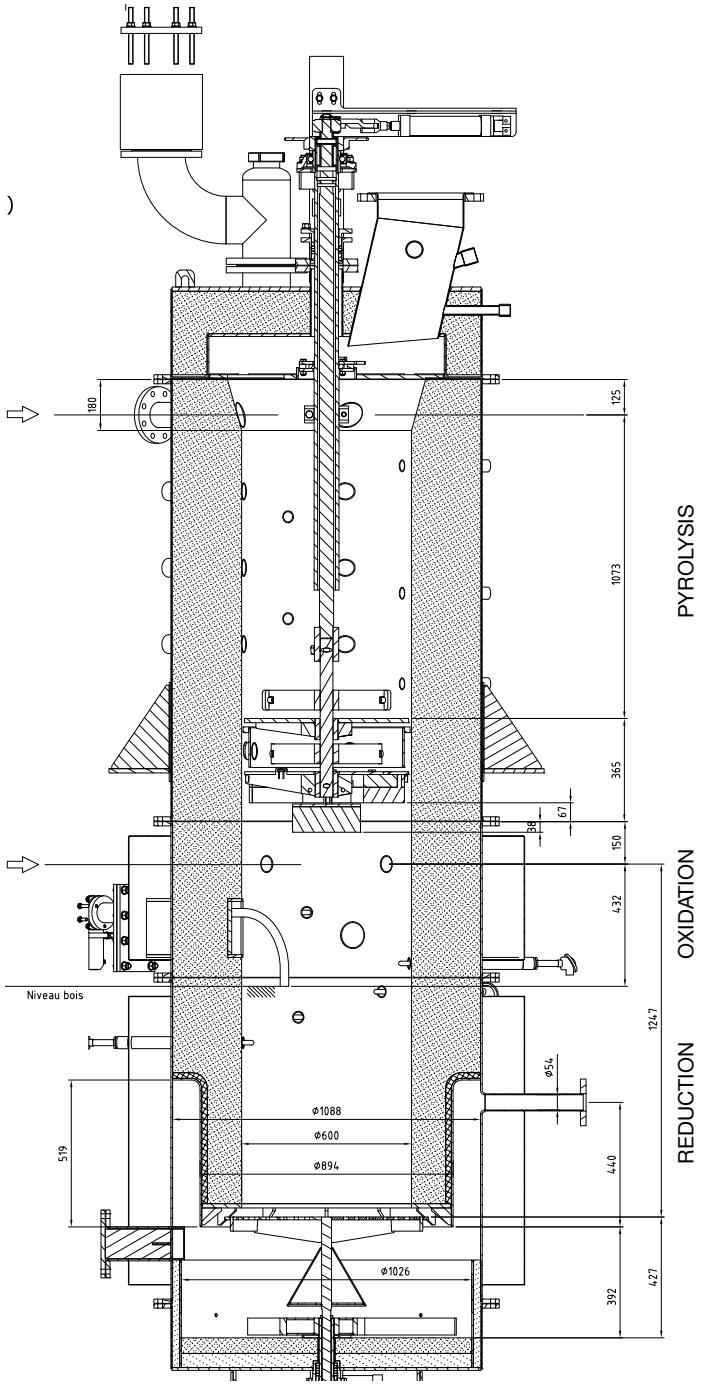


***Figure 3.6*** *– Dimensions of the different reactive zones of T.G.P.*

The gasifier has a great thermal inertia due to the fact that the concrete and insulation layers are the same as on industrial gasifier. The construction material are the same since the temperatures reached in each zone are the same and thus required the same insulation and mechanical properties. As it has significantly less power, the ratio between the concrete mass and the power of the gasifier is much worse on T.G.P. This is a disadvantage when it comes to starts and transient states as more time is needed to heat the concrete and insulation layer. It also presents an advantage at steady-state since it smoothes the variations in the process temperatures as the thermal inertia of the concrete plays the role of a thermal buffer. The temperature measurements are made close to the wall as the movements of solid particles forbid to place them at the center of the reactor (see Section 3.2.5). The gasifier is also equipped with pressure sensors to measure the pressure losses of the porous beds. It allows to monitor the clogging of the particle beds, a phenomenon that is common to downdraft technologies and occurs generally at the bottom of the reduction bed.

The flow of gas through the gasifier is ensured by a side channel vacuum pump from Becker International. It is controlled though a frequency converter and regulated on the air flow measurement. For safety reasons, the maximal pressure authorised on the experimental reactor is 0.4 $[barg]$. The air is then divided into two circuits to feed the primary injection loop and the secondary injection loop. Each loop distributes the air into four tuyeres. The ratio of air inside each loop is regulated thanks to two butterfly valves that are controlled by the operator in order to set the air ratio. The flows are influenced by the pressure drops of the reactive beds that are fluctuating constantly so it needs several adjustments per hour to maintain the chosen air ratio. On the pyrolysis zone, the air distribution loop and the tuyere are normally located above the biomass particle bed. This can be modified on T.G.P. in order to investigate the injection into porous medium for the pyrolysis zone. There are 4 potential positions for the primary air injection as presented in Figure 3.7. The secondary injection has only one potential position as there is no interest for porous medium injection in the oxidation zone.

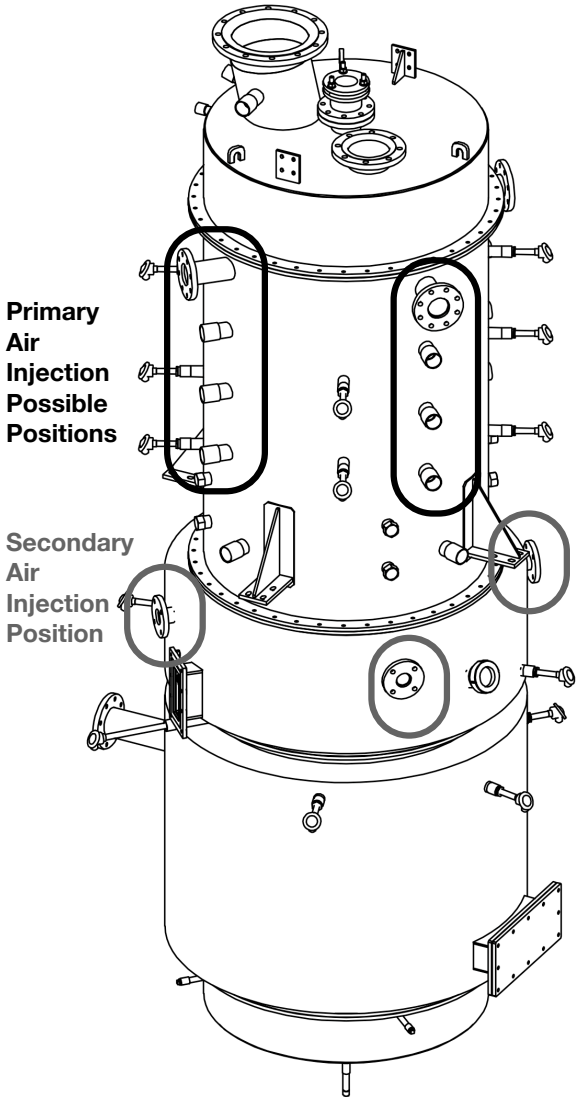


***Figure 3.7*** *– Illustration of the four possible positions for the primary air injection and the only position for the secondary air injection.*

### 3.2.2 Biomass feeding system and circulation

The gasifier is fed thanks to an automated screw worm of approximately 4 meters mounted at the bottom of a $2.5m^3$ hopper. This hopper offers from 7 to 12 hours of autonomy depending on the power regime of the gasifier. However, as the plant is only aimed at research it is generally only fuelled with $1m^3$ of biomass in order to monitor the biomass consumption more precisely. At the top of the screw worm, biomass falls into an airlock before entering the gasifier. As mentioned before, the air is pushed inside the gasifier using a blower, the pressure in the gasifier is always slightly above atmospheric pressure (maximum of 0.3 bar(g) at the exhaust of the blower). The airlock is there to avoid the release of pyrolysis gases (containing combustible and toxic gases) to the surroundings of the gasifier during the filling of the gasifier with biomass. This airlock forbids continuous feeding of biomass since it can only work by batches. It is constituted of two sliding gate valves that can never be open at the same time to avoid to open the reactor to the atmosphere.

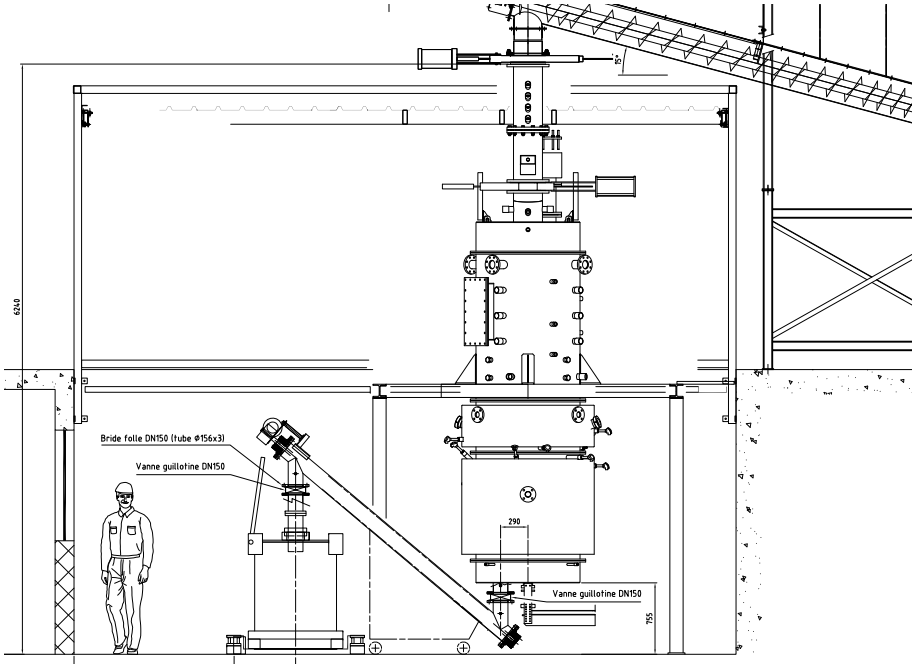


***Figure 3.8*** *– Schematics of the gasifier illustrating the gasification reactor with its biomass feeding system and the ash extraction system.*

As a matter of fact, the flow of gas is continuous while the flow of solid is discontinuous. As shown further in the experimental results, differences in the flows of gas and solids through the whole process leads to fluctuations in syngas composition. It is thus interesting to reduce the fluctuations in the solid flow as much as possible. After the airlock, the biomass thus enters the reactor through a first buffer zone aimed at reducing these discontinuities in the solid flow.

The flow of biomass in the gasifier is not controlled directly. The consumption of biomass depends of the air mass flow rate. The flow of biomass is thus not forced by the operator in order to respect a defined consumption, instead, it is imposed by the air settings. In order to achieve that and to maintain steady-state conditions in the gasifier, the level of the reacting beds of biomass are maintained as constants as possible. The top of the pyrolysis zone is located just after the airlock buffer and the end of the pyrolysis zone has a physical separation at the bottom of it, also acting as a buffer before the oxidation and reduction zone. The heights of the two beds are controlled independently as illustrated by Figure 3.9.

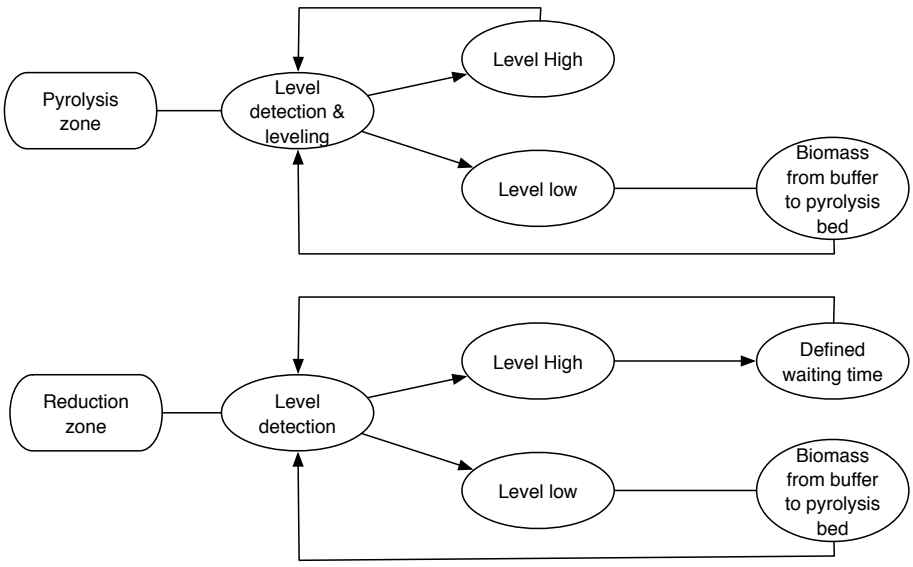


***Figure 3.9*** *– Brief illustration of the loops controlling the levels of the particle beds.*

The filling of the pyrolysis zone from the buffer is made on a quarter of the gasifier, making the filling and the bed level uneven. The top of the bed is thus equipped with a mechanical rake with 10 centimetre teeth that rotates around the axis of the reactor to equalise the bed level. This ensures that the top of the bed stays homogeneous and flat, thus reducing the risk of creating preferential paths inside the particle bed. The mechanical rake is also used to measure the bed level as the resistance is changing regarding the depth of the teeth inside the solid particle bed. The filling of the reduction bed from the pyrolysis is made thanks to a rotating mechanism that fills it on the whole surface of the bed, making it globally even and cancelling the need of an equaliser. The height of the bed is measured through a rotating sensor that can measure if the bed is high (first detection point), medium (second detection point) or low (no detection at all). In both zones, the measurement triggers the same output: if the level is below a certain value, biomass is injected into the reaction zone. This allows to reduce the fluctuations in the flows even if it does not cancel them as presented in the results.

The flow of biomass entering the gasifier is regulated through constant bed heights but there is still the problem of extraction of unconverted biomass at the bottom of the gasifier. As said before, the biomass flow is linked to the consumption but part of the biomass is not transformed into syngas in the process. This solid residue, often called ashes, is made of carbon that did not react and minerals or metals present in the biomass at the inlet. It has to be extracted in order to avoid accumulation in the reactor. This extraction is regulated on the pressure losses created by the reduction bed. The reduction bed lays on a grid. With the consumption of the biomass, the particles shrink and in a co-current gasifier, the flow of gas tends to push the bed downwards, creating a plug at the bottom of the gasifier, increasing the pressure drops created by the biomass bed. To maintain the gas flow, the blower increases the inlet pressure and the phenomenon worsens itself. In order to reduce the pressure drop created by the bed, the grid rotates quickly to create a movement of the bed that rearranges the particles inside the bed. The particles small enough to cross the grid fall down and the consequence of these actions is a decrease in the pressure drop. The grid is thus regulated on the pressure losses created by the reduction bed. The risk is that if the biomass conditioning (shape, density, size, dust content, drying process etc.) creates a high pressure drop, the extraction rate will in-

crease and will not respect the required residence time in the reduction zone for a good gasification. The conditioning of the biomass is thus critical for the process.

Finally, the ashes that fall through the grid are collected and evacuated through an airlock that has the same role as the inlet one. They are then conveyed through a screw worm to a sealed container that can contain approximately 40 hours of operations. The container can be changed during a test, the change takes less than 15 minutes and the bottom of the gasifier can accumulate ashes for more than two hours so there is no consequence for the quality of the steady-state of the process.

Those 4 regulation mechanisms (grid movement, reduction zone filling, pyrolysis zone filling and buffer zone filling) are independently controlled but they are obviously influencing each other. Figure 3.10 illustrates how one control loop influences the other. Rectangles represent evolution of the state of the gasifier, rounded corner rectangles represent a detection by a sensor and ovals represent actions. The solid lines represent consequences that follow an action and the dotted lines represent potential consequences that may or may not follow actions. For example, when the pyrolysis level is low, the filling of this zone starts, emptying the buffer zone located above it. If the detector in this zone reaches the low level position, it will start an airlock filling sequence, if not, the sequence is not started.

Figure 3.10 shows, for example, that the movement of the grid, activated to reduce the pressure losses inside the reduction bed, can trigger a chain reaction in all the other mechanisms. The grid movement can potentially bring the reduction bed level below its detection level, triggering the filling of this zone. The filling of the reduction zone decreases the height of the pyrolysis bed and can potentially bring it below the desired level, triggering the filling of this zone as a consequence. As said in the previous paragraph, this can trigger an airlock filling sequence. The link between the different loop of the filling sequence represents conditional actions that are triggered by a detection sensor. For example, when the grid movement is activated, the sensor level does not automatically detect the variation of level of the reduction bed so the reduction filling sequence may not activate after the grid movement sequence.

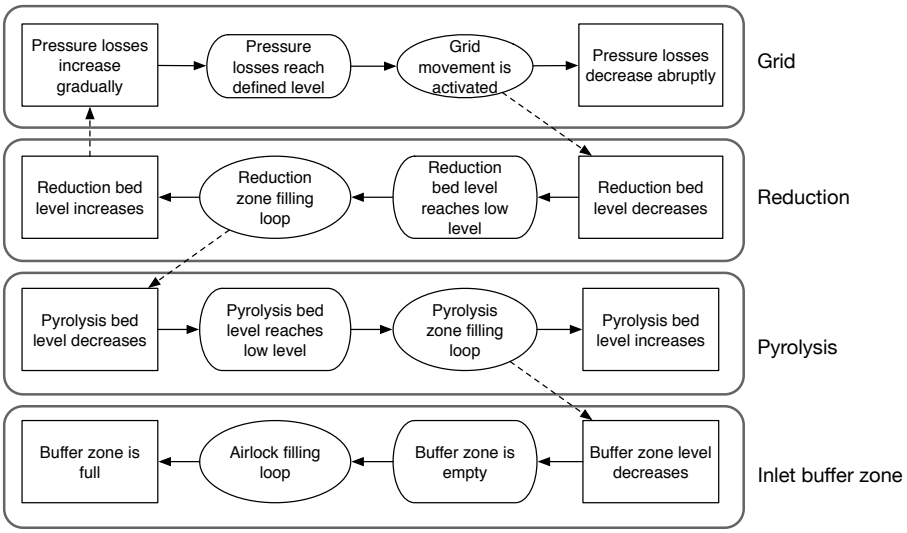


***Figure 3.10*** *– Illustration of the loops interactions. Solid lines represents certain consequences and dotted lines represent potential consequences.*

These potential consequences are represented by the dotted lines between the loops in Figure 3.10.

Another example is the grid sequence. The grid movement could result in a decrease of the height of the bed not large enough to bring the reduction bed to a low level. The rearrangement of the bed particles due to the grid movement (which is always the same) is random so the influence on the bed height cannot be predicted. The movement of particles during the filling of the reduction and pyrolysis zone are also random so the quantity of mass transferred during one filling sequence fluctuates. It is thus not possible to predict the number of filling sequences required to decrease the previous bed level to a low position. Moreover, the particles in the reduction bed are consumed by the reactions and the particles in the pyrolysis zone are going through a shrinking phenomenon due to their pyrolysis. All these factors justify that the loops have to be controlled independently.

### 3.2.3 Gas cleaning system

In order to use the gas into an IC engine, it needs to be cooled down (usually at least below 25 $[°C]$) to avoid knocking and to increase the volumetric efficiency.

During this cooling, tars condense and can cause clogging issues, they thus need to be removed. Traditionally, Xylowatt used a biodiesel cleaning system for its industrial applications. It allows a high heat exchange rate with a great tar removal efficiency. Some tar cleaning systems are well-known and very efficient (like the OLGA cleaning system from ECN [72]) but they come at a certain cost.

As the tar content decreased by a factor of approximately 50 with the NOTAR® technology, simpler (than on industrial gasifier and previous technology) cleaning system with reduced capital expenses was considered on the T.G.P. The aim was also to develop a cleaning system using water as a cooling agent to use in places were biodiesel is not widely available. The system chosen consists in a water injection into the gas to cool it very quickly with the heat required by the state transformation of evaporating water. The water is then condensed in a heat exchanger by water cooled itself by a small cooling fan outside the laboratory.

The cleaning system, presented in Figure 3.11 is composed of:

- a dust cyclone at the outlet of the reactor to remove fine ashes,
- a water injection followed by a venturi to saturate the syngas with water,
- an counter current heat exchanger with a water injection at the top to ensure that the walls of the heat exchanger are not dry in order to avoid tar accumulation on the walls,
- a second cyclone to remove droplets entrained by the flow,
- a final granular filter filled with wood sawdust to remove impurities that could still be present at this stage.

On industrial gasifiers, the gas is cooled down to temperature as low as 5 degrees Celsius so a chiller is also installed if industrial conditions need to be reproduced. The final cooling temperature, depending on the application required by the process can thus be between 5 (thanks to the chiller) and 35°C (depending on the outside atmospheric conditions). Tars are thus collected in the water at the bottom of the condenser. The water system works in a closed loop as water (containing tars) at the bottom of the condenser is cooled down and is re-injected at the top of the condenser. The excess water produced by condensation of steam in the syngas (from the drying and oxidation) at the outlet of the gasifier is evacuated to a decantation tank. This water has to be

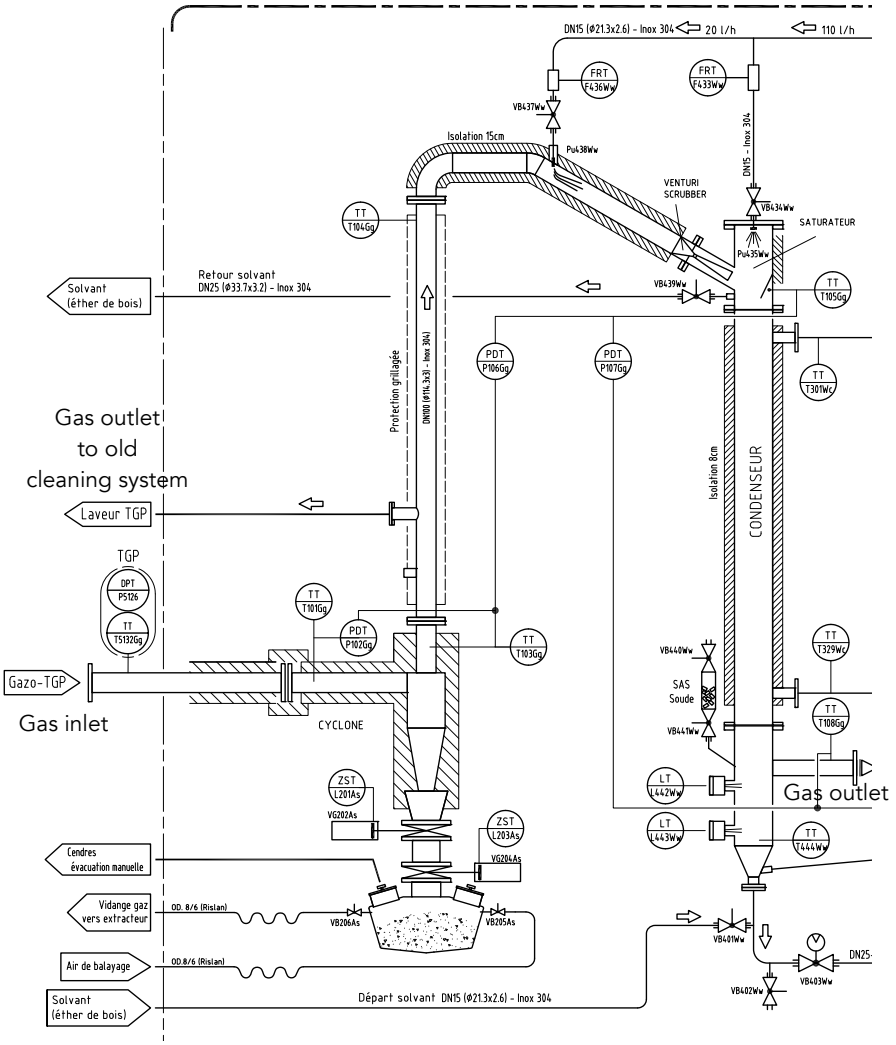


***Figure 3.11*** *– Schematics of the dust cyclone and gas condenser of the gas cleaning system.*

treated due to its tars and fine particles (solid particles entrained by the gas flow) contents. Depending on the feedstock, some other condensed pollutants like ammonia can be found in the water. Therefore, this type of cleaning system does not solve the treatment of pollutants, it displaces it in the water. The gas goes out of the heat exchanger saturated with water. A cyclone stands at the outlet of the condenser to remove the droplets that could potentially be entrained by gas flow or appear due to the saturation state of the gas.

The gas also contains some solid particles that need to be removed. These small particles, called fine ashes have the same origin as ashes but are small enough to be entrained by the gas flow. A major part of them is removed before the condenser at the outlet of the gasifier thanks to a dust cyclone. Finally, a cylindrical tank filled with wood sawdust acts as final filter before the use of the syngas in case the previous gas treatments did not remove all the impurities completely. This filter is placed at the end of the line to protect the engines connected to the gasifier in the event of a failure or of poor efficiency of the previous cleaning system elements.

### 3.2.4 Engines and flare

On TGP, depending on the focus of the research, the gas produced by the gasifier can be directed to 3 different types of applications. Syngas can either be burned in a flare if investigations only focus on gasification process or can be directed to two engine benches or a burner if investigations focus on the end-use of the syngas.

The flare is the most simple use as it is only aimed at burning the syngas in order to avoid pollutant emissions to the atmosphere. To ensure that the flare never shuts down, it is maintained with a premixed natural gas flame that is regulated with a temperature measurement and an igniter. The flare can be replaced by a gas burner. The connection to a burner can be useful to reproduce boiler conditions using TGP syngas. For example, it allowed to measure the flame temperature for glass industry applications.

There are two different benches where engines working with syngas can be tested. On the first bench there is one clean and cold gas supply, coming from

the outlet of the cleaning system. Two types of Diesel engines modified for syngas can be connected to this bench. The first engine is an industrial four cylinder Diesel engine from Greaves Cotton Limited with a displacement of 4.5 litres. It is modified to work with syngas as a spark ignition (SI) engine. The maximum electrical output of this engine is 40 $kWe$ when using the syngas from the experimental gasifier. This engine was the subject of a master's thesis in 2014 [73]. The second engine is a Diesel engine modified to work with vegetable oil. It is used to test co-firing of Diesel and syngas.

On the second bench, there are two syngas supplies, one similar to the first bench and the other one with hot uncleaned but filtered syngas for special applications. The second bench hosts an homogeneous charge compression ignition (HCCI) engine, an uncommon type of engine that could potentially use hot syngas from the outlet of the gasifier. The engine is still a prototype. This bench is the subject of the Ph. D. thesis of Subir Bhaduri [74] and a paper [75] on the use of unscrubbed biomass syngas produced using TGP during 36 hours.

### 3.2.5 Instrumentation

The gasifier is a pilot plant, meaning it stands between two scales: it is larger than usual lab scale equipment and it is smaller than industrial gasifiers. The number of parameters to control and measure is increased in comparison to a small scale laboratory experiment but the quantities to measure are smaller than at industrial scale. In order to characterise the NOTAR® process, the gasifier is equipped with a lot of sensors and sampling points. This subsection describes the instruments installed to acquire data on the gasifier. Specific instruments for the sampling of tar and char are described later in Section 5.1.

#### Temperature measurements

The gasifier is equipped with 11 thermocouples in the pyrolysis zone and 11 thermocouples in the oxidation and reduction zones. Their position is shown in Figure 3.12. The zone without thermocouples between the last one of the pyrolysis zone and the first one in the oxidation zone is the mechanism that allows to have a gaseous phase in this oxidation zone. Due to its presence it is more difficult to place temperature measurements in this zone.

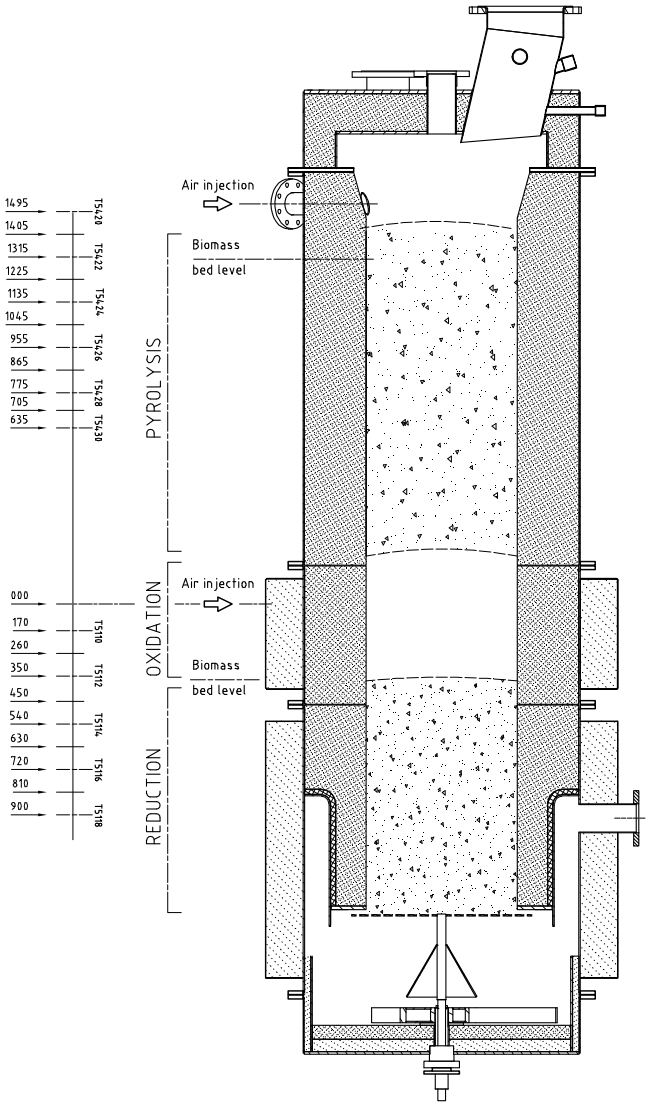


***Figure 3.12*** *– Schematics of the gasifier illustrating the location of the thermocouples.*

The 3 thermocouples in the oxidation zone are from Type 'R' with a range from 0 to 1600 [$°C$] to resist high temperature. The 19 other thermocouples are from Type 'K' with a range from 0 to 1100 [$°C$].

The thermocouples are placed at different heights but also at different positions within the gasifier as every thermocouple is shifted by approximately 90 degrees (depending on the position of other equipment e.g. level detectors, manhole, etc) in comparison to the previous and the next one. Figure 3.13 illustrates this shift in the placement of thermocouples. The placement of all the thermocouples draws a spiral form inside the gasifier. This allows to ensure that the gasifier temperature profile is distributed on the whole perimeter of the gasifier. Inhomogeneities can thus appear in the observed temperature profile as thermocouples are not aligned. The temperature profile measured is not truly the temperature profile to which one biomass solid particle is exposed. The first thermocouple will take the temperature on the north side on the gasifier while the third one will consider the south part of the gasifier. This can disturb the reader when looking at the data and need to be remembered when analysing the results obtained.

As there is no physical separation between the oxidation zone and the reduction bed, the thermocouples can either measure the oxidation zone temperature or the reduction bed temperature depending on the reduction bed height. As said before, the solid flow is discontinuous and the bed height varies during an experiment. Though the average position of the bed is fixed thanks to a height measurement that allows to control the flow of biomass. The typical setup places the top of the bed at the fourth thermocouple. This thermocouple is thus part of the time covered by char and the other part of the time in the gaseous oxidation zone. The thermocouple at the interface between the two zones thus shows great temperature variations and is generally not taken into account to calculate the mean temperature of reaction zones.

The thermocouples are placed inside the gasifier inside the biomass bed but near the concrete wall. At first, thermocouples were inserted 5 centimetres inside the bed but due to the biomass movement, they were bended against the concrete. The thermocouples are thus now approximately only 1 centimetre inside the reaction zones (as illustrated in Figure 3.14). The solid particle

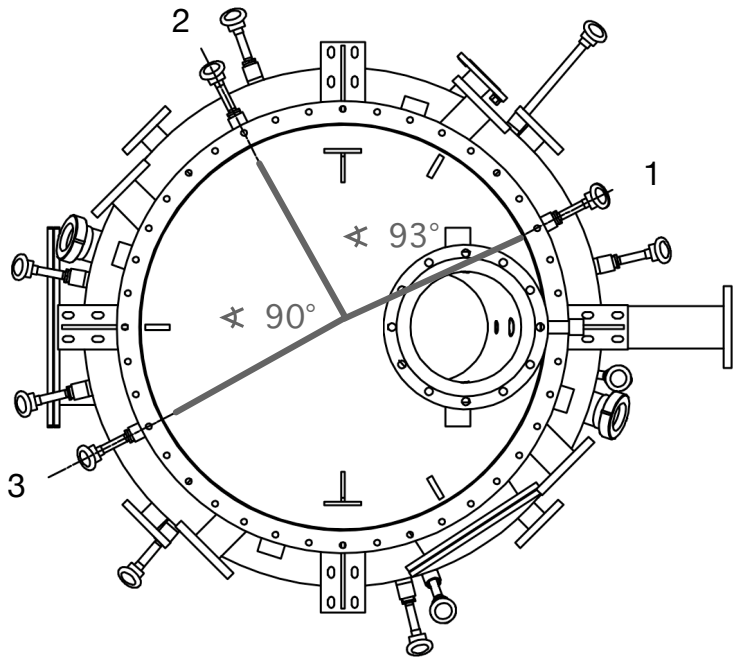


***Figure 3.13*** *– Illustration of the placement of three thermocouples of the pyrolysis zone, the angle between the second thermocouples and the previous one (1) is 93° while the angle between the second thermocouple and the third one is 90°.*

movements forbid to capture the profile between the center of the bed and the external layer without disturbing the biomass flow.

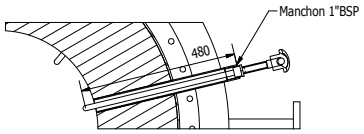


***Figure 3.14*** *– Schematics of the gasifier illustrating the location of the thermocouples.*

### Pressure measurements

The monitoring of the pressure drops inside the process is really important. They are used to control the ash extraction and to monitor the need of maintenance operations on the cleaning part of the process. The overall pressure of the process is also measured for safety reasons. The gasifier measures the differential pressure before and after:

- the blower
- the pyrolysis bed
- the reduction bed
- the dust cyclone
- the condenser
- the water cyclone
- the granular filter

The gas flows are also measured thanks to pressure drop measurements through orifices. The measurement of the air flow is accurate since the temperature of the inlet air is measured constantly and the moisture of the air in the room is measured several times during a run (and it does not vary greatly). The outlet gas flow measurement is more difficult as it requires the knowledge of the syngas composition at the moment of the measurement and this composition is constantly slightly fluctuating. The uncertainties implied by these measurements are discussed in details in the mass and energy balance section 4.1.

**Gas measurements**

As seen in the introduction, 99% of the outlet gas from natural wood gasification is composed by only 6 compounds. These components are, from the one with the highest content to the one with the smallest content: $N_2$, $CO$, $H_2$, $H_2O$ (its content depends on the moisture content of biomass and the operating conditions so its order can vary greatly), $CO_2$ and $CH_4$. In order to measure the quality of the process, it is thus critical to analyse the composition of the producer gas. The gas is always measured on a dry basis, meaning the water content is not measured directly and only calculated on the amount of water collected by accumulation in the condenser. The water content is thus not instantaneous and it is thus an average made on a minimum of 20 minutes of run translating into a poor quality of measurement. It means that does not capture the influence of small variations of the process that appear even at steady-state. Nevertheless, it is not critical for the process as the water is always condensed before the use of the syngas into an IC engine.

Three components, $CO$, $H_2$ and $CH_4$, are measured using an infrared on-line analyser system SIEMENS ULTRAMAT 23. $H_2$ is measured using an on-line analyser SIEMENS CALOMAT 62 which is a Thermal Conductivity Detector Analyser (TCD). It is based on the difference of thermal conductivity between the measured gas and a reference gas that is nitrogen. It is used to measure hydrogen concentration as its thermal conductivity differs significantly from other diatomic gases. As the producer gas contains other components than nitrogen and hydrogen, the measurement is influenced by the presence of other species. The measurement is thus corrected automatically with the data from the infrared analyser. Nitrogen is not measured and is considered as the rest. The ULTRAMAT 23 also measured oxygen to ensure that there is no more oxygen in the syngas for safety reasons. The oxygen measurement can also allow a measurement of the gas with air dilution if the maximum of the measurement range were to be reached. These two instruments are calibrated with two reference bottles presenting different compositions in order to adapt the calibration to the composition of the producer gas when using different gasifying agents.

### Tar measurements

There are two methods implemented on the experimental setup for the tar content measurement at the outlet of the gasifier. The first one is an homemade instrument using a cold filter and the second one is an application of the TAR PROTOCOL. The first method is a gravimetric method. It only measures the tar content but not their composition while the second method allows the measurement of the tar content and the tar composition. The second method is described in details in section 5.1.1.

The gravimetric method is quiet simple. Figure 3.15 presents an illustration of the gravimetric tar content instrumentation.

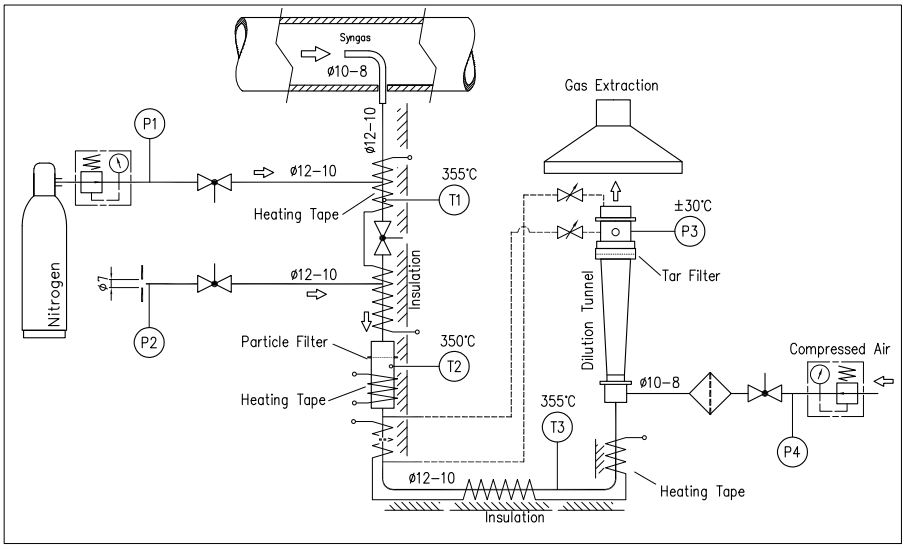


***Figure 3.15*** *– Schematics of the gravimetric tar content measurement setup presenting the sampling probe, the heated pipe and filter, the temperature set points and the most important part: the dilution tunnel at the end of witch is the tar filter.*

The gas is sampled through a probe at the exit of the gasifier and maintained at high temperature. It passes through a particle filter at more than 300 $[°C]$ and is quenched inside a dilution tunnel thanks to cold compressed air. The air is also used to control the gas flow thanks to an ejector design. The tars and water contained in the syngas then condense on the filter. The filter is weighted before the measurement and is then dried at 70 $[°C]$ to remove the water before being weighted again. The syngas flow going through the filter is also measured constantly during the experiment thanks to an orifice plate, allowing to calcu-

late the tar content in the syngas. The precision of the weighting machine used to weight the filter and the small amount of tars in the syngas requires a high measurement time (approximately 30 minutes) in order to accumulate enough tars on the filter. Another default of the measurement is that it does not allow to measure lighter tars such as benzene but they are not critical as they are considered unharmful for the engine.

Table 3.1 presents the results of a measurement realised by the CIRAD laboratory using the TAR PROTOCOL and measurements made by the gravimetric method with similar conditions. The composition is not measured in the case of the gravimetric method. The instruments could not be placed in parallel on the gasifier so the measurement are not simultaneous but there is a good agreement between the order of magnitude between the two measurements once the benzene -that cannot be taken into account by the gravimetric method- is deduced from the total of tar measured. All the tar measurements at the outlet of the gasifier presented in this thesis were made using the gravimetric method. The TAR PROTOCOL measurement method is only applied at the outlet of the pyrolysis.

| Compound | Gravimetric method $[mg/Nm^3]$ | TAR PROTOCOL $[mg/Nm^3]$ |
|---|---|---|
| Benzene | ND | 42.3 |
| Phenol | ND | 1.4 |
| Naphtalene | ND | 2.60 |
| Naphtalene-1-methyl | ND | 0.4 |
| Naphtalene-2-methyl | ND | 0.3 |
| Phenanthrene | ND | 0.6 |
| Anthracene | ND | 0.7 |
| Total | 5 to 8 | 48.34 |
| Total without benzene | 5 to 8 | 6.14 |

***Table 3.1*** *– Comparison between measurements made using the UCL gravimetric measurement and TAR PROTOCOL measurements made by the CIRAD laboratory on T.G.P. during tests on air gasification. Note that ND stands for not determined as the composition is not measured in the case of the gravimetric method.*

### 3.2.6 Uncertainty analysis

In order to assess the quality of the measurements made on T.G.P., an uncertainty analysis with a bottom-up approach is presented in this subsection. One of the main interest of the gasification process is its efficiency. It is thus important to characterise the energy inlets and outlets and the uncertainty around them in order to assess the quality of the efficiency measurement.

The main components analysed in order to evaluate the uncertainty on the efficiency are thus the following:

- Mass inlets and their energy
- Mass outlets and their energy

#### Inlets

The mass inlets are composed of wood and air. The energy inlets are of two types: sensible enthalpy of air and wood and LHV of wood. The chain of uncertainties leading to the calculation of the power input is shown in Figure 3.16.

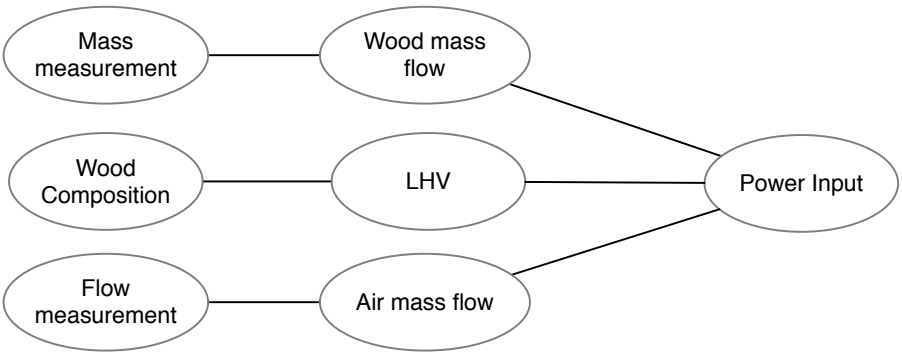


***Figure 3.16*** *– Chain of uncertainties on the power input.*

The inlet mass of wood is measured thanks to an electronic balance and is thus easy to assess. The weighting machine used to measure the mass of wood entering the reactor is composed of a SCAIME F60X bending beam load cell. Its error is given by the manufacturer as $\pm 0.008$ % of the nominal load which is here 300 kg. The uncertainty for such a rectangular distribution with an interval of confidence of 95% is thus given by: $U_{95,woodm} = \frac{2\ 0.008\ 300}{\sqrt{3}} = 2.7713\ [kg]$.

The average size of a load of wood is approximately 175 kg, giving a relative uncertainty on the mass of wood of around 1.58%.

The LHV is measured by the CIRAD laboratory according to the standard XP CEN/TS 14918 that limits the error to 300 J/g. The uncertainty in this case is thus given by: $U_{95,woodLHV} = \frac{2\ 300}{\sqrt{3}} = 346.41\ [J/g]$. Considering the LHV was measured at 16790 $[J/g]$, this gives a relative uncertainty of 2.06 %.

The combined uncertainty on the energy contained in a load of wood is thus:

$$\begin{aligned} U_{95,woodP} &= \sqrt{LHV_{wood}^2 * U_{95,woodm}^2 + M_{wood}^2 * U_{95,woodLHV}^2} \\ &= 76420\ [kJ] \end{aligned}$$

The relative uncertainty on the energy contained in a load of wood is thus given as 2.6 %.

The air mass flow is measured through an orifice using ISO5167 standard. The air inlet is divided in two before entering the gasifier between the primary and secondary injection. The flows are measured individually in order to control the flow injected in each reaction zone. The mass flows are calculated through two differential pressure sensors. The reference for the sensors is Endress+Hausser Deltabar PMD235-NN4A2EH1C. These pressure sensors have each been calibrated and tested on 12 points of measurements to evaluate their uncertainty. Both sensors show good accuracy and a global uncertainty of respectively 1.2 and 1 Pa for the primary and secondary air injections sensors. As their range is 0-1000Pa, the relative uncertainty are $u_{95,psensor1} = 0.12\%$ and $u_{95,psensor2} = 0.1\%$.

The uncertainty on the air flow is thus given by the standard ISO5167 as 0.76 % for the primary air flow measurement and 0.75 % for the secondary air flow measurement, giving us a global uncertainty on the air flow of 0.755 %.

Considering that the enthalpy of air at ambiant temperature is approximately 0.03 % of the energy at the inlet of the gasifier, the influence of the uncertainty on the energy content of air is negligible.

Table 3.2 presents a summary of uncertainties at the inlet of the gasifier.

| Measurement | Relative uncertainty |
|---|---|
| Wood Mass | 1.58 % |
| Wood LHV | 2.06 % |
| Inlet power on wood | 2.60 % |
| Air mass flow | 0.76 % |

***Table 3.2*** *– Uncertainty on quantities at the inlet of the gasifier.*

### Mass outlet

The total mass flow outlet is the sum of char, water and gas outlets. The energy outlets are of three types: sensible heat of syngas, char and water, latent heat of polluted water and LHV of syngas and char. The chain of uncertainties leading to the calculation of the power output is shown in Figure 3.17.

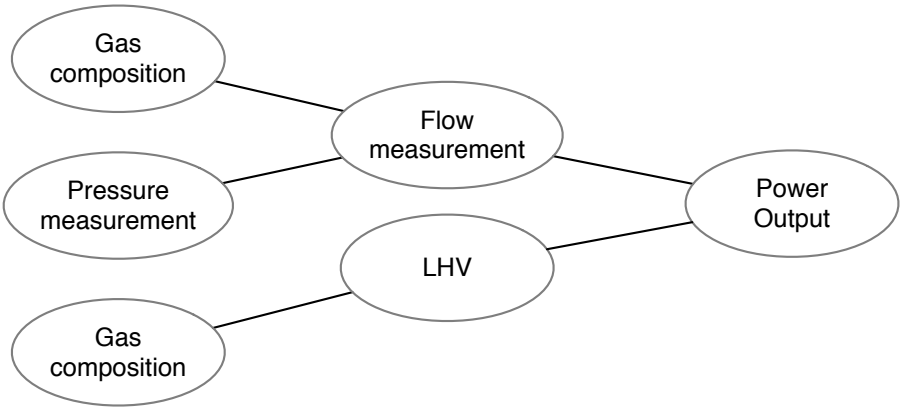


***Figure 3.17*** *– Chain of uncertainties on the power input.*

The char mass is constantly measured on a dedicated weighting machine installed beneath the char container. The weighting machine is homemade and composed of three SCAIME F60X bending beam load cells. Their errors are, as written before, given by the manufacturer as ±0.008 % of the nominal load. The nominal load of each sensor is here again 300 kg. The overall absolute uncertainty on the three sensors is thus calculated as 4.1569 kg or 1.39% for the relative uncertainty.

The LHV of the char is also measured by the CIRAD laboratory according to the standard XP CEN/TS 14918 that limits the error to 300 J/g. The uncertainty in this case is thus the same as for wood ans is given by: $U_{95,charLHV} = \frac{2\ 300}{\sqrt{3}} = 346.41\ [J/g]$. Considering that the LHV of char (30390 $[J/g]$) is higher than wood (16790 $[J/g]$), the relative uncertainty is thus smaller at 1.14 %.
The combined uncertainty on the energy contained in the char is thus:

$$\begin{aligned} U_{95,charP} &= \sqrt{LHV_{char}^2 * U_{95,charm}^2 + M_{char}^2 * U_{95,charLHV}^2} \\ &= 42219\ [kJ] \end{aligned}$$

The relative uncertainty on the energy contained in the char is thus given as 15.88 %. This uncertainty is important because the tare weight of the weighting machine is very big in comparison to the weighted mass as the container mass is three times larger than the mass of char it can contain.

The water mass is measured by batches every time the water collector is emptied. The balance has a precision of 0.05 kg and the mass of a batch is approximately 5 kg. The absolute uncertainty for a rectangular distribution is thus $U_{95,water} = 0.0577kg$ and the relative uncertainty is thus 1.15 %.

The gas flow is more difficult to measure as it combines the composition measurement to a orifice measurement, inducing more sources of uncertainty. The gas mass flow is measured through a orifice using ISO5167 standard. The mass flow is calculated through one differential pressure sensor which is also a Endress+Hausser Deltabar PMD235-NN4A2EH1C. This pressure sensor is calibrated and tested on 12 points of measurements to evaluate its uncertainty. The sensor shows a pretty good accuracy and a global uncertainty of 1 Pa . As its range is 0-1000Pa, the relative uncertainty are $u_{95,dpsensor} = 0.1\%$.

The gas composition is taken into account by the standard ISO5167 through the gas constant $R^* = \frac{R}{M_m}$. For air, the gas constant presents a normal distribution with an uncertainty $u_{95,air} = 1.14\ 10^{-4}$. In the case of syngas, the uncertainty of the gas composition is bigger than the uncertainty on the composition of air. The relative uncertainty on each gas analysed by the CALOMAT and ULTRAMAT analysers is calculated as follows $U_{95,gas\ i} = 1.15$ %. The combined

uncertainty on the gas constant is thus $u_{95,syngas} = 3.39\ 10^{-4}$. This should lead to a bigger uncertainty on the measurement of the flow as the uncertainty on air gas constant is just $u_{95,air} = 1.14\ 10^{-4}$. Nevertheless, the section of the pipes where the syngas flow is measured is bigger than the section of the pipes where the air flow is measured. As the absolute uncertainty on the geometry of the pipes is the same, the relative uncertainty on the diameter is lower and the overall uncertainty is globally better for the syngas measurement at 0.73 %.

Table 3.3 presents a summary of uncertainties at the outlet of the gasifier.

| Measurement | Relative uncertainty |
|---|---|
| Char Mass | 1.39 % |
| Char LHV | 1.14 % |
| Outlet power on char | 15.88 % |
| Syngas mass flow | 0.73 % |

***Table 3.3*** *– Uncertainty on quantities at the outlet of the gasifier.*

In the next chapters, all the figures present raw data measurements without error bars. The uncertainty analysis is thus there to give a global overview of the uncertainty of measurement but for readability reasons, they will not be presented further in the figures presenting experimental data. The curves are also often not filtered in order to reflect the time variations induced by the flow discontinuities of the process.

## 3.3 Chapter summary

The technology presented in this chapter has several advantages: a low tar content in the syngas, a small residence time at high temperature for solid particles (decreasing the risk of clinkers formation) and the production of a syngas with a relatively high LHV (in comparison to other gasification technologies). These good performances are due to the implementation of the two-stage air injection and the core of the technology: the gaseous phase oxidation zone. The chapters also presented the experimental setup which is a scale-down of industrial installation well instrumented in order to be able to investigate the operating conditions and performances more precisely. The next chapter presents the results of the investigation lead on this experimental installation.

# Chapter 4

# Experimental investigations of gasification

The investigations carried out on the experimental installation (T.G.P.) can be divided into two categories.
The first category concerns investigations on the technology in the conditions it was designed for. These studies are run with natural wood and serve as reference for other tests. The studies are focused on the parameters introduced by the new two-stage concept. .
The second category concerns investigations aimed at widening the range of possibilities of the technology. They are aimed at the use of alternative gasifying agents or alternative fuels. They study the influence of such changes on the performances of the process in comparison to air gasification of natural wood.

These two types of experiments are described in the two last sections of this chapter. The first section describes mass and energy balances (M&EB) made on continuous operation for long periods of time (more than 24 hours) in order to characterise the experimental tool that is T.G.P. before starting comparative campaigns.

## 4.1 Mass and Energy balances

Balances realised to measure the inputs and the outputs of mass and energy (more precisely enthalpy) are presented in this section in order to characterise

the gasifier and to be able to compare its performance with state of the art technologies. In those balances the gasifier is considered as a black box with several entries (biomass and air) and exits (syngas and char) as illustrated in Figure 4.1.

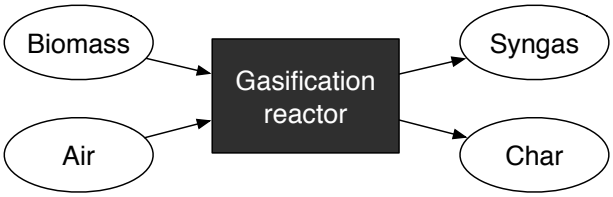


***Figure 4.1*** *– The M&EB only consider inputs and outputs of the gasification reactor.*

The mass balances consist of two different types of balances as the mass can be measured globally and then taken species by species $(C, H, O, N)$. It thus contains a second important information on the conversion of the different species, for example, the carbon conversion pathways are really important.

In total, three types of mass and energy balances are detailed in this section but before the description of those balances, the need for tests on long periods of time (more than 24 hours) needs to be explained. The interest for a long time experiment is justified by several factors:

- the thermal inertia of the T.G.P. ;
- the discontinuous solid flows ;
- the potential mass accumulation inside the gasifier.

Those three factors are detailed in the next paragraphs.

**Startup and steady-state**

The T.G.P. reactor high thermal inertia is due to the fact that its insulation and concrete layers are the same as in an industrial gasifier as described in section 3.2. The T.G.P. thus requires several hours of heating (from 5 to 10 hours depending on the startup conditions) before reaching steady-state. Due to unsteady conditions, the data collected through this transitory state is not relevant and is not taken into account for the balances.

The gasifier has 3 phases of ignition before stabilisation to steady-state. The first phase is the ignition of the pyrolysis zone, achieved thanks to a hot air injection directly inside the porous bed. The second phase (which can be simultaneous to the first phase) is the ignition of the reduction bed thanks to a hot air ignition above the char bed. At first it acts as a combustion bed since there is not enough pyrolysis gases and no combustion gases to realise a reduction. The third phase is the gas phase ignition when there is sufficient hot pyrolysis gases and hot air to ignite a flame in the oxidation zone. Those three phases can be observed on the gas composition presented in Figure 4.2 for what can be described as a "hot" start. [1]

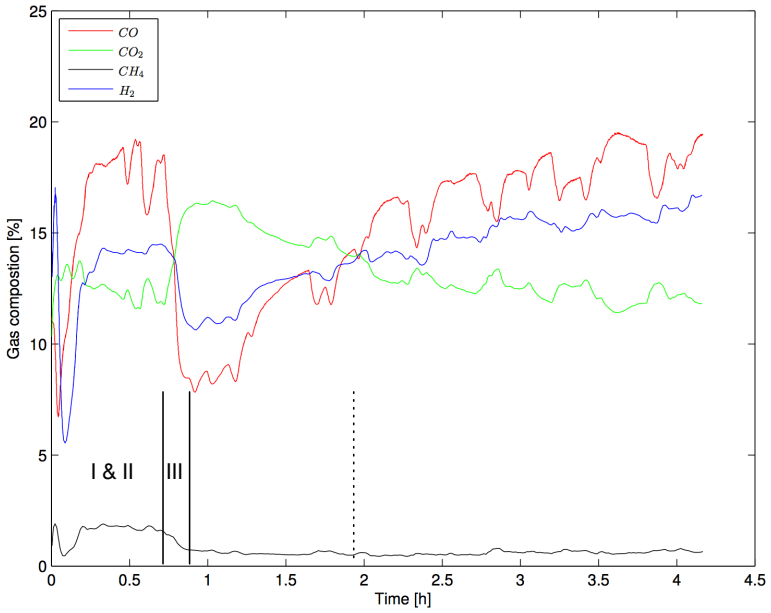


***Figure 4.2*** *– Gas composition ($\%mol_{dry\ basis}$) during ignition of T.G.P. for hot start showing ignition phases I, II and III. It also presents the transition from combustion to gasification at the dotted line.*

At first, the gasifier acts as a very poor burner, producing between 10 to 15$\%_{vol}$ of carbon monoxide due to the lack of oxygen. This could seem a gas potentially interesting but it contains a lot of tars. The ignition of the oxidation zone is characterised by a fall in the carbon monoxide content and an increase in the carbon dioxide content. These trend changes are due to the fact that the combustion quality is increasing in the oxidation zone.

[1] The gasifier ran the day before so it did not cool down to room temperature and the startup phase is thus reduced.

After these three phases, the reactor is transitioning from combustion to gasification. The conversion efficiency is really low at the start of this phase and is slowly increasing. The gasifier needs several hours to reach steady-state. This time is even more important if the particle beds need to be renewed (e.g. to test a different type of biomass) but this will not be discussed further in the present work. The long time required to reach steady-state is again due to the thermal inertia. The other factor justifying the required heating time is the heating power available. As the reduction reactions are highly endothermic, when the reactors starts gasifying, the power available for heating decreases drastically, increasing the heating time. Another important point observed during this transition to steady-state is the moment when the carbon monoxide content surpasses the carbon dioxide content. At this point, the gasifier is considered to gasify more than to burn the biomass (after around 2 hours in Figure 4.2).

The advantage of the thermal inertia is that it damps the variations in the process, resulting in a more stable process. The inconvenient is that it requires more time to observe trends change in the operating conditions. This inconvenient also pleads for longer runs.

Figure 4.3 shows the gas composition for a long run when the gasifier is at steady-state. The grey areas are excluded from the data as they do not represent steady-state, they are left in the figure to illustrate the transition phases of the gasifier.

The large variations in Figure 4.3, observed after the 18th and 21st hours, are linked to variations in the air inlet flows. Those variations are presented in Figure 4.4. They are induced by pressure drop variations in the reduction bed. As explained in subsection 3.2.2, the reduction bed porosity reduces during the test and pressure losses increase. The grid maintaining the bed is thus periodically rotated to modify the bed arrangement and create new pathways, resulting in a sudden decrease of the reduction bed overall pressure drop. The smaller variations, occurring at a higher frequency, are caused by the movement of the biomass particles from one reactive zone towards another. These variations are the reason why the curve is not smooth because they occur several times per hour (depending on the power inlet).

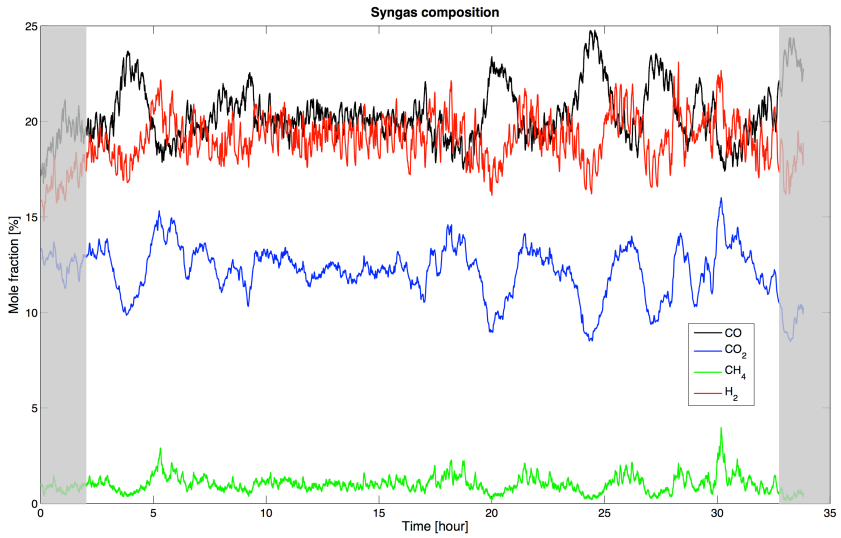


***Figure 4.3*** *– Gas composition ($\%mol_{dry\ basis}$) during steady-state of T.G.P.*

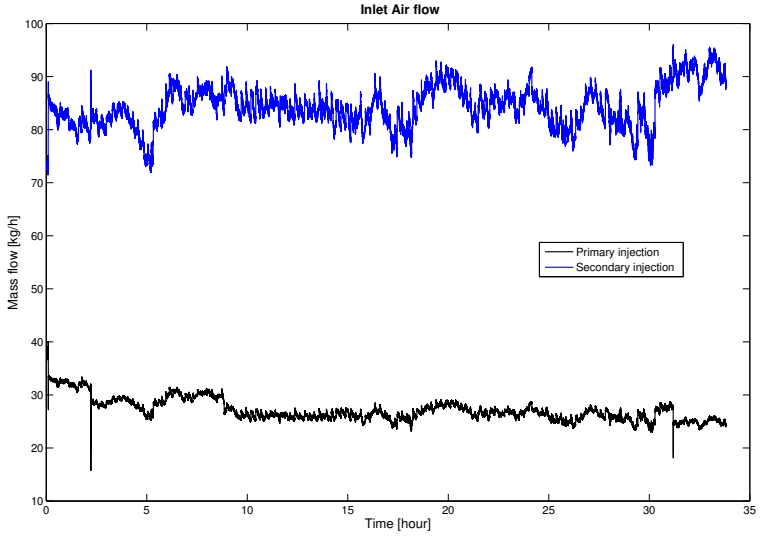


***Figure 4.4*** *– Gas composition ($\%mol_{dry\ basis}$) during steady-state of T.G.P.*

### Solid flows

The solid flows inside the gasifier are not continuous and difficult to measure. They can only be measured at the inlet and the outlet. The feeding of the gasifier is, as described in chapter 3.2, made through an airlock. The biomass input airlock is located between the hopper and the pyrolysis zone and allows the transfer of wood from atmospheric conditions to reactor conditions. This airlock is filled with biomass to a level measured with a level detector. Its regulation is thus volumetric but it cannot be used to measure the biomass flow as the bulk density of biomass inside the airlock varies from one filling to the other.

The inlet mass is thus measured before filling the hopper with a scale made with a bending beam load cell. The smallest achievable measurement of solid flows is thus the size of the load inside the hopper. The mass inside the hopper can be divided by the number of airlocks realised with one load to get an estimation of the mass inside one airlock. One airlock filled with biomass is consumed within 15 to 45 minutes depending on the selected power of the gasifier and the type of biomass (e.g. its moisture content, its density).

On T.G.P., due to the pilot scale, the considered masses are significant and a normal hopper load of wood is consumed in four hours. The time required for an analysis of the solid flows is thus much longer than for the gases flows that can be measured online every second.

### Mass inside the gasifier

The mass balance starts from the evolution of the mass in an open system:

$$\frac{dM}{dt} = \sum_i \dot{m}_i \ ,$$

where $M$ is the mass inside the system and $\dot{m}_i$ are the mass fluxes at the input and output. Indeed, the amount of mass inside the gasifier at any moment is unknown. Several components of the gasifier can accumulate small quantities of solid mass, e.g. the ash collector at the bottom of the gasifier. This accumulation effect aims to allow them to act as buffers and reduce the discontinuities caused by the solid flow.

The consequence is that the mass conservation is not respected at a given time, it can be expressed as:

$$\sum_{i,inlet} \dot{m}_i(t) \neq \sum_{j,outlet} \dot{m}_j(t) \ .$$

The difference between these two terms is oscillating around zero. If A is defined as the amount of mass that could be accumulated in the buffer zones of the gasifier, the sum of the differences between the inlet and outlet mass fluxes for a given period of time should be between $[-A; A]$. However, considering a longer period of time increases the total amount of mass taken into account and allows to limit the impact of the accumulation ability of the gasifier as the relative difference between the inlet and outlet mass will decrease.

The fluxes can be continuous mass fluxes like the air supply or discrete mass exchange like the biomass supply. On T.G.P., some instantaneous values are impossible to measure and some kind of averaging is thus required to estimate the evolution of the mass:

$$\Delta M = \int_{t_0}^{t_f} \frac{dM}{dt} dt = \int_{t_0}^{t_f} \sum_i \dot{m}_i dt \ .$$

Here, some definition must be introduced to simplify the notation. An average value over the whole run duration is defined by

$$\overline{x} = \frac{1}{t_f - t_0} \int_{t_0}^{t_f} x(t) dt = \frac{1}{\Delta t} \int_{t_0}^{t_f} x(t) dt \ .$$

The instantaneous value is thus the sum of the average and of a fluctuating part,

$$x(t) = \overline{x} + x'(t) \ ,$$

with the properties that the average of the fluctuating part is zero ($\overline{x'(t)} = 0$). Given these definitions, the mass balance can be written:

$$\Delta M = \sum_i \overline{\dot{m}_i} \Delta t \quad \text{or} \quad \frac{\Delta M}{\Delta t} = \sum_i \overline{\dot{m}_i} \ .$$

This equation illustrates the fact that the impact of the mass variations in the system decreases with the running time. It also points out that a systematic error (on the right hand of the equation) of measurement increases with the

running time, leading to incoherent balances. As the mass variation inside the system is known from the initial and final masses, the mass balance cannot be applied instantaneously but only to average values.

This concludes the explanation of the long duration tests to realise good mass and energy balances. The next subsections then describe the way the mass and energy balances are developed on T.G.P. before presenting the experimental results obtained during the test campaigns.

### 4.1.1 Mass balance

The basic idea of a mass balance is pretty straightforward: the mass measured at the inlet of the gasifier is put in balance with the mass measured at the outlet for a determined period and those amounts should logically be equal. The practical application of the M&EB is much more complex as many quantities are only approximately known or even not measured. For example, the amount of water contained by the biomass is measured on a biomass sample and estimated for the whole biomass consumed by the gasifier.

For two-stage gasification, the inlets are biomass and air (or another gasifying agent) and the outlets are carbon rich ashes (simply called ashes) and syngas, containing water and impurities (tars and solid particles called fine ashes). The mass fluxes are presented in Figure 4.5.

The mass flux balance can be written as:

$$\dot{m}_{biomass} + \dot{m}_{air} = \dot{m}_{ashes} + \dot{m}_{syngas}.$$

This subsection starts by detailing the inlet and outlet mass fluxes of the gasification reactor. It then presents in details the results of one $M\&EB$ test and summarises the results of three long durations tests.

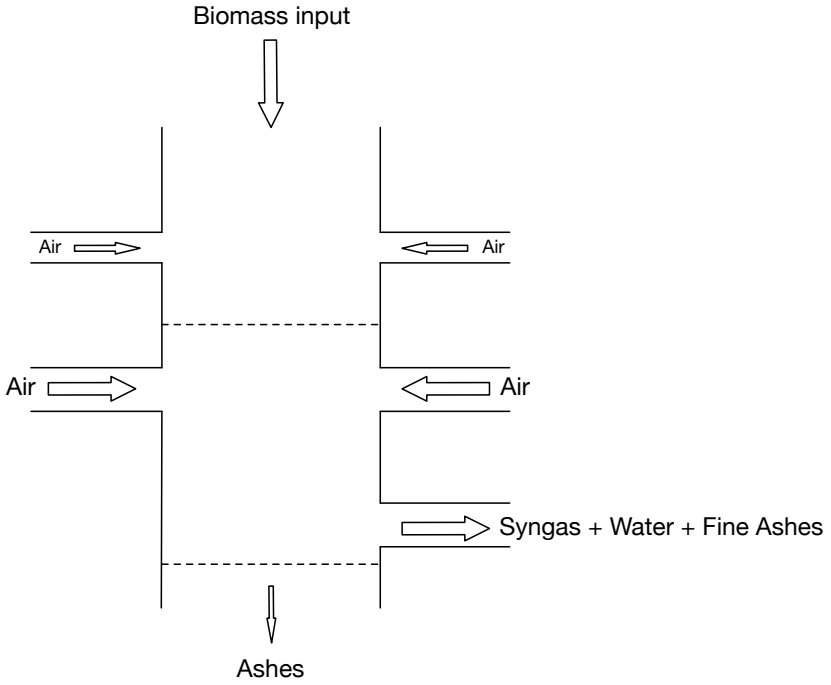


***Figure 4.5*** *– Illustration of the mass fluxes of the gasification reactor.*

**Biomass**

The biomass entering the gasifier is weighed before filling the hopper. The time measurement starts with the first airlock filling (see subsection 3.2.2 for details on feeding system). The time measurement stops when the hopper and the airlock are empty again. The consumption of the airlock is based on the measurement of the level of the pyrolysis bed, hence the uncertainty on the level measurement leads to potential time measurement discrepancy. Again, the importance of this error decreases with the test duration.

The biomass used for the characterisation tests is natural wood chips. The wood chips are dried below 10% moisture in order to increase the efficiency of the process.

In order to be able to make a mass balance element by element (called elemental balance), proximate and ultimate analyses of the wood used during these tests are performed. The results of this analysis are presented in Table 4.1.

The wood used can be defined by the formula $CH_{1.45}O_{0.66}$ which is typical for natural wood.

| Proximate analysis | | Ultimate analysis | |
|---|---|---|---|
| Moisture content(% Wet basis) | 7.50 | Carbon content(% Dry basis) | 49.10 |
| Ash content(% Dry basis) | 1.30 | Hydrogen content(% Dry basis) | 5.94 |
| Volatile matter content(% Dry basis) | 81.80 | Nitrogen content(% Dry basis) | 0.25 |

***Table 4.1*** *– Proximate and ultimate analyses of wood chips.*

The proximate and ultimate analyses are performed according to the XP CEN/TS 15104 and the ASTM D 5373 standards on solid biofuels and char. The elemental analysis uses combustion to oxidise the sample into simple combustion products easier to measure. The oxygen content is thus not mentioned as it is constitutes the rest of the components on dry basis. Oxygen content can thus be calculated as: $O_{\%} = 100 - C_{\%} - H_{\%} - N_{\%} - Ash_{\%}$.

**Air**

As written in the chapter 3.2.6, the air flow is measured with a orifice flow meter according to the ISO-5167 standard. The moisture content is measured several times during the run and, as its variations are low, an average value is considered for the whole test. The composition of dry air is not measured and is taken as standard (typical mixture of air and nitrogen). The temperature and pressure of the inlet air are measured every second.

**Syngas**

The syngas output can be divided into three components: dry syngas, water and impurities (fine ashes and tars). The dry syngas is measured with a orifice flowmeter using the composition given by the SIEMENS CALOMAT and ULTRAMAT described in section 3.2.5. The piping to the gas analysis instruments induces a time delay between the temperature and pressure measurement that is difficult to measure precisely. The bad synchronisation between the gas composition, the temperature and pressure measurements can lead to significant discrepancies on the orifice flowmeter. In order to get more accurate results, an assumption on nitrogen balance is made to verify the syngas flow. The assumptions are that the nitrogen from air does not react inside the process and

that the nitrogen content of the wood can be neglected. The flow of nitrogen is thus considered as constant and the rest of the flow is calculated thanks to the gas composition measurement.

The water content in the syngas at the outlet of the gasification reactor is estimated thanks to the water collected at the bottom of the condenser. The level of the water at the bottom of the condenser is kept between two levels. When water reaches the highest level sensor, the water is evacuated till the level reaches the lowest level sensor. Water is collected in a weighted container and the time between the two sensor signals is registered by the data acquisition software in order to calculate the flow of condensed water. The time of collection (between two levels of the sensors) is around 30 minutes.

The water collected is polluted with tars and fine ashes. This water is not analysed and the tars and ashes contents are roughly assimilated to pure water in the mass balance. Moreover, tars have been measured several times on the gasifier and are below 50 $[mg/Nm^3]$ and can be neglected. At the outlet of the condenser, the syngas is still saturated with water. The temperature of the syngas is measured and the water content of saturated syngas is estimated and added to the condensed water.

The fine ashes are collected at the bottom of the dust cyclone. Their production is so limited that intermediate measurements are not relevant. The measurement is thus only made once at the end of the tests and the total amount is added to the total mass balance. Table 4.2 presents the results of the proximate and ultimate analyses of fine ashes. The ultimate analysis shows that these fine ashes are mainly composed of carbon and mineral matter (oxygen and hydrogen are presents in small quantities).

| Proximate analysis | | Ultimate analysis | |
|---|---|---|---|
| Moisture content(% Wet basis) | 8.30 | Carbon content(% Dry basis) | 60.80 |
| Ash content(% Dry basis) | 31.20 | Hydrogen content(% Dry basis) | 0.60 |
| Volatile matter content(% Dry basis) | 3.40 | Nitrogen content(% Dry basis) | 0.52 |

***Table 4.2*** *– Proximate and ultimate analyses of fine ashes.*

### Ashes

The ashes are collected at the bottom of the gasifier. They are evacuated by a worm drive that is built to play the role of an airlock. The ashes are then stored in a weighted container. The sequence of the screw worm fills the container every 5 -10 minutes (the timers that control the sequence can be adjusted). The extraction is thus discontinuous and should thus be considered on long periods of time in order to avoid error from the buffer capacity of the ash collector at the bottom of the reactor.

Table 4.3 presents the results of the elemental and immediate analysis of ashes. The elemental analysis shows that the ashes are mainly made of carbon and mineral matter with a significant amount of oxygen (around 12%).

| Proximate analysis | | Ultimate analysis | |
|---|---|---|---|
| Moisture content(% Wet basis) | 2.40 | Carbon content(% Dry basis) | 36.20 |
| Ash content(% Dry basis) | 52.1 | Hydrogen content(% Dry basis) | 0.25 |
| Volatile matter content(% Dry basis) | 2.50 | Nitrogen content(% Dry basis) | 0.31 |

***Table 4.3*** *– Proximate and ultimate analyses of ashes.*

### Operating conditions

Three long duration tests are presented in this section. The reference test is detailed to illustrate the $M\&EB$ procedures and they are all summarised at the end of this subsection.

The first test is made at medium power ($\pm 160$ $[kW]$ on syngas LHV) with an average value for the air ratio of $\alpha = 0.38$. The second test is also made at medium power ($\pm 170$ $[kW]$ on syngas LHV) with a reduced air ratio of $\alpha = 0.23$. The higher air ratio generally reduces the tar content in the syngas but induces a reduction of the stability of the process. This second test is used as the reference test. The third test is made at high power ($\pm 220$ $[kW]$ on syngas LHV) with an air ratio close to the reference test at $\alpha = 0.25$.

### Results

This subsection presents the results obtained during the long duration reference test. The overall test took approximately 36 hours but the mass and energy balances started after the heating and ended before the shut down of the gasifier.

Figure 4.6 presents the gas composition at the outlet of the reactor during the reference mass and energy balance of the experimental setup. It shows great stability considering the scale of time observed.

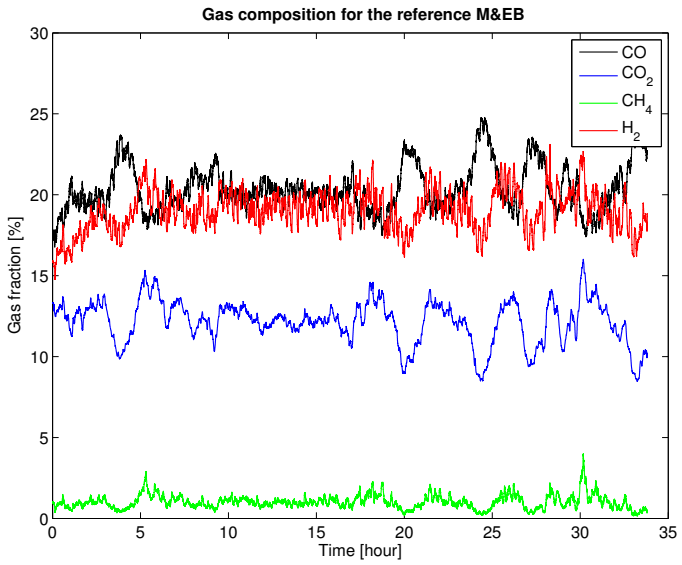


***Figure 4.6*** *– Gas composition ($\%mol_{dry\ basis}$) during the reference M&EB of T.G.P.*

Figure 4.7 presents time-zooms on the gas composition presented in Figure 4.6 to illustrate that the variations in the composition are lower when observed on smaller time scale even for the period that presents the biggest oscillations (on the right graph). The left graph presents a typical steady-state gas composition.

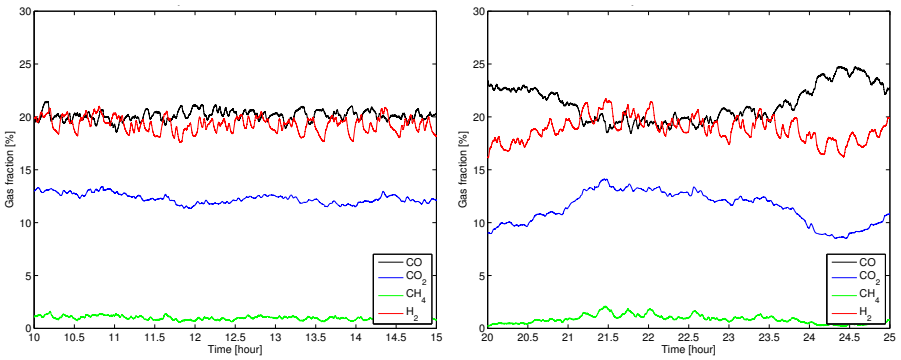


***Figure 4.7*** *– Zoom on the gas composition for specific periods of the reference M&EB of T.G.P. showing a great stability on the left and oscillations on the right.*

Another good indicator of the stability of the process during the reference mass and energy balance is the temperature in the different reaction zones. It is presented in Figure 4.8. The temperature in the pyrolysis and oxidation zone seems to reach stability faster because the heat available for wall heating is reduced in the reduction zone so it only stabilises after more than 5 hours of run. This temperature is a near wall temperature and does not reflect the fact that the process is at steady-state since the second hour of test.

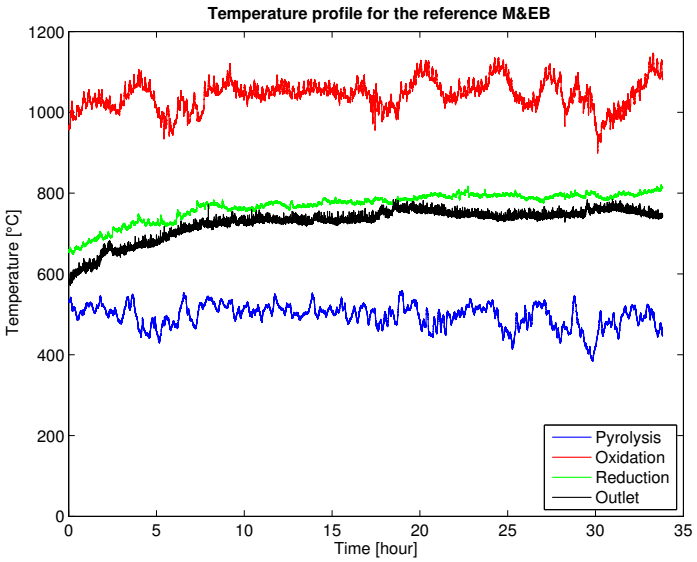


***Figure 4.8*** *– Temperature profile during the reference M&EB of T.G.P.*

Once the stability of the process is established, mass balance can be analysed. As a reminder, the total mass of flows in and out of the reactor during a test can be detailed as:

$$\begin{aligned} m_{in} &= m_{biomass} + m_{air}, \\ m_{out} &= m_{syngas} + m_{ashes} + m_{fine\ ashes} + m_{polluted\ water}. \end{aligned}$$

The total inlet and outlet mass are summarised in Table 4.4. The value of 2.8% referred as error in Table 4.4 is the relative difference between the mass measured at the inlet and the mass measured at the outlet. It can be considered as accurate regarding the uncertainty analysis presented in section 3.2.6 and the size of the installation. The difference in the mass measurements is positive, meaning that some outlet mass is unaccounted or some inlet mass is overestimated. The uncertainty on measurements has already been discussed. Nevertheless, it is interesting to note that the whole test bench presents leaks that cannot be measured or accurately quantified. It represent the only mass loss of the system and this should not influence the balance (there is a leak detection test at the beginning of each day to ensure a sufficient sealing level) but it could justify the assumption that the measured outlet mass is smaller than the inlet mass. The global accuracy is considered as sufficient to evaluate the global performances of the NOTAR® gasification process.

| Mass In [kg] | Mass Out [kg] | Error [%] |
|---|---|---|
| 3427.68 | 3331.82 | 2.80 |

***Table 4.4*** *– Mass balance.*

Figures 4.9a and 4.9b present the distribution of mass for inlet and outlet flows. It is interesting to note that the gasifying agent, air in this case, represent nearly two thirds of the inlet mass while biomass only accounts for a third.

It is also interesting to observe that syngas represents 93% of the outlet mass and that the fine ashes mass can, as said before, be neglected. The total mass of ashes is 3%, meaning that approximately 8.5% of biomass is not converted into syngas. This is due to the fact that in opposition to updraft gasifier, downdraft

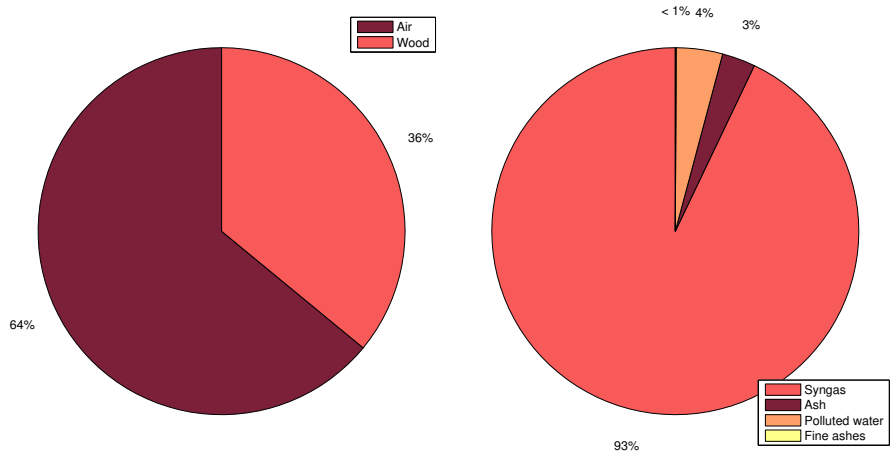


***(a)*** *Inlet* ***(b)*** *Outlet*

***Figure 4.9*** *– Mass distribution.*

gasifiers have difficulties to reach a high carbon conversion ratio. The reactions occurring in the reduction bed are highly endothermic so the temperature of the bed decreases quickly after the oxidation zone and the char at the bottom of the bed is thus in a lower temperature reactive zone. Moreover, the carbon found in this zone is less reactive as the highly reactive carbon already reacted in the high temperature zone. This phenomenon forbids the production of white ashes (without carbon) in downdraft gasifiers.

Table 4.5 presents the elemental balance. The outlet flow of syngas is corrected through the nitrogen balance. As the syngas measurement is difficult, it is adjusted so that the amount of nitrogen in the air is found at the outlet in the syngas. The error on nitrogen should thus be equal to zero but it presents a negligible difference that comes from the small amount of nitrogen inside the biomass. It is not taken into account for the gaseous nitrogen balance assumption. The nitrogen from biomass probably reacts though the process into ammonia that is not measured on T.G.P. due to its low content. Moreover, it condenses with water during the cleaning treatment. The discrepancies on the other compounds may come from uncertainties on the gas and tar compositions. The gas composition presents a measurement uncertainty discussed in section 3.2.6 and neglects heavier hydrocarbon compounds such as ethane, butane or aromatic compounds like benzene or toluene.

| | Mass In [kg] | Mass Out [kg] | Error [%] |
|---|---|---|---|
| Carbon | 560.45 | 509.16 | 9.15 |
| Hydrogen | 80.34 | 74.14 | 7.72 |
| Oxygen | 1101.42 | 1066.69 | 3.15 |
| Nitrogen | 1670.62 | 1666.61 | 0.24 |

***Table 4.5*** *– Elemental balance.*

Measuring the composition more precisely (i.e. measure more compounds) would decrease the nitrogen content and, as the flow is calculated on nitrogen balance, increase the syngas flow. This shall also reduce the difference on the total mass balance. It shall be noted that hydrogen content presents more variations and is thus more difficult to quantify precisely, also increasing the uncertainties. The composition of polluted water and the tars it contains does not have a significant influence on the mass balance due to the low tar content of the water collected.

Figures 4.10a and 4.10b present the distribution of carbon for inlet and outlet flows.

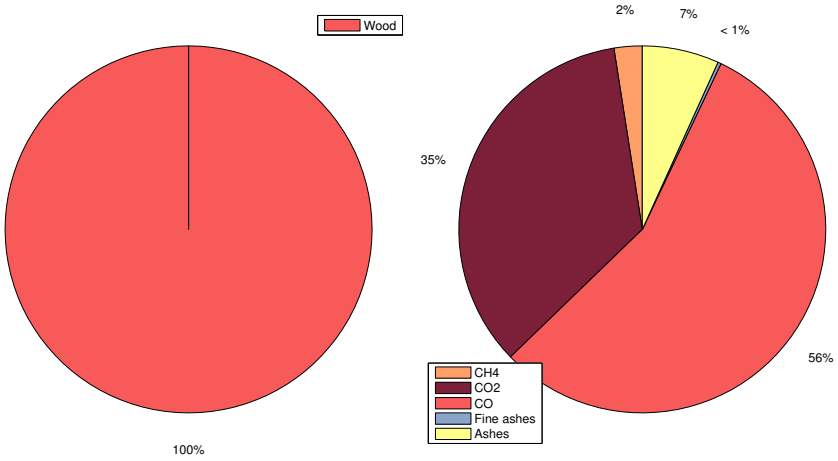


***(a)*** *Inlet* ***(b)*** *Outlet*

***Figure 4.10*** *– Carbon distribution.*

The carbon is logically only found in the biomass at the inlet as shown in Figure 4.10a. At the outlet, it is interesting to note that approximately 7% of the total mass of carbon is not converted into syngas and stays in the ashes as

shown in Figure 4.10b. As the carbon in the ashes presents a high LHV, its presence has even more effect on the energy balance that it has on the mass balance that will be discussed in the next section on energy balance.

Figure 4.11a presents the hydrogen content at the inlet. The hydrogen mainly comes from the dry wood as the wood chips are dried below 10% of moisture content. The moisture content of the inlet air has a limited influence on the hydrogen balance as it only represents 3% of the hydrogen mass while the moisture content of the wood occupies a significant part with 13% of the total hydrogen inlet mass.

Figure 4.11b shows the importance of the water content of the syngas. The water content of the syngas at the outlet of the reactor is collected at two point, the condensed water polluted with tars and the moisture content of the gas after the condenser. These two together represent nearly 30% of the total mass of hydrogen at the outlet of the gasifier. This means that approximately 15% of the hydrogen contained in the dry wood is not converted into fuel.

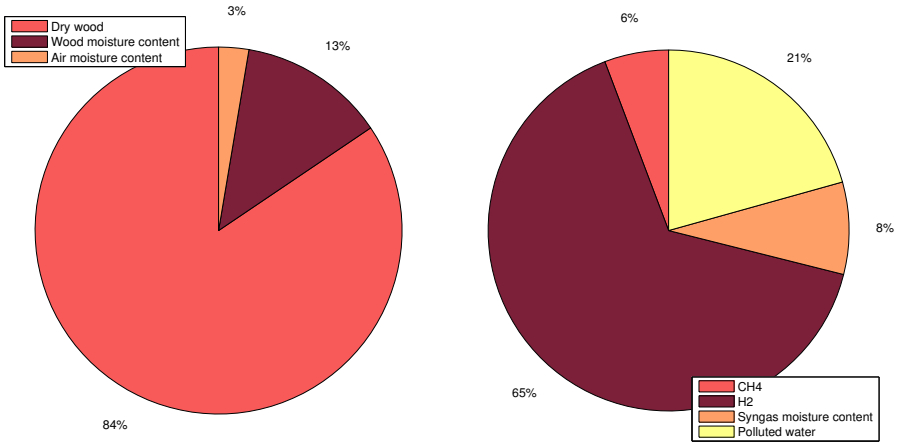


*(a) Inlet* *(b) Outlet*

***Figure 4.11** – Hydrogen distribution.*

Figure 4.12a presents the oxygen distribution at the inlet. It is interesting to note that the amount of oxygen contained in the wood chips is equivalent to the one in the air at respectively 45% and 46% of the total inlet mass of oxygen.

The moisture content of the air has again a low influence while the moisture content of the wood has again a significant part of the mass of the oxygen at 7%.

Figure 4.12b shows that the importance of the water content of syngas is smaller than for the hydrogen balance. The two compounds together totalise only 17% of the total mass of oxygen at the outlet of the gasifier.

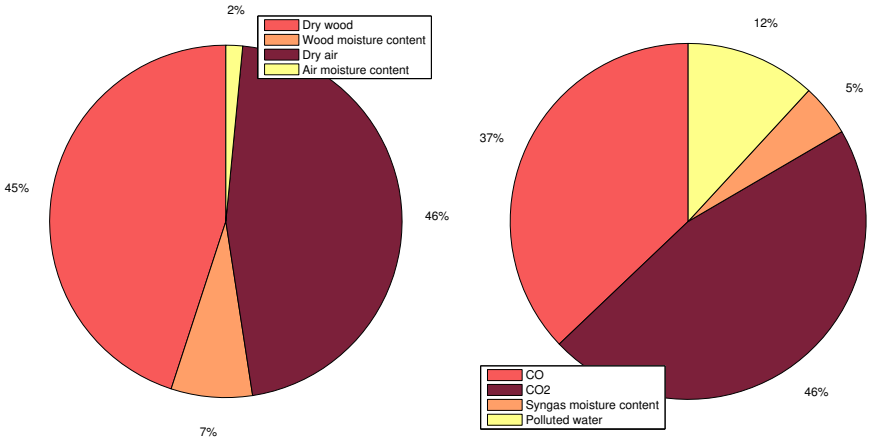


*(a) Inlet* *(b) Outlet*

***Figure 4.12** – Oxygen distribution.*

The nitrogen distribution is not presented as the amount of nitrogen found in the wood is neglected, it only comes from air at the inlet. The nitrogen content in the ashes and fine ashes is so low that it is rounded to zero. The nitrogen is thus only found in the syngas at the outlet.

### 4.1.2 Energy balance

The same method used to realise the mass balance of the gasification reactor can be applied to the energy balance. The inlet and outlet flows of mass are the same but the calculation of their energy input needs to be defined. Moreover, the gasifier also exchanges heat with the atmosphere and this exchange represents an additional flux to consider as illustrated in Figure 4.13.

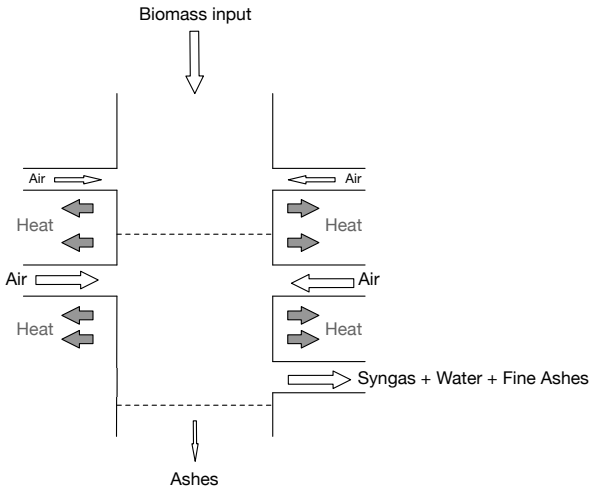


***Figure 4.13*** *– Illustration of the energy fluxes of the gasification reactor.*

The energy fluxes can be defined in a similar way as the mass balance by:

$$\dot{E}_{biomass} + \dot{E}_{air} = \dot{E}_{char} + \dot{E}_{syngas} + \dot{E}_{wall\ losses}.$$

This subsection details the energy fluxes of the gasification reactor.

**Biomass**

The energy from the biomass entering the gasifier can be divided into two categories: sensible enthalpy and formation enthalpy. It is defined as:

$$\dot{E}_{biomass} = c_{p,biomass}\ (T_{biomass} - T_{ref}) + LHV_{biomass},$$

where $LHV_{biomass}$ is the Lower Heating Value of the biomass (measured by CIRAD Laboratory cfr. Appendix A).

It can also be calculated with the HHV estimation based on the elemental analysis with the formula given by Reed [30]:

$$HHV_{biomass} = 34.1C + 132.2H - 1.53A - 12.0(O + N) \quad [kJ/g],$$

where C, H, A, O and N are the weight fractions of carbon, hydrogen, ash, oxygen and nitrogen in the fuel. The LHV is calculated by subtracting the heat of

evaporation of the water from the $HHV$: $LHV = HHV - 2500\ \frac{y}{2}\ \frac{M_{m,H_2O}}{M_{m,biomass}}$, where y comes frome the $CH_yO_x$ formula.

The LHV of the wood chips, as measured by CIRAD laboratory, is: $LVH_{wood} = 16790\ [kJ/kg]$ on wet basis or $LVH_{wood} = 18000\ [kJ/kg]$ on dry basis.

**Air**

The energy content of the air is really low as it only consists in sensible enthalpy and the air is admitted nearly at room temperature. There is a slight heating effect at the blower but its order of magnitude is not comparable with the energy content of biomass. Nevertheless, in order to take it into account, the temperature and pressure of the inlet air are measured after the blower and considered as the inlet conditions of the reactor.

**Syngas**

As for the mass balance, the syngas output can be divided into three components: dry syngas, water and impurities (ashes and tars). The balance of energy is taken at the outlet of the reactor where those three components are at high temperature (more than 600 $[°C]$).

The energy content of the dry syngas is thus the sum of sensible enthalpy and formation enthalpy (LHV) of each constituant. The sensible enthalpy in this case is quite important due to the high temperature.

The water content here plays a major role due to the high sensible enthalpy and the heat of vaporisation it contains. The contribution of water is calculated on the mass flow of water that is divided into two terms: one is weighted through collection in polluted water (i.e. at the bottom of the condenser) and the rest is estimated by considering that the syngas at the outlet of the condenser is saturated with water vapour. In order to evaluate the level of water vapour in the syngas, the temperature is taken at the outlet of the condenser.

The tar content is again neglected in the balance and the fine ashes are measured but their share is close to zero and thus neglected (even if they present a LHV of $18378[kJ/kg]$ on wet basis).

### Ashes

The ashes still contain a significant amount of carbon translating into a significant amount of energy. Their LHV is equal to 10358$[kJ/kg]$ on wet basis. Their sensible enthalpy is low in comparison to their LHV.

### Wall heat losses

The wall heat losses are estimated by the measurement of the external temperature of the reactor. The temperature is taken at five different points on the external surface of the gasifier and the reactor is divided into five zones where the measured temperature is taken as the reference for the external wall temperature. Within each of this five zones, the heat flow is calculated as: $\dot{Q} = k_{wall}\ S\ (T_{in} - T_{external})$. The effective heat transfer coefficient $k_{wall}$ is calculated considering the four constituants of the wall: refractory concrete, insulation concrete, insulation and stainless steel as illustrated in Figure 4.14 for the oxidation zone. The composition is the same for all the zones but the thickness of each component varies a little in order to reduce the costs in regions exposed to lower temperatures.

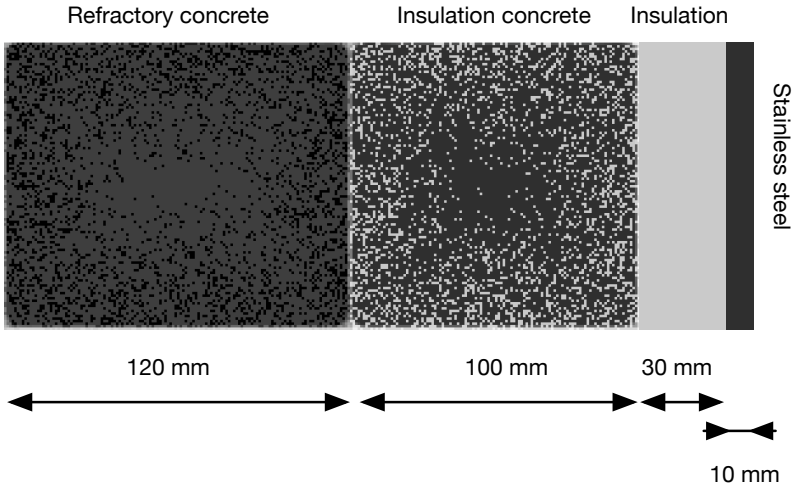


***Figure 4.14*** *– Illustration of the composition of the reactor wall for the oxidation zone.*

For example, the wall of the oxidation zone is 0.26 m thick and is composed of (from exterior to interior):

- 0.03 [m] of super insulation WAKER WDR ($\lambda = 0.06[W/m.K]$)
- 0.10 [m] of insulation concrete ($\lambda = 0.45[W/m.K]$)
- 0.12 [m] of refractory concrete ($\lambda = 1.4[W/m.K]$)
- 0.01 [m] of stainless steel ($\lambda \approx 30[W/m.K]$)

The external and internal convection coefficients cannot be measured but they are calculated at approximatively $h_{ext} = 10[W/m^2.K]$ and $h_{int} = 30[W/m^2.K]$. Due to the high quantity of insulating material, the influence of the value taken for the convection terms is low on the overall transfer coefficient. The overall effective coefficient of transfer is given as $\sigma = 1.06[W/m^2.K]$.

**Results**

The total energy in and out of the gasification reactor during a M&EB can be detailed as:

$$\begin{aligned} E_{in} &= E_{biomass} + E_{air} \\ E_{out} &= E_{dry\ syngas} + E_{fine\ ashes} + E_{water} + E_{ashes} + E_{wall\ losses} \end{aligned}$$

The energy balance and its error presented in Table 4.6 should not be compared to the mass balance and its error. Sure, the energy balance is largely based on the mass balance but the energy content varies from one compound to another (meaning the errors in mass does not have the same impact on the energy errors) and the energy balance presents an additional term in comparison to the mass balance: wall heat losses.

| Energy Input [kJ] | Energy Output [kJ] | Error [%] |
|---|---|---|
| 2.07e+07 | 2.05e+07 | 1.04 |

***Table 4.6*** *– Energy balance.*

Figures 4.15a and 4.15b present the distribution of energy for inlet and outlet flows. As expected, the gasifying agent, air in this case, does not bring energy into the gasifier. It is interesting to note that 88% of wood's energy is transferred into syngas. The ashes represent 5% of the energy balance while they represent only 3% of the mass balance.

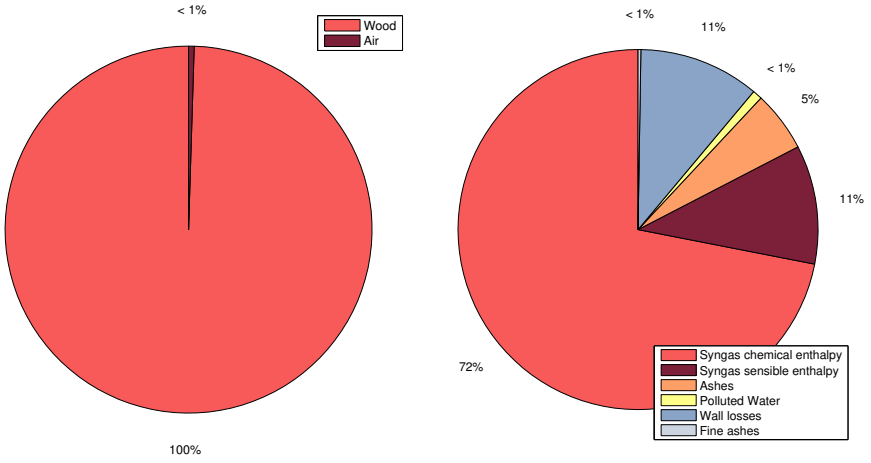


***(a)*** *Inlet* ***(b)*** *Outlet*

***Figure 4.15*** *– Energy distribution*

Wall losses are the main energy losses but they contain several assumptions that make them less precise than other measurements. They may be overestimated but the order of magnitude is correct.

The fuel energy conversion rate can be defined as the ratio of chemical energy in the syngas to chemical energy in biomass. It can be written as:

$$\eta_C = \frac{LHV_{syngas}\ \dot{m}_{syngas}}{LHV_{biomass}\ \dot{m}_{biomass}} = 71.21\%.$$

For biomass to power application, the gas still needs to be used into an engine for example, considering an efficiency between 35-40%, the total biomass to electricity conversion efficiency would be between 25 to 30%. The heat recovery should be around 45-55%, bringing the total CHP energy efficiency around 70-80%.

The mass and energy balances presented here were the subject of two master theses realised by Catherine Debucquois & Charly Raisière [76] and Elisabeth Bries & Arthur Leveau [77]. Table 4.7 shows the synthesised results of the mass and energy balances for three different long duration tests realised on T.G.P. The results are very similar in terms of conversion efficiency $\eta_c$ even if the air ratio $\alpha$ is modified between run 1 and run 2 and the power is modified between the run 3 and the other runs.

| Data | Units | Run 1 Reference | Run 2 Modified $\alpha$ | Run 3 High power |
|---|---|---|---|---|
| $P_{th}$ $[kW_{PCI}]$ | $[kW_{LHV}]$ | 169.25 | 162.93 | 217.34 |
| Average biomass consumption | $[kg/h]$ | 51.42 | 47.80 | 64.38 |
| Average air flow | $[kg/h]$ | 90.62 | 83.31 | 111.31 |
| $LVH_{syngas}$ | $[kJ/kg]$ | 4744.7 | **4820.3** | 4798.5 |
| ER | [-] | 0.30 | 0.29 | 0.29 |
| $\alpha$ (air ratio) | [-] | 0.23 | 0.38 | 0.25 |
| SV | $[m/s]$ | 0.12 | 0.12 | 0.16 |
| $Y_{gaz}$ | $[N_{m^3}/kg]$ | 2.46 | 2.45 | 2.46 |
| SGR | $[kg/m^2/h]$ | 180.01 | 169.07 | 227.72 |
| $\eta_c$ | [-] | 0.71 | **0.73** | 0.72 |
| $[CO]$ | $[\%_{vol}]$ | 19.06 | 19.77 | **19.84** |
| $[CO_2]$ | $[\%_{vol}]$ | 11.85 | 12.49 | 11.89 |
| $[CH_4]$ | $[\%_{vol}]$ | 0.83 | 1.16 | 1.00 |
| $[H_2]$ | $[\%_{vol}]$ | 19.13 | **19.30** | 18.54 |

***Table 4.7*** *– Comparison of the performances for three long duration tests of the T.G.P. installation.*

## 4.2 Influence of gasification key parameters

Two-stage technologies increased the interest for downdraft gasification thanks to improved performances and reduced maintenance costs. They also introduced new controlling and monitoring parameters. On a single-stage gasifier, the only control parameter is the amount of air injected in the gasifier as it can be modified during a test. Other parameters like bed heights investigated in this thesis require a shut down of the reactor to be modified.

The amount of air regulates the flow of biomass since, as described in Section 3.2, it determines its consumption. In theory, the wood consumption should be proportional to the air flow but it is not actually the case as the efficiency of gasification varies with the power input (and thus with the air flow). Nevertheless, there is generally no way to control the biomass flow independently from the air flow so even if the link is not linear, the relation is fixed by the experimental setup.

As explained in Sections 1 and 3.2, downdraft gasifiers can present high pressure drops in the reduction bed. As the gas flow is pushing the char against the grid at the bottom of the gasifier, trying to counter-act by increasing the injection pressure increases the problem. In updraft gasifiers, the gas flow pushes the particle upwards, helping to keep a good porosity of the bed and limiting the pressure drops without the need of mechanical action. On the contrary, downdraft gasifiers are often equipped with a system that allows to create a movement inside the reduction bed in order to break the clogging structure and evacuate the ashes from the reduction zone. For example, in T.G.P., the mechanism is a grid that can be rotated as described in Section 3.2.

These pressure drop control systems influence the biomass flow but they cannot control it. If the ash extraction system at the bottom of the gasifier is forced too much (extraction rate higher than required by pressure drops), the gasifier will not run properly (poor efficiency, increased tar level, etc.). This absence of independent control lead to an ER that is nearly constant once the design is fixed. This is also the reason why biomass shape is critical for the process of gasification because biomass with a high clogging tendancy will require a high extraction rate and reduce the residence time of the particles in each reaction zones, leading to low gasification efficiency.

These observations indicate that air inlets are the main parameter to control the whole process. The two-stage gasification splits the air injection into two, introducing a new parameter to control, the air ratio between the two injections. The investigations on air ratio are the first experiments described in this section.

The physical separation between the pyrolysis zone and the oxidation and reduction zone leads to a second parameter: heights of the pyrolysis bed and of the reduction bed. In single stage technology, there is only one bed and the reaction zone sizes are fixed by design and by the biomass characteristics. In T.G.P. gasifier, the bed heights are independent and the flexibility of this experimental gasifier allows to modify the size of the reaction zones independently. The modification of the bed heights are in fact a modification of the particle residence time in each reaction zone. These bed heights investigations are described in the second part of this section.

Finally, the new technology introduced gaseous phase injection for both pyrolysis and oxidation zones for an homogeneous air distribution but the interest was less obvious for the pyrolysis zone. The last subsection discusses a third parameter which is the influence of porous medium air injection in the pyrolysis zone.

### 4.2.1 Air ratio

The improvements brought by the two-stage gasification process come with added complexity in comparison to the single stage gasifiers [31]. The main new parameter is the air ratio $\alpha$. The definition of the air ratio, as mentioned in Section 1.3 is the ratio between the primary air injection flow and the total flow of air injected in the gasifier. As a reminder, it can be written as:

$$\alpha = \frac{\text{Primary air flow}}{\text{Total air flow}} = \frac{\text{Primary air flow}}{\text{Primary air flow} + \text{Secondary air flow}}.$$

The air ratio usually takes values between 0.2 and 0.35 at steady-state for woody biomass. The aim is to inject the right amount of air into the pyrolysis zone to ensure a good pyrolysis and the rest into the oxidation zone to produce the heat required for the reduction reactions. The amount of air into the pyrolysis zone has an optimum value that depends on the type of biomass. On the one hand, if too much air is injected, the biomass will not only pyrolyse and burn pyrolysis gases but will also consume char needed for the reduction reaction. This will translate into a higher carbon dioxide content in the syngas, reducing the conversion efficiency of biomass to syngas. On the other hand, if

the amount of air is too low, the temperatures reached will not be sufficient to have a good pyrolysis, translating into higher tar content in the syngas and ultimately, if the temperatures are really low, there reactions will not sustain themselves and the gasification process will shut down.

Figures 4.16a and 4.16b show the influence of the air ratio on carbon monoxyde and dioxyde production. Each dot represent an average on approximately one hour of test at steady-state. When $\alpha$ increases, meaning that more air is sent to the primary air injection, the carbon dioxyde content increases and the carbon monoxide content decreases. This means that the lower air ratios produce a better syngas.

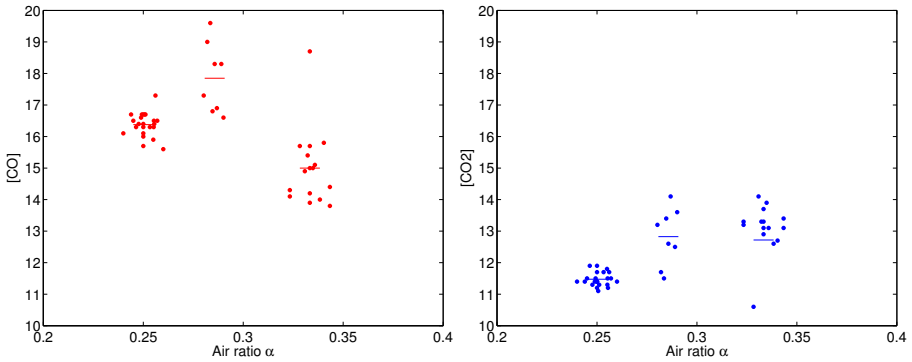


***(a)*** *CO* ***(b)*** $CO_2$

***Figure 4.16*** *– Influence of the air ratio on the carbon monoxyde molar fraction (on the left) and carbon dioxyde molar fraction (on the right) content of syngas from natural wood.*

Figure 4.16a also shows that the carbon monoxyde decreases if the air ratio is too low, meaning there is not enough air for the pyrolysis zone. This investigation shows that for this particular type of wood and moisture content (<10%, see 4.1.1), the optimum air ratio is approximately $\alpha = 0.3$.

Figures 4.17a and 4.17b show that the air ratio also influences the hydrogen and methane content. The ratio of 0.3 is again the best even if the differences for methane are not significant. In fact, as explained in section 1.3, methane is interesting for LHV but is usually linked to a higher tar content.

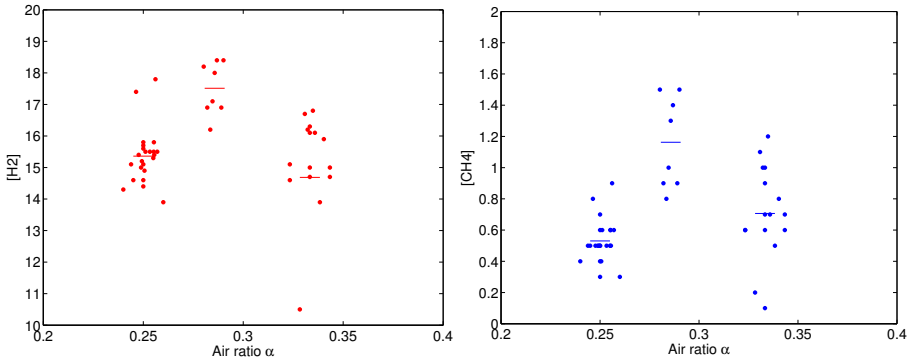


*(a)* $H_2$ *(b)* $CH_4$

***Figure 4.17*** *– Influence of the air ratio on the hydrogen molar fraction (on the left) and methane molar fraction (on the right) content of syngas from natural wood.*

Unfortunately, tar content measurements could not confirm that the air ratio influences the tar content in syngas. Figure 4.18 shows the mass fraction of tar samples for different air ratios. The samples are taken during a period of approximately 30 minutes at steady-state. The air ratio is the same for sample 0 to 6, 8 to 13 and 14 to 17. No clear trend could be outlined from these results.

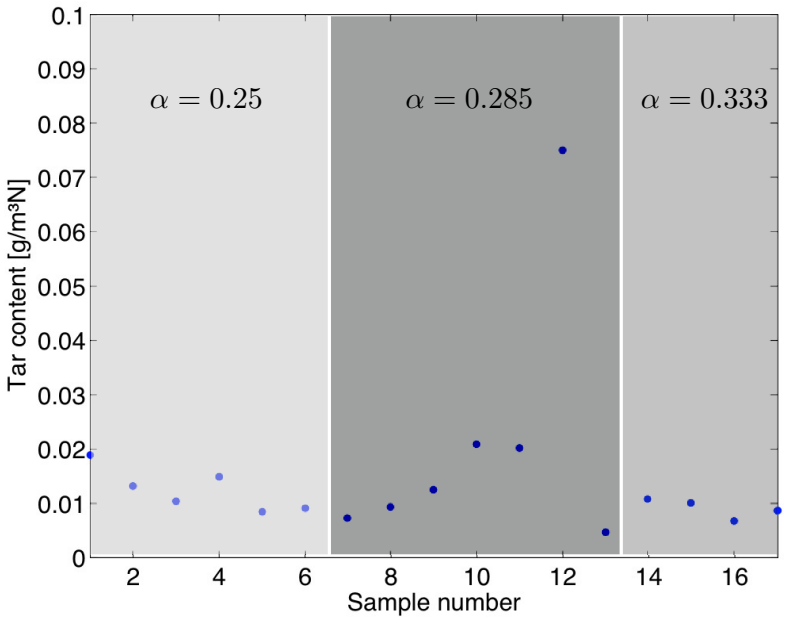


***Figure 4.18*** *– Tar content measurements for different air ratios.*

All the samples, except sample 12, present concentration below 25 $[mg/Nm^3]$ which it roughly 40 times less than typical values for single stage technology. Sample 12 which presents a tar content of 74 $[mg/Nm^3]$ (more than three times other sample) should be excluded because it was taken during a reduction zone filling sequence launched manually in order to capture the effect of the filling on tar content. During these sequences, the biomass from the bottom of the pyrolysis zone at approximately 600 $[°C]$ reaches the top of the reduction at approximately 850 $[°C]$ and emits pyrolysis gases that are not fully cracked as they are emitted after the high temperature oxidation zone. These sequences are also observed on the temperature curves as explained in section 4.1.

### 4.2.2 Bed heights

Bed heights are a major parameter for the gasifier since for a fixed power, the flow of solid is constant and the bed heights determine the residence time of solid particles in each reaction zones. Higher particles beds mean longer residence time. Long residence time are usually considered as better for the reaction but, for the same power, the heat is diluted in a bed of bigger size, reducing the temperature reached. These temperatures are important since pyrolysis kinetics follow Arrhenius schemes which depend on the temperature exponentially. The influence of temperature in the pyrolysis process is more detailed in section 5.2.

The residence times inside the pyrolysis zone are estimated with the solid biomass flow and apparent density of biomass. For these investigations, the average wood flow was 30 $kg/h$ which is approximately 200 $m^3/h$. Neglecting the volume reduction of wood in the pyrolysis bed (due the shrinking induced by pyrolysis [78]), the speed of solid particles in this zone is approximately 1.4 $m/h$. Three pyrolysis bed heights were tested resulting in three residence times as follow:

- Maximum height on T.G.P. of 980mm, equivalent to 42 minutes.
- Intermediate height on T.G.P. of 800mm, equivalent to 34 minutes.
- Minimum height on T.G.P. of 620mm, equivalent to 27 minutes.

The smallest residence time is actually the closest to industrial gasifiers. The aim of this study is to check the effect of an increase of the residence time on industrial gasifiers. The effect of the residence time is more difficult to analyse than the air ratio since the size of the bed has a major impact on the temperature profile of the pyrolysis zone. This profile will thus also be discussed in this section.

The partial injection of air is made at the top of the pyrolysis zone but the partial combustion of pyrolysis gases only occurs inside the particle bed. This particular flameless combustion is called smoldering combustion and it determines the temperature profile of the whole pyrolysis zone. The combustion front is moving, hence making the control of smoldering combustion difficult. The speed of the smoldering front occurring inside particles bed is difficult to stabilise as it depends on the air flow. For a fixed bed, depending on the air flow, the front either goes in the same (called forward smoldering) or in the opposite direction (called reverse smoldering) than the air flow. For low air flows, the front move towards the air inlet when it is pushed away for higher air flows. In a fixed bed, the flame is thus moving downwards or upwards depending mainly on the chosen air flow.

On downdraft gasifiers, the added complexity comes from the fact that the bed is moving downwards. This downward movement of the solid particles needs to happen at a speed equal to the opposite of the speed of the reaction front in order to have a stable smoldering front. In this case, the smoldering thus needs to be a reverse one. This opposite movements are illustrated in Figure 4.19 and can lead to difficulties to reach steady-state in the pyrolysis zone. This behaviour can also induce adjustments on the settings during an experiment. Nevertheless, the major discontinuities observed in the syngas composition come from the discontinuous flow of biomass.

Typically, the top of the bed is at ambient temperature, below the top, it increases to drying temperatures. Below the drying front, it increases to higher temperatures in the smoldering front (approx. 600 $[°C]$) and then cools down due to diffusion inside the biomass particles and heat losses. At the bottom of the pyrolysis zone the temperature are thus lower at approximately 500 $[°C]$. The whole temperature profile is illustrated in Figure 4.19.

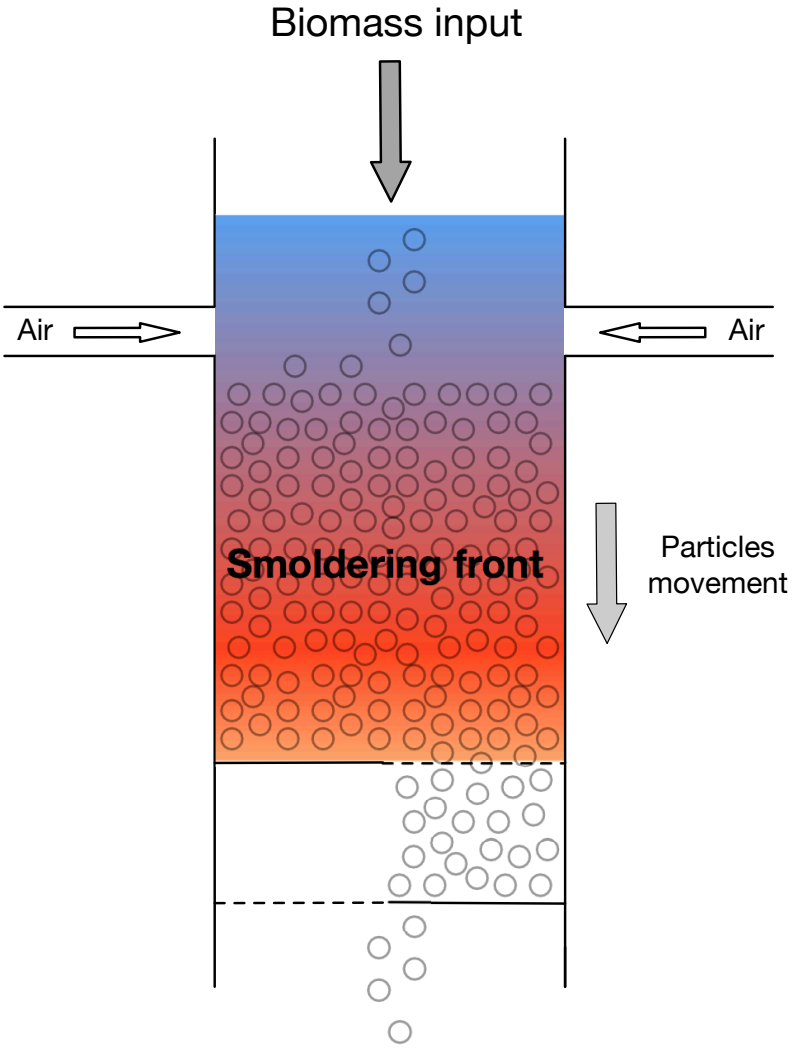


***Figure 4.19*** *– Illustration of the position of the smoldering front inside the particles bed. The blue colour representing low temperatures while the red colour represents the high temperatures.*

Figure 4.20 illustrates the position of the thermocouples inside the pyrolysis zone along with the approximative position of the top of the bed for the different cases. The thermocouples are numbered from 1 to 11, the first one is placed 9 centimetres below the air injection and all the others are placed 9 centimetres below the previous ones around the gasifier with an shift of 90° between two thermocouples as detailed in section 3.2.5.

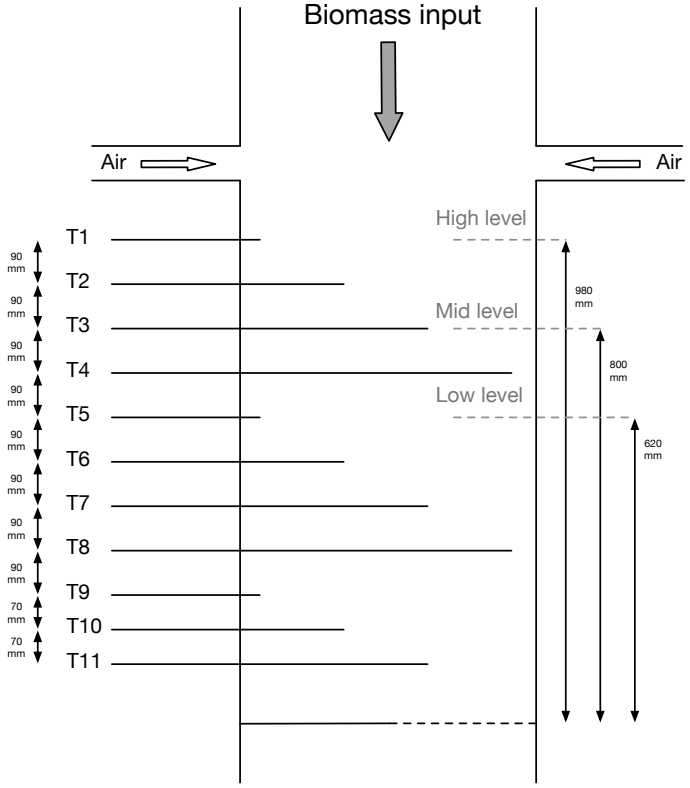


***Figure 4.20*** *– Illustration of the position of the thermocouples inside the particles bed.*

The figures 4.21, 4.22 and 4.23 present the temperatures in the pyrolysis zone for a complete experimental test. The first two hours of each test are transient state while the rest can be considered as steady-state in terms of temperature.

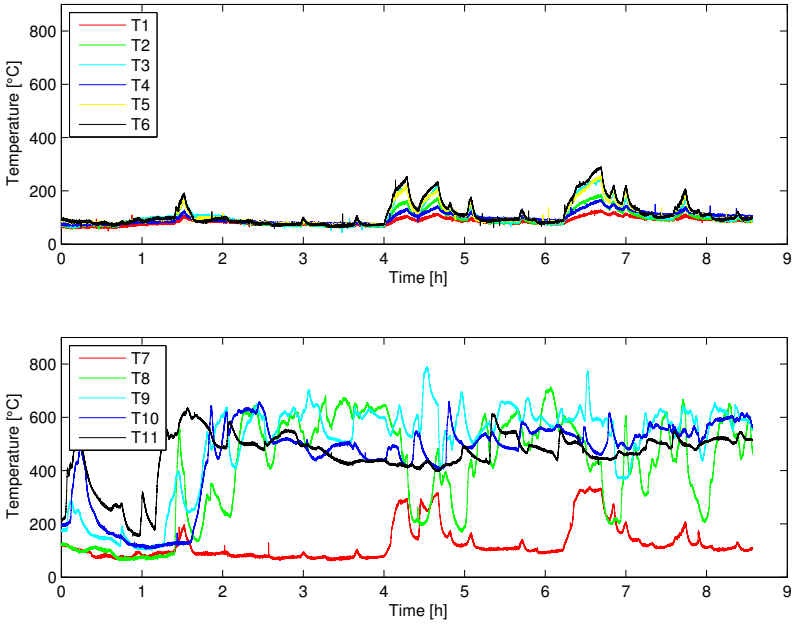


***Figure 4.21*** – *Evolution of the measured temperatures in the pyrolysis zone for the minimal bed height (620 [mm]).*

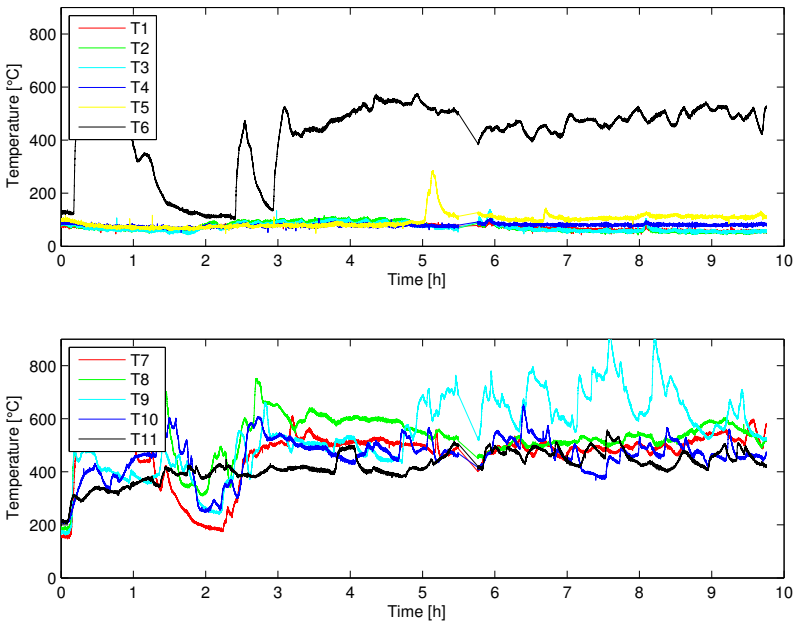


***Figure 4.22*** – *Evolution of the measured temperatures in the pyrolysis zone for the intermediate bed height (800 [mm]).*

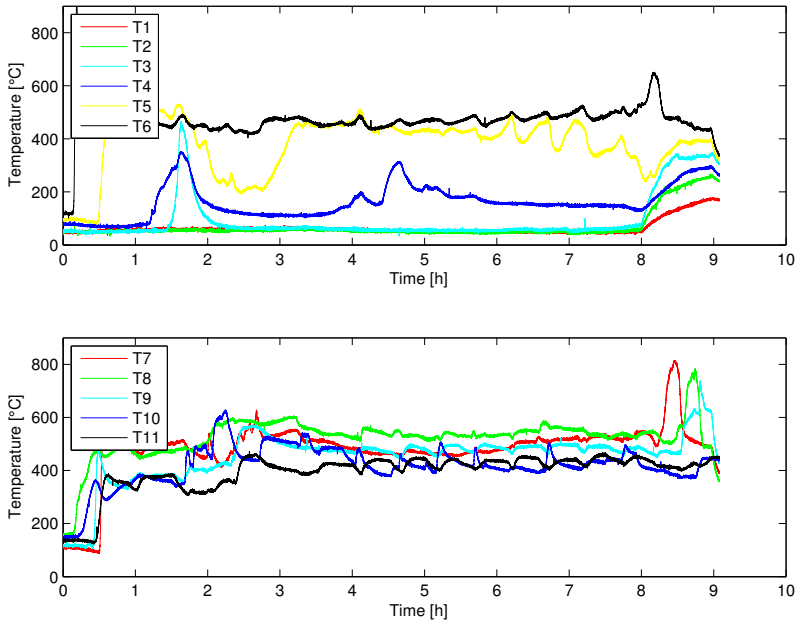


***Figure 4.23*** *– Evolution of the measured temperatures in the pyrolysis zone for the maximal bed height (980 [mm]).*

On the Figure 4.21 that presents the minimal residence time, the six first measurement show low temperature, meaning they are far from combustion front, mainly due to the fact that the top of the bed is on average located approximately at T5. The maximum temperatures reached by T9, T10 and T11 are more than 700°C.

Rather than only considering the total residence time or the height of the pyrolysis bed, it is also interesting to observe the location of the smoldering front or the distance between the smoldering front and the bottom of the pyrolysis zone. This distance allows to calculate the residence time at a high temperature. It could be interesting to see if this height is influenced by the total size of the bed. If not, increasing the height of the bed may not have any effect on the operating conditions and performances of the gasifier. The experiments show modification of the position of the smoldering front for the three cases, it is located around T7 for the lowest level, above T6 for the medium level and above T5 for the highest level.

The second and third figures (4.22 & 4.23) show a greater stability with less temperature variations. This is due to the fact that the volume of particles at high temperature is higher and translates into higher thermal inertia of the bed. They also show that the profile is wider and the average temperature of the thermocouples at the bottom of the pyrolysis zone are lower. This improved stability simplifies the control of the pyrolysis zone.

Figure 4.24 presents the evolution of the average temperature of the pyrolysis zone during the three tests. The lower bed height presents an average temperature below the two other tests because the thermocouples at the top of the bed are cold as shown by the profile of average temperatures presented in Figure 4.25. The significant difference between the three tests is the decreased stability for the temperature for the lowest bed.

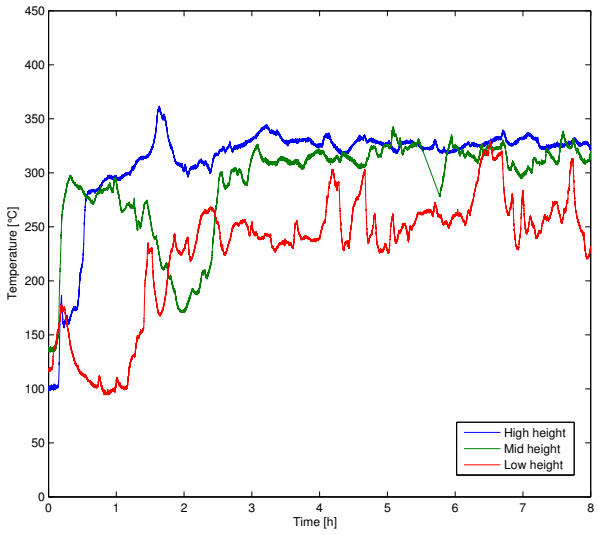


***Figure 4.24*** *– Average temperature for the eleven thermocouples in the pyrolysis zone for the three bed heights (Maximum, Medium and Minimum.*

Figure 4.25 shows that the lowest bed height presents a similar maximal temperature (approx. 750 [K]) with a shift toward the bottom of the gasifier. The main difference is thus the residence time at high temperature rather than the reached temperature itself. The reactive zone of the lowest bed is approximately 300 [mm] ($\approx$ 760 [$s$]) shorter than the highest bed and 180 [mm] ($\approx$ 460 [$s$]) shorter than the medium bed.

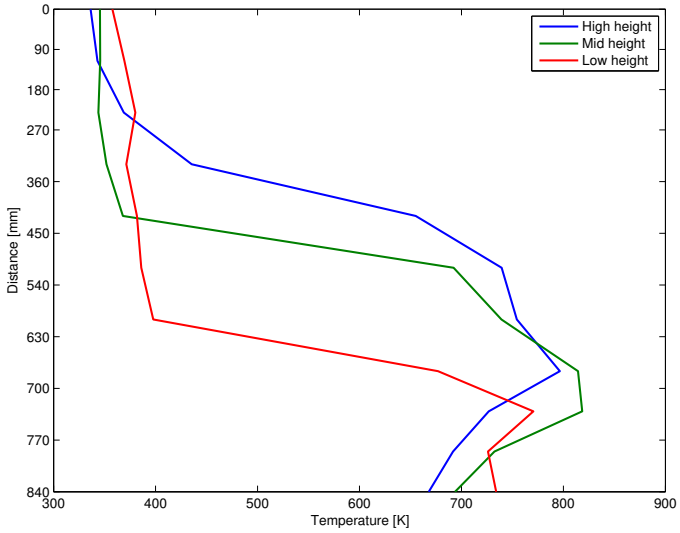


***Figure 4.25*** *– Profiles of time average temperatures for the three bed heights.*

During these tests, the temperature in the combustion zone was not affected by the pyrolysis and was similar for all bed heights. The air ratio tested was the same so the differences shown by the gas composition at the outlet of the gasifier are all due to the bed heights variations.

The Figure 4.26 shows the gas composition for the intermediate level pyrolysis bed. It is presented first as it is between the two other levels and will then be used as a reference to compare the effect of an increased or decreased bed height. It shows the evolution of the syngas quality during a test. Even if the temperature profiles are stable after 2 or 3 hours, the gas quality is improving for 5 to 6 hours and still shows improvement potential at the end of the test, the state of the gasifier after 6 hours can be considered close to steady-state. The evolution is typical, at start, the different phases observed are described in section 4.1. The quality of syngas is considered good after 2 to 3 hours of operation which can be put in parallel to the time when stable temperatures are reached.

It is interesting to notice that variations due to discontinuity in the solid flows can also be observed on syngas composition. The average composition, near steady-state, for the intermediate bed height contains 20% of $CO$, 16% of $H_2$,

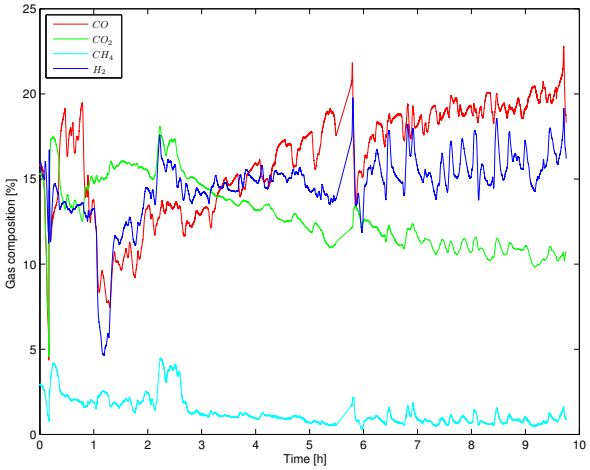


***Figure 4.26*** *– Gas molar composition for the intermediate pyrolysis bed height (800 [mm]).*

12 % of $CO_2$ and 1% of $CH_4$, the rest is nitrogen from air and other compounds in negligible amounts (tars, light hydrocarbons, fine particles).

Figure 4.27 presents syngas composition for the minimum pyrolysis bed height. The composition reached at steady-state is approximately 22% of $CO$, 18% of $H_2$, 12 % of $CO_2$ et 1% of $CH_4$. This quality is higher than the one obtained with the intermediate bed height. Sudden drops and peaks at hour 7 are calibration measurement and should not be taken into account. They are presented to keep raw data intact.

Figure 4.28 confirms that an increased height has a negative effect on syngas quality with an average composition at steady-state of 18% of $CO$, 15% of $H_2$, 11 % of $CO_2$ and less than 1% of $CH_4$. The end of this test should be excluded since the solid flow from pyrolysis zone is stuck and no biomass is coming in the reduction bed, leading to the production of a high carbon monoxyde gas due to char gasification. This gas composition can seem really interesting but presents a low hydrogen content is only due to a transient state where the char bed is going to be consumed really quickly and is not renewed. When biomass flow is restored, the carbon monoxide content drops, the hydrogen and methane content rises inducing a high tar production. These operating conditions are thus avoided because they create significant variations in the gas composition and *in fine* produce a higher average tar content.

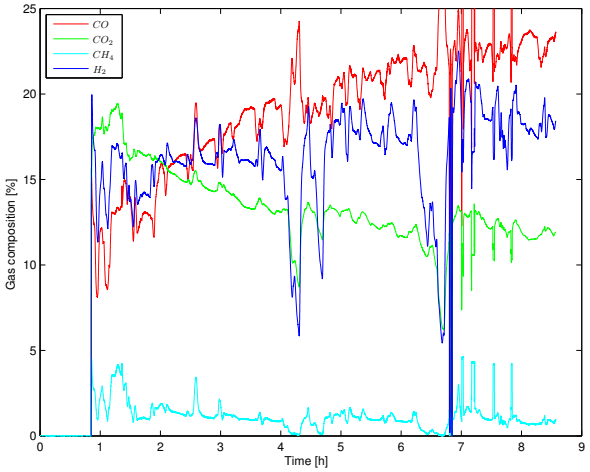


***Figure 4.27*** *– Gas molar composition for the minimal pyrolysis bed height (620 [mm]). Sudden drop near $7^{th}h$ are due to calibration.*

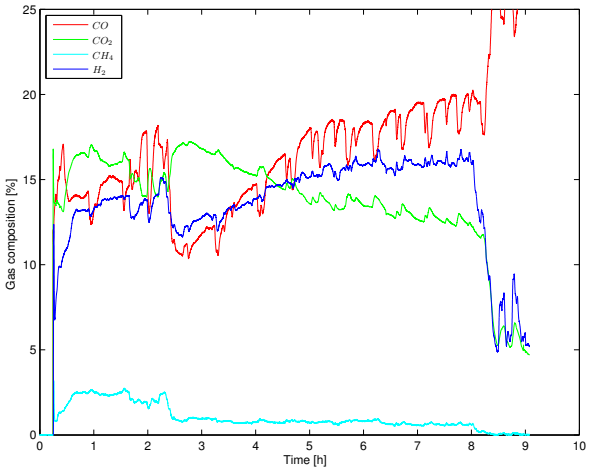


***Figure 4.28*** *– Gas molar composition for the highest pyrolysis bed height (980 [mm]).*

The gas composition tends to show that there is no interest to increase the pyrolysis bed height. This conclusion should be balanced by the stability brought by the higher bed height. A compromise between stability and syngas quality could be found by combining the two effects.

Tar measurements for different bed heights are presented in Figure 4.29. The average tar content of the minimal bed height ($0.004 \pm 0.001[g/Nm^3]$ [95%]) is not significantly lower than for the highest bed height ($0.006 \pm 0.0005[g/Nm^3]$ [95%]) considering the uncertainty on the measurement. Tar cracking below the front apparently does not play a significant role. The tar content cannot be linked clearly to the bed height of the pyrolysis zone

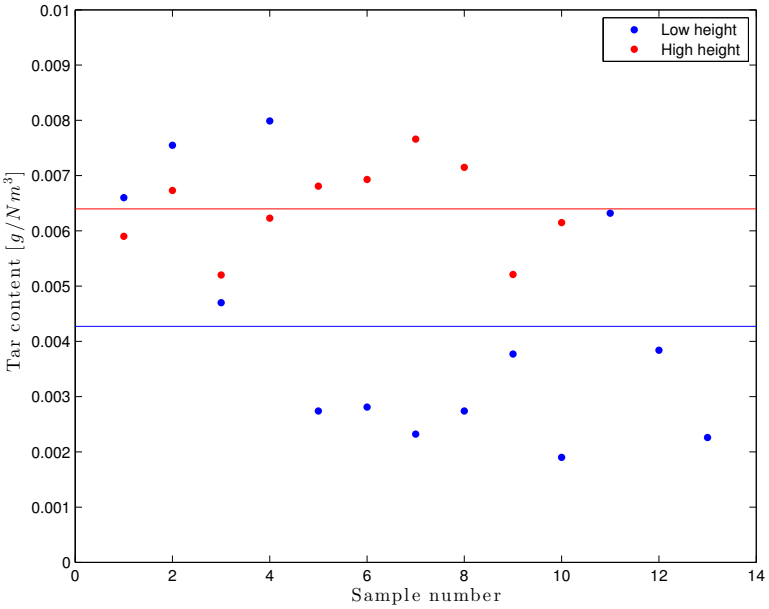


***Figure 4.29*** *– Tar measurement for the maximal and minimal height with respectively 10 and 13 samples analysed. Straight line is the average of the samples.*

### 4.2.3 Air injection in the porous medium

All the reactors based on the concept of single stage technology (illustrated in Figure 4.30) presents a similar temperature profile. The top of the particles bed is cold ($\approx$ 25 [$^{\circ}C$]) then the temperature increases to a maximum ($\approx$ 1000 [$^{\circ}C$]) close to the air injection and decreases along the reduction bed (exit at $\approx$ 500 [$^{\circ}C$]).

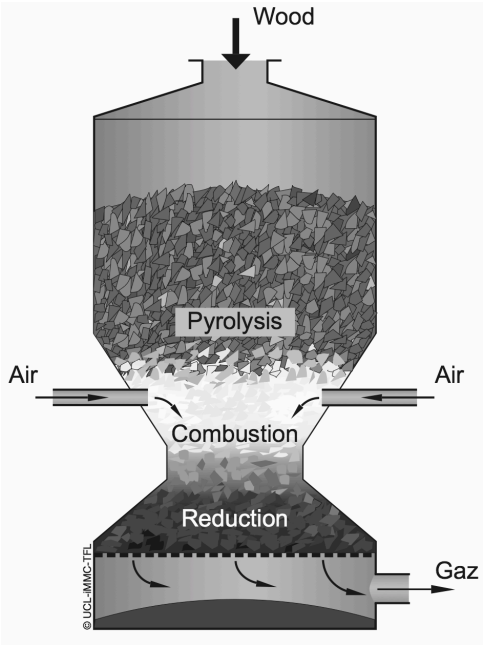


***Figure 4.30*** *– Single stage gasifier principle.*

In a two-stage gasifier, the production of the heat required for pyrolysis is achieved through a primary air (or gas) injection or external heating and it modifies the temperature profile. The oxidation and reduction zones present similar temperature profiles as the single stage technologies but the temperature profile in the pyrolysis zone may vary from one technology to another depending on the location of the primary air injection, the geometry of the reactor and process operating conditions.

In the NOTAR® concept, the air injection is by default placed at the top of the pyrolysis zone, above the wood bed to avoid hot zones at injection points where clinkering and slagging could appear with high ashes content biomass.

In two-stage technologies, the temperature profile is divided in two. The first part of the profile is the pyrolysis zone and the second part is the combustion and reduction zone. The second part of the profile is similar in all technologies. The temperature profile of the pyrolysis front on T.G.P. is inverted in comparison to single-stage technologies. In single-stage reactors, the temperature is increasing during the whole pyrolysis ($\approx 650$ $[°C]$) as the biomass is heating through heat conduction from the combustion zone ($\approx 1000$ $[°C]$). In industrial NOTAR® applications, the profile is a constantly decreasing profile as the partial combustion occurs at the air injections at the top of the bed ($\approx$ 550 $[°C]$). The temperature then decreases due to heat losses and heat transfer to the core of the solid particles. The disadvantage is that the end of the pyrolysis is at lower temperature ($\approx 400$ $[°C]$). Blondeau et al. [78] showed that in order to achieve a good pyrolysis, temperature should increase rather than decrease as a complete pyrolysis is harder to achieve due to the insulating properties of the char. The profile presented by T.G.P. is thus not optimal in regards to Blondeau conclusions. Nevertheless, pyrolysis is influenced by two parameters: temperature and residence time. The residence times at sufficient temperatures are actually higher than required for a complete pyrolysis, promoting the pyrolysis of the two-stage process.

As seen in Section 3.2 T.G.P. design allows to investigate several positions for the location of the primary air injection. The idea was to investigate the influence of porous medium injection (of primary air) on the operating conditions (temperature profile, quality of pyrolysis, etc.) of the pyrolysis zone. Theoretically, the benefit could be a better pyrolysis thanks to higher temperatures ($\approx 650$ $[°C]$) reached even with decreased residence times. As the kinetics of the pyrolysis are of Arrhenius type, the increase in temperature could have an effect more positive than the negative effect induced by the decrease in residence time. Porous medium injection was avoided to avoid the risk of an inhomogeneous air distribution leading to poor pyrolysis in certain zones and a decrease on the overall efficiency of the pyrolysis. Nevertheless, it is interesting to see if the potential improvement of porous medium injection is worth the risk.

Unfortunately, first tests on T.G.P. showed a behaviour different from the one observed on industrial version of the NOTAR® technology. Even with air injection located at the top of the gasifier as on industrial gasifiers, the com-

bustion front was located inside the particle bed. On industrial gasifiers, there is a flame located at the air injection created by the combustion of pyrolysis gases present thanks to recirculation loops inside the pyrolysis zone. The temperature profile usually observed on industrial gasifiers could not be reproduced. The assumption is that it the flame in industrial NOTAR® reactors is maintained thanks to the larger surface of concrete above the top of the bed that reflects the flame radiation and the larger diameter that allows more pyrolysis gas recirculation.

Anyway, the results obtained on T.G.P. presented similar syngas composition and tar content with an improved stability of the process. These observations lead to changes in the management of the industrial gasifiers. The operating conditions on industrial gasifiers were changed and the combustion above the bed was forsaken in favour of an in-bed combustion similar to the one observed on T.G.P. Nevertheless, porous medium injection was investigated on T.G.P. to evaluate its influence on the temperature profile and the quality of pyrolysis.

Figure 4.31 presents the gas composition for tests with air injection above and inside the particles bed in the pyrolysis zone.

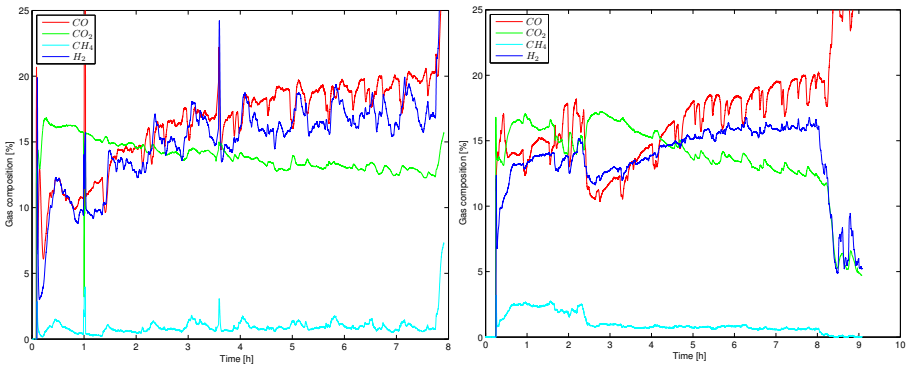


*(a) Porous medium injection* *(b) Injection at the top of the bed*

***Figure 4.31*** *– Gas composition with porous medium injection on the left and above the bed injection on the right. Note: peaks near hour 1 and 3.7 on the left graph are due to calibration of the gas analysers.*

The carbon monoxide content is increased by approximately 2% on average while the hydrogen content is increased by nearly 3% on average. The methane content is also increased. The lower position for the air injection thus increases

syngas quality for the same bed height. This effect could be combined with a higher residence time (higher bed height) in order to gain in quality without decreasing the stability of the process.

Tar measurements (presented in Figure 4.32) for different injections show no influence of the location of the injection (above or inside the particles bed) inside the pyrolysis zone on the production of tars. The average value for both bed height is around $6.5[mg/Nm^3]$ and with an equivalent confidence interval (at 95%) of $\pm 0.5[mg/Nm^3]$. The choice on the bed height to use can thus be made without considering the potential effect on the tar content as it is apparently not influenced by this parameter.

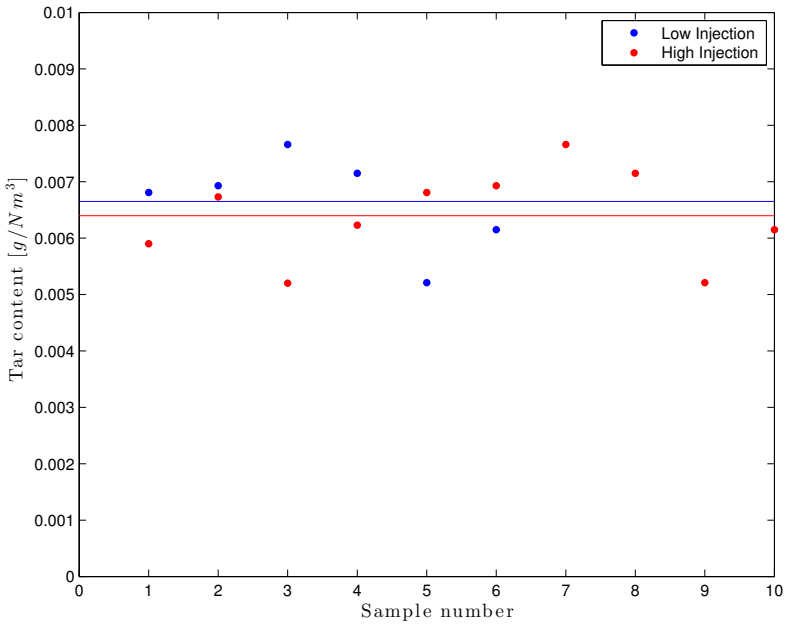


***Figure 4.32*** *– Tar measurements for the two types of injection.*

The temperature profile presented in Figure 4.33 shows that the stability is similar to the one seen in Figure 4.23 for the injection above the porous bed. This shows that the stability of the pyrolysis zone is not affected by air injection location.

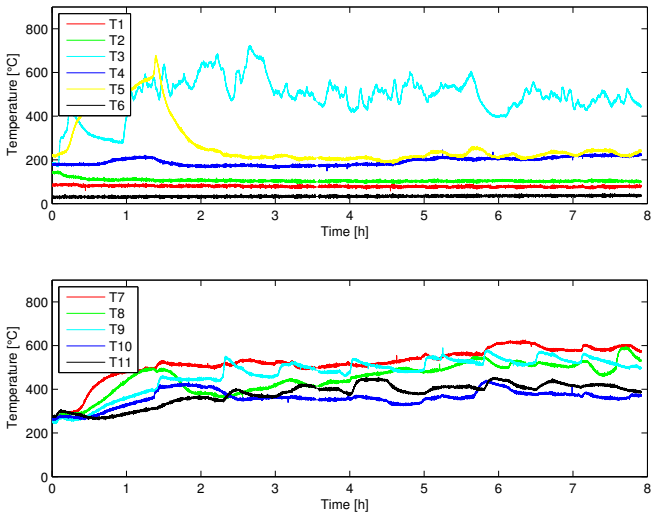


***Figure 4.33*** *– Temperature profile in the pyrolysis zone for porous medium injection.*

## 4.3 Oxygen enriched air gasification

The low LHV of syngas can become an issue when it comes to applications where the flame temperature is critical for the process. Methane substitution by syngas requires a higher producer gas LHV for some specific burners (e.g. burners used in the glass industry). The aim of this research is to address this issue by using oxygen enriched air as a gasification agent into a two-stage fixed bed downdraft gasifier [79].

As said in the introduction, there are two advantages from the use of oxygen enriched air. The first one is an increase of the syngas LHV. Syngas from air gasification usually contains 45 to 50 % of nitrogen: removing nitrogen could increase the LHV by a factor of 1.8 to 2.

The second advantage is to allow an increase of power for the same gasifier. The gasifier flow (and thus power) is typically limited by losses related to pressure drop occurring at the pyrolysis and reduction beds. Reducing the volume of gas going through the gasifier, thanks to nitrogen removal, allows to increase the power of the gasifier. The investment cost per power unit is thus drastically reduced, allowing to balance the additional costs specific to oxygen enrichment.

Tests were made replacing air injection in the combustion zone by pure oxygen injection while the injection in the pyrolysis zone (first stage) remained pure air. The reason is double: the stability of the pyrolysis zone and the risk of carbon consumption. The reduced gas mass flow could reduce the heat convection inside the particles bed and decrease the stability of the process. Moreover, the use of pure oxygen could increase the risk of consuming the char instead of pyrolysis gases, reducing the carbon conversion efficiency. For those reasons, the secondary injection is the only one using oxygen enriched air. The use of pure oxygen in the pyrolysis zone could be investigated in further developments.

The modification of the gasifying agent modifies the calculation of the air ratio defined in section 1.3. The air ratio when using oxygen enriched air is thus based only on oxygen mass flows. With an oxygen ratio similar to air gasification ratio, the two injections combined resulted in overall enriched air mixture containing 50% of oxygen and 50% of nitrogen. This represents a volumetric reduction of approximately 35% in comparison to air gasification at equivalent power. It allows to increase the LHV from $5000 - 5500$ $[J/Nm^3]$ to $8500 - 9000$ $[kJ/Nm^3]$.

This section describes the preliminary results of investigations on the influence of oxygen injection on the temperatures of the process and on the gas composition and LHV.

### 4.3.1 Influence on the temperature

As the primary injection is not modified for these tests, there is no modification, compared to air gasification, on the temperature profile along the axis of the pyrolysis zone. This subsection is thus focused on the temperature measurements of the oxidation and reduction zone only. The temperature of the oxidation zone is supposed to increase significantly while the temperature of the reduction zone is supposed to have a slight increase due to improvement of the efficiency.

The increase in temperature was estimated using the small equilibrium model presented in Section 2. Figure 4.34 shows the increase of the equilibrium temperature expected at the outlet of the gasifier as of function of the oxygen enrichment for constant oxygen to fuel equivalence ratio of 0.3.

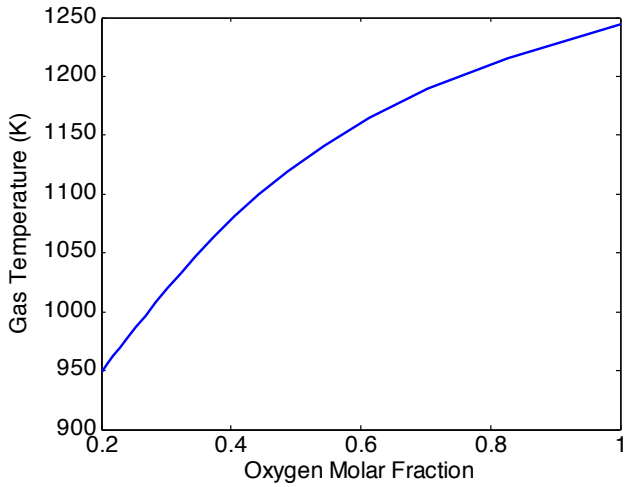


***Figure 4.34*** *– Theoretical temperature at the outlet of the gasifier as a function of the oxygen molar fraction in the air fed to the reactor. The equivalent ratio is fixed at 0.3, the value predicted by the equilibrium model.*

The estimated temperature increase at constant equivalence ratio is for the 50% mixture a little smaller than 200 [$°C$]. This increase cannot be considered directly as the air enrichment modifies the optimal gasification oxygen to fuel ratio (conversion of the air to fuel ratio for oxygen enriched air characterisation). The optimal gasification oxygen to fuel ratio needs to be calculated again, giving a new equilibrium temperature for every oxygen enrichment percentage as shown in Figure 4.35 for 5 different enrichments. The evolution of the optimal oxygen to fuel ratio is presented by the green line in Figure 4.35. It decreases with the air enrichment, leading to an optimal ratio of 0.26 for the 50% enrichment tests realised on T.G.P. in comparison to 0.3 for air gasification. The theoretical increase in temperature is thus moderate and below 100 [$°C$] for the 50% enrichment predictions.

As said in Section 3.2, there is no physical separation between the oxidation and reduction zone: the boundary between the two reactive zones is not fixed. In addition, the bed height varies during a run and can be adapted between experiments. The chosen division sometimes differs from the experimental observation. This has no influence on the results and should thus not disturb their reading.

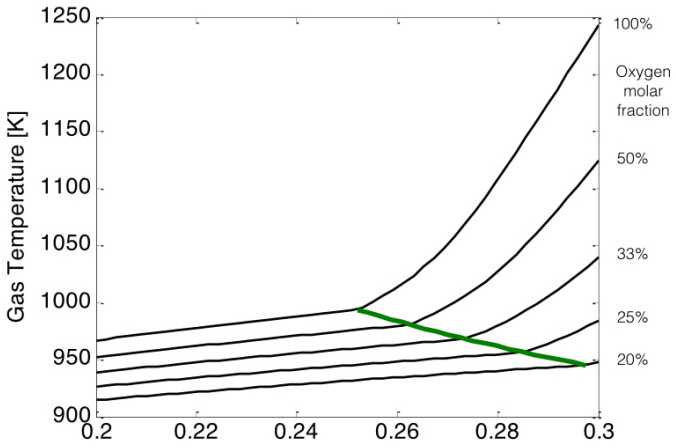


***Figure 4.35*** *– Theoretical temperature at the outlet of the gasifier as a function of the equivalent ratio for different oxygen molar fraction as predicted by the equilibrium model. The evolution of the optimal oxygen to fuel ratio is presented by the green line.*

Figure 4.36 presents the data from the three first temperature measurements in the oxidation and reduction zone during a test using air as the gasifying agent.

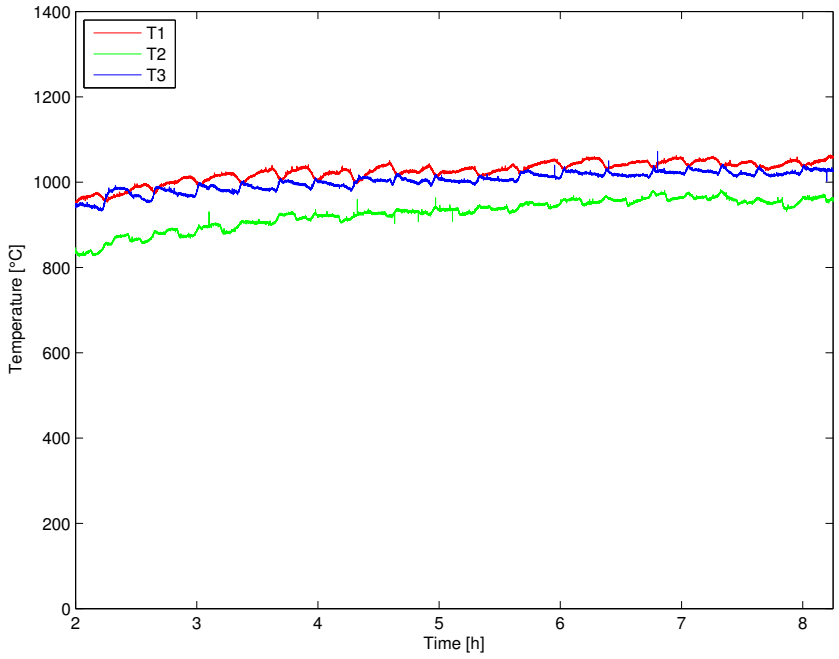


***Figure 4.36*** *– Temperatures in the oxidation zone for air gasification. T1 is the measurement at the top of the zone, T2 is located 9cm below T1 and T3 is located 9 cm below T2.*

These measurements are always located above the reduction bed, in the gaseous phase. They are thus considered as representative of the oxidation conditions. They show great stability with small variations due to the discontinuity in the solid flows.

Figure 4.37 presents the same temperature measurements for a test using oxygen-enriched air as the gasifying agent. The temperatures reached after five hours (near steady-state) are, as expected, higher but the increase in temperature is contained to approximately 150°C. The variations observed in the graph are due to the discontinuities in the solid flows as for the previous graph. The influence of theses discontinuities leads to more important variations in the case of oxygen-enriched air gasification, probably due to a smaller thermal inertia of the gas.

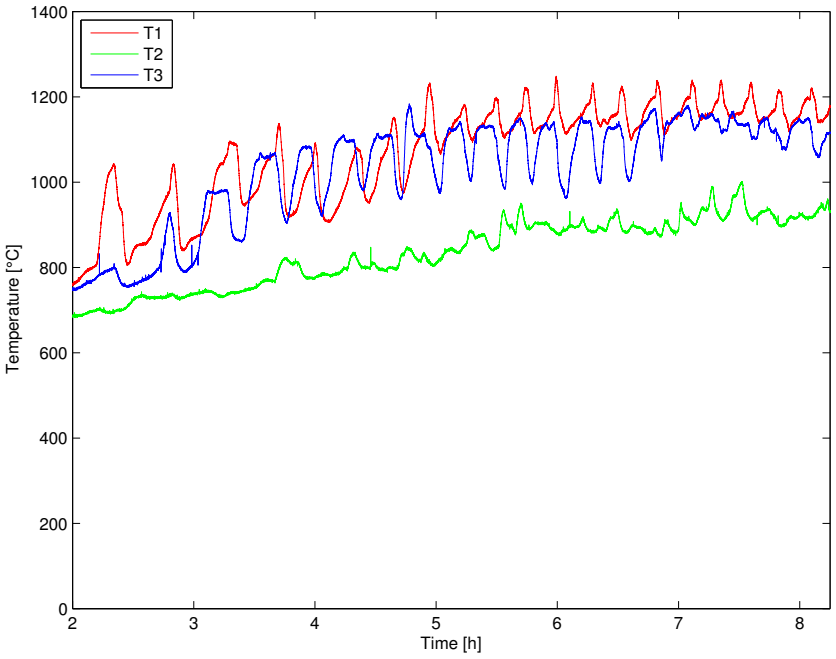


***Figure 4.37*** *– Temperatures in the oxidation zone for oxygen enriched air gasification. T1 is the measurement at the top of the zone, T2 is the second and T3 is the third.*

The average temperature for both tests is close with 1030°C for air gasification and 1050°C for oxygen-enriched air gasification. The difference stands in the

maximum temperature reached that peaks at 1200°C for oxygen-enriched air gasification in comparison to less than 1100°C for air gasification.

Figures 4.38 and 4.39 present the temperature measurements of the thermocouples placed below those presented in Figure 4.36 and 4.37. They are thus closer to or inside the reduction bed. As the first two temperature measurements of this zone are not permanently above the solid particles bed, these are associated with the reduction zone. Actually, the top of the bed is in average located at the level of the temperature measurement showing great periodic variations. The thermocouple that shows these variations in measurement is in fact going in and out of the solid particles bed, measuring sometimes the bed temperature and sometimes the gaseous phase temperature. In Figure 4.38, the temperature measurement T2 is the one at the boundary of the reaction zones and in Figure 4.39 it is T1 that is placed there. This means that bed height has been slightly moved upwards for the test using oxygen-enriched air.

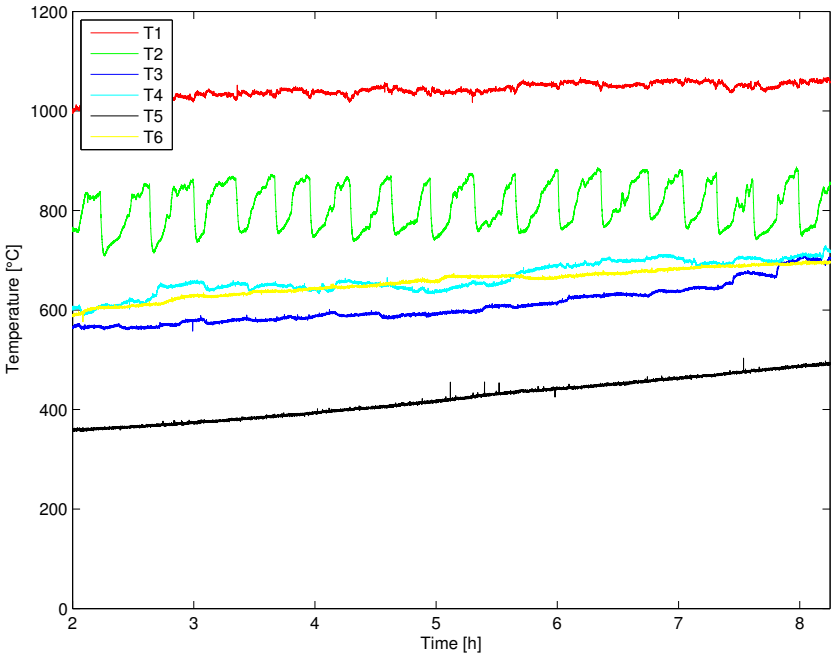


***Figure 4.38*** *– Temperatures in the reduction zone for air gasification. T1 is the measurement at the top of the zone, T2 is the second, T3 is the third, etc.*

Figure 4.39 shows that all the temperatures, including the outlet temperature of the reduction bed are only slightly higher, even with a bigger particle bed, as those predicted by the equilibrium modelling. If looking at temperature measurements T3, T4 and T6, the difference of temperatures are really small (on average the difference is approximately 80°C, 750°C for air and 830°C for oxygen-enriched air) and could lead to the conclusion that influence of oxygen on gasifier materials in the reduction zone is negligible.

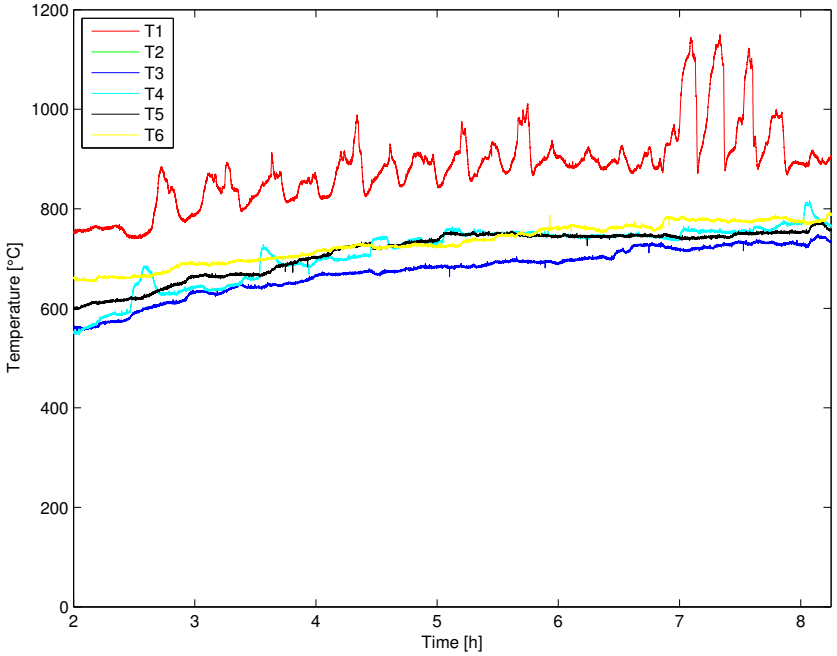


***Figure 4.39*** *– Temperatures in the reduction zone for oxygen-enriched air gasification. T1 is the measurement at the top of the zone, T2 is the second, T3 is the third, etc.*

### 4.3.2 Gas composition and LHV

Figures 4.40 and 4.41 present the gas composition for air and oxygen-enriched air gasification experiments. In both experiments, the gas quality is still slightly improving at the end of the experiment. It can be observed that hydrogen is the most subject to fluctuations for air gasification.

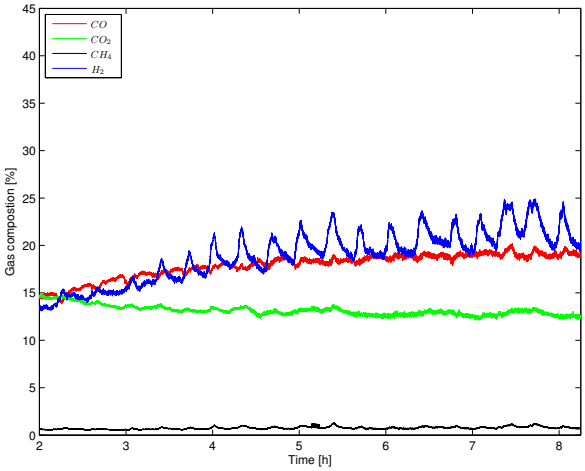


***Figure 4.40*** *– Gas composition in molar fractions as a function of time for air gasification.*

The average composition on the whole experiment (thus including transient state) for the air gasification (presented in Figure 4.40) is: 19.5% of $CO$, 22% of $H_2$, 1% of $CH_4$, 13% of $CO_2$ and 44.5% of $N_2$. The LHV obtained at the end of the test is 5500 $[kJ/Nm^3]$ for an average composition of: 20.3% of $CO$, 23.3% of $H_2$, 1% of $CH_4$, 12.8% of $CO_2$ and 42.6% of $N_2$.

Figure 4.41 shows that the variations in the gas composition are higher. This is easily explained by the nitrogen removal. When looking at the variations as a percentage of the total value, they are in fact similar if not smaller.

The average composition on the whole experiment (thus including transient state) for the oxygen-enriched air gasification (presented in Figure 4.41) is: 27% of $CO$, 25% of $H_2$, 2% of $CH_4$, 19% of $CO_2$ and 27% of $N_2$. The LHV obtained at the end of the run is as high as 8500 $[kJ/Nm^3]$ for an average composition of: 31.7% of $CO$, 29% of $H_2$, 1.8% of $CH_4$, 18.7% of $CO_2$ and 18.8% of $N_2$. This represents an increase of the LHV of 54%. In comparison on nitrogen free basis, it can be observed that the LHV increase is higher than the one calculated on a nitrogen removal base. This means that, as expected, the conversion efficiency is increased.

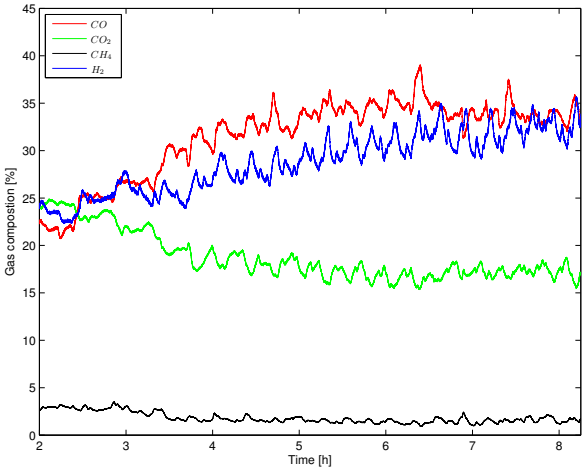


***Figure 4.41*** *– Gas composition in molar fractions as a function of time for oxygen-enriched air gasification.*

Figure 4.42 presents the $CO/CO_2$ ratio. This ratio is complementary to the carbon conversion ratio. The carbon conversion ratio measures the amount of carbon converted from solid to gaseous species, mainly in carbon monoxides and dioxides with the operating conditions of T.G.P. The $CO/CO_2$ ratio compares the amount of carbon converted into a fuel (carbon monoxide) on the amount of carbon converted into a useless species (carbon dioxide). The goal is thus to maximise this ratio in order to get as much fuel as possible.

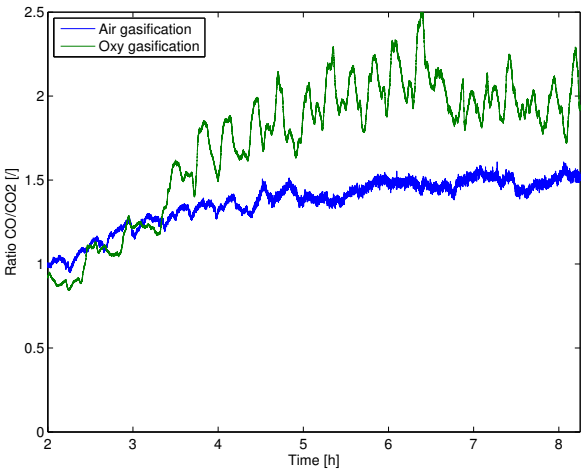


***Figure 4.42*** *– $CO/CO_2$ ratio for air and oxygen-enriched air gasification.*

The equilibrium model predicts a ratio of 2.5 for air gasification and an increase to 3.5 for the use of a 50% oxygen mixture. This increase can be observed experimentally as the $CO/CO_2$ ratio increases from approximately 1.5 to 2 as shown in Figure 4.42. This also tends to prove that the chemical equilibria are displaced and that the carbon conversion efficiency is increased by the addition of oxygen. To verify this assumption, carbon content of the ashes will be analysed in a near future.

Figure 4.43 presents the $CO/CO_2$ ratio as a function of temperature in the oxidation zone. The points are taken every 3 minutes during the whole run and the measurements start after the third hour of operations. The dispersion of the points is higher for the oxygen tests because, as seen in Figure 4.42, the composition and the $CO/CO_2$ ratio present bigger variation for oxygen gasification. Nevertheless, the trends indicate that the $CO/CO_2$ ratio increases with the temperature.

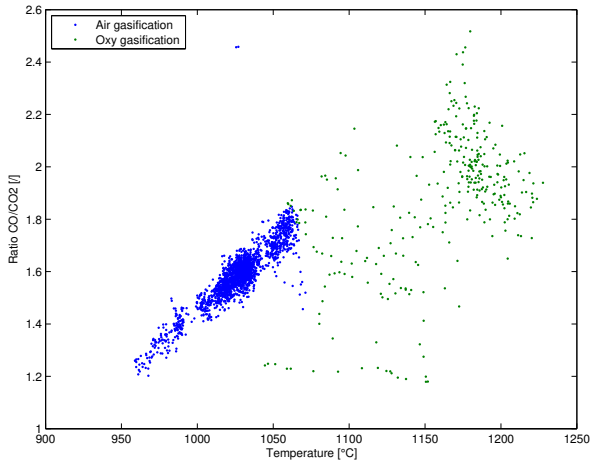


***Figure 4.43*** *– $CO/CO_2$ ratio as a function of temperature for air and oxygen-enriched air gasification.*

This preliminary research proved the interest for oxygen-enriched air gasification to increase the LHV and the carbon conversion efficiency of biomass.

## 4.4 Waste gasification

As the competition for wood utilisation is increasing (construction, energy, furniture, etc), new biomass become of interest for gasification. This section presents results of research on waste biomass that show great potential for energy production. The first one is sewage sludge which is really interesting thanks to his huge supply [80]. The second one is creosoted wood from railroads ties: they are made of wood so the only additional parameter is the pollutant and great quantities of ties are also available for energy recovery [81, 82].

### 4.4.1 Sewage sludge

Sludge management first aims are waste reduction and stabilisation. More recently, another goal has been added which is energy recovery to reduce the negative costs of water and sludge treatment. Gasification could meet both objectives by recovering energy and reducing the amount of wastes drastically. The other ways of treatment are digestion and incineration which have respectively a lower stabilisation potential and a lower energy recovery efficiency as illustrated by Figure 4.44.

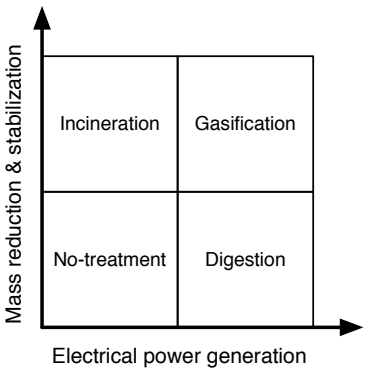


***Figure 4.44*** *– Illustration of the advantages of using gasification for sewage sludge treatment.*

At the outlet of the gasification process, the pollutants contained in the sludge are found in two flows: the solid ashes and the syngas. The mineral content of sewage sludge (including metals in certains cases) is found in the ashes at the bottom of the gasifier meaning that no special treatment is required for

the syngas in order to collect this unwanted part of biomass. These ashes can be disposed in a landfill since they are inert. They can also be incinerated to recover the carbon that could not be converted in the gasification process if its share in the ashes is significant but they could induce slagging depending on their composition. As they often contain heavy metals or other pollutant, they should not be used on agricultural soil as fertiliser. The gaseous pollutants (e.g. ammonia) found at the outlet of the reactor can (if needed) be treated more easily than in incineration plants since it can be done before combustion. The treatment can thus be applied on cold gas ($< 20$ $[°C]$ at the outlet of the gas cleaning system) when pollutant concentrations are higher than in flue gases (where pollutants are diluted by the nitrogen of the air of combustion).

| Elementary analysis | Wood | Sludge A | Sludge B |
|---|---|---|---|
| C | 0.5 | 0.36 | 0.39 |
| H | 0.06 | 0.04 | 0.06 |
| O | 0.44 | 0.24 | 0.27 |
| N | 0 | 0.05 | 0.04 |
| Ashes | 0.01 | 0.3 | 0.25 |
| y | 1.44 | 1.48 | 1.69 |
| x | 0.66 | 0.49 | 0.52 |
| z | 0 | 0.12 | 0.08 |

***Table 4.8*** *– Chemical composition (mass fraction dry basis) of wood, sludge A and sludge B and numerical values for the $CH_yO_xN_z$ ash free formula.*

Sewage sludge composition on dry and ash free basis is close to wood as shown in Table 4.8. The main difference comes from ash content and has a major impact on the LHV. The LHV of wood is found to be between 16 and 19 MJ/kg while dried sludge tested is approximately 12MJ/kg. The low LHV is a minor problem for the gasification process but the thermal inertia of the minerals is a significant one. For the same amount of energy injected in the pyrolysis zone, minerals will lower the pyrolysis temperature that is critical for a proper gasification. Such conditions must be avoided to ensure the quality of the syngas. To reach sufficient pyrolysis temperatures, it is possible to mix the sludge with wood chips in different proportions to lower the concentration of minerals and decrease the influence of differences of kinetics. For this reason, the gasification of different mixtures of sludge and wood has been studied. High mineral matter

content could also lead to problematic clinkers production because of the low melting point of some components even if the ash content has proven to be less important than the nature of ashes [83]. However, in a two-stage gasification unit, the residence time at high temperature is very short, avoiding the risk of melting.

The two types of sludge tested differ from the processes they come from, giving them a slightly different compositions but a major difference in their conditioning. Their geometrical differences lead to differences in gasification performances. Sludge A was made of small spheres and could only be gasified successfully by mixing them with wood in 50/50 proportion. Sludge B was made of small cylinders and could be gasified successfully without the addition of wood.

The two types of sludge presented very close ThermoGravimetric Analysis (TGA) results. The TGA were performed on ground sludge and showed similar results as expected as their composition is similar (cfr. Table 4.8). The assumption is that the physical properties of the sludge acquired through the conditioning process conferred to the two type of sludge very different heat conductivities. The bulk density of sludge A was roughly 400 $[kg/m^3]$ when the bulk density of sludge B was roughly 800 $[kg/m^3]$. This lead to significant differences in the heat transfer inside the particles and the particles bed and on the pyrolysis process. This hypothesis could be confirmed by a macro-TGA but this test could not be performed during these experimental campaigns.

Table 4.9 shows the gas composition obtained in similar conditions for the two types of sludge. The natural wood results are also presented as a reference even if waste gasification is not really comparable to wood gasification..

| | Wood | Sludge A | | Sludge B | | | |
|---|---|---|---|---|---|---|---|
| Proportion of sludge | 0% | 50% | 75% | 50% | 60% | 75% | **100%** |
| $CO$ | 16.2% | 13.3% | 7.8% | 16.1% | 14.3% | 16% | **13.8%** |
| $H_2$ | 15.5% | 11.5% | 10.5% | 16.4% | 15.3% | 18.4% | **16.6%** |
| $CO_2$ | 12.1% | 10.3% | 11.3% | 13.3% | 12.5% | 11.1% | **10.9%** |
| $CH_4$ | 0.7% | 0.3% | 1.8% | 1.1% | 1.1% | 1.8% | **1.7%** |

***Table 4.9*** *– Gas composition (volume fraction) of syngas tests with wood and sludge A & B.*

The hydrogen, carbon monoxide and carbon dioxide contents are comparable between wood and tests with sludge B. The biggest difference is the methane content that is normally a sign of increased tar content. It should be interesting to test the level of tars for sludge gasification in further developments.

Analysis were also made on heavy metal capture and they revealed that 90% of metals contained in the sludge were left in the facility. Only 10% of them were found in the gas, mainly chromium and antimony (N.B. no mercury in studied sludges).

### 4.4.2 Creosoted wood

The wooden railroad ties have a lifespan of approximately 50 years. When replaced, they need to be stored and destroyed very carefully because they are impregnated by creosote and polluted by the rail use. The main problem of these ties are the polycyclic aromatic hydrocarbons (PAHs) they contain. They need to be burnt at high temperature to be destroyed, releasing the heavy metals contained in the ties. They thus require heavy gas treatment in suitable incinerators. Gasification could present an alternative as it possesses a high temperature combustion zone followed by a colder char bed that acts as a filter for heavy metals. This thus solves the two issues posed by creosoted ties.

As it is only polluted wood impregnated with tar, the operation conditions are similar to natural wood gasification, the metal content is too small to have any influence at all. Figure 4.45 shows that the composition of the syngas is similar to the one obtained with natural wood. The main differences reside on the

stability of the process, which is slightly lower for creosoted wood due to the management of pressure losses.

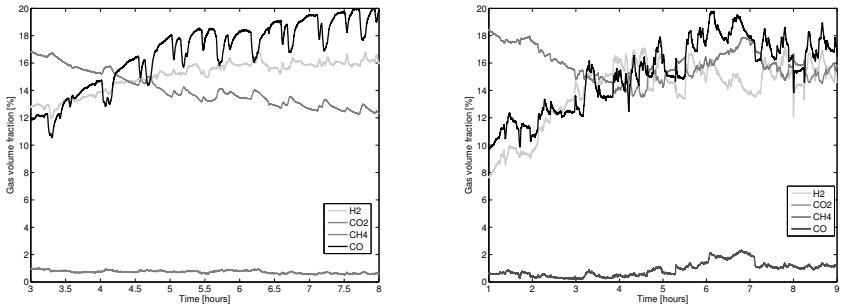


***Figure 4.45*** *– Syngas composition comparison for a test using natural wood (on the left) and creosoted wood (on the right). Methane is represented in grey between 0 and 2%, Carbon monoxide is dark grey, Carbon dioxide is light grey and Hydrogen is black. The syngas composition is similar for both feedstocks.*

The only interest of this campaign is to look at pollutant capture and PAH destruction. The gas was injected into a cogeneration engine to measure pollutant at the exit of the engine, and compare the emissions to the regulation regarding class B wastes incineration centers. Figure 4.46 presents emissions at the outlet of the gasifier and compares it to the regulation limits. Carbon monoxide is the only emission exceeding the limit. Nevertheless as syngas contains 20 % of it, the presence of a carbon monoxide content higher than the regulation is not a sign of a poor combustion (as it is usually for other fuels) and it could be discussed with the regulator. The only other important emission is mercury because it is not well captured by the char reduction bed due to its low melting point (below 0 $[°C]$).

The gas analysis on this campaign allowed to develop a small empirical predictive tool. Based on the concentrations of pollutants (e.g. heavy metal or PAHs) in the biomass, it is possible to estimate the concentration in the gas at the outlet of the engine. The gas yield and the dilution into the engine flue gas gives a theoretical maximum concentration considering all the pollutants are found in the gas. A second approximation is made considering that the pollutant capture potential of the process is the same as the lowest measured one during experimental campaigns. This tool can help determine if an ad-

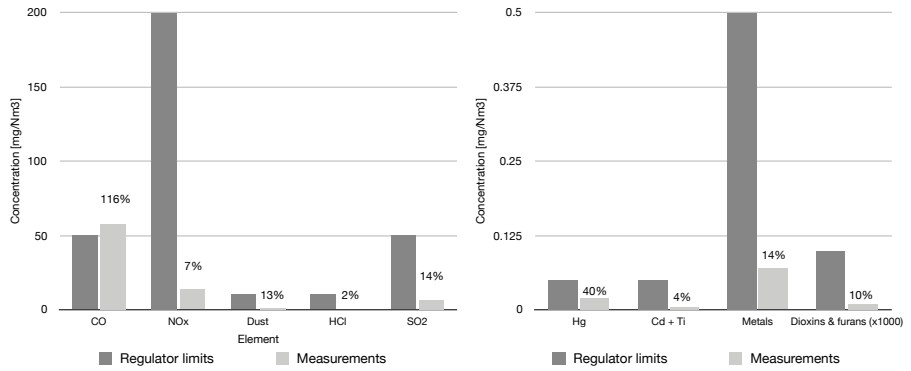


***Figure 4.46*** *– Engine emissions in light grey compared to the emission limits in Europe in dark grey.*

ditional treatment on the gas will be mandatory. Of course as it is based on experiments, additional tests are required to validate the pollutant content at the outlet of the engine.

Table 4.10 presents the efficiency of filtering of the gasification process when using polluted biomass.

| Element | Filtering efficiency |
|---|---|
| Cadmium & Thalium | 98.3 % |
| Chlorine | 99.6 % |
| Fluorine | 98.4 % |
| Mercury | 28.5 % |
| Sulfur | 94.5 % |
| Other metals | 99.9 % |

***Table 4.10*** *– Filtering ratio measure.*

The measurements from Table 4.10 were made during tests using creosoted wood as a feedstock. The efficiency is calculated as the amount of pollutants removed (difference between pollutant at the inlet and the outlet) on the total amount of pollutants at the inlet of the gasifier. It can be noted as:

$$\text{Filtering efficiency} = \frac{\dot{m}_{Poll,inlet} - \dot{m}_{Poll,outlet}}{\dot{m}_{Poll,inlet}}.$$

Table 4.10 shows that Chlorine, Fluorine and heavy metals are filtered by the gasifier as only a small percentage is found in the syngas. The hypotheses are that metals are found in the ashes while chlorine and fluorine may be present in the ashes and in the polluted water produced by the gasifier. Unfortunately, the other output of the process (ashes, fine ashes or polluted water) or the wood sawdust filter were not analysed so there is no data to validate these hypotheses.

Table 4.10 shows that sulfur filtering efficiency is high too even if a little bit lower than for the other compounds. If sulfur is captured by the polluted water, its pH can become acidic and lower the filtration efficiency on longer runs. For industrial applications, a pH regulation system is thus considered on the water filter to maintain the pH level in a desired range and avoid saturation of the water.

Finally, tests showed that mercury, the lightest metal, is going through the whole process with only a slight filtering effect. It is thus found in significant amount at the outlet of the engine and should be considered with more attention.

## 4.5 Chapter summary

This chapter presented four types of experimental results obtained on the T.G.P. The first ones are the validation of the experimental setup through mass and energy balances. They point out that the main energy losses of the system are the unconverted char and the wall losses. If the char conversion ratio could not be improved further, a valorisation of this char could improve the energy efficiency of the overall process.

The second experimental results presented in this chapter focus on key parameters of the process that are the air ratio, the pyrolysis zone residence time and the porous medium injection in the pyrolysis zone. The air ratio investigations showed that an optimal air ratio could be found depending on the biomass used. This optimum presents the best syngas composition while maintaining a low level of tars in the syngas. The influence of the residence time show that a reduced residence time at higher temperature presented a small improvement

of the syngas quality while the stability of the process decreased. The porous medium injection showed an increased stability of the process while maintaining a similar syngas quality and the combination of these two modifications should be investigated further.

The third section of this chapter presented the promising results of oxygen enriched air gasification. The syngas LHV is increased along with the conversion efficiency and further developments to increase even more the oxygen content should be investigated further.

Finally this chapter presented successful tests of waste gasification. I also showed that the gasifier could act as a filter and propose an alternative to current waste treatment technologies.

The next chapter will focus on the pyrolysis step with experimental results and numerical simulations.

# Chapter 5

# Oxidative pyrolysis step of the gasification process

The experimental campaigns lead on T.G.P. proved that the pyrolysis step is critical for the gasification process and the resulting tar content in the syngas. Tests with biomass having similar composition and LHV showed significantly different operating condition in the gasifier, mainly due to their pyrolysis characteristics (measured thanks to a thermo gravimetric analysis - TGA). This chapter details the investigations lead in order to increase the knowledge on this critical step of the gasification process.

The first section of this chapter describes the experimental measurements of the products of the pyrolysis zone on T.G.P. The other sections describe the numerical tools developed and the results obtained in this thesis in order to help predict the pyrolysis products. The second section presents the general context that lead to the choice of a coupling between a particle model and a flow simulation. The third section presents the first numerical tool that is a particle model named SPY, developed by J. Blondeau [78], adapted and used in the present work to produce pyrolysis data. The fourth section of this chapter presents the numerical model for the pyrolysis zone flow and the fifth section discusses the results obtained with this model. The chapter ends with the comparison between the numerical and experimental results and a summary of the key points of the chapter.

## 5.1 Experimental measurements of the pyrolysis products

As the pyrolysis revealed itself critical for the gasification process, some measurement tools were implemented on the gasifier in order to investigate it in more details. This chapter presents the tools and results of the experimental campaign on the pyrolysis process. It starts with the description of the tar protocol installed on the setup, it then moves to the description of the char sampling instrument and ends with the results obtained thanks to these two apparatuses.

### 5.1.1 TAR PROTOCOL

As mentioned in the introduction, the pyrolysis of wood produces a wide variety of molecules going from the light volatile hydrocarbons to large polyaromatic hydrocarbons. In order to characterise the composition of pyrolysis gases, they are divided into two categories: non-condensables and condensables regarding their state (respectively gaseous or liquids) at ambiant temperature or at the reference temperature of the process. Condensable gases represent a relatively small number of species including $H_2$,$CO$, $CO_2$, $CH_4$ and some light hydrocarbons like $C_2H_4$. Gaseous species measurement is not difficult, even if it requires adapted analysers and a rigorous use. It can be made online and continuously. Measuring pyrolysis condensable species is less known and in order to standardise the discussions on the pyrolysis products, a measurement method applicable to all types of gasification was developed as said in the introduction. Its name is the TAR PROTOCOL.

The standardised sampling method has been defined by an association of scientists and is detailed in a paper from 2000 [8]. The TAR PROTOCOL is a series of guidelines and recommandations adapted to the type of application. The TAR PROTOCOL implementation installed on TGP is presented in Figure 5.1. It is constituted of:

- A non iso-kinetic probe inside the gasifier. The iso-kinetic probe is not required as particulate matter content is not measured and the sampling is made at a temperature above 350[$^\circ C$] (cfr. [7]).

- A heated pipe to avoid condensation of the tars before the sampling bottles.
- A heated dust filter to capture the solid particles without condensing the tars.
- A series of 4 impinger bottles placed in a water bath at ambient temperature to collect heavier tars. It is made of 1 empty bottle and 3 bottle containing isopropanol.
- A second series of 3 bottles in a glycolated water bath maintained at -20$[^{\circ}C]$ to collect lighter tars. It is made of 2 bottles containing isopropanol and one empty bottle with a sintered quartz. The P&ID shows 3 parallel lines of bottles in the cooled chamber. The three lines are used to repeat tests quickly as everything is already at the required temperature.
- A final filtering bottle containing silica gel (placed at the outlet of the cooling chamber). Its goal is protecting the rest of the line, not collecting samples like the other bottles.
- A volumetric pump and a valve mounted in parallel to ensure the control of the flow.
- A rotameter to measure the flow though the apparatus.
- A volumetric flow meter to measure the volume of gas analysed during a test. The line is equipped with a temperature and a pressure measurement in order to adjust the volumetric measurement.
- The gas analysis system is made of 3 systems in parallel:
  - A gas chromatography with a Thermal Conductivity Detector (TCD) and a Flame Ionisation Detector (FID). The GC is saturated by the permanent gases contained in pyrolysis gas so it requires additional gas analysers. The GC is a model N611-00B from Perkin-Elmer. The gas sampling is realised with an Hamilton gas syringe of 1 $[ml]$. Refer to [84, 85] for detailed description of the GC-FID-TCD setup.
  - A thermal conductivity detector for $H_2$
  - An infrared analyser for $CO$, $CO_2$ and $CH_4$

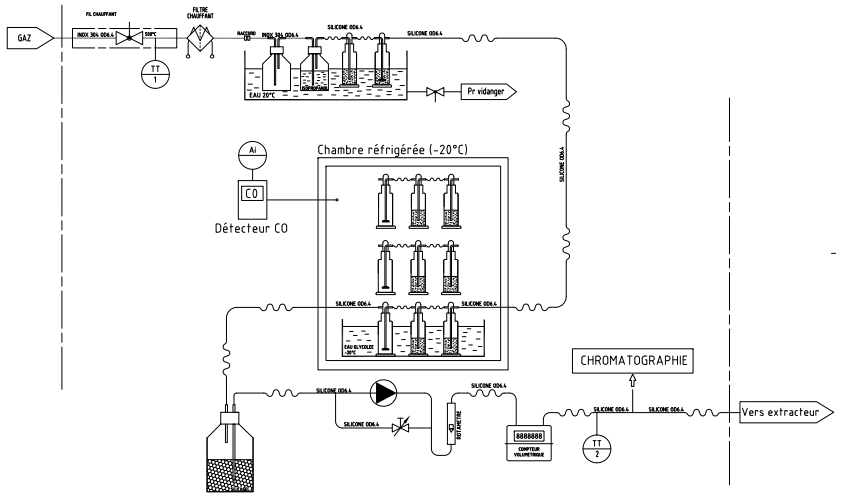


***Figure 5.1*** *– P&ID of the tar protocol system installed on the pyrolysis zone of T.G.P.*

This system allows the measurement of permanent gases and some light hydrocarbons and the collection of samples of heavier compounds that have been analysed in an external laboratory (CIRAD, Montpellier).

### 5.1.2 Char sampling

It is easy to extract gas from the pyrolysis zone to analyse it. However, it is more difficult to extract solid particles of biomass at the bottom of the pyrolysis zone. A special probe has been designed to collect biomass char samples from the pyrolysis zone. The probe, presented in Figure 5.2, is a cylinder containing a worm with an opening on one half of the cylinder at the end of the probe. The probe is filled with char by rotating the handle of the probe. This handle is connected to the worm gear which advances the char thanks to its helicoidal shape. The probe is inserted inside the gasifier through an airlock in order to avoid gas leaks to the atmosphere.

Once the probe is full of pyrolysed biomass, it is retrieved inside the airlock where nitrogen at ambient temperature cools it down in order to prevent further reactions. The char is thus "frozen" in its end of pyrolysis state. It is then sent for immediate and elemental analysis at an external laboratory (CIRAD, Montpellier).

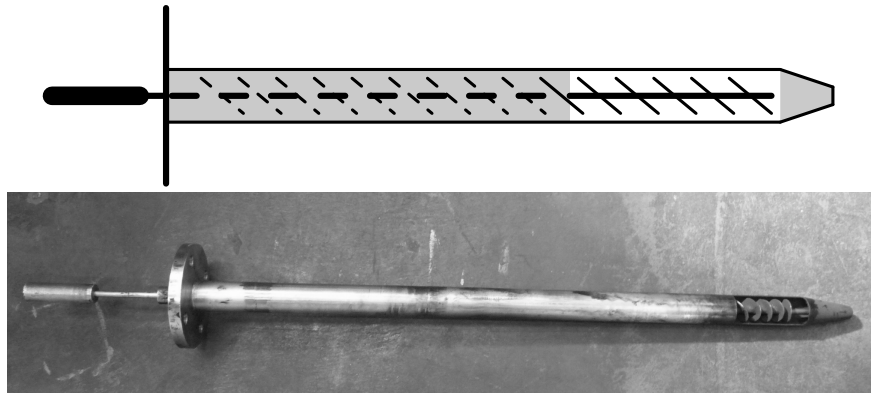

***Figure 5.2*** *– Illustration and picture of the char sampling probe.*

### 5.1.3 Wood gasification results

Several tests were made and the results are detailed in the master thesis of Elisabeth Bries & Arthur Leveau [77]. This section presents one test representative of the whole tests made on the pyrolysis zone. Table 5.1 summarises the operating conditions of the reactor for the test presented in this section.

| Characteristics | Units | NOTAR® data |
|---|---|---|
| Reactor diameter | $[m]$ | 0.60 |
| Mean pressure | [atm] | 1.133 |
| Mean temperature | $[°C]$ | 530 |
| Air flow | [kg/h] | 18.4 |
| Biomass flow | [kg/h] | 42.5 |
| Biomass moisture | $[\%_{dry\ basis}]$ | 5.90 |
| ER (for pyrolysis zone only) | [-] | 0.073 |
| SGR | $[kg_{biomass}/(m^2h)]$ | 150.24 |

***Table 5.1*** *– Summary of the operating conditions.*

Some non-condensable gases ($CO$,$CH_4$ and $CO_2$), measured through the IR analyser are also measured by the GC-TCD-FID setup and present similar results (when the GC-TCD-FID sensor is not saturated due to different scales for the two experimental apparatuses).

Figure 5.3 presents the estimated distribution of mass at the outlet of the pyrolysis zone. The gaseous species represent more than 60% of the mass while

water and char account for approximately 20% of the mass each. Tars represent only one percent of the total mass which can not be neglected as even a small amount of tars can cause problems for industrial applications.

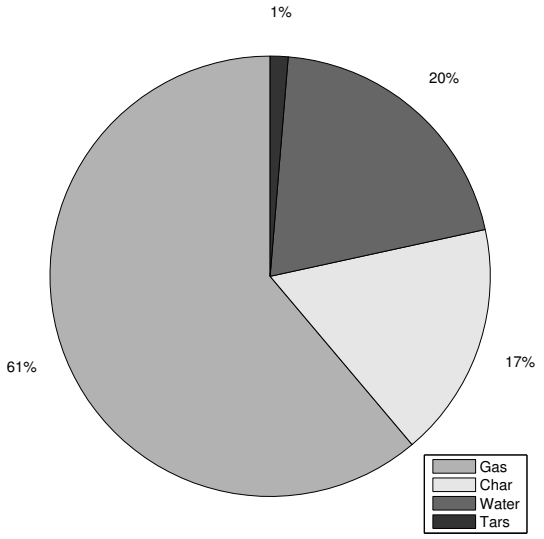


***Figure 5.3*** *– Composition of the pyrolysis products at the outlet of the pyrolysis zone.*

Figure 5.4 presents the composition of the permanent gases measured through the IR analyser during a sampling of the pyrolysis gases using the tar protocol. Before starting the measurement, the piping and all the elements of the tar protocol are filled with nitrogen to forbid reactions between pyrolysis gases and oxygen that could be present if the sampling system was open to the atmosphere. It takes approximately 3 minutes to evacuate the nitrogen. This is due to the low volumetric flows in comparison to the volume of the sampling installation (all the impinger bottles and filters). After that, the composition shows a good stability and low fluctuations in the measurement during the rest of the test.

The gas with the highest content is obviously nitrogen coming from the air injected in the pyrolysis zone. The second gas in concentration is the carbon dioxide produced by the partial combustion of pyrolysis gases. Hydrogen and carbon monoxide are also in significant proportions. They are produced by the incomplete partial combustion and the cracking of the heavier species in the pyrolysis products, not by a reduction reaction as it is the case for the third re-

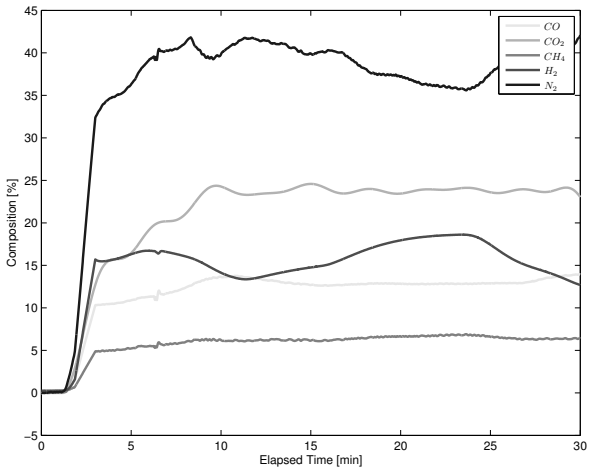


***Figure 5.4*** *– Composition of the fraction of permanent gases at the outlet of the pyrolysis zone.*

action zone of the process. The hydrogen content shows the biggest variations during the test and this is not explained as all the parameters of the process are steady. The assumption is that variations in hydrogen are caused by variations in the moisture content of the wood. When wood starts to pyrolyse, it releases its water, hence modifying the quality of the partial combustion locally and producing more or less hydrogen depending on the moisture content. This assumption could not be verified as the measurements of carbon monoxide and dioxide contents are constant. As mentioned earlier, the nitrogen content is not measured but deduced by the measurement of other gases so its variations are a consequence of the variations of the hydrogen content.

Table 5.2 presents a detailed analysis of the permanent gases obtained at the outlet of the sampling system. The composition reflects the species still present in the gaseous phase after the impinger bottles at -20 [$°C$]. The gas is sampled in a 5 ml syringe and injected into the GC-FID-TCD analyser. The results show a good agreement for the gases measured with the IR analyser and that molecules heavier than methane do not have a fraction higher than one percent. Adding all that heavier molecules measured by the analyser only represent less than 2 % in volume.

| $CO$ [%] | $CO_2$ [%] | $CH4$ [%] | $H_2$ [%] | $C_2H_4$ [%] | $C_2H_6$ [%] | $C_3H_6$ [%] | $C_3H_8$ [ppm] | $C_4H_{10}$ [ppm] | $EtOH$ [ppm] | $C_3H_6O$ [ppm] |
|---|---|---|---|---|---|---|---|---|---|---|
| 13.30 | 23.82 | 6.39 | 14.78 | 0.90 | 0.58 | 0.29 | 674.0 | 349.0 | 120.6 | 40.5 |

***Table 5.2*** *– Permanent gases composition.*

During these tests, the collected mass of tars was equivalent to a content below 30 $[g/Nm^3]$ at the outlet of the pyrolysis zone. This can be compared to the values met in updraft gasifiers were all the tars are found in the syngas due to the sequential order of the reactions in the updraft process.

Table 5.3 presents a summary of the analysis made on one sample of tars collected.

| Class | Measured concentration $[mg/l]$ | Concentration in pyrolysis gas $[mg/Nm^3]$ |
|---|---|---|
| Acids | 912.74 | 2.336 |
| Alcohols | Not Detected | ND |
| Aldehyde and ketones | 482.29 | 1.234 |
| Aromatics | 2866.61 | 7.337 |
| Furans | 483.5 | 1.238 |
| Guaiacols | 92.57 | 0.237 |
| HAPs | 236.00 | 0.604 |
| Nitrogenous aromatics | 29.22 | 0.075 |
| Phenols | 3506.06 | 8.974 |
| Sugars | 189.56 | 0.485 |
| Terpenes | Not Detected | ND |
| Total | 8798.55 | 22.52 |

***Table 5.3*** *– Condensed results of the tar analysis made by the CIRAD laboratory on one collected tar sample, full report in Appendix A.*

Table 5.3 shows that 72% of the tar collected are aromatics and phenols. It is also interesting to note that no alcohol was found in the sampled tars while ethanol was measured in the non condensable gas in traces.

The development of such tools and the collection of experimental data in the pyrolysis is useful for the development and the validation of numerical models of the oxidative pyrolysis of biomass occurring in this type of reactors.

## 5.2 Numerical simulation of the pyrolysis in the NOTAR® gasifier - General principles

There are several approaches to gasification modelling. As seen in Chapter 2 on alternative gasifying agents, the simplest models of gasification are equilibrium models. These models are not able to take the tars into account. They treat gasification as a black box: one reactor where all the reactions occur at the same time and are at equilibrium. To consider the production of tars, a more detailed model is required.

Di Blasi et al. propose a dynamic model of a fixed bed gasification reactor in order to capture its complexity [19]. The pyrolysis zone is particular as it is sustained by a partial combustion of the pyrolysis gases as in the NOTAR® technology. This type of combustion, called smoldering combustion, can be unstable and the dynamics inside such stratified beds arouses interest. Di Blasi et al. model is a quasi-continuous model where the solid phase and the gas phase co-exist at every point of the modelling domain. This type of model gives good prediction results when the gradients (temperature, gas concentrations) inside the particles are not significant. These limitations forbid a good prediction of the tar evolution inside the pyrolysis zone as it is influenced by the size of the wood chips.

Anca-Couce et al. [86] consider that the problem is multi scale as it involves flow simulations at the level of the reactor and thermal and chemical computations at the level of the particle. The most detailed solution for such problem is the Discrete Particle Model where each particle in the bed is considered and modelled in addition to the fluid phase flow and reactions. These types of models have high computational costs. For example, a team from the Exascale Computing Project [87] realised a simulation with MFIX-DEM of a lab-scale gasifier that tracks over a million particles and their interaction with the gas phase. Their goal is now to achieve a tracking of more particles to simulate a pilot scale plant.

Anca-Couce et al. [86] propose to use a model that is in between the quasi-continuous models like the one from Di Blasi and the DPM models as illustrated in Figure 5.5. This is the Representative Particle Model where one particle is

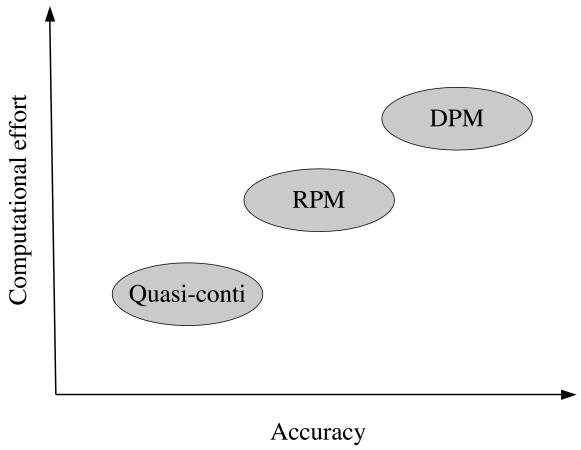


***Figure 5.5*** *– Comparison of performances between quasi continuous, DPM and RPM models. Illustration from Anca-Couce et al. [86].*

chosen as representative of a segment of the reactor as illustrated in Figure 5.6. This strongly reduces the computational costs in comparison to DPM models and allows a better prediction of the tar evolution than the quasi-continuous models.

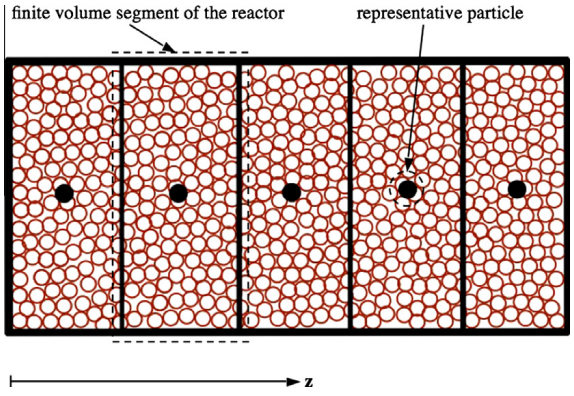


***Figure 5.6*** *– Illustration of the Representative Particle Model from Anca-Couce et al. [86].*

The model developed in this thesis is based on Anca-Couce et al. multi-scale idea of coupling a particle model to flow simulations. The two models do not work in parallel but interact together sequentially (the outputs from one model are used as inputs for the other). This is illustrated in Figure 5.7. The

algorithm starts with the particle model named "SPY" that stands for Single particle PYrolysis model developed by Julien Blondeau in his thesis [78]. The particle model has been slightly adapted to simulate pyrolysis of larger particles during increased residence times in comparison to the initial conditions it was built for. For the first iteration, SPY uses the experimental data from T.G.P. (i.e. the temperature profile in the pyrolysis zone). SPY simulates the gaseous emissions of the solid particles. The results are then transferred to Fluent® that realises a flow simulation with gas phase reactions using the data produced by SPY as inputs. Fluent® then calculates the temperature profile inside the pyrolysis zone that is afterwards transferred to SPY in order to produce a better approximation of the source terms from the solid particles. The loop illustrated in Figure 5.7 should converge in a few iterations. It is interesting to note that it mixes an Eulerian approach for the fluid simulation to a Lagrangian approach for the particle model. The model does not take solid phase reactions into account in order to keep it as simple as possible and reduce computational costs. It should be interesting to evaluate the influence of solid phase reactions and the interest to add them to the model.

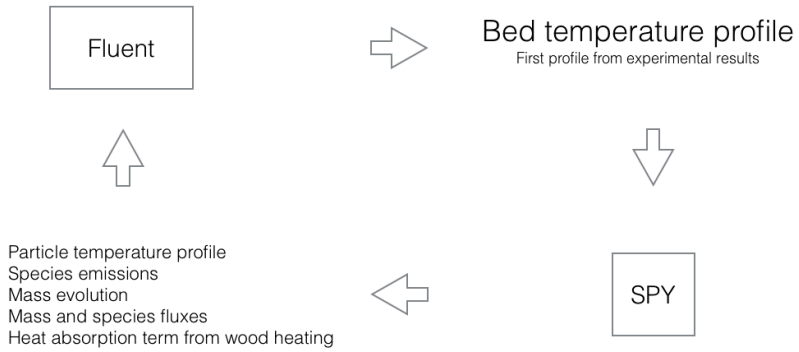


***Figure 5.7*** *– Illustration of the coupling of SPY and Fluent®.*

## 5.3 The particle model - SPY

This section briefly describes the particle model developed by Julien Blondeau [78]. The original model was developed to cope with problems encountered in industrial boilers working with pulverised woody biomass. Pulverised fuel boilers are a well known technology used in coal and biomass powered steam cycles.

The problem appearing when converting this type of boilers to biomass is that the particles of biomass are generally larger than coal particles after grinding (due to mechanical properties). The shape of the particles is also different, quasi-spherical particles for coal and quasi-cylindrical for wood. They can be of different shapes when using other sources of biomass. These differences induce modifications in the thermal behaviour. The problem that is generally thermally thin for pulverised coal particles becomes thermally thick for pulverised biomass particles. Also, the model was developed for particles of the size of 1-2 $[mm]$ and a residence time of several seconds and was adapted in the present work to be used for particles of the size of 1-4 $[cm]$ and a residence time of several hundreds seconds.

This section will start by describing the inputs and outputs of the particle model used in this thesis. It will then explain in details the particle geometry and the size distribution used in the simulations.

### 5.3.1 Particle model inputs and outputs

#### Inputs

The particle model describes the thermal decomposition of wood using kinetic schemes. As mentioned before, as wood particles are thermally thick, it also includes the heat conduction and the gas diffusion inside the particle. It is thus taking into account the thermal characteristics of the particle. The kinetic mechanisms used are based on the works of Miller & Bellan [88] and Ranzi [89].

Wood particles are decomposed into five main components: cellulose, hemicellulose, lignin, water and ash. The biomass is thus described using the mass fraction of these five components. At the moment, the model does not handle feedstocks that cannot be described by these components (e.g. sewage sludge, plastics).

The model uses the particle geometry and composition, the kinetic mechanisms and the thermal conditions to calculate the gaseous species emission as a function of time. On top of the residual charcoal, the model considers a thermal decomposition into 10 gaseous species (including water) and 10 tar species that are given in Table 5.4.

| Name | Atomic composition | CAS number |
|---|---|---|
| Gases | | |
| Hydrogen | $H_2$ | 1333-74-0 |
| Carbon monoxide | $CO$ | 630-08-0 |
| Carbon dioxide | $CO_2$ | 124-38-9 |
| Methane | $CH_4$ | 74-82-8 |
| Formaldehyde | $CH_2O$ | 50-00-0 |
| Methanol | $CH_4O$ | 67-56-1 |
| Ethylene | $C_2H_4$ | 74-85-1 |
| Acetaldehyde | $C_2H_4O$ | 75-07-0 |
| Ethanol (ETOH) | $C_2H_6O$ | 64-17-5 |
| Water vapor | $H_2O$ | 7732-18-5 |
| Tars | | |
| Hydroxyacetaldehyde (HAA) | $C_2H_4O_2$ | 141-46-8 |
| Glyoxal | $C_2H_2O_2$ | 107-22-2 |
| Propanal | $C_3H_6O$ | 123-38-6 |
| Propanedial | $C_3H_4O_2$ | 542-78-9 |
| 5-hydroxymethyl-furfural (HMFU) | $C_6H_6O_3$ | 67-47-0 |
| Levoglucosan (LVG) | $C_6H_{10}O_5$ | 498-07-7 |
| Xylose monomer (XYLAN) | $C_5H_8O_4$ | - |
| Paracoumaryl alcohol (p-Coumaryl) | $C_9H_{10}O_2$ | 3690-05-9 |
| Phenol | $C_6H_6O$ | 108-95-2 |
| Sinapaldehyde | $C_{11}H_{12}O_4$ | 4206-58-0 |

***Table 5.4*** *– Species produced by the decomposition of wood according to Ranzi's mechanism [89] used in SPY. The CAS number is the identifier delivered by the Chemical Abstracts Service.*

The model is time-dependent so the temperature profile has to be given as a function of time. In the gasification reactor, the particles are moving in a reactor considered at steady-state. The temperature profile inside the reactor is thus space-dependent. In order to use the particle model with an experimental profile to predict the particle emissions inside the pyrolysis zone, a conversion from space-dependent profile to time-dependent profile has to be made. This conversion is detailed in Section 5.4.4. The hypothesis is that the particles are moving with a constant speed through the reactive zone. This hypothesis links the space and time together and allows an easy conversion from one to the other. The speed is calculated by taking into account several parameters: the mass flow of biomass, the bulk density of biomass and the section of the reactor. This assumption is not exact as the solid bed movements are made by batches and the particle size changes through the pyrolysis process hence changing the bulk density of the biomass bed.

The experimental profile used as a starting point for the simulation is shown in Figure 5.8. It is taken from a test representative of typical conditions met at nominal power for air gasification with a high level of the pyrolysis bed, pyrolysis air injection above the particles bed and an air ratio around 0.25. The origin of the graph, the starting time, is the top of the particle bed. It is at room temperature. The first thermocouple presenting a temperature in the bed above the fresh wood temperature is reached by a particle after 1500 seconds and show a slight increase in temperature but not enough to trigger any chemical reaction (not even drying). The other thermocouples are reached at 1830s, 2200s, 2560s, 2930s and 3215s. To establish a first profile, they are connected together with a linear evolution.

Figure 5.8 shows a temperature of the fifth thermocouple that is lower than the fourth one which is normally not expected. This is due to the fact that the thermocouples are not one above each other as mentioned in the description of the measurement tools in Section 3.2.5. Anyway, the data is kept raw as iterations between the two models should smooth out experimental irregularities.

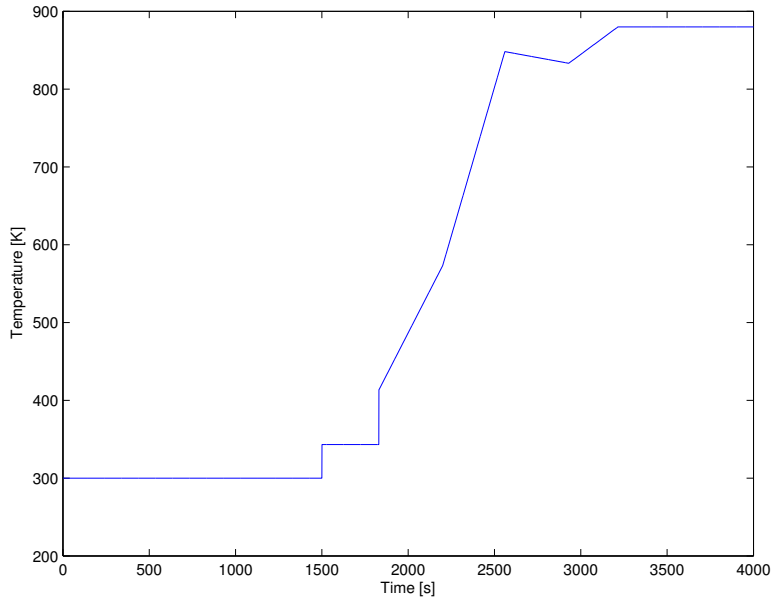


***Figure 5.8*** *– Experimental temperature profile observed by a solid particle inside the pyrolysis zone.*

### Outputs

SPY uses the temperature profile to calculate the emissions of gases as a function of time. It also calculates the heat absorbed by the particle during pyrolysis and its temperature profile. It thus gives the temperature of the emitted gases at the moment they leave the particle. This allows the calculation of their total enthalpy at the time of emission. This enthalpy is required by the flow model.

SPY outputs are processed and entered into the flow simulation model. The flow simulation model produces a new temperature profile that can be entered into SPY to iterate the solution. An example of profile produced by the flow simulation using a simplified gas phase mechanism is given in Figure 5.9. It will be discussed further in Section 5.4.4.

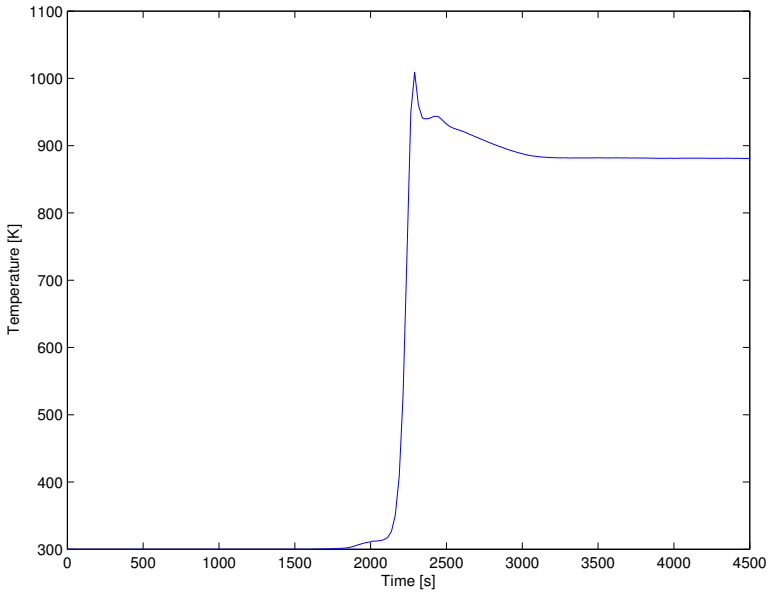


***Figure 5.9*** *– Temperature profile produced by the flow simulation using a simplified kinetic mechanism after one iteration on the particle model output.*

### 5.3.2 Particle characteristics

#### Particle geometry

The biomass used in the numerical study is natural wood in order to compare the results to the experimental ones obtained on T.G.P. The wood is conditioned into wood chips of different sizes and shapes.

In the model, the wood particles are assimilated to small cylinders with anisotropic characteristics due to the wood fibres. To reflect the variation of particle sizes in the biomass bed, three sizes were investigated in this thesis in order to emphasise the effect of the particles size on the results. The minimum size for particles is cylinders of 2 centimetres in height and 1 centimetre in diameter. The maximum size for particles is cylinders of 8 centimetres in height and 4 centimetres in diameter even if those larger particles represent a small part of the distribution. The model can calculate the data for the pyrolysis of different sizes and mix them together with a weighted average to obtain the data for a mix of particles.

Figure 5.10 presents the relative mass evolution limited to 3 different sizes of particles and the resulting profile for a mixture of particles from these 3 different sizes presenting the same composition and a moisture content of 5.9 $\%_w$ on dry basis. The mixture is composed of 30 $\%_w$ of the smallest particles, 15 $\%_w$ of the largest particles and 55 $\%_w$ of medium particles. The medium particles have an height of 4 $[cm]$ and a diameter of 2 $[cm]$.

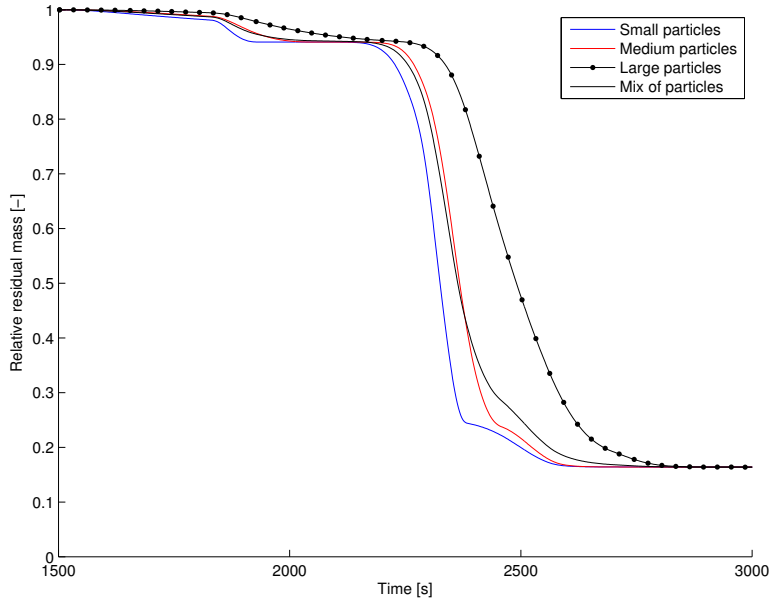


***Figure 5.10*** *– Relative mass evolution for 3 different sizes of particles and the resulting profile for a mixture of particles from different sizes.*

All the particles are exposed to the same temperature profile. This profile is taken from experimental data of the pyrolysis zone from T.G.P. (see Figure 5.8). The starting time of the profile is the top of the pyrolysis bed which is at ambiant temperature. The evolution is thus only shown for a residence time higher than 1500 seconds because the temperature before this time (below 80 $[°C]$) is not sufficient enough to trigger any significant reaction in the biomass particles.

The comparison of these mass evolutions illustrates the importance of simulating several representative particle sizes. The first decrease of mass observed on the particles corresponds to drying which occurs globally at the same pe-

riod for all particles. The drying of the particles shows only a slight difference (logically longer for the largest particles). On the other hand, the pyrolysis is much slower for the largest particles.

As the temperature profile inside the particle depends on the size, the pyrolysis process evolution will also show differences. The flows of gaseous species emitted by the particle is logically not similar. Figures 5.11 and 5.12 present the gas flow rates of the lighter gaseous species emitted respectively from small and large particles. Tars follow a similar trend. For the small particles, the flows are concentrated on a peak around the partial oxidation front while it is more spread out for the larger particles.

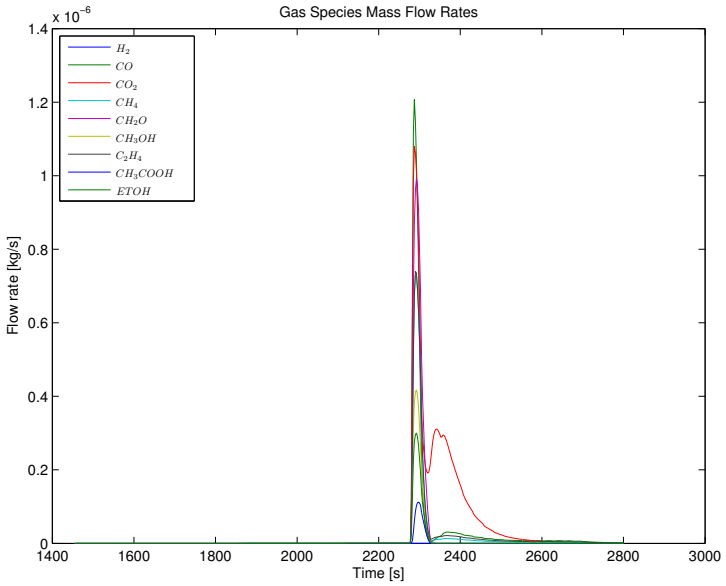


***Figure 5.11*** *– Emission rate of gaseous species for particles of 2 cm of height and 1 cm of diameter (moisture* $5.9\%_{db}$*).*

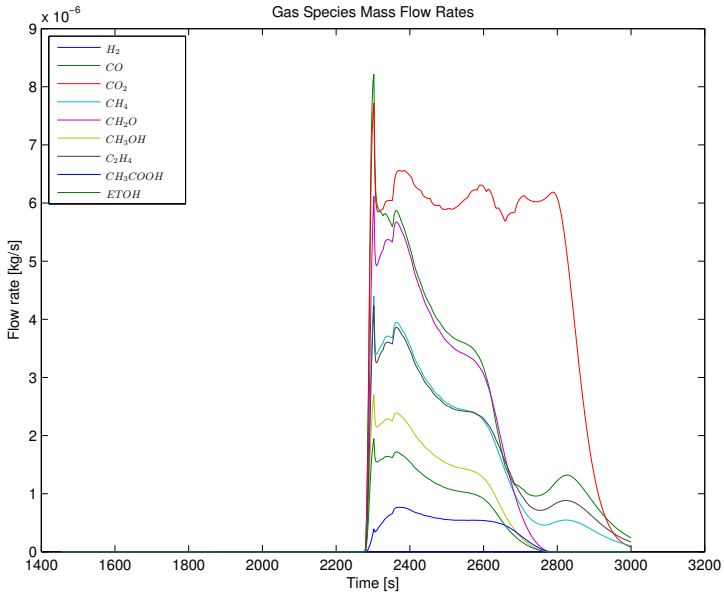


***Figure 5.12*** *– Emission rate of gaseous species for particles of 8 cm of height and 2 cm of diameter (moisture* $5.9\%_{db}$*).*

Table 5.5 presents the different reaction times for the small and large particles exposed to the temperature profile from Figure 5.9 with a combustion front between 2100 and 2500 [s].

| Size | End of drying | Start of pyrolysis | End of pyrolysis |
|---|---|---|---|
| Small particles (1x2cm) | 1950 [s] | 2100 [s] | 2600 [s] |
| Large particles (4x8cm) | 2200 [s] | 2250 [s] | 2900 [s] |

***Table 5.5*** *– Reaction times for small and large particles.*

One important conclusion is that the composition of gaseous and tar species emitted is globally the same for all particle sizes, as shown in Figures 5.13 and 5.14 that present the tar cumulated emissions expressed as a mass fraction of the initial mass of the particle. SPY seems to overestimate the production of Levoglucosan, a problem that is not critical and already observed and discussed in Julien Blondeau's work [78].

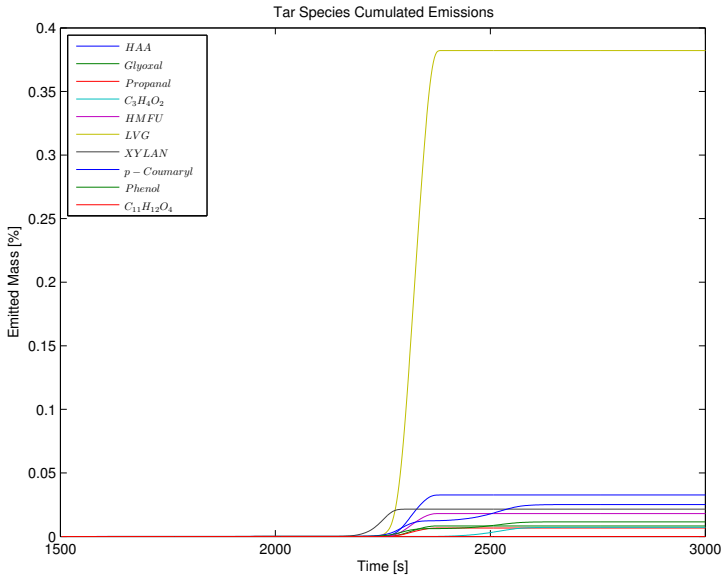


***Figure 5.13*** *– Total emitted mass of gaseous species for one particle of 2 cm of height and 0.5 cm of diameter presenting a moisture content of* $5.9\%_{db}$.

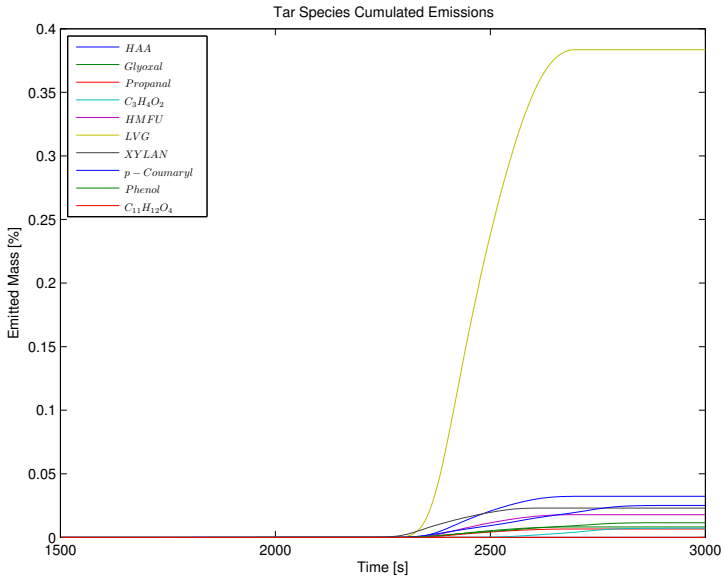


***Figure 5.14*** *– Total emitted mass of gaseous species for particles of 8 cm of height and 2 cm of diameter presenting a moisture content of* $5.9\%_{db}$.

For high residence times, the SPY model is not influenced by the moisture content. Most of the moisture content is evaporated during a first drying phase and the pyrolysis of dried wood is similar after this drying step. Figures 5.15 & 5.16 present the total relative emitted mass on dry basis of tars emitted for a case with $1.9\%_{db}$ moisture content and a case with $9.9\%_{db}$. They show that the moisture content does not influence the composition of the tars emitted by the particles. The conclusion is the same for gases on dry basis, the main difference is the water content.

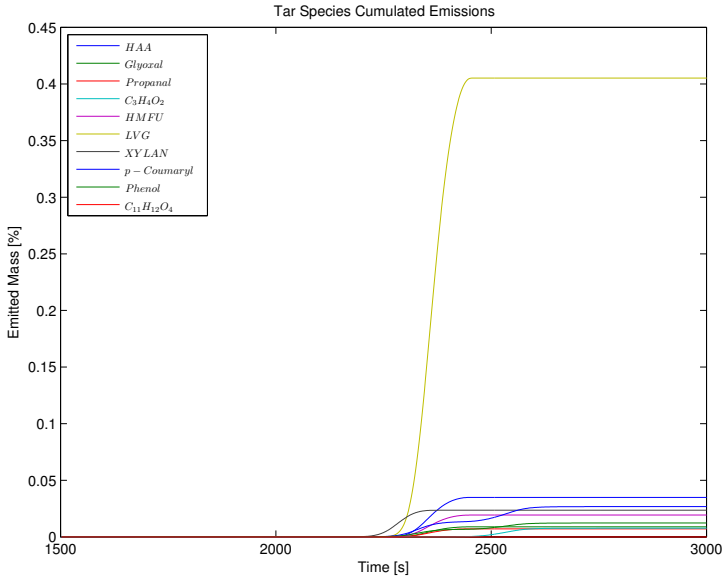


***Figure 5.15*** *– Total emitted mass of gaseous species for one particle of 4 cm of height and 1 cm of diameter presenting a moisture content of* $1.9\%_{db}$.

The variation of the moisture content induces a variation on the energy absorbed by the particles for the drying part of the process. On the experimental setup, an increase in the moisture content leads to a decrease in temperature of all the reactive zones if all other parameters are kept the same.

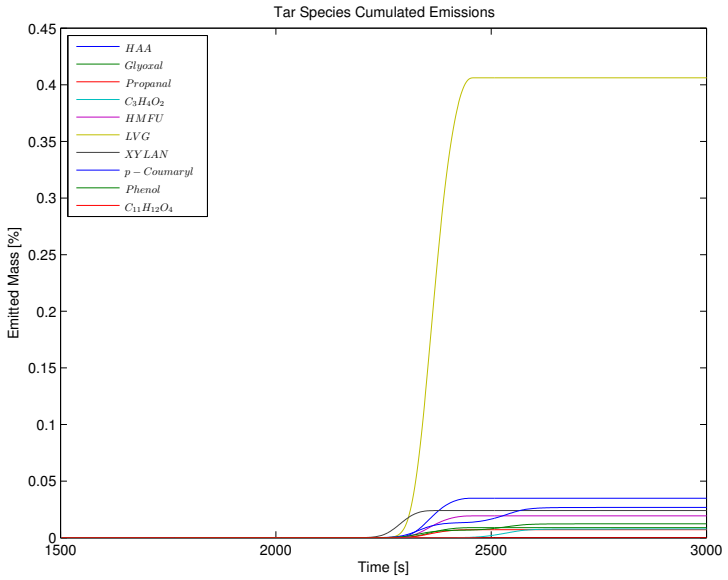


***Figure 5.16*** *– Total emitted mass of gaseous species for particles of 4 cm of height and 1 cm of diameter presenting a moisture content of* $9.9\%_{db}$.

### Biomass particle composition

The SPY model is, at the moment, implemented and validated for woody biomass. It is designed to consider particles with a composition made of a mix of cellulose, hemicellulose and lignin. The biomass is described by the mass fraction of these three compounds. The model also considers the moisture content of the biomass particle. Other compounds could be implemented easily, the only requirement is to have their pyrolysis kinetic scheme. SPY uses a modified version of the Ranzi mechanism [89] for hemicellulose, cellulose and lignin decomposition.

The composition chosen for the biomass is based on the ultimate analysis made on the wood used in the experimental campaigns. These analyses, presented in Table 5.6, allow to determine the composition of the wood and a generic formula for the biomass used in our experimental campaign as $CH_{1.423}O_{0.65}N_{0.0057}$.

| Characteristics | Experimental data |
|---|---|
| Moisture content (Mass % on wet basis) | 5.9 |
| Ash content (Mass % on dry basis) | 2.6 |
| Volatile matter (Mass % on dry basis) | 79.1 |
| Carbon content (Mass % on dry basis) | 48.9 |
| Hydrogen content (Mass % on dry basis) | 5.8 |
| Oxygen content (Mass % on dry basis) | 42.37 |
| Nitrogen content (Mass % on dry basis) | 0.33 |

***Table 5.6*** *– Ultimate analysis for wood used in the experimental campaigns.*

When looking at compositions in the literature, wood is generally composed of 50% of cellulose and the rest of hemicellulose and lignin. The proportions of cellulose, hemicellulose and lignin were chosen to be close to data found in literature and respect the ultimate analysis. The composition taken is thus given in Table 5.7.

| | |
|---|---|
| Cellulose (Mass % on dry basis) | 49.72 |
| Hemicellulose (Mass % on dry basis) | 26.52 |
| Lignin (Mass % on dry basis) | 23.76 |

***Table 5.7*** *– Estimated composition of wood in terms of molecules.*

As the model does not take ash and nitrogen into account, the chosen composition is selected to fit the wood composition on a dry, ash and nitrogen free basis. Table 5.8 gives the element composition used in the model with respect to the composition of the wood used for the experimental campaigns. The table also presents the experimental char formula that is taken as pure carbon in the particle model.

| Characteristics | Experimental data | Model data |
|---|---|---|
| Moisture content (Mass % on wet basis) | 5.9 | 5.9 |
| Carbon content (Mass % on dry & ash free basis) | 50.2 | 50.39 |
| Hydrogen content (Mass % on dry & ash free basis) | 5.95 | 5.98 |
| Oxygen content (Mass % on dry & ash free basis) | 43.5 | 43.63 |
| Nitrogen content (Mass % on dry & ash free basis) | 0.34 | 0 |
| Wood formula | $CH_{1.423}O_{0.65}N_{0.006}$ | $CH_{1.423}O_{0.65}$ |
| Char formula | $CH_{0.21}O_{0.04}$ | $C$ |
| Gas and Char content (produced by SPY model) | 84.2%/15.8% | 83.6%/16.4% |

***Table 5.8*** *– Ultimate analysis for test wood.*

## 5.4 Modelling the pyrolysis zone

This section presents the flow model used for the numerical simulation of wood pyrolysis in the pyrolysis zone of a NOTAR® gasifier. The first part of this section describes the flow model and the assumptions taken for the simulation. The second part of this section describes the geometry of the pyrolysis zone used in the simulations. The second part of this section presents the physical parameters taken as inputs in parallel to the choices made for the numerical simulation.

### 5.4.1 Geometry

The geometry used for the simulations is 2D axisymmetric. This choice was made in regard to the high computational cost induced by a full 3D simulation. The model is thus not able to capture the effect of the non-homogeneity of the air distribution. These effects are negligible as the size of the porous medium acts as a buffer.

The dimensions of the pyrolysis zone are as close as possible to the dimensions of the experimental gasifier T.G.P. The pyrolysis zone is divided into two parts. The first zone where the air is injected is located above the solid particle bed. This zone thus represents a gaseous plenum. The second zone starts at the top of the bed which can be set at several positions as seen in Section 4.2.2. For the simulation, it is set at the highest level which is the most stable one in experimental conditions. As said in the description of the process, the height of the pyrolysis bed is variable during the experiments but for the simulations, it is fixed at the mean position of the top of the bed. The wood particles forming the bed are represented by a porous medium.

The dimensions are shown on the left of Figure 5.17. The air injection is uniformly distributed on the perimeter of the pyrolysis zone in the simulation (the inlet is presented in red on the upper right corner of the pyrolysis zone) in opposition to the four points injection of the experimental setup. The first zone measures 200 [mm] while the second zone measures 950 [mm].

The biomass is fresh at the top of the porous bed then heats up and pyrolyses inside the particle bed just before the smoldering front where partial oxidation takes place as illustrated on the right of Figure 5.17.

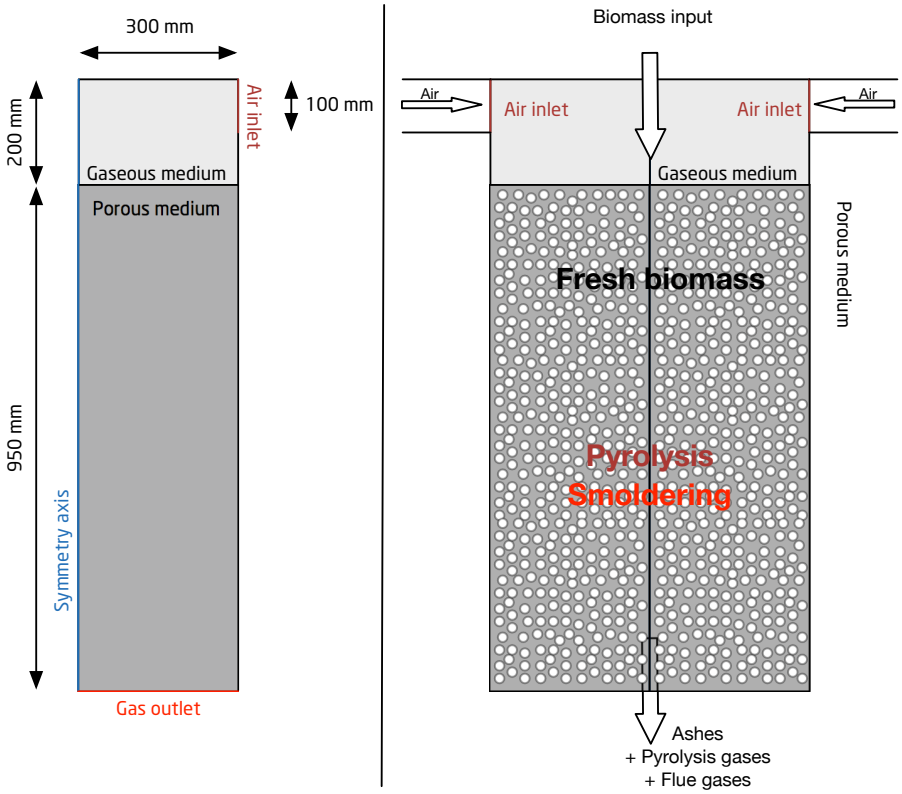


***Figure 5.17*** – *On the left: the pyrolysis zone is simplified into an axisymmetric model with dimensions corresponding to the T.G.P. gasifier. On the right: a representation of the full pyrolysis zone modelled with Fluent®.*

### 5.4.2 Flow characteristics

The flow through the pyrolysis zone is first evaluated thanks to experimental measurements in order to select the correct flow model. As the pyrolysis zone is divided into two zones, the flow will be analysed independently in each zone.

At the top of the reactor, the air injection in the pyrolysis zone varies from 12 to 25 $Nm^3/h$. This represents a mass flow of air of approximately 15 to 35 kg/h or 0.004 to 0.009 kg/s. For the following calculations, the air inlet mass flow is taken at the maximum value of 0.009 kg/s. The speed through the gaseous medium after the air inlet is thus:

$$\begin{aligned} u_{air} &= \dot{m}/(\rho \text{ x } S) \\ &= \frac{0.009\ [kg/s]}{1.25\ [kg/m^3] * \pi * 0.3^2\ [m^2]} \\ &= 0.0255\ [m/s] \end{aligned}$$

That allows to approximate the Reynolds number of the flow above the top of the porous zone as:

$$Re = \frac{\rho\ u\ D}{\mu} \approx 1050\ [/]$$

The flow through the gaseous phase can thus be considered as globally laminar even at the maximum inlet flow.

For the second part of the flow, the gas emitted by the wood particles have to be taken into account in order to evaluate the total maximum gas flow going through the porous medium. At the outlet of the pyrolysis zone, the volatile fraction of the wood is converted into gas so approximately 80% of the wood mass flow is added to the mass flux of air. The nominal flow of wood is approximately 40$[kg/h]$ or 0.1111$[kg/s]$. Hence the total flow of gas (air inlet & pyrolysis gases) should be approximately 0.0014 $[kg/s]$.

The composition of the reacting mixture of air and pyrolysis gas can vary hence the density is not a priori known. Nevertheless, an approximation can be made to estimate the Reynolds number as the density of the gas does not vary more than roughly 30%. The average molar mass is around 24 $[kg/kmole]$ and the maximal temperature measured at the outlet of the pyrolysis zone around 600 $[°C]$. This gives an approximate density for the partially oxidised pyrolysis gases of $\rho_g = \frac{M_m p}{RT} = 0.36\ [kg/m^3]$. This allows to estimate $u_g$ and $Re_g$ as:

$$\begin{aligned} u_g &= \frac{0.014\ [kg/s]}{0.3\ [kg/m^3] * \pi * 0.3^2\ [m^2]} \approx 0.165\ [m/s] \\ Re &= \frac{\rho_g\ u_g\ D}{\mu} \approx 5000\ [/] \end{aligned}$$

The flow through the porous medium is thus also globally laminar. The flow through the pores of the porous region may present a higher Reynolds number locally but porous medium flows at this Reynolds are not considered as turbulent. It could be important to simulate the flow through porous medium more precisely in order to capture the pressure drops accurately but it is not the objective of this work as the pressure drops measured on T.G.P. in the pyrolysis zone are negligible in comparison to the ones in the reduction zone.

### 5.4.3 Flow modelling

The Fluent® model is a 2D axisymmetric simulation of the flow through the pyrolysis zone. The biomass particle bed is modelled as a porous medium that includes a source of gases emitted by the biomass particles calculated by SPY.

The Fluent® model solves the Navier-Stokes equations for an incompressible flow with the presence of a source term. As shown in Subsection 5.4.2, the characteristics of the flow are globally laminar so terms linked to turbulence are neglected.

The equation of conservation of mass is given by:

$$\frac{\partial \rho}{\partial t} + \nabla \cdot (\rho \mathbf{v}) = S,$$

where $\mathbf{v}$ is the velocity vector, $\rho$ is the fluid density and S is the source term.

In the case of a reacting flow, the equation for each species is given by:

$$\frac{\partial}{\partial t}(\rho m_i) + \nabla \cdot (\rho \mathbf{v} m_i) = -\nabla \cdot \mathbf{J}_i + R_i + S_i,$$

where $m_i$ is the mass fraction of species $i$, $\mathbf{J}_i$ is the diffusion flux of species $i$ (due to gradient of concentration and temperature - defined by Fick's law), $R_i$ is the reaction rate of species $i$ given by the chemical reactions (hereby determined by Arrhenius kinetic expression) and $S_i$ is the species source term (hereby defined thanks to the data produced by SPY and detailed in Section 5.4.4).

The momentum conservation equation is given by:

$$\frac{\partial}{\partial t}(\rho \mathbf{v}) + \nabla \cdot (\rho \mathbf{v}\mathbf{v}) = -\nabla p + \nabla \cdot (\boldsymbol{\tau}) + \rho \mathbf{g} + \mathbf{F},$$

where $p$ is the static pressure, $\boldsymbol{\tau}$ is the stress tensor, $\mathbf{g}$ is the gravitational constant and $\mathbf{F}$ is the term linked to the mass source term $S$.

The energy equation solved by Fluent for the fluid phase above the particles bed is quite simple as it does not contain any source term or reaction, it is given by:

$$\frac{\partial}{\partial t}(\rho E) + \nabla \cdot (\mathbf{v}(\rho E + p)) = \nabla \cdot (k \nabla T - \sum_i h_i \mathbf{J}_i + (\boldsymbol{\tau} \cdot \mathbf{v})),$$

where $E$ is the total energy given by $E = h - \frac{p}{\rho} + \frac{v^2}{2}$ (with $h$ the sensible enthalpy of the fluid) and $k$ is the fluid thermal conductivity.

For the gas phase inside the porous medium, the energy equation is modified to take the porous medium presence into account. The assumption of thermal equilibrium is taken as the process is supposed at steady-state.

The equation is therefore given by:

$$\frac{\partial}{\partial t}(\gamma\rho_f E_f + (1-\gamma)\rho_s E_s) + \nabla\cdot(\mathbf{v}(\rho_f E_f + p)) = \nabla\cdot(k_{eff}\nabla T - \sum_i h_i \mathbf{J}_i + (\boldsymbol{\tau}\cdot\mathbf{v})) + S_f^h,$$

where $\gamma$ is the porosity of the porous medium, indices $_f$ are for fluid phase while indices $_s$ are for solid phase, $k_{eff}$ is the effective thermal conductivity (volume average of the fluid and solid conductivities) and $S_f^h$ represents sources/sinks of energy, in this case it is the sum of the sensible enthalpy of the mass source term and the energy absorbed by the wood bed (both terms are defined thanks to the data produced by SPY and detailed in Section 5.4.4).

### 5.4.4 Mesh

The mesh used for the simulation is made of 40680 rectangular cells. Rectangular cells are chosen as the geometry is regular. With the porous medium and the low velocity of the gases, the velocity in the radial direction is low, except in the gaseous zone. The mesh is thus fine at the walls to capture boundary effects (important temperature gradient) and then grows rapidly toward the center as the gradients in the radial direction are small. As the Reynolds is low, the constraint on the size of the cells imposed by the flow is low. In the reactive region, the mesh is refined due to high temperature gradients and high reaction rates.

Figure 5.18 presents the mesh with a zoom on the refinement made to capture temperature and reaction rate gradients in the reactive zone. It can be observed that the mesh is also refined radially near wall to capture wall effects.

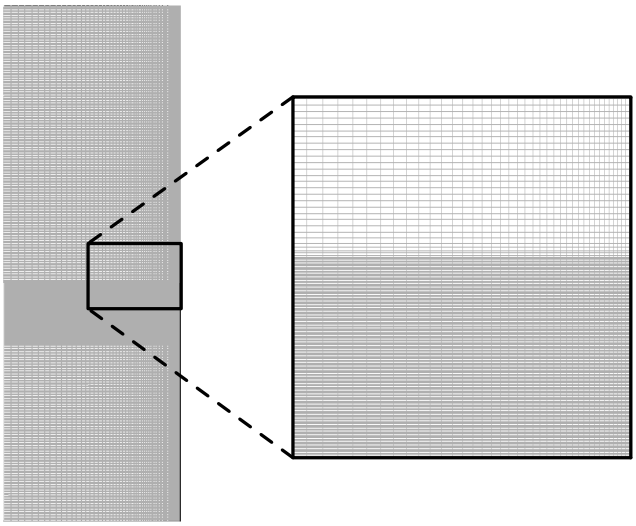

***Figure 5.18*** *– Illustration of the mesh of the pyrolysis zone with a zoom on the refined mesh around the reactive zone.*

### Viscous solver

This subsection presents the conditions applied on the viscous solver selected in Fluent®. The flow being globally laminar (see Subsection 5.4.2), the solver selected in Fluent® is the "Laminar solver".

The inlet condition is imposed in the model as a mass flow inlet. At the outlet of the reactor, located at the bottom, the imposed condition is the outlet pressure, based on experimental data. The inlet pressure is thus calculated by Fluent® in order to respect the mass flow inlet in regards to the pressure drops created by the particle bed and determined by the solver. These pressure losses are not significant as the gas velocity in the pyrolysis zone is low.

Pressure drops are mainly dictated by the porous medium properties so they have to be selected accurately. According to the work of Mayerhofer et al. [90], particles bed of irregular shaped wood particles present resistance that differ regarding the direction of the flow going though it. Their results show that for the largest particles (8.7 mm of diameter in their case), the value given for the permeability when the flow is axis to the bed is more than twice the one

when the flow is perpendicular to the bed. For the smallest particles, the ratio between the two permeabilities is only 1.4, suggesting that the permeability in the axis direction increases with the size of the particles. The value for largest particles is $K_{\parallel} = 26.4\ 10^{-8}[m^2]$ for the absolute permeability in the axis direction and $K_{\perp} = 13.0\ 10^{-8}[m^2]$ in the radial direction. This means that the flow is more difficult in the axis direction than in the radial one and axial movements are more limited than radial ones. These values are used in the numerical simulations presented in this thesis even if the impact on the flow characteristics is limited.

The porosity of the bed is also estimated, it stands at: $\epsilon = 60\%$, based on experimental measurements of wood beds inside a mockup reactor.

**Species Model**

The reactions occurring in the gaseous phase of the pyrolysis zone can be assimilated to a partial combustion of the pyrolysis gases released by the biomass. The air is injected above the top of the bed and is homogeneously distributed thanks to four nozzles located in the gaseous phase and thanks to the pressure drop created by the porous medium. The global reaction is thus a combustion occurring at a very low equivalence ratio (between 0.1 and 0.15).

The species emitted by the porous medium are taken from the SPY model and a suitable mechanism is then required. Dias et al. developed a kinetic mechanism for hydrocarbons containing as high as 12 carbon atoms [91, 92]. This mechanism is validated and well known by the UCL team so it can be easily adapted to suit the needs of the pyrolysis gases application. As the UCL mechanism covers too many hydrocarbons, it was decided to use a reduced mechanism that included hydrocarbons from $C_1$ to $C_6$, $H_2$ and $C_6H_6O$ to reduce the computational cost.

The list of species included in the reduced version of the UCL mechanism is: $H_2$, $H$, $O$, $O_2$, $OH$, $C_2H_5CHO$, $C_2H_5CO$, $H_2O$, $HO_2$, $CH_3$, $CH_4$, $CO$, $CO_2$, $HCO$, $CH_2O$, $C_2H_2$, $C_2H_3$, $C_2H_4$, $C_2H_5$, $HCCO$, $CH_2CO$, $H_2O_2$, $C_3H_3$, $C_6H_6$, $C_6H_5$, $C_6H_6O$, $C_6H_5O$, $C_5H_6$, $C_5H_5$, $CH_3CHO$, $CH_3CO$, $CH_3O$, $CH_3OH$, $CH_2OH$, $C_2H_5OH$, $CH_2CHO$ and $CH_3CH_2O$.

Unfortunately, this mechanism lack certains species that are present in the pyrolysis model from Blondeau. As the SPY pyrolysis mechanism is based on Ranzi et al. work, the combustion mechanism was extended using parts of the combustion mechanism from Ranzi et al. Their combustion mechanism [89, 93, 94], available on their website can be used for several types of applications and is thus too complex for the purpose of this thesis. It includes species that are not considered by SPY so these species and the reactions they were involved in have been removed. Afterwards, preliminary validations allowed to select the main conversion paths and remove the other species and their related reactions in order to reduce the mechanism and the computational costs it induces.

The list of species coming from Ranzi et al. mechanism is: $C_4H_6O_2$, $C_9H_{10}O_2$, $C_6H_8O_4$, $C_6H_{10}O_5$, $C_5H_8O_4$, $C_5H_4O_2$, $C_6H_6O_3$, $C_2H_2O_2$, $C_2H_4O_2$ and $C_{10}H_8$.

The full mechanism used in the numerical simulation is presented in Appendix B. It includes the 48 species mentioned earlier and is made of 227 reactions.

### Source terms Modelling

The Fluent® model used simulates the fluid flow through a porous medium. The interactions between the solid particles and the fluid are only considered with a Darcy law for the flow and the mass and energy exchanges are implemented using User Defined Functions (UDFs). These functions allow to expand Fluent® capabilities by allowing the user to modify characteristics of the simulation before the start of the simulation or during the simulation at each iteration. UDFs are coded in C and can call a library of predefined functions to access the simulation data. This subsection presents the implementation of UDFs to simulate the interaction between the solid particles and the gas flow.

The first part of this subsection focuses on the description of the mass source terms while the second part presents the energy source terms.

**From time dependence to space dependence -** The Fluent® model includes source terms based on the distribution of gas emission given by the SPY model. As mentioned earlier, SPY model gives the production of gases as a function of time while the flow modelling from Fluent® requires the gases emissions as a function of space. The SPY profile is thus converted into a space-dependent function thanks to the assumption of a constant speed for the solid particles. The biomass consumption is approximately $40kg/h$ with an apparent density of 200 $[kg/m^3]$ in the experimental gasifier with an intern diameter of 0.6 $[m]$, leading to a speed of: $u_s = \frac{\dot{m}}{\rho\ S} = 0.0002\ [m/s]$. The speed is the same for all the tests as the moisture content and particles size influences on the density (on dry wood) are neglected.

As the time and space discretisation do not have the same discretisation steps, the values of the detailed source terms are interpolated linearly. The description of this interpolation is given in this section.

It starts by converting the time vector with a discretisation step of 1 second into a space vector with a discretisation step of the size of the solid particle speed $u_s$. The position is given as:

$$l(t) \quad = \quad t * u_s,$$

with $t$ the time equivalent from the SPY model and $u_s$ the speed of the solid particles.

The algorithm used in Fluent® then acquires the values of the center of all cells in the mesh domain and stores it into a vector $x$. In order to calculate the emission of the cell, the difference of the mass at the inlet and the outlet of the cell is calculated. The source term in Fluent® is expressed in emission per unit of volume. It then multiplies this factor by the volume of each cell. The assumption made is that the emission rate is constant in a slice of the pyrolysis zone, as there is no significant radial gradient inside the reactive zone. The only important parameter is thus the thickness of the slice.

In order to take that into account, the position of the slice faces, $x_1$ and $x_2$ have to be calculated. These positions are illustrated in Figure 5.19.

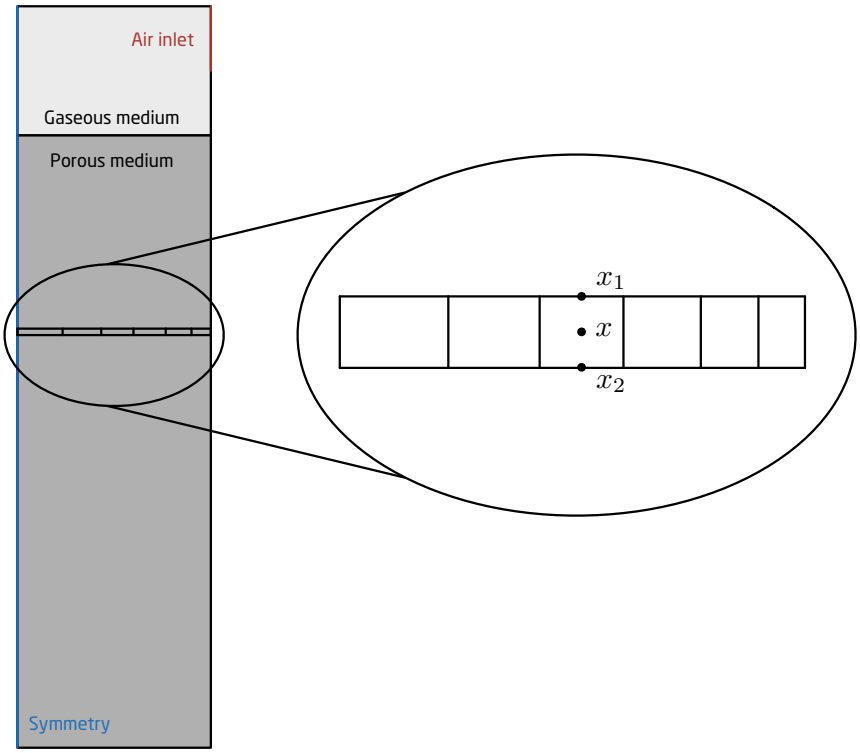


***Figure 5.19*** *– Illustration of the position of the cell faces for the space discretisation.*

The location of the cell faces can be expressed as:

$$\begin{aligned} x_1 &= x - d/2, \\ x_2 &= x + d/2, \end{aligned}$$

with $x$ the center of the cell, $d$ the height of the raw of cells, $x_1$ and $x_2$ the coordinates of the faces of the cell.

As the mass of the emitted gas is given on discrete positions that do not exactly match the positions of the faces, the mass values are interpolated as follows:

$$\begin{aligned} & \text{for} \quad l(t) < x_1 < l(t+1) \ : \\ m(x_1) &= m\Big(l(t)\Big) + \frac{x_1 - l(t)}{l(t+1) - l(t)} \ \Big(m\Big(l(t+1)\Big) - m\Big(l(t)\Big)\Big), \\ & \text{for} \quad l(t) < x_2 < l(t+1) \ : \\ m(x_2) &= m\Big(l(t)\Big) + \frac{x_2 - l(t)}{l(t+1) - l(t)} \ \Big(m\Big(l(t+1)\Big) - m\Big(l(t)\Big)\Big). \end{aligned}$$

The total amount of gas released by the cells between the two faces $x_1$ and $x_2$ is expressed as:

$$m_{\%} = \frac{m(x_1) - m(x_2)}{m_{total}}.$$

Figure 5.20 illustrates the calculation for the mass source term for a position $x$ that stands between $x_1$ and $x_2$.

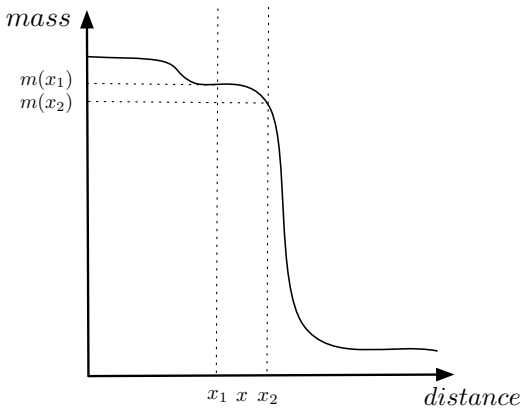


***Figure 5.20*** *– Illustration of the mass source term calculation.*

The conversion between the two different discretisation schemes presents an error of approximately 0.15 % due to interpolation errors.

This fraction of mass is then converted into a volumetric emission term using the volume of a slice of the pyrolysis zone of one cell height. As it is a fraction, it can be adapted to the chosen flow of biomass. The source term is thus given as:

$$\text{Mass}_{source} = m_{\%} * \dot{m}/\text{Volume}_{section}$$

The main assumption made to convert from time-dependence to space-dependence is the constant speed of solid particles (the particle shrinking due to pyrolysis is neglected). The flow of dry biomass is hereby determined thanks to experimental data and fixed for the simulations. Hence the wet biomass flow is calculated in regards to the biomass moisture content to maintain the same flow of dry biomass matter. The moisture content does not influence the speed of particles (linked to their volume and not their weight) but it will change the species emission profile and the amount of water released by the particles.

**Energy Source and Sink terms -** There are two types of energy terms that are implemented in the model. The first one is a source term linked to the enthalpy of the emitted gases and the second one is a sink linked to the heat absorption by the solid particles.

The first energy term is the enthalpy of the gas emitted by the particles. When adding a gas source term in Fluent®, it is composed of 3 different user defined sources. The first term is the mass and was described earlier.

The second one is the chemical composition of the source term. It is given as a mass flow species by species to give Fluent® the full composition of the added mass. The information of the first term can seem redundant as the total of the species mass flows is equal to the first source term but it is a requirement from Fluent®.

The third term is an energy source term equivalent to the enthalpy of the additional mass, i.e. an image of the temperature at which the mass is inserted in the simulation domain. This temperature comes from the SPY model results. The reference temperature is set in Fluent® at 25[°C] so if no energy source term is specified, the inserted mass will have an equivalent temperature of 25[°C]. The enthalpy source term of the gas can thus be expressed as:

$$\text{Source}_{gas\ enthalpy} = m_i \int_{T_{ref}}^{T_{g,SPY}} c_{p,i}(T)dT,$$

where $m_i$ and $c_{p,i}$ are the mass and heat capacity of the species $i$, $T_{ref}$ is 25[°C] and $T_{g,SPY}$ is the temperature of the emitted gas calculated by SPY.

The second energy term simulates the heat absorption of the solid wood bed. It is calculated by averaging the external temperature of a single particle coming from SPY data to calculate the convective external heat transfer between the gas and the particles (the radiative transfer is neglected). It can be expressed as:

$$\text{Sink}_{particles} = -h_e\ (T_g - T_p)\ S_p\ \rho\ \gamma,$$

where $h_e$ is the convection coefficient between the gas and the solid particles, $T_g$ is the temperature of the gaseous phase calculated by Fluent®, $T_p$ is the temperature of the outer layer of the particle calculated by SPY, $S_p$ is the specific surface of the particle, $\rho$ the particle density and $\gamma$ the porosity of the bed.

The value of the convection coefficient $h_e$ is difficult to chose properly and this value is used in the simulations as an adjustment variable in order to ensure the global energy balance of the simulation.

**Wood thermal conductivity**

The thermal transfer inside the porous bed is, as every heat transfer phenomenon, due to 3 factors. The first one, convection, is linked to the hot gas flow exchanging with the solid particles. The convection transports heat in the same direction as the flow (from top to bottom). The two other ones are radiation and conduction and are independent of the flow. They thus go in all directions.

The radiative transfer is difficult to estimate. It is usually taken into account through an effective thermal conductivity combining the radiative and conductive effect. The wood thermal conductivity takes values between $0.1 - 0.2W/m.K$ according to Phyllis2 biomass characteristics database [95]. The literature gives effective conductivity of particle bed between $0.3 - 0.4W/m.K$ [90, 96, 97, 98]. The influence of the conductivity on the results is limited when considering a conductivity below $1W/m.K$ which is the case for wood particle beds. The whole porous bed is thus taken constant at $0.346W/m.K$ which is twice the default conductivity of wood inside Fluent® database and stands in the interval found in the literature.

### Wall thermal losses

The heat losses at the wall are calculated assuming a constant external temperature and wall properties from the experimental reactor. In order to simplify the model, the wall properties from the oxidation zone are taken as a reference for the whole reactor. The wall of the oxidation zone composition and heat transfer coefficient are detailed in subsection 4.1.2. The effective heat transfer coefficient (taking convection inside and outside the reactor into account) is low at $\sigma = 1.06[W/m^2.K]$ thanks to the good insulation of this zone. The outside temperature is taken constant at $300[K]$. The wall heat flux can thus be calculated as:

$$\text{Wall heat flux} = -\sigma * (T_{wall} - 300) \quad [W/m^2]$$

### Initialisation

In order to simulate the reactions inside the pyrolysis zone, the simulation needs to be initialised. First, the non-reactive flow simulation is calculated and converged with the air inlet and the mass sources terms inside the porous medium. The two energy source terms are activated during the non reactive simulation but only the enthalpy term plays a role in non-reactive simulation. The heat absorption term is in fact equal to zero as the overall temperature never surpasses the temperature of the particle inside the SPY model. These non-reactive calculations are obtained using a steady-state solver.

Once the non-reactive flow is converged, the reactions are started using a high temperature patch in the zone where pyrolysis gas are emitted. The combustion problem is stiff and requires the use of the stiff chemistry solver inside Fluent®. The convergence is again obtained using a steady solver.

### Model control

To validate the accuracy of the model, mass and energy balances are investigated. The overall mass balance is not sufficient to determine the validity of the simulations as the elemental mass balance can present discrepancies even if the overall mass balance is correct. The best way to determine if the elemental mass balance is accurate enough is to observe nitrogen which does not react in the kinetic model used for these simulations and is calculated as the rest of the mass balance after calculating the reactions of all the other species by Fluent®. When the nitrogen balance presents a sufficient accuracy, the simulation can be assumed as fully converged.

For the energy, the balance in the simulation is missing the terms linked to the solid phase as the simulations only model the solid phase as a porous medium. The input of energy of the model is the enthalpy of air and the enthalpy and LHV of gases injected into the porous medium.

The mass balance of the numerical simulations is expressed as:

$$\dot{m}_{air} + \dot{m}_{gas,1} = \dot{m}_{gas,2},$$

where $\dot{m}_{gas,1}$ is the gas emitted by the biomass particles and $\dot{m}_{gas2}$ is composed of gas emitted by the biomass particles and flue gases produced by the partial oxidation.

The energy balance of the numerical simulations is expressed as:

$$\dot{m}_{air}\Delta h_{air} + \dot{m}_{gas,1}(\Delta h_{gas,1} + LHV_{gas,1}) =$$
$$\dot{m}_{gas,2}(LHV_{gas,2} + \Delta h_{gas,2}) + \text{Energy Sink.}$$

The energy contained in the air is really small as it is injected at $300K$ and the reference temperature is 25°C ($298.15K$). The power of the air injection is equal to $P_{air} = 9W$.

The inputs for the energy balance are:

$$\begin{aligned} \dot{m}_{air} &= 0.005\ [kg/s] \\ \Delta h_{air} &= 25\ [kJ/kg] \\ \dot{m}_{gas} &= 0.0067\ [kg/s] \\ \Delta h_{gas} &= 800\ [kJ/kg] \\ LHV_{gas} &= 13.325\ [MJ/kg] \end{aligned}$$

The outputs for the energy balance are:

$$\begin{aligned} \dot{m}_{fluegas} &= 0.0059\ [kg/s], \\ \Delta h_{fluegases} &= 650\ [kJ/kg], \\ \dot{m}_{gas2} &= 0.0058\ [kg/s], \\ LHV_{gas2} &= 13.325\ [MJ/kg]. \end{aligned}$$

The gas composition is based on the SPY model which allows to calculate the $CH_yO_x$ formula for the pyrolysis gases. This then gives the equivalence ratio of the combustion considering that all the oxygen is consumed. The calculated ER (on gas only) is: 0.13. This ER allows to calculte the volume of gas that reacts with oxygen and the heat release by the combustion reaction.

The corresponding powers are calculated for an input temperature of $300K$ and an output temperature of $870K$. The power contained in the gas emitted by the particles is approximated at the average temperature of $770K$. In the simulations, this temperature is not constant as it is taken from the temperature profile of the particles given by SPY (it varies between $600K$ and $950K$).

The results of the balance are the following:

$$\begin{aligned} P_{s,air} &= 0.009\ [kW] \\ P_{s,gas} &= 5\ [kW] \\ P_{LHV,gas} &= 89\ [kW] \\ P_{LHV,gas2} &= 77\ [kW] \\ P_{Reaction} &= 12\ [kW] \\ P_{s,fluegases} &= 4.6\ [kW] \\ P_{s,gas2} &= 5.3\ [kW] \\ P_{out} &= 87\ [kW] \\ P_{in} &= 94\ [kW] \end{aligned}$$

The difference between the outlet and the inlet is justified by the heat required to heat up the wood and modelled through the Heat Sink. The heat sink does not appear in the results produced by Fluent®. This means that the heat absorbed by the heat sink representing the heating of wood particles is approximately 7 $[kW]$. The order of magnitude is the same that when calculating the heat required by considering the heat capacity and the mass flow of the wood. This can be estimated by the formula: $P_{wood} = \dot{m}\ c_{p,wood}\ (T_{wood} - T_{ref}) \approx 9\ [kW]$ using values found in the literature for the heat capacity of wood.

### 5.4.5 Model validation

This section presents the results of the numerical simulations made in Fluent®. It starts with the preliminary results obtained with a simplified kinetic mechanism used for the validation of the different User Defined Functions implemented in Fluent®. It then describes the results obtained with the mechanism adapted for this work and based on Ranzi et al. work.

#### User Defined Functions validation

In order to validate the parameters of the numerical simulation and, more importantly, the use of the different User Defined Functions (mass source term, energy source term, species source term), simulation were made using a highly simplified kinetic scheme. The kinetic mechanism includes 14 species and 29 reactions. The mechanism is based on the work of Yetter et al. [99] with the addition of a carbohydrate to represent the tars contained in the pyrolysis gas. This carbohydrate decomposes directly into methane, carbon monoxide and carbon dioxide.

Figure 5.21 presents the velocity profile for the simulations in Fluent® using the reduced mechanism. The air is injected on the top right corner and then spreads before entering the pyrolysis zone. As expected, the flow is close to a 1D flow in the porous region. The axisymmetric approach is interesting for the addition of the oxidation zone for further developments as this zone is more subject to 2D effects. The flow then accelerates due to the mass source term first and the increase in temperature due to the reactions. the flow then slightly decelerates due to the temperature decrease. This decrease is due to the fact that all the oxygen is consumed and the porous medium heat sink is still absorbing heat (because in the experiments the wood is still not at the temperature of the gas phase). The consumption of oxygen is illustrated in Figure 5.22 that presents the oxygen mass fraction profile from the numerical simulations. The oxygen fraction at the intake is the one from the air. It then decreases by dilution with water due to the drying of the particles and then it is consumed by the reactions in the smoldering front.

Figure 5.23 presents the temperature profile obtained with the numerical simulations from Fluent®. It shows that position of the smoldering front corresponds to the oxygen rapid consumption.

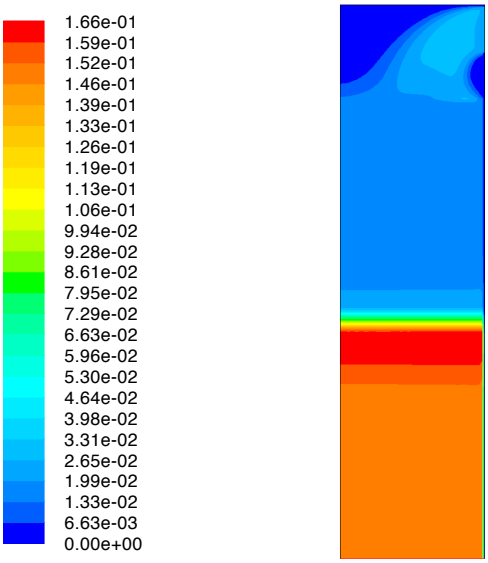


***Figure 5.21*** *– Velocity profile ([m/s]) obtained with the numerical simulations (with conditions from experimental data) from Fluent®.*

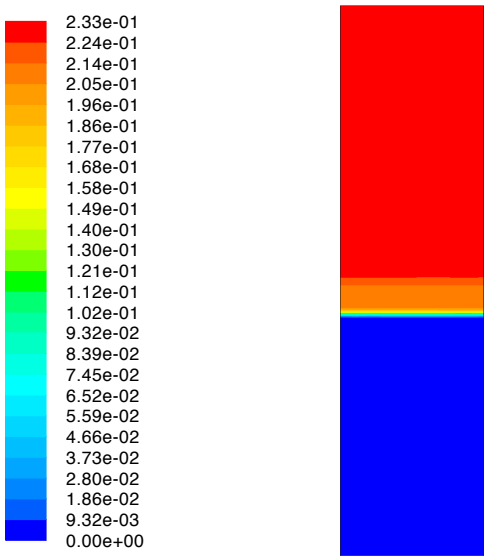


***Figure 5.22*** *– Oxygen mass fraction profile ([/]) obtained with the numerical simulations (with conditions from experimental data) from Fluent®.*

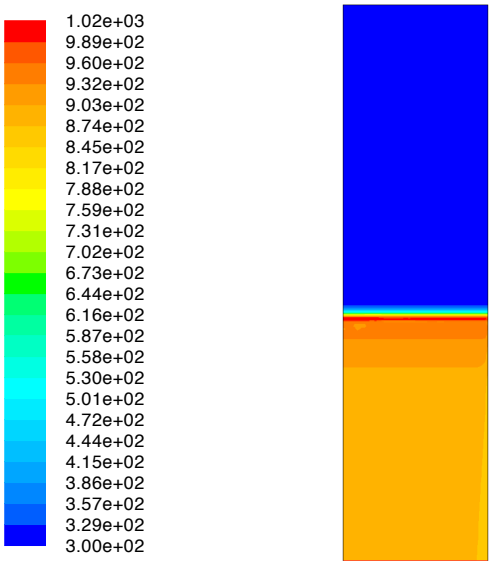


***Figure 5.23*** *– Temperature profile ([K]) obtained with the numerical simulations (with conditions from experimental data) from Fluent®.*

Figure 5.24 compares the temperature profile obtained with the numerical simulations (with conditions from experimental data) to the experimental profile measured on T.G.P. and used as reference in the SPY model. The temperature increase in the simulation is more stiff than the one observed in the experiments. This could be reduced by increasing the conductivity of the porous medium but it is already high in comparison to experimental data found in the literature. There is a perfect agreement between the simulated temperature outlet of these simulations and the temperature outlet of the experiments thanks to the adjustment variable that is the convection factor of the energy sink term.

These simulations present a good agreement for the temperature profile but due to the simplicity of the mechanism the tar content at the outlet is always equal to zero for all the configurations tested. All the tars are converted into smaller elements so this could not help predict any influence of the operating conditions of the pyrolysis zone on the tar content at the outlet of this zone. Figure 5.25 presents the tars mass fraction profile where the emission of tar can be observed. The tars are quickly emitted and consumed completely.

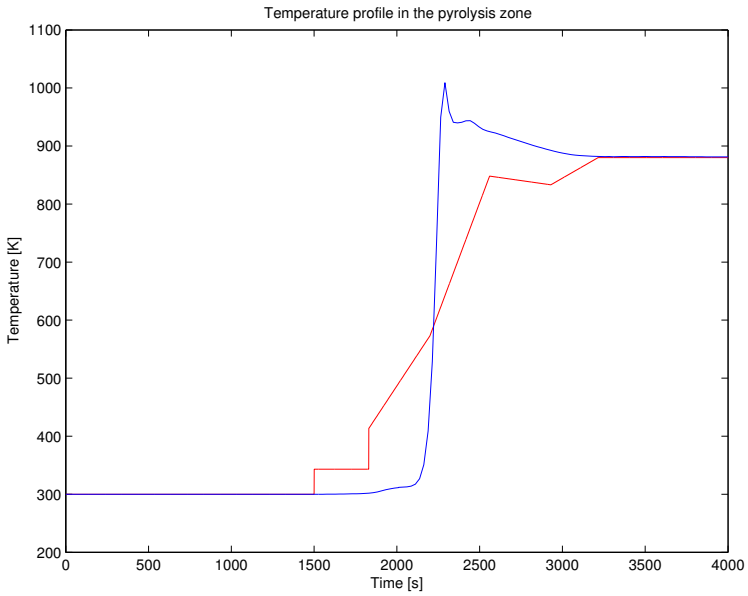


***Figure 5.24*** *– Temperature profile obtained with the numerical simulations (with conditions from experimental data) in blue and the experimental profile measured on T.G.P. and used as reference in the SPY model in red.*

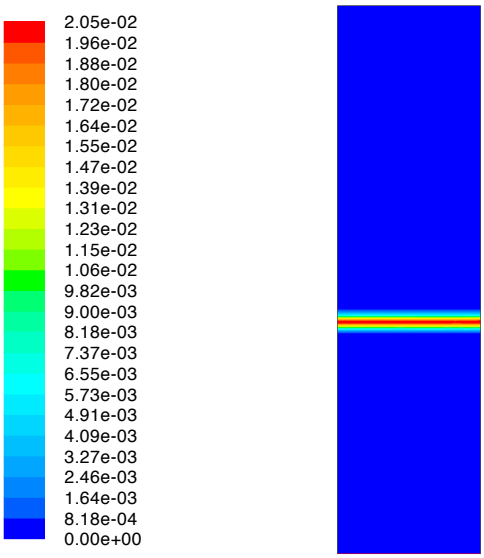


***Figure 5.25*** *– Tar ($C_8H_{12}O_6$) mass fraction profile ([/]) obtained with the numerical simulations (with conditions from experimental data) from Fluent®.*

Moreover, the composition at the outlet of the pyrolysis zone cannot be compared with the experimental data from T.G.P. as the quality of the conversion into gaseous fuel is much higher for these simulations as presented in Table 5.9. The tars, representing approximately half of the gas emitted by the particles is directly converted into methane, carbone monoxide and carbon dioxide. Methane later reacts with oxygen to produce carbon monoxide and hydrogen. This results in a gas with a really high content of carbon monoxide, carbon dioxide and hydrogen. Nevertheless, it allowed to validate the good implementation of the different User Defined Functions that simulates the mass source of gases (and the enthalpy of emitted gases), the wall heat losses and the heat sink (representing the heat required to heat up the biomass particles).

| Gas | Mass fraction % Simulation | Molar fraction % Simulation | Molar fraction % Experimental data |
|---|---|---|---|
| $CO$ | 29.22 | 24.16 | 10.6 |
| $H_2$ | 1.94 | 22.3 | 11.82 |
| $CO_2$ | 28.32 | 14.9 | 19 |
| $CH_4$ | 5.21 | 7.52 | 6 |
| $H_2O$ | 4.18 | 5.37 | 20 |
| $N_2$ | 31.13 | 25.74 | 31.84 |

***Table 5.9*** *– Gas composition (mass and volume fraction) of the simulation using the reduced mechanism in order to validate the User Defined Functions.*

### Detailed mechanism

Once the User Defined Functions are validated thanks to the simplified mechanism, they need to be adapted to a larger number of species in order to take the tars into account. As said in the previous section, the simulation is initialised with a non-reactive flow simulation that allowed to validate that the new source terms were working properly. Figure 5.26 presents the temperature profile inside the pyrolysis zone for the non-reactive simulation. Even without reactions, the temperature profile is not uniform because the gases injected using User Define Functions have a higher temperature than the air injected at the top of the reactor. There is also a radial gradient as the wall losses are cooling the gas near it.

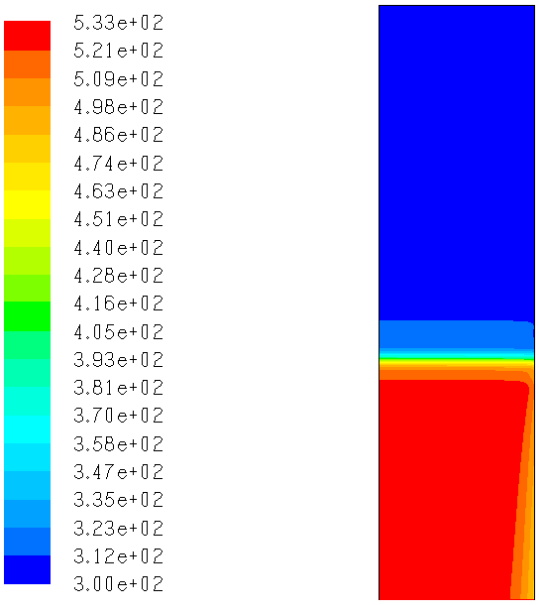


***Figure 5.26*** *– Temperature profile inside the pyrolysis zone for the non reactive simulations. The temperature is not uniform as the gas injected into the porous medium is hot and there are wall heat losses.*

Figure 5.27 presents the axial and radial velocity profiles inside the pyrolysis zone for the non-reactive case. It illustrates the fact that the speeds in this zone are low (below 7 [cm/s]) and mainly in the axial direction. Figure 5.27a allows to locate the air inlet on the top right corner and the emission of gases due to the mass source terms a little under the middle of the pyrolysis zone where gases accelerate due to the increase of the mass and volumetric flows (also due to the increase in temperature observed on Figure 5.26). Figure 5.27b shows a little recirculation above the porous medium but nearly no radial variation inside the porous medium. This indicates that the 3D effects are limited for this simulation.

A temperature patch of high temperature (approximately 1800 [K]) is thus added to the zone where the mass species source term is the highest as it should represent the zone with the smoldering combustion front. Figure 5.28 presents the temperature profile inside the pyrolysis zone after the addition of the temperature patch to initialise the reactions. This patch starts the reactions and iterations are required to diffuse the heat in the rest of the pyrolysis

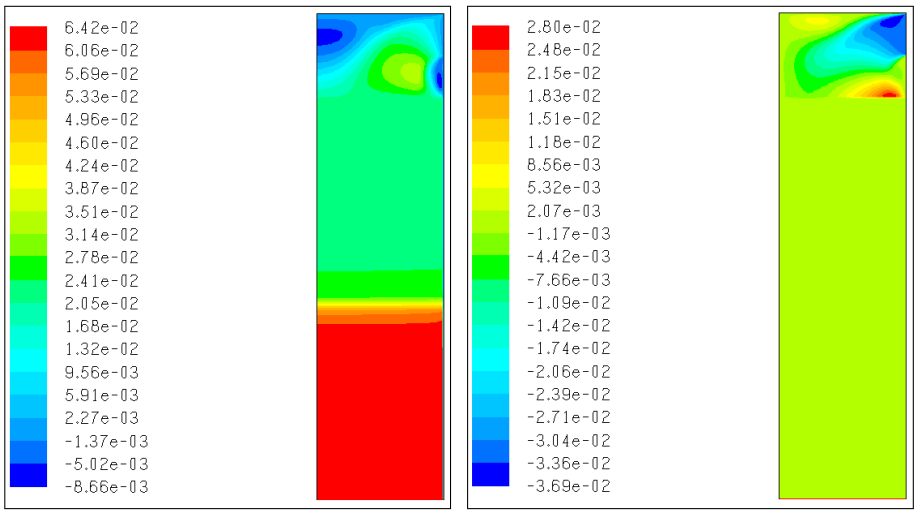


***(a)*** *Axial Velocity* ***(b)*** *Radial Velocity*

***Figure 5.27*** *– Velocity profiles inside the pyrolysis zone for the non-reactive flow simulation.*

zone and reached a converged solution.

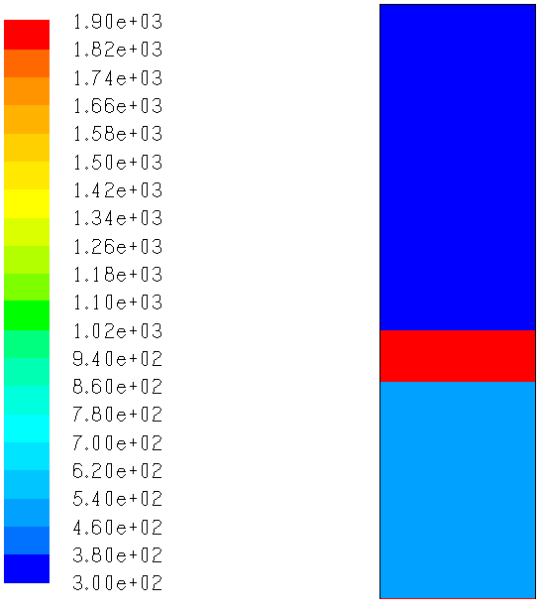


***Figure 5.28*** *– Temperature profile inside the pyrolysis zone after the addition of the temperature patch to initialise the reactions.*

Figure 5.29 presents the establishment of the temperature profile in the pyrolysis zone during the iterative calculations. Even if there are not a lot of 3D effects, the influence of the wall is visible on Figure 5.29a. The influence of the wall is reduced at steady-state when the convergence is reached. The maximal temperature observed on 5.29b is over 1710 [K] which is roughly 750 [K] more than in the experimental measurements. This temperature in the model is controlled by the heat absorption terms implemented by User Defined Functions. It can thus in theory be adjusted to meet a good agreement with the experimental results. The problem met during these tests is that if the temperature of the front decreases below 1700 [K], the reactive front cannot be maintained.

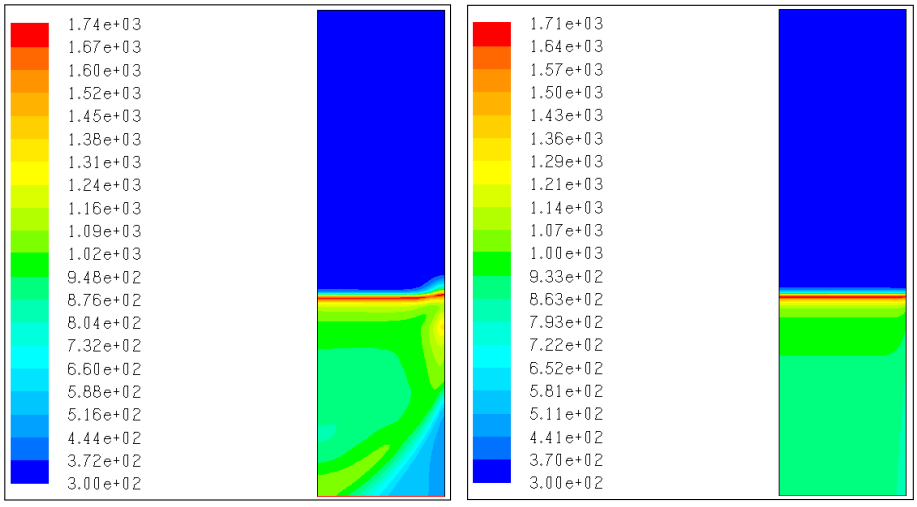


***(a)*** *Transitory: diffusion of heat* ***(b)*** *Steady-state*

***Figure 5.29*** *– Temperature profiles [K] inside the pyrolysis zone for the intermediate simulation (a) and fully converged simulation (b).*

This extinction phenomenon is illustrated in Figure 5.30. Figure 5.30a presents a stabilised front with a reduced heat absorption term (resulting in a 2000 [K] reactive front). When increasing the heat absorption of the bed particles through a User Defined Function in order to increase the agreement with experimental data, the front becomes unstable and non reactive as illustrated in Figure 5.30b. No explanation could be found for this behaviour. The reduced ChemKin mechanism was tested at lower temperature with OpenSmoke to see if the problem came from the mechanism itself or its interactions with

Fluent®. The tests were passed successfully by the mechanism at temperature as lows as 850[K]. The heat transfer to the wall and the no slip conditions at the wall were disabled in order to see if the heat losses or the flow were the cause of the problem. The results were the identical as the extinction phenomenon happened at the same temperature level. Refinements on the mesh were also tested unsuccessfully (refined mesh showed same phenomenon and unrefined mesh crashed due to the stiffness of the chemistry). Unfortunately, after several efforts and tests, the origin of the problem could not be found. As the mechanism was tested independently, the origin of the problem is probably the interactions between the Fluent® chemistry solver and the kinetic mechanism.

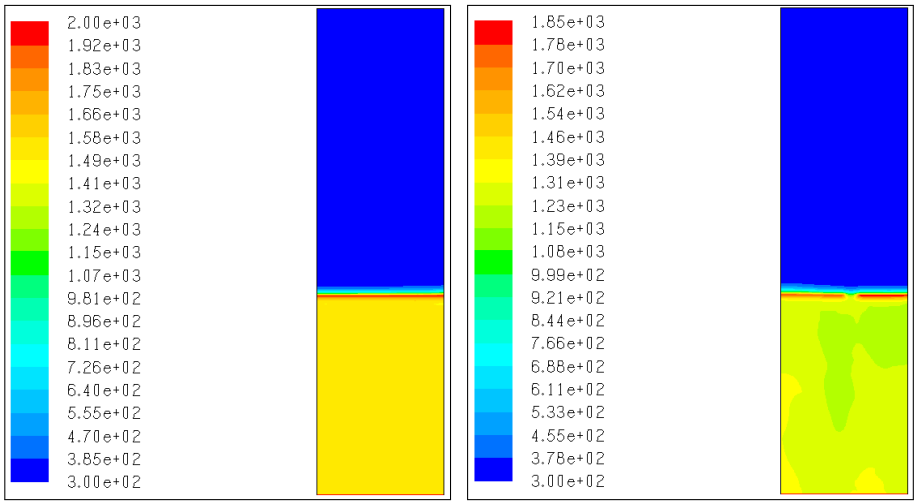


***(a)*** *Stabilised reactive zone* ***(b)*** *Extinction of the reactive front*

***Figure 5.30*** *– Temperature profiles [K] inside the pyrolysis zone for a stable simulation and failing simulation due the reactive front instability.*

The problems of extinction described force to decrease the heat sink to ensure the stabilisation of the front. The consequence is the presence of a temperature peak illustrated in Figure 5.31.

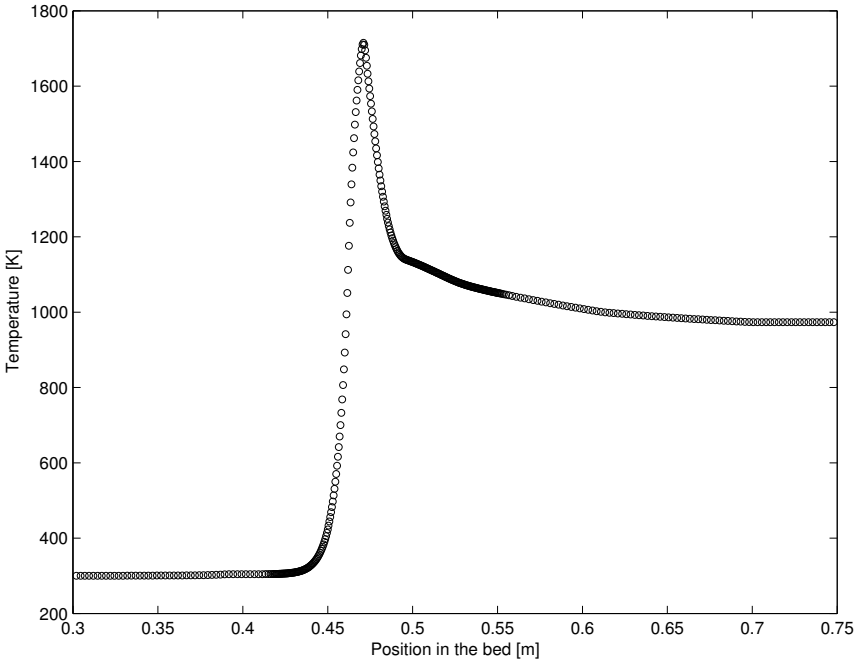


***Figure 5.31*** *– Temperature profile in the pyrolysis zone showing a peak of temperature.*

## 5.5 Numerical results

Regardless of the peak temperature problems presented in Subsection 5.4.5, the results obtained with the model at the outlet of the pyrolysis zone are of interest. The main parameters interesting to investigate are the size of the particles and their moisture content. As said before, three particle sizes and three different moisture contents are chosen, thus making it 9 different test cases to analyse. The reference names of the tests are given in Table 5.10.

| Size (Dxh) / Moisture | 1cm x 2cm | 2cm x 4cm | 4cm x 8 cm |
|---|---|---|---|
| $1.9\%_{wb}$ | S1H1 | S2H1 | S3H1 |
| $5.9\%_{wb}$ | S1H2 | S2H2 | S3H2 |
| $9.9\%_{wb}$ | S1H3 | S2H3 | S3H3 |

***Table 5.10*** *– Numerical simulations matrix.*

Each test is realised with particles of the same size rather than a mix of different sizes in order to emphasise the influence of the particles size. The moisture contents chosen are also significantly higher than the variations usually observed on the wood chips used in the experimental setup in order to emphasise the influence of the moisture content.

The parameters used for particles of size 1 and 2 are exactly the same. The size 3 particles simulations presented a lower stability, forcing the reduction of the heat sink in order to maintain the smoldering front. Unfortunately, the simulation of large particles with the highest moisture content forced to reduce the heat sink even more, presenting inconsistent results.

Figure 5.32 presents the temperature profiles obtained for the different tests. The temperature profiles are similar (due to the heat sink adjusting the outlet temperature to the experimental data) and the main differences are observed on the smoldering front.

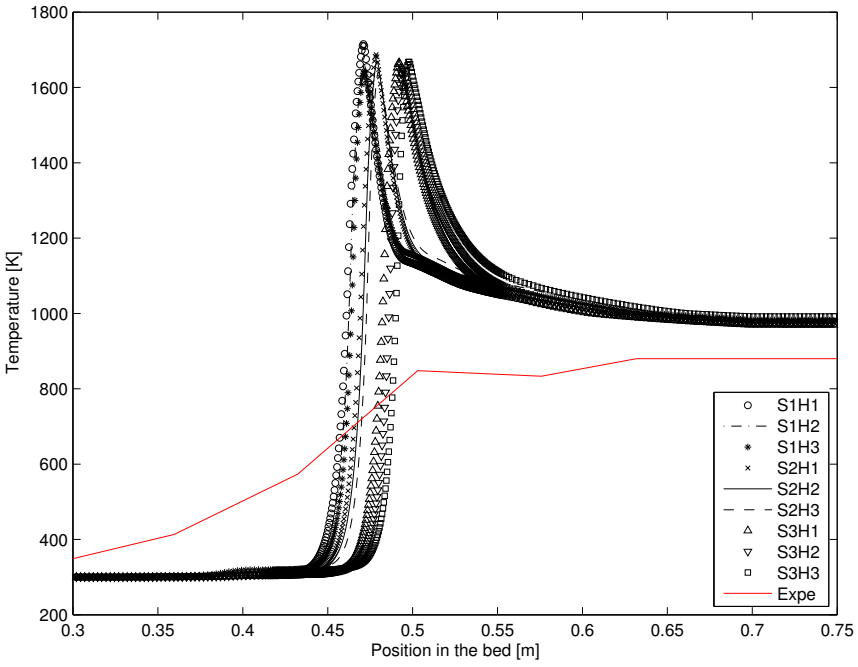


***Figure 5.32*** *– Temperature profile [K] in the pyrolysis zone for the different test cases. The differences are limited and mainly concentrated in the reactive front.*

A zoom on the temperatures in the reactive front is presented in Figure 5.33. The size of the particles slightly affects the spatial position of the reactive front as the gas are emitted at different times but the composition of the emitted species is the same, as described in Section 5.3. The size of the particles has no other observable effect. A higher moisture content slightly decreases the maximum temperature in the smoldering front and slightly displaces the position of the front towards the bottom of the pyrolysis zone. The outlet temperature increases with the moisture content as the conversion from sensible to chemical enthalpy decreases with the moisture content.

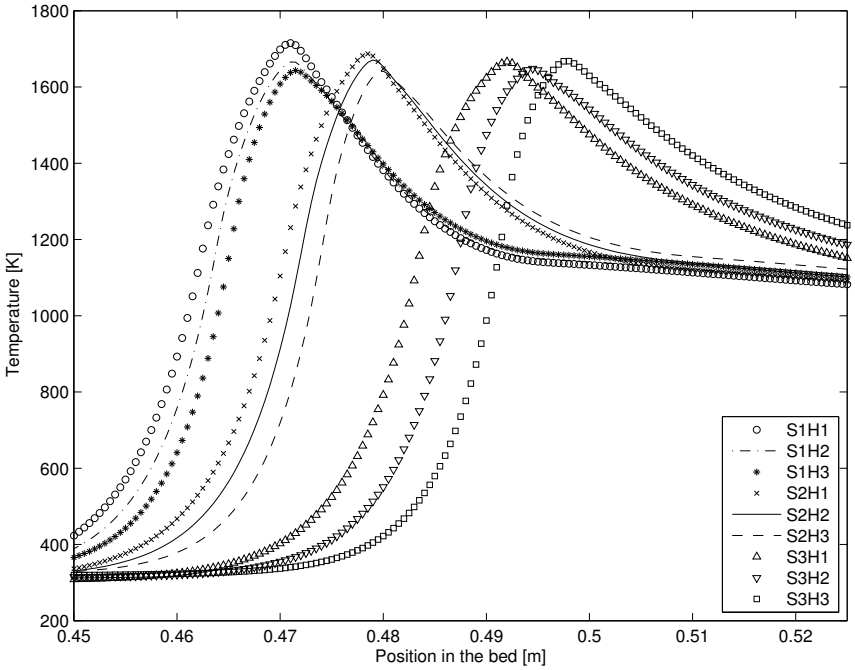


***Figure 5.33*** *– Temperature profile [K] in the pyrolysis zone for the different test cases. The differences are limited and mainly concentrated in the reactive front.*

Table 5.11 presents the power balances for each numerical simulation. As the flow of air and its inlet conditions do not vary, the energy contained in the air is the same for all the tests and is negligible in comparison to the other inputs.

It is interesting to note that as the size does not influence the composition of the gas emitted by the particles, it has no effect on the power input from the emitted gas either. It is also interesting to note that the heat sink that

| | S1H1 | S1H2 | S1H3 | S2H1 | **S2H2** | S2H3 | S3H1 | S3H2 | S3H3 |
|---|---|---|---|---|---|---|---|---|---|
| Air | | | | | | | | | |
| Total Enthalpy $[W]$ | 14 | 14 | 14 | 14 | **14** | 14 | 14 | 14 | 14 |
| Gas emitted by particles | | | | | | | | | |
| Total Enthalpy $[kW]$ | -40.1 | -45.0 | -50.2 | -40.1 | **-44.9** | -50.1 | -39.9 | -44.7 | -49.9 |
| Sensible Enthalpy $[kW]$ | 2.5 | 2.5 | 2.6 | 2.5 | **2.6** | 2.7 | 2.7 | 2.7 | 2.8 |
| Formation Enthalpy $[kW]$ | -42.6 | -47.5 | -52.8 | -42.6 | **-47.5** | -52.8 | -42.6 | -47.5 | -52.8 |
| Gas outlet | | | | | | | | | |
| Total Enthalpy $[kW]$ | -49.5 | -54.4 | -59.1 | -50.2 | **-54.2** | -59.0 | -50.3 | -54.4 | -58.7 |
| Sensible Enthalpy $[kW]$ | 14.1 | 14.5 | 15.1 | 13.9 | **14.6** | 15.3 | 13.8 | 14.5 | 15.4 |
| Formation Enthalpy $[kW]$ | -63.6 | -68.9 | -74.2 | -64.1 | **-68.8** | -74.3 | -64.1 | -68.9 | -74.0 |
| Heat Sink $[kW]$ | -9.4 | -9.4 | -8.9 | -10.1 | **-9.3** | -8.9 | -10.4 | -9.7 | -8.8 |

***Table 5.11** – Comparison of the power inputs and outputs for each test case.*

calibrates the temperature is influenced by the size as it is linked to the temperature profile that depends on the moisture content. The simulations show that with the same simulation parameters, the heat sink slightly decreases with the size of the particles. In reality, the size should not impact the amount of energy absorbed by the wood but should only impact the heat absorption profile if the mass flows are identical.

The water content influences the formation enthalpy of the gas emitted by the wood particles but this difference (approximately 5kW for 4% of moisture content) is logically also observed at the outlet of the pyrolysis zone.

The emitted gas enthalpy increases with the moisture content. It is due to the fact that the gas in each case is emitted using the temperature profile produced by SPY and based on experimental data. The dry biomass flow is maintained constant, meaning that the total mass flow increases with moisture content.

The heat sink should be linked to the moisture content as there is more mass to heat up. The opposite is observed on the results as the heat sink is calibrated on the difference of temperature between the gas and the experimental particle profile. When the moisture content increases, the temperature reached in the reactive front are lower, thus reducing the heat sink. Simulations with a heat sink increasing with moisture content lead to extinction of the reactive front.

Table 5.12 presents the composition of the light gases found at the outlet of the pyrolysis zone for the 9 simulations. The light gases and the tar content are expressed on a dry gas basis while the water content is given on wet basis. The test S2H2 is highlighted as it presents the initial conditions that are the closest to experimental conditions with the medium size particles and the moisture content of 5.9% on dry basis. There is a good agreement for the nitrogen, carbon dioxide and water content.

The simulations overestimate methane content while underestimating carbon monoxide and hydrogen content. There are two explanations for these differences. First, when looking at the mass balance species by species it seems that the air to wood ratio is overestimated for the simulations. Reducing the amount of air should reduce the nitrogen and carbon dioxide fractions while increasing

| Case | $H_2$ $[\%_{vol,dry}]$ | $CO$ $[\%_{vol,dry}]$ | $CO_2$ $[\%_{vol,dry}]$ | $CH_4$ $[\%_{vol,dry}]$ | $N_2$ $[\%_{vol,dry}]$ | $H_2O$ $[\%_{vol,wet}]$ | Tar $[g/Nm^3]$ |
|---|---|---|---|---|---|---|---|
| **Exp.** | **14.78** | **13.30** | **24.00** | **7.29** | **39.8** | **20** | **22.38** |
| S1H1 | 12.14 | 9.92 | 22.99 | 13.27 | 40.89 | 14.71 | 14.97 |
| S1H2 | 12.11 | 9.46 | 23.39 | 13.24 | 41.03 | 17.63 | 14.83 |
| S1H3 | 12.33 | 9.60 | 23.25 | 12.99 | 41.05 | 20.71 | 15.95 |
| S2H1 | 11.95 | 9.70 | 23.31 | 13.25 | 40.94 | 14.36 | 14.30 |
| **S2H2** | **12.25** | **9.82** | **23.12** | **13.13** | **40.92** | **17.60** | **12.81** |
| S2H3 | 12.74 | 10.02 | 23.28 | 13.23 | 40.00 | 20.33 | 12.24 |
| S3H1 | 12.03 | 10.09 | 23.04 | 13.05 | 40.74 | 14.09 | 13.00 |
| S3H2 | 12.23 | 10.23 | 22.90 | 12.89 | 40.74 | 17.24 | 12.31 |
| S3H3 | 12.45 | 10.17 | 22.85 | 12.82 | 40.78 | 20.47 | 11.40 |

***Table 5.12*** *– Comparison of volumetric composition for the permanent gases at the outlet of the pyrolysis zone between the different simulations and the experimental data. Test S2H2 is emphasised as it is the one with initial conditions that are the closest to experimental data.*

other fractions. Secondly, the wood to char ratio is not equivalent between the experimental data and the SPY data. This is due to the fact that SPY does consider that char is pure carbon and that the char content is calculated by SPY and not imposed to fit the experimental data. Moreover, the char to wood ratio is based on the measurement of char samples at the bottom of the pyrolysis zone that also induces uncertainty (e.g. homogeneity, completeness of the pyrolysis at the sampling probe, etc).

The effect of the size and moisture content of particles on the composition is not significant but it points towards an increase of the fuel gases ($H_2$, $CO$ and $CH_4$) production with the moisture content and size. This observation is in contradiction with the expectations as high moisture content and large particles lead to lower temperatures and longer residence times required for pyrolysis. One hypothesis is that it is due to the limitation of the heat sink calibrated on the temperature profile to maintain the reactive front.

The production of tars is also reduced with large particles and a high moisture content. This is again in contradiction with expectations as the tar content at the outlet of the gasifier increases with the moisture content in experiments.

Table 5.13 presents the complete tar composition for the simulations and the experimental data. While the order of magnitude of the tar content is similar, the compositions are quite different. Aromatics are the main component in experimental measurements with 70% of the mass of tars while they only represent 8% of the mass of tars in the simulations. Aldehydes and cetons represent more than 50% of the mass of tars in the simulations while only representing 5% of the mass in the experimental measurement. The model is thus unfortunately not suitable to predict the composition of tars at the outlet of the gasifier.

Further developments should concentrate on resolving the extinction phenomenon in the partial oxidation zone in order to get a better understanding of the tar formation problem in the pyrolysis zone. This development could allow the use of a better heat sink, calibrated on mass flow.

## 5.6 Chapter summary

This chapter presented experimental and numerical tools aimed at investigating the oxidative pyrolysis in the NOTAR® reactor. Char and gas (containing tars) could be collected and analysed successfully at the outlet of the pyrolysis zone, allowing to gather reference data for numerical simulations.

The particle model SPY adapted to larger particles presents plausible results with a concentration of levoglucosan probably overestimated as already observed by Blondeau. The flow model with simplified mechanism gives results in good agreement with experimental data. Unfortunately, due to interactions between the detailed mechanism and Fluent®, the numerical temperature profile could not match experimental data, making the model unsuitable for tar content prediction. Further work should focus on solving the handling of the mechanism by the chemistry solver and on the addition of solid phase reactions to the simulations.

| | **Exp.** | S1H1 | S1H2 | S1H3 | S2H1 | **S2H2** | S2H3 | S3H1 | S3H2 | S3H3 |
|---|---|---|---|---|---|---|---|---|---|---|
| Aldehydes & cetons $[g/Nm^3]$ | **1.23** | 11.42 | 10.90 | 4.21 | 11.45 | **11.04** | 14.4 | 6.97 | 6.07 | 4.68 |
| Acids $[g/Nm^3]$ | **2.336** | / | / | / | / | / | / | / | / | / |
| Alcohol $[g/Nm^3]$ | / | 5.51 | 5.41 | 3.11 | 6.09 | **5.73** | 5.51 | 7.62 | 7.13 | 6.37 |
| Aromatics $[g/Nm^3]$ | **16.39** | 1.32 | 1.33 | 2.03 | 1.27 | **1.21** | 1.10 | 1.25 | 1.35 | 1.49 |
| PAH $[g/Nm^3]$ | **0.60** | 3.60 | 3.19 | 3.41 | 1.75 | **1.70** | 1.70 | 0.97 | 1.22 | 1.46 |
| HC $[g/Nm^3]$ | / | 136.59 | 135.37 | 132.30 | 135.84 | **133.42** | 131.21 | 130.72 | 128.06 | 126.85 |
| Furans $[g/Nm^3]$ | **1.24** | 1.03 | 1.09 | 0.73 | 0.98 | **0.95** | 0.93 | 0.66 | 0.61 | 0.63 |
| Glucids $[g/Nm^3]$ | **0.49** | 5.48 | 5.04 | 5.57 | 4.97 | **4.59** | 4.53 | 2.90 | 3.06 | 3.15 |
| Total $[g/Nm^3]$ | **22.28** | 164.94 | 162.32 | 151.36 | 162.35 | **158.64** | 155.55 | 151.09 | 147.52 | 144.62 |
| Total (without Alcohol & HC)$[g/Nm^3]$ | **22.28** | 22.84 | 21.55 | 15.95 | 20.42 | **19.50** | 18.83 | 12.75 | 12.32 | 11.39 |

***Table 5.13** – Comparison of volumetric composition for the permanent gases at the outlet of the pyrolysis zone between the different simulations and the experimental date.*

# Conclusion and perspectives

Biomass gasification is an interesting conversion pathway for the future of the energy production sector. The types of gasification process have to be chosen carefully regarding the biomass used and the gas composition expected for a specific application (See Chapters 1 & 2).

The two-stage fixed bed gasification process presented in this thesis allows to produce a gas with a low tar content and a high LHV, making it suitable for small scale combined heat and power applications.

The development of the experimental installation T.G.P. lead to a better understanding of the gasification process. The experimental results translated into direct improvements on industrial gasifiers like the operating conditions in the pyrolysis zone and a different management of the air injections in the pyrolysis zone.

A full characterisation of the installation through Mass and Energy Balances allowed to point out that the main energy losses are the unconverted carbon and the wall losses. Carbon conversion and reactor insulation are the areas were the main efforts should concentrate in order to further increase the efficiency of the process. Note that carbon conversion could also be improved through secondary measures (after the gasification reactor) with, for example, ashes post-treatment in an external reactor or boiler.

Experimental investigations also highlighted the existence of an optimal air ratio between the primary and secondary injections. This optimal air ratio allowed the production of a syngas with a higher LHV while the tar level was not significantly influenced by the air ratio. The residence time of solid particles in

the pyrolysis zone was also investigated, showing that a reduced time allowed an increase in syngas quality while decreasing the stability of the process. Again no significant influence on the tar content could be observed. The last parameter tested was the air injection into the porous medium in the pyrolysis zone that lead to an increase in the stability of the process. The first objective of the thesis has thus been successfully achieved. Further developments should focus on testing the combination of a reduced residence time of solid particles in the pyrolysis zone and air injection into the porous medium in the pyrolysis zone to see if it could improve the syngas quality while maintaining the stability of the process.

Sewage sludge from waste water treatment plants and creosoted wood were tested successfully, widening the range of biomass accepted by the process and allowing new conversion pathways for these difficult feedstocks. The measurements of pollutant emissions allowed to investigate the suitability of the process for polluted biomass. All measurements for creosoted railroad ties stood below European emission standards (except $CO$ for which an exemption was accepted by the regulator due to the nature of syngas). The measurement of pollutants at the exhaust of the CHP engine ensured that the gaseous outlet respected environmental regulations in Belgium for waste treatment plants. Further research should focus on the potential accumulation of pollutants inside the cleaning system of the process (e.g. in the final filter). Sewage sludge tests also highlighted the importance of the biomass density in the gasification process. Further research should investigate modifications of the design in order to treat high density biomass like agro-residues pellets (e.g. rice husk pellets).

An alternative gasifying agent was tested though experiments with oxygen enriched air. The tests showed a good potential with a LHV increased more than simply due to the nitrogen removal thanks to the displacement of reaction equilibria. Further developments should focus on increasing the overall air enrichment to investigate the temperature increase in each reaction zone and the modification of the thermal wear induced by this increase.

Finally, the last objective on the development of a prediction tool for the pyrolysis zone was partially achieved. A flow model of the pyrolysis zone, combining a particle model and flow simulations, has been developed in order to predict the influence of different process parameters on the tar content of the pyrolysis gases. The results of each part of the model are interesting to look at. The results of the particle model show that considering this high residence times, the size of the particles has no effect on the overall composition of emitted gases.

Getting exploitable results with a coupling of two models (flow and particle) revealed very difficult due to kinetic reactions management by the chemistry solver. Further developments should thus focus on solving the interactions between the kinetic mechanism and the chemistry solver in order to remove the high temperature zone that appears in the simulation. Another interesting development could be the addition of solid phase reactions to the model.

Finally, future work should consider the other steps of the gasification process (e.g. the oxidation and cracking of the pyrolysis gases) in order to predict the tar content at the outlet of the gasifier. This is even more interesting that it could be implemented easily as the reactions are only gas phase reactions and are already included in the kinetic mechanism for the oxidative pyrolysis.

# Bibliography


[1] B. J. de Vries, D. P. van Vuuren, and M. M. Hoogwijk. Renewable energy sources: Their global potential for the first-half of the 21st century at a global level: An integrated approach. *Energy Policy*, 35(4):2590–2610, April 2007.

[2] G. Berndes, M. Hoogwijk, and R. van den Broek. The contribution of biomass in the future global energy supply: a review of 17 studies. *Biomass and Bioenergy*, 25(1):1–28, July 2003.

[3] W. van Swaaij, S. Kersten, and W. Palz. *Biomass Power for the World: Transformations to Effective Use*. Pan Stanford Series on Renewable Energy. Pan Stanford, 2015.

[4] R. C. Brown. *Thermochemical processing of biomass conversion into fuels, chemicals and power*. Wiley, Chichester, West Sussex, 2011.

[5] J. Ruiz, M. Juárez, M. Morales, P. Muñoz, and M. Mendívil. Biomass gasification for electricity generation: Review of current technology barriers. *Renewable and Sustainable Energy Reviews*, 18:174–183, February 2013.

[6] T. A. Milne, N. Abatzoglou, and R. J. Evans. Biomass gasifier" tars": their nature, formation, and conversion. *NREL technical report*, 1998.

[7] S. V. B. Van Paasen, J. H. A. Kiel, J. P. A. Neeft, H. A. M. Knoef, G. J. Buffinga, U. Zielke, K. Sjostrom, C. Brage, P. Hasler, P. A. Simell, and others. Guideline for sampling and analysis of tar and particles in biomass producer gases. *Final report documenting the Guideline, R& D work and dissemination*, page 95, 2002.

[8] J. P. A. Neeft, H. A. M. Knoef, U. Zielke, K. Sjöström, P. Hasler, P. A. Simell, M. A. Dorrington, and C. Greil. TAR PROTOCOL. DEVELOPMENT OF A STANDARD METHOD FOR THE MEASUREMENT OF ORGANIC CONTAMINANTS ("TAR") IN BIOMASS PRODUCER GASES. In *TAR Protocol*. Biomass for energy and industry. Proc. 1st World conference and exhibition, held in Sevilla (Spain), 2000.

[9] K. Maniatis and A. Beenackers. Tar protocols. IEA bioenergy gasification task. *Biomass and bioenergy*, 18(1):1–4, 2000.

[10] L. P. L. M. Rabou, R. W. R. Zwart, B. J. Vreugdenhil, and L. Bos. Tar in Biomass Producer Gas, the Energy research Centre of The Netherlands (ECN) Experience: An Enduring Challenge. *Energy & Fuels*, 23(12):6189–6198, December 2009.

[11] Y. Neubauer and F. Behrendt. Online Tar Analysis with Laser Mass-Spectrometry for Biomass Gasifiers. *Eurasian Chemico-Technological Journal*, 11(2):97–104, 2016.

[12] P. Basu. *Biomass gasification and pyrolysis practical design and theory*. Academic Press, Burlington, MA, 2010.

[13] R. Warnecke. Gasification of biomass: comparison of fixed bed and fluidized bed gasifier. *Biomass and Bioenergy*, 18(6):489–497, June 2000.

[14] P. McKendry. Energy production from biomass (part 3): gasification technologies. *Bioresource technology*, 83(1):55–63, 2002.

[15] E. Bocci, M. Sisinni, M. Moneti, L. Vecchione, A. Di Carlo, and M. Villarini. State of Art of Small Scale Biomass Gasification Power Systems: A Review of the Different Typologies. *Energy Procedia*, 45:247–256, 2014.

[16] M. Puig-Arnavat, J. C. Bruno, and A. Coronas. Review and analysis of biomass gasification models. *Renewable and Sustainable Energy Reviews*, 14(9):2841–2851, December 2010.

[17] L. Devi, K. J. Ptasinski, and F. J. Janssen. A review of the primary measures for tar elimination in biomass gasification processes. *Biomass and Bioenergy*, 24(2):125–140, February 2003.

[18] J.-M. Seynhaeve, H. Jeanmart, and F. Navez. Use of CFD FLUENT code to simulate the air flow through a wood particles bed for the design of

large downdraft gasifiers. In *Science in Thermal and Chemical Biomass Conversion*. 2004.

[19] C. D. Blasi. Dynamic behaviour of stratified downdraft gasifiers. *Chemical Engineering Science*, 55(15):2931–2944, August 2000.

[20] A. K. Sharma. Experimental study on 75kwth downdraft (biomass) gasifier system. *Renewable Energy*, 34(7):1726–1733, July 2009.

[21] M. J. Groeneveld. The change from fossil to solar and biofuels needs our energy. 2008.

[22] G. GE Jenbacher. JENBACHER Technical guidelines TI No 1000-0300, August 2005.

[23] L. Van de steene, J. Tagutchou, F. Mermoud, E. Martin, and S. Salvador. A new experimental Continuous Fixed Bed Reactor to characterise wood char gasification. *Fuel*, 89(11):3320–3329, November 2010.

[24] H. E. M. Stassen and H. A. M. Knoef. Small-scale gasification systems. *The Netherlands: Biomass Technology Group, University of Twente*, 1993.

[25] P. Plis and R. Wilk. Theoretical and experimental investigation of biomass gasification process in a fixed bed gasifier. *Energy*, 36(6):3838–3845, June 2011.

[26] M. Nacken, L. Ma, S. Heidenreich, and G. V. Baron. Performance of a catalytically activated ceramic hot gas filter for catalytic tar removal from biomass gasification gas. *Applied Catalysis B: Environmental*, 88(3-4):292–298, May 2009.

[27] S. Heidenreich, M. Müller, and P. U. Foscolo. *Advanced biomass gasification: new concepts for efficiency increase and product flexibility*. Elsevier/Academic Press, Amsterdam ; Boston, 2016.

[28] L. Taylor. *Bottom feed - updraft gasification system*. Google Patents, July 1999. US Patent 5,922,092.

[29] D. T. Pedroso, E. B. Machín, J. L. Silveira, and Y. Nemoto. Experimental study of bottom feed updraft gasifier. *Renewable Energy*, 57:311–316, September 2013.

[30] T. B. Reed and A. Das. *Handbook of biomass downdraft gasifier engine systems*. Biomass Energy Foundation, 1988.

[31] B. Berger, A. Bacq, H. Jeanmart, and F. Bourgois. Experimental and numerical investigation of the air ratio on the tar content in the syngas of a two-stage gasifier. *European Biomass Conference and Exhibition Proceedings*, Plenary sessions(PC1.2):20–25, 2010.

[32] A. Gómez-Barea, B. Leckner, A. Villanueva Perales, S. Nilsson, and D. Fuentes Cano. Improving the performance of fluidized bed biomass/waste gasifiers for distributed electricity: A new three-stage gasification system. *Applied Thermal Engineering*, 50(2):1453–1462, February 2013.

[33] S. Heidenreich and P. U. Foscolo. New concepts in biomass gasification. *Progress in Energy and Combustion Science*, 46:72–95, February 2015.

[34] E. Bocci. European UNIfHY Project, 2012.

[35] T. Bui, R. Loof, and S. Bhattacharya. Multi-stage reactor for thermal gasification of wood. *Energy*, 19(4):397–404, April 1994.

[36] S. C. Bhattacharya, A. H. Mizanur Rahman Siddique, and H.-L. Pham. A study on wood gasification for low-tar gas production. *Energy*, 24(4):285–296, 1999.

[37] Z. Zainal, A. Rifau, G. Quadir, and K. Seetharamu. Experimental investigation of a downdraft biomass gasifier. *Biomass and Bioenergy*, 23(4):283–289, October 2002.

[38] P. Brandt, E. Larsen, and U. Henriksen. High Tar Reduction in a Two-Stage Gasifier. *Energy & Fuels*, 14(4):816–819, July 2000.

[39] S. C. Bhattacharya, S. Shwe Hla, and H.-L. Pham. A study on a multi-stage hybrid gasifier-engine system. *Biomass and Bioenergy*, 21(6):445–460, 2001.

[40] M. Barrio. *Experimental investigation of small-scale gasification of woody biomass*. PhD thesis, The Norwegian University of Science and Technology, Trondheim, 2002.

[41] A. Surjosatyo, F. Vidian, and Y. S. Nugroho. A review on gasifier modification for tar reduction in biomass gasification. *An International Journal of Jurnal Mekanikal*, 31:62–77, 2010.

[42] T. Koch. Perspectives for the TK Energi 3-stage Gasification Technology in Austria, presentation, 2005.

[43] R. Kramreiter, M. Url, J. Kotik, and H. Hofbauer. Experimental investigation of a 125 kW twin-fire fixed bed gasification pilot plant and comparison to the results of a 2 MW combined heat and power plant (CHP). *Fuel Processing Technology*, 89(1):90–102, January 2008.

[44] J. D. Martínez, E. E. Silva Lora, R. V. Andrade, and R. L. Jaén. Experimental study on biomass gasification in a double air stage downdraft reactor. *Biomass and Bioenergy*, 35(8):3465–3480, August 2011.

[45] A. L. Galindo, E. S. Lora, R. V. Andrade, S. Y. Giraldo, R. L. Jaén, and V. M. Cobas. Biomass gasification in a downdraft gasifier with a two-stage air supply: Effect of operating conditions on gas quality. *Biomass and Bioenergy*, 61:236–244, February 2014.

[46] Y.-I. Son, S. J. Yoon, Y. K. Kim, and J.-G. Lee. Gasification and power generation characteristics of woody biomass utilizing a downdraft gasifier. *Biomass and Bioenergy*, 35(10):4215–4220, October 2011.

[47] Z. Ma, Y. Zhang, Q. Zhang, Y. Qu, J. Zhou, and H. Qin. Design and experimental investigation of a 190 kWe biomass fixed bed gasification and polygeneration pilot plant using a double air stage downdraft approach. *Energy*, 46(1):140–147, October 2012.

[48] P. Raman, N. Ram, and R. Gupta. A dual fired downdraft gasifier system to produce cleaner gas for power generation: Design, development and performance analysis. *Energy*, 54:302–314, June 2013.

[49] J. W. Judex, M. Gaiffi, and H. C. Burgbacher. Gasification of dried sewage sludge: Status of the demonstration and the pilot plant. *Waste Management*, 32(4):719–723, April 2012.

[50] T.-Y. Mun, J.-W. Kim, and J.-S. Kim. Air gasification of dried sewage sludge in a two-stage gasifier: Part 1. The effects and reusability of additives on the removal of tar and hydrogen production. *International Journal of Hydrogen Energy*, 38(13):5226–5234, May 2013.

[51] E. Natarajan, A. Nordin, and A. Rao. Overview of combustion and gasification of rice husk in fluidized bed reactors. *Biomass and Bioenergy*, 14(5):533–546, May 1998.

[52] R. A. Narváez Cueva. Use of Rice Crops Waste for Energy Production in Ecuador. *Energy & Power*, 3(3):27–36, 2013.

[53] M. Dogru, C. R. Howarth, G. Akay, B. Keskinler, and A. A. Malik. Gasification of hazelnut shells in a downdraft gasifier. *Energy*, 27(5):415–427, 2002.

[54] V. Suzdalenko, I. Barmina, A. Lickrastina, and M. Zake. The Effect of Co-Gasification of the Biomass Pellets with Gas on the Thermal Degradation of Biomass. *fuel*, 5(1):2–3, 2011.

[55] J.-W. Kim, T.-Y. Mun, J.-O. Kim, and J.-S. Kim. Air gasification of mixed plastic wastes using a two-stage gasifier for the production of producer gas with low tar and a high caloric value. *Fuel*, 90(6):2266–2272, June 2011.

[56] M. Niu, Y. Huang, B. Jin, and X. Wang. Oxygen Gasification of Municipal Solid Waste in a Fixed-bed Gasifier. *Chinese Journal of Chemical Engineering*, 22(9):1021–1026, September 2014.

[57] T.-Y. Mun, B.-S. Kang, and J.-S. Kim. Production of a Producer Gas with High Heating Values and Less Tar from Dried Sewage Sludge through Air Gasification Using a Two-Stage Gasifier and Activated Carbon. *Energy & Fuels*, 23(6):3268–3276, June 2009.

[58] Z. Zainal, R. Ali, C. Lean, and K. Seetharamu. Prediction of performance of a downdraft gasifier using equilibrium modeling for different biomass materials. *Energy Conversion and Management*, 42(12):1499–1515, August 2001.

[59] F. D. Rossini. JANAF thermochemical tables. *The Journal of Chemical Thermodynamics*, 4(3):509–510, May 1972.

[60] A. K. Sharma. Equilibrium modeling of global reduction reactions for a downdraft (biomass) gasifier. *Energy Conversion and Management*, 49(4):832–842, April 2008.

[61] G. Schuster, G. Löffler, K. Weigl, and H. Hofbauer. Biomass steam gasification - an extensive parametric modeling study. *Bioresource Technology*, 77(1):71–79, March 2001.

[62] A. V. Bridgwater. Renewable fuels and chemicals by thermal processing of biomass. *Chemical Engineering Journal*, 91(2):87–102, 2003.

[63] V. B. Silva and A. Rouboa. Using a two-stage equilibrium model to simulate oxygen air enriched gasification of pine biomass residues. *Fuel Processing Technology*, 109:111–117, May 2013.

[64] J. Ahrenfeldt, U. Henriksen, T. K. Jensen, B. Gøbel, L. Wiese, A. Kather, and H. Egsgaard. Validation of a Continuous Combined Heat and Power (CHP) Operation of a Two-Stage Biomass Gasifier. *Energy & Fuels*, 20(6):2672–2680, November 2006.

[65] U. Henriksen, J. Ahrenfeldt, T. K. Jensen, B. Gøbel, J. D. Bentzen, C. Hindsgaul, and L. H. Sørensen. The design, construction and operation of a 75kw two-stage gasifier. *Energy*, 31(10-11):1542–1553, August 2006.

[66] S. Jarungthammachote and A. Dutta. Experimental investigation of a multi-stage air-steam gasification process for hydrogen enriched gas production. *International Journal of Energy Research*, 36(3):335–345, March 2012.

[67] R. Zhang, K. Cummer, A. Suby, and R. C. Brown. Biomass-derived hydrogen from an air-blown gasifier. *Fuel Processing Technology*, 86(8):861–874, May 2005.

[68] B. Acharya, A. Dutta, and P. Basu. An investigation into steam gasification of biomass for hydrogen enriched gas production in presence of CaO. *International Journal of Hydrogen Energy*, 35(4):1582–1589, February 2010.

[69] C. V. Huynh and S.-C. Kong. Performance characteristics of a pilot-scale biomass gasifier using oxygen-enriched air and steam. *Fuel*, 103:987–996, January 2013.

[70] K. Jaojaruek, S. Jarungthammachote, M. K. B. Gratuito, H. Wongsuwan, and S. Homhual. Experimental study of wood downdraft gasification for

an improved producer gas quality through an innovative two-stage air and premixed air/gas supply approach. *Bioresource Technology*, 102(7):4834–4840, April 2011.

[71] M. Gupta, J. Yang, and C. Roy. Predicting the effective thermal conductivity of polydispersed beds of softwood bark and softwood charâ˜†. *Fuel*, 82(4):395–404, March 2003.

[72] H. Boerrigter, M. Bolhár-Nordenkampf, E. P. Deurwaarder, T. Eriksson, J. W. Könemann, R. Rauch, S. V. B. Van Paasen, and J. Palonen. OLGA optimum. *Energy research Centre of the Netherlands, ECN-E-06-048*, 2006.

[73] Q. Osterrieth and G. Ryelandt. Adaptation au syngas et régulation de l'alimentation d'un moteur stationnaire. Master's thesis, Université catholique de Louvain, 2014.

[74] S. Bhaduri. *Experimental studies on HCCI combustion of biomass syngas towards tar tolerant operation.* PhD thesis, Université catholique de Louvain, Louvain-la-Neuve, 2017.

[75] S. Bhaduri, B. Berger, M. Pochet, H. Jeanmart, and F. Contino. HCCI engine operated with unscrubbed biomass syngas. *Fuel Processing Technology*, 157:52–58, March 2017.

[76] C. Debucquois and C.-A. Raisière. Caractérisation d'une installation expérimentale de gazéification à lit fixe bi-étagé. Master's thesis, Université catholique de Louvain, 2014.

[77] E. Bries and A. Leveau. Caractérisation expérimentale de la zone de pyrolyse d'un gazogène de type NOTAR. Master's thesis, Université catholique de Louvain, 2016.

[78] J. Blondeau and H. Jeanmart. Biomass pyrolysis at high temperatures: Prediction of gaseous species yields from an anisotropic particle. *Biomass and Bioenergy*, 41:107–121, June 2012.

[79] B. Berger, A. Bacq, T. André, T. Bach, F. Bourgois, and H. Jeanmart. Oxygen Enriched Air Gasification in an Experimental Two-Stage Gasifier. Vienna, 2015.

[80] B. Berger, C. Peregrina, A. Bacq, F. Saidi, J. Audic, F. Mosnier, F. Bourgois, and H. Jeanmart. Experimental investigation of sewage sludge gasification using a two-stage fixed bed downdraft gasifier. Venice, 2012.

[81] B. Berger, A. Bacq, H. Jeanmart, and F. Bourgois. Experimental Investigation on the gasification of creosoted wood using a two-stage gasifier. Berlin, 2011.

[82] J. Damon, A. Bacq, B. Berger, P. Dubois, F. Bourgois, and H. Jeanmart. Environmental Benefits with Used Railway Sleepers Fuelling Xylowatt's Notar Gasification Technology. pages 1026 – 1032, Milan.

[83] L. De Fusco. *Assessment of ash agglomeration and fouling in combustion by theoretical and experimental biomass fuels characterization.* PhD Thesis, UCL UCL - SST/IMMC/TFL - Thermodynamics and fluid mechanics Ecole Polytechnique de Louvain, 2017.

[84] J. Vandooren, M. Branch, and P. Van Tiggelen. Comparisons of the structure of stoichiometric CH4î—¸N2oî—¸Ar and CH4î—¸O2î—¸Ar flames by molecular beam sampling and mass spectrometric analysis. *Combustion and Flame*, 90(3):247–258, September 1992.

[85] V. Dias. *Etude de la formation des précurseurs des suies dans les flammes riches prémélangées d'éthylène.* PhD thesis, Université catholique de Louvain, 2003.

[86] A. Anca-Couce, N. Zobel, and H. A. Jakobsen. Multi-scale modeling of fixed-bed thermo-chemical processes of biomass with the representative particle model: Application to pyrolysis. *Fuel*, 103:773–782, January 2013.

[87] P. Messina. The Exascale Computing Project. *Computing in Science & Engineering*, 19(3):63–67, June 2017.

[88] R. MILLER and J. BELLAN. A Generalized Biomass Pyrolysis Model Based on Superimposed Cellulose, Hemicelluloseand Liqnin Kinetics. *Combustion Science and Technology*, 126(1-6):97–137, July 1997.

[89] E. Ranzi, A. Cuoci, T. Faravelli, A. Frassoldati, G. Migliavacca, S. Pierucci, and S. Sommariva. Chemical Kinetics of Biomass Pyrolysis. *Energy & Fuels*, 22(6):4292–4300, November 2008.

[90] M. Mayerhofer, J. Govaerts, N. Parmentier, H. Jeanmart, and L. Helsen. Experimental investigation of pressure drop in packed beds of irregular shaped wood particles. *Powder Technology*, 205(1-3):30–35, January 2011.

[91] V. Dias, J. Vandooren, and H. Jeanmart. An experimental and modeling study of the addition of acetone to H 2 /O 2 /Ar flames at low pressure. *Proceedings of the Combustion Institute*, 35(1):647–653, 2015.

[92] V. Dias, J. Vandooren, and H. Jeanmart. Experimental and Modeling Study of Propanal/H2/O2/Ar Flames at Low Pressure. *Combustion Science and Technology*, 188(4-5):556–570, May 2016.

[93] C. Dupont, L. Chen, J. Cances, J.-M. Commandre, A. Cuoci, S. Pierucci, and E. Ranzi. Biomass pyrolysis: Kinetic modelling and experimental validation under high temperature and flash heating rate conditions. *Journal of Analytical and Applied Pyrolysis*, 85(1-2):260–267, May 2009.

[94] M. Corbetta, A. Frassoldati, H. Bennadji, K. Smith, M. J. Serapiglia, G. Gauthier, T. Melkior, E. Ranzi, and E. M. Fisher. Pyrolysis of Centimeter-Scale Woody Biomass Particles: Kinetic Modeling and Experimental Validation. *Energy & Fuels*, 28(6):3884–3898, June 2014.

[95] ECN. ECN Phyllis 2 Database.

[96] N. Parmentier. *Experimental characterization and numerical simulation of packed beds of wood particles.* PhD thesis, Université catholique de Louvain, 2015.

[97] W. Guo, C. J. Lim, X. Bi, S. Sokhansanj, and S. Melin. Determination of effective thermal conductivity and specific heat capacity of wood pellets. *Fuel*, 103:347–355, January 2013.

[98] Y. Asako, H. Kamikoga, H. Nishimura, and Y. Yamaguchi. Effective thermal conductivity of compressed woods. *International journal of heat and mass transfer*, 45(11):2243–2253, 2002.

[99] R. A. YETTER, F. L. DRYER, and H. RABITZ. A Comprehensive Reaction Mechanism For Carbon Monoxide/Hydrogen/Oxygen Kinetics. *Combustion Science and Technology*, 79(1-3):97–128, September 1991.

# Appendix A

# CIRAD analysis resulsts

cirad
LA RECHERCHE AGRONOMIQUE POUR LE DÉVELOPPEMENT

Montpellier, le 06 juin 2016

Objet : Rapport d'Analyse

| Réf. CIRAD | Réf. échantillon | Date réception échantillon | Remarques |
|---|---|---|---|
| 16_05_01 | Solide 1 Charbon | 03/05/2016 | RAS |
| 16_05_02 | Solide 2 Biomasse | 03/05/2016 | RAS |

**Référence échantillon 16_05_01** : ***Solide 1 Charbon***

| | |
|---|---|
| Teneur en humidité *(% m)* | 0.6 |
| Teneur en Cendres *(% m sur base sèche)* | 9.9 |
| Teneur en Matières Volatiles *(% m sur base sèche)* | 4.3 |
| Teneur en Carbone *(% m sur base sèche)* | 83.6 |
| Teneur en Hydrogène *(% m sur base sèche)* | 1.51 |
| Teneur en Azote *(% m sur base sèche)* | 0.27 |
| PCS sur brut *(J/g)* | 30 720 |
| PCS sur anhydre *(J/g)* | 30 900 |
| PCI sur anhydre *(J/g)* | 30 580 |
| PCI sur brut *(J/g)* | 30 390 |

www.cirad.fr Innovons ensemble pour les agricultures de demain

CIRAD – UPR BioWooEB -TA B-114/16 – 73, Rue J.F. Breton –34398 MONTPELLIER CEDEX 5.
Tél : 33 (0) 4.67.61.59.05 – Fax : 33 (0) 4.67.61.65.15

Etablissement public à caractère industriel et commercial (EPIC) – SIREN 331596270 – RCS Paris B 331 596 270

cirad
LA RECHERCHE AGRONOMIQUE POUR LE DÉVELOPPEMENT

**Référence échantillon 16_05_02 : *Solide 2 Biomasse***

| | |
|---|---|
| Teneur en humidité *(% m)* | 5.9 |
| Teneur en Cendres *(% m sur base sèche)* | 2.6 |
| Teneur en Matières Volatiles *(% m sur base sèche)* | 79.1 |
| Teneur en Carbone *(% m sur base sèche)* | 48.9 |
| Teneur en Hydrogène *(% m sur base sèche)* | 5.8 |
| Teneur en Azote *(% m sur base sèche)* | 0.33 |
| PCS sur brut *(J/g)* | 18 090 |
| PCS sur anhydre *(J/g)* | 19 220 |
| PCI sur anhydre *(J/g)* | 18 000 |
| PCI sur brut *(J/g)* | 16 790 |

cirad

# RAPPORT D'ANALYSE GC-MS

**Nom de l'échantillon :** **UCL condensables**
Date de l'expérience : 7 juin 2016
Date de l'analyse : 7 juin 2016
Date de traitement : 16 juin 2016

Colonne : DB1701 - Cpsil19CB 14% cyanopropylphényl et 86% dimethylpolysiloxanne
Chromatographe : GC Agilent 6890
Détecteur : Spectromètre de Masse Agilent 5975

| CAS | Alcools | [] mg/L |
|---|---|---|
| 67-56-1 | Methanol | <LQ (200) |
| | ***Total Alcools*** | ***0,00*** |

| CAS | Aldehydes et cétones | [] mg/L |
|---|---|---|
| 50-00-0 | Formaldehyde | <LQ (50) |
| 75-07-0 | Acetaldehyde | 348,73 |
| 23147-58-2 | Glycolaldehyde | <LQ (50) |
| 116-09-6 | 2-Propanone,1-hydroxy- | <LQ (50) |
| 930-30-3 | 2-cyclopenten-1-one | 133,56 |
| 2758-18-1 | 2-cyclopenten-1-one-3-methyl | <LQ (1) |
| 5077-67-8 | 2-Butanone,1-hydroxy- | <LQ (50) |
| 765-70-8 | 3-methyl-1,2-cyclopentanedione | <LQ (10) |
| 10493-98-8 | 2-hydroxy-2-cyclopenten-1-one | <LQ (10) |
| 592-20-1 | 1-acetyloxy-2-propanone | <LQ (2) |
| | ***Total Aldehydes et cétones*** | ***482,29*** |

| CAS | Acides | [] mg/L |
|---|---|---|
| 64-18-6 | Formic_acid | <LQ (200) |
| 64-19-7 | Acetic_acid | 912,74 |
| 79-09-4 | Propionic_acid | <LQ (50) |
| | ***Total acides*** | ***912,74*** |

| CAS | Furanes | [] mg/L |
|---|---|---|
| 98-01-1 | Furfural | 94,37 |
| 98-00-0 | 2-furanmethanol | 125,68 |
| 271-89-6 | Benzofuran | 171,45 |
| 620-02-0 | 2-furancarboxaldehyde,5-methyl | <LQ (1) |
| 625-86-5 | 2,5-dimethylfuran | 92,00 |
| 67-47-0 | 5-hydroxymethylfurfural | <LQ (10) |
| | ***Total furanes*** | ***483,50*** |

| CAS | Aromatiques azotés | [] mg/L |
|---|---|---|
| 110-86-1 | Pyridine | 19,57 |
| 109-06-8 | Pyridine-2-methyl | <LQ (1) |
| 91-22-5 | Quinoline | 9,65 |
| 119-65-3 | Isoquinoline | <LQ (4) |
| | ***Total aromatiques azotés*** | ***29,22*** |

| CAS | Aromatiques | [] mg/L |
|---|---|---|
| 71-43-2 | Benzene | 1.378,75 |
| 108-88-3 | Toluene | 821,64 |
| 100-41-4 | Ethylbenzene | 93,84 |
| 108-38-3 et 106-42-3 | (m+p)-xylene | 131,59 |
| 95-47-6 | O-xylene | 52,02 |
| 100-42-5 | Styrene | 245,76 |
| 95-13-6 | Indene | 143,02 |
| 2177-47-1 | 2-methylindene | <LQ (1) |
| 536-74-3 | Phenylethyne | <LQ (1) |
| | ***Total aromatiques*** | ***2.866,61*** |

| CAS | Sucres | [] mg/L |
|---|---|---|
| 498-07-7 | Levoglucosan | <LQ (2) |
| 113781-13-8 | LAC | <LQ (4) |
| 4451-30-3 | DGP | 189,56 |
| | ***Total Sucres*** | ***189,56*** |

| CAS | Phenols | [] mg/L |
|---|---|---|
| 108-95-2 | Phenol | 2.530,00 |
| 95-48-7 | Phenol-2-methyl | 455,33 |
| 106-44-5 et 108-39-4 | Phenol-3-methyl+Phenol-4-methyl | 302,35 |
| 95-65-8 | 3,4-dimethylphenol | <LQ (1) |
| 105-67-9 | 2,4-dimethylphenol | 188,66 |
| 90-15-3 | 1-naphthalenol | 12,03 |
| 135-19-3 | 2-naphthalenol | 17,69 |
| 123-31-9 | Hydroquinone | <LQ (1) |
| | ***Total phénols*** | ***3.506,06*** |

| CAS | Guaiacols | [] mg/L |
|---|---|---|
| 90-05-1 | Phenol-2-methoxy | 55,81 |
| 93-51-6 | Phenol-2-methoxy-4-methyl | 4,72 |
| 91-10-1 | 2,6-dimethoxyphenol | 19,31 |
| 2785-89-9 | Phenol-4-ethyl-2-methoxy | 5,23 |
| 97-53-0 | Eugenol | <LQ (1) |
| 97-54-1 | Isoeugenol | 7,49 |
| 7786-61-0 | 2-methoxy-4-vinylphenol | <LQ (1) |
| 4812-20-8 | 2-isopropoxyphenol | <LQ (1) |
| | ***Total Guaiacols*** | ***92,57*** |

| CAS | HAPs | [] mg/L |
|---|---|---|
| 91-20-3 | Naphthalene | 120,89 |
| 90-12-0 | Naphthalene-1-methyl | 31,35 |
| 91-57-6 | Naphthalene-2-methyl | 31,35 |
| 208-96-8 | Acenaphthylene | 20,27 |
| 83-32-9 | Acenaphthene | 9,19 |
| 86-73-7 | Fluorene | 9,54 |
| 85-01-8 | Phenanthrene | 13,42 |
| 120-12-7 | Anthracene | <LQ (1) |
| 206-44-0 | Fluoranthene | <LQ (1) |
| 129-00-0 | Pyrene | <LQ (1) |
| 56-55-3 | Benzo(a)anthracene | <LQ (1) |
| 218-01-9 | Chrysene | <LQ (1) |
| 205-99-2 | Benzo(b)fluoranthene | <LQ (1) |
| 207-08-9 | Benzo(k)fluoranthene | <LQ (1) |
| 50-32-8 | Benzo(a)pyrene | <LQ (1) |
| 191-24-2 | Benzo(ghi)perylene | <LQ (1) |
| 53-70-3 | Dibenzo(ah)anthracene | <LQ (1) |
| 193-39-5 | Indeno(123cd)pyrene | <LQ (1) |
| | ***Total HAPs*** | ***236,00*** |

| CAS | Terpenes | [] mg/L |
|---|---|---|
| 7785-70-8 | 1-R-a-pinene | <LQ (1) |
| | ***Total Sucres*** | ***0,00*** |

| | [] mg/L |
|---|---|
| ***Total général*** | ***8.798,55*** |

# Appendix B

# ChemKin Mechanism

```
ELEMENTS
    O H C N
END

SPECIES
    N2
    H2 H O O2 OH H2O2
    C2H5CHO C2H5CO H2O HO2
    CH3 CH4 CO CO2 HCO CH2O C2H2
    C2H3 C2H4 C2H5 HCCO CH2CO C3H3
    C6H6 C6H5 C6H6O C6H5O C5H6 C5H5
    CH3CHO CH3CO CH3O CH3OH CH2OH
    C2H5OH CH2CHO CH3CH2O
    C4H6O2 C9H10O2 C6H8O4 C6H10O5 C5H8O4
    C5H4O2 C6H6O3 C2H2O2 C2H4O2 C10H8
END

REACTIONS
    H+O2=OH+O 1.040000E+014 0.000000E+000 1.529000E+004
    H2+O=H+OH 5.080000E+004 2.670000E+000 6.292000E+003
    OH+H2=H2O+H 4.380000E+013 0.000000E+000 6.990000E+003
    H2O+O=OH+OH 2.970000E+006 2.020000E+000 1.340000E+004
    H2+M=H+H+M 4.577000E+019 -1.400000E+000 1.044000E+005
    H2O /1.200000E+001/ H2 /2.500000E+000/ CO /1.900000E+000/ CO2 /3.800000E+000/
    O+O+M=O2+M 6.165000E+015 -5.000000E-001 0.000000E+000
    H2O /1.200000E+001/ H2 /2.500000E+000/ CO /1.900000E+000/ CO2 /3.800000E+000/
    H+OH+M=H2O+M 3.500000E+022 -2.000000E+000 0.000000E+000
    H2O /3.650000E+000/ H2 /7.300000E-001/ CO /1.900000E+000/ CO2 /3.800000E+000/
    H+O2(+M)=HO2(+M) 4.650000E+012 4.400000E-001 0.000000E+000
    LOW /1.737000E+019 -1.230000E+000 0.000000E+000/
    H2O /1.000000E+001/ H2 /1.300000E+000/ CO /1.900000E+000/ CO2 /3.800000E+000/
    H+HO2=OH+OH 7.079000E+013 0.000000E+000 2.950000E+002
    H2+O2=H+HO2 5.176000E+005 2.430000E+000 5.350000E+004
    HO2+O=O2+OH 3.250000E+013 0.000000E+000 0.000000E+000
    OH+HO2=H2O+O2 2.456000E+013 0.000000E+000 -4.970000E+002
    HO2+HO2=O2+H2O2 1.300000E+011 0.000000E+000 -1.630000E+003
```

```
DUPLICATE
HO2+HO2=O2+H2O2 3.658000E+014 0.000000E+000 1.200000E+004
DUPLICATE
H2O2(+M)=OH+OH(+M) 2.000000E+012 9.000000E-001 4.875000E+004
LOW /2.490000E+024 -2.300000E+000 4.875000E+004/
H2 /3.700000E+000/ O2 /1.200000E+000/ CO /2.800000E+000/ CO2 /1.600000E+000/
H2O2+H=HO2+H2 2.150000E+010 1.000000E+000 6.000000E+003
OH+H2O2=HO2+H2O 1.740000E+012 0.000000E+000 3.180000E+002
DUPLICATE
OH+H2O2=HO2+H2O 7.590000E+013 0.000000E+000 7.269000E+003
DUPLICATE
H+O+M=OH+M 4.714000E+018 -1.000000E+000 0.000000E+000
H2O /1.200000E+001/ H2 /2.500000E+000/ CO /1.500000E+000/ CO2 /2.000000E+000/
CO+OH=CO2+H 7.015000E+004 2.050000E+000 -3.557000E+002
DUPLICATE
CO+OH=CO2+H 5.757000E+012 -6.600000E-001 3.318000E+002
DUPLICATE
H+CH2O=HCO+H2 5.740000E+007 1.900000E+000 2.740000E+003
O+CH2O=HCO+OH 1.070000E+013 5.700000E-001 2.762000E+003
OH+CH2O=HCO+H2O 1.800000E+013 0.000000E+000 4.360000E+002
CH2O+M=HCO+H+M 3.300000E+039 -6.300000E+000 9.990400E+004
H2 /2.000000E+000/ CO /1.500000E+000/ CH2O /3.000000E+000/
H+HCO=CO+H2 7.340000E+013 0.000000E+000 0.000000E+000
O+HCO=CO2+H 3.000000E+013 0.000000E+000 0.000000E+000
O+HCO=CO+OH 3.020000E+013 0.000000E+000 0.000000E+000
OH+HCO=CO+H2O 1.020000E+014 0.000000E+000 0.000000E+000
O2+HCO=CO+HO2 7.580000E+012 0.000000E+000 4.100000E+002
HCO+M=CO+H+M 4.750000E+011 6.600000E-001 1.487000E+004
H2O /1.200000E+001/ H2 /2.000000E+000/ CO /1.500000E+000/ CO2 /2.000000E+000/
O+HCCO=CO+CO+H 9.640000E+013 0.000000E+000 0.000000E+000
CO+O(+M)=CO2(+M) 1.362000E+010 0.000000E+000 2.384000E+003
LOW /1.173000E+024 -2.790000E+000 4.191000E+003/
H2O /1.200000E+001/ H2 /2.000000E+000/ CO /1.750000E+000/ CO2 /3.600000E+000/
CO+O2=CO2+O 1.119000E+012 0.000000E+000 4.770000E+004
HO2+CO=CO2+OH 1.570000E+005 2.180000E+000 1.794000E+004
O+CH2CO=HCO+HCO 2.290000E+012 0.000000E+000 1.352000E+003
CH3CHO+O2=CH3CO+HO2 3.000000E+013 0.000000E+000 3.910000E+004
CH3CHO+OH=CH3CO+H2O 2.350000E+010 7.300000E-001 -1.110000E+003
CH3CHO+O=CH3CO+OH 5.800000E+012 0.000000E+000 1.800000E+003
CH3CO+O=CH2CO+OH 3.900000E+013 0.000000E+000 0.000000E+000
CH3CO+O=CH3+CO2 1.000000E+013 0.000000E+000 0.000000E+000
CH3CO+OH=CH2CO+H2O 1.200000E+013 0.000000E+000 0.000000E+000
H+CH4=H2+CH3 1.320000E+004 3.000000E+000 8.041000E+003
O+CH4=OH+CH3 9.030000E+008 1.560000E+000 8.489000E+003
OH+CH4=H2O+CH3 1.560000E+007 1.830000E+000 2.783000E+003
CH3+H(+M)=CH4(+M) 1.270000E+016 -6.300000E-001 3.830000E+002
LOW /2.477000E+033 -4.760000E+000 2.440000E+003/
TROE /7.830000E-001 7.400000E+001 2.941000E+003 6.964000E+003/
H2 /2.000000E+000/ H2O /6.000000E+000/ CO /1.500000E+000/ CO2 /2.000000E+000/
CH4 /2.000000E+000/
O+CH3=CH2O+H 8.430000E+013 0.000000E+000 0.000000E+000
O2+CH3=CH2O+OH 3.310000E+011 0.000000E+000 8.946000E+003
OH+CH3=CH2O+H2 8.000000E+012 0.000000E+000 0.000000E+000
CH3+CH2O=HCO+CH4 4.090000E+012 0.000000E+000 8.847000E+003
```

CH3+CH3=C2H5+H 8.000000E+014 0.000000E+000 2.660000E+004
CH3+CH3=C2H4+H2 1.000000E+016 0.000000E+000 3.201300E+004
C2H3+O2=C2H2+HO2 1.000000E+011 0.000000E+000 0.000000E+000
C2H3+OH=C2H2+H2O 2.000000E+013 0.000000E+000 0.000000E+000
O+C2H3=CH2CO+H 3.000000E+013 0.000000E+000 0.000000E+000
C2H3+H=C2H2+H2 1.200000E+013 0.000000E+000 0.000000E+000
H+C2H2(+M)=C2H3(+M) 5.600000E+012 0.000000E+000 2.400000E+003
LOW /3.800000E+040 -7.270000E+000 7.220000E+003/
TROE /7.507000E-001 9.850000E+001 1.302000E+003 4.167000E+003/
O+C2H2=HCCO+H 1.350000E+007 2.000000E+000 1.900000E+003 !GRI
OH+C2H2=CH2CO+H 2.180000E-004 4.500000E+000 -1.000000E+003
O2+C2H3=CH2O+HCO 5.420000E+012 0.000000E+000 0.000000E+000
OH+C2H2=CH3+CO 4.830000E-004 4.000000E+000 -2.000000E+003
C2H2+O2=HCCO+OH 2.000000E+008 1.500000E+000 3.010000E+004
HCCO+C2H2=C3H3+CO 1.000000E+011 0.000000E+000 3.000000E+003
C2H4+O=HCO+CH3 1.920000E+007 1.830000E+000 2.200000E+002
OH+C2H4=C2H3+H2O 2.050000E+013 0.000000E+000 5.944000E+003
H+C2H4=H2+C2H3 1.100000E+014 0.000000E+000 8.500000E+003
C2H5+O=CH3CHO+H 1.100000E+014 0.000000E+000 0.000000E+000
C3H3+O2=CH2CO+HCO 3.000000E+010 0.000000E+000 2.868000E+003
C5H6+O2=C5H5+HO2 5.000000E+013 0.000000E+000 3.540000E+004
C5H6+OH=C5H5+H2O 3.430000E+009 1.200000E+000 -4.470000E+002
C5H6+O=C5H5+OH 1.810000E+014 0.000000E+000 3.080000E+003
C5H6+H=C5H5+H2 2.800000E+013 0.000000E+000 2.259000E+003
C6H5+O=C5H5+CO 1.000000E+014 0.000000E+000 0.000000E+000
C6H6+H=C6H5+H2 6.020000E+008 1.810000E+000 1.640000E+004
C6H6+O2=C6H5+HO2 6.300000E+013 0.000000E+000 6.000000E+004
C6H6+OH=C6H5+H2O 2.386100E+004 2.680000E+000 7.730000E+002
C6H6+OH=C6H6O+H 1.300000E+013 0.000000E+000 1.060000E+004
C6H6+O=C6H5O+H 6.660000E+012 0.000000E+000 2.332000E+003
C6H5+OH=C6H5O+H 1.000000E+013 0.000000E+000 0.000000E+000
C6H5O+H=CO+C5H6 3.000000E+013 0.000000E+000 0.000000E+000
C6H5+O2=C6H5O+O 2.600000E+013 0.000000E+000 6.120000E+003
DUPLICATE
C6H5+O2=C6H5O+O 3.000000E+013 0.000000E+000 8.991000E+003
DUPLICATE
C6H5O=CO+C5H5 2.510000E+011 0.000000E+000 4.390000E+004
C6H6O+OH=C6H5O+H2O 6.000000E+012 0.000000E+000 0.000000E+000
C6H6O+H=C6H5O+H2 1.150000E+014 0.000000E+000 1.240000E+004
C6H6O+O=C6H5O+OH 2.810000E+013 0.000000E+000 7.352000E+003
CH3+O2=CH3O+O 2.050000E+018 -1.570000E+000 2.922900E+004
CH3O+H=CH3+OH 1.000000E+013 0.000000E+000 0.000000E+000
CH3O+M=CH2O+H+M 1.000000E+014 0.000000E+000 2.500000E+004
CH3O+H=CH2O+H2 2.000000E+013 0.000000E+000 0.000000E+000
CH3O+OH=CH2O+H2O 5.000000E+012 0.000000E+000 0.000000E+000
CH3O+O=CH2O+OH 1.000000E+013 0.000000E+000 0.000000E+000
CH3O+O2=CH2O+HO2 6.300000E+010 0.000000E+000 2.600000E+003
CH3O+H=CH2OH+H 3.400000E+006 1.600000E+000 0.000000E+000
CH3OH+OH=CH3O+H2O 5.300000E+003 2.650000E+000 -8.840000E+002
CH3OH+O=CH3O+OH 1.300000E+005 2.500000E+000 5.000000E+003
CH3OH+H=CH3O+H2 4.000000E+012 0.000000E+000 6.101000E+003
O+CH3OH=OH+CH2OH 3.880000E+005 2.500000E+000 3.100000E+003
H+CH3OH=CH2OH+H2 3.070000E+005 2.550000E+000 5.440000E+003
OH+CH3OH=CH2OH+H2O 4.800000E+013 0.000000E+000 4.500000E+003

```
CH2OH+H=CH3+OH 1.000000E+013 0.000000E+000 0.000000E+000
CH2OH+M=CH2O+H+M 1.000000E+014 0.000000E+000 2.500000E+004
CH2OH+H=CH2O+H2 2.000000E+013 0.000000E+000 0.000000E+000
CH2OH+OH=CH2O+H2O 1.000000E+013 0.000000E+000 0.000000E+000
CH2OH+O=CH2O+OH 1.000000E+013 0.000000E+000 0.000000E+000
CH3O+HCO=CH2O+CH2O 6.030000E+012 0.000000E+000 0.000000E+000
CH3+HO2=>CH4+O2 3.600000E+012 0.000000E+000 0.000000E+000
CH4+O2=>CH3+HO2 5.177000E+015 -3.300000E-001 5.796000E+004
CH3+OH(+M)=CH3OH(+M) 6.300000E+013 0.000000E+000 0.000000E+000
LOW /2.700000E+038 -6.300000E+000 3.100000E+003/
TROE /2.105000E-001 8.350000E+001 5.398000E+003 8.370000E+003/
H2 /2.000000E+000/ H2O /6.000000E+000/ CH4 /2.000000E+000/ CO /1.500000E+000/
CO2 /2.000000E+000/
CH3+HO2=CH3O+OH 2.000000E+013 0.000000E+000 0.000000E+000
C2H5OH(+M)=CH3+CH2OH(+M) 5.940000E+023 -1.680000E+000 9.116300E+004
lOw /2.880000E+085 -1.890000E+001 1.099140E+005/
trOe /5.000000E-001 2.000000E+002 8.900000E+002 4.600000E+003/
H2O /5.000000E+000/ H2 /2.000000E+000/ CO2 /3.000000E+000/ CO /2.000000E+000/
C2H5OH(+M)=C2H5+OH(+M) 2.950000E+022 -2.200000E+000 9.660000E+004
lOw /3.800000E+088 -1.970000E+001 1.150000E+005/
trOe /2.094000E+000 1.653900E+004 1.114000E+000 1.613600E+002/
C2H5OH(+M)=C2H4+H2O(+M) 4.900000E+009 1.400000E+000 6.580000E+004
lOw /2.400000E+080 -1.790000E+001 8.480000E+004/
trOe /2.126000E+000 1.356800E+004 9.690000E-001 1.604000E+002/
C2H5OH(+M)=CH3CHO+H2(+M) 7.240000E+011 9.500000E-002 9.100700E+004
lOw /4.460000E+087 -1.942000E+001 1.155860E+005/
trOe /9.000000E-001 9.000000E+002 1.100000E+003 3.500000E+003/
H2O /5.000000E+000/
C2H5OH+OH=CH3CH2O+H2O 2.810000E+002 2.970000E+000 -5.800000E+002
C2H5OH+H=CH3CH2O+H2 5.550000E-023 1.060000E+001 -4.459000E+003
C2H5OH+O=CH3CH2O+OH 1.580000E+007 2.000000E+000 4.448000E+003
CH3CH2O+H=CH3+CH2OH 3.000000E+013 0.000000E+000 0.000000E+000
CH3CH2O+H=C2H4+H2O 3.000000E+013 0.000000E+000 0.000000E+000
CH3CH2O+OH=CH3CHO+H2O 1.000000E+013 0.000000E+000 0.000000E+000
CH3CHO+OH=CH2CHO+H2O 3.370000E+011 0.000000E+000 -6.200000E+002
CH3CHO+O=CH2CHO+OH 3.720000E+013 -2.000000E-001 3.556000E+003
CH3CHO+H=CH2CHO+H2 1.850000E+012 4.000000E-001 5.359000E+003
CH3CO+M=CH3+CO+M 2.000000E+013 0.000000E+000 1.708700E+004
C2H3+O2=CH2CHO+O 1.080000E+013 -6.100000E-001 5.260000E+003
CH2CHO=CH3+CO 1.170000E+043 -9.830000E+000 4.375600E+004
H+CH2CO(+M)=CH2CHO(+M) 4.865000E+011 4.220000E-001 -1.755000E+003
LOW /1.012000E+042 -7.630000E+000 3.854000E+003/
TROE /4.650000E-001 2.010000E+002 1.773000E+003 5.333000E+003/
H2 /2.000000E+000/ H2O /6.000000E+000/ CH4 /2.000000E+000/ CO /1.500000E+000/
CO2 /2.000000E+000/
CH2CHO+O2=CH2CO+HO2 1.580000E+010 0.000000E+000 0.000000E+000
CH2CHO+O2=CH2O+CO+OH 2.510000E+010 0.000000E+000 0.000000E+000
CH2CHO+O=CH2O+HCO 3.980000E+013 0.000000E+000 0.000000E+000
CH2CHO+OH=CH2CO+H2O 2.000000E+013 0.000000E+000 0.000000E+000
C6H5O+O=C5H5+CO2 1.000000E+013 0.000000E+000 0.000000E+000
C5H5+H=C5H6 2.710000E+063 -1.479000E+001 2.105000E+004
CH2O+HO2=HCO+H2O2 3.010000E+012 0.000000E+000 1.307600E+004
CH2O+O2=HO2+HCO 1.000000E+014 0.000000E+000 4.000000E+004
CH2O+M=CO+H2+M 2.500000E+014 0.000000E+000 2.821500E+004
```

H2O2+H=OH+H2O 2.410000E+013 0.000000E+000 3.974000E+003
H2O2+O=OH+HO2 9.550000E+006 2.000000E+000 3.970000E+003
H+HO2=H2O+O 3.010000E+013 0.000000E+000 1.721000E+003
CH2CHO+OH=CH2OH+HCO 3.010000E+013 0.000000E+000 0.000000E+000
CH3CHO+H=CH3CO+H2 1.200000E+014 0.000000E+000 7.000000E+003
CH2CHO+H=CH3+HCO 2.200000E+013 0.000000E+000 0.000000E+000
CH2CHO+H=CH2CO+H2 1.100000E+013 0.000000E+000 0.000000E+000
CH2CO+O=HCCO+OH 1.000000E+013 0.000000E+000 8.000000E+003
H+C2H5CHO=H2+C2H5CO 1.200000E+014 0.000000E+000 7.000000E+003
O+C2H5CHO=OH+C2H5CO 5.850000E+012 0.000000E+000 1.808000E+003
C2H5CO=C2H5+CO 5.890000E+012 0.000000E+000 1.440000E+004
OH+C2H5CHO=H2O+C2H5CO 2.690000E+010 7.600000E-001 -3.400000E+002
C2H5CO=CH2CO+CH3 2.740000E+009 1.410000E+000 3.583000E+004
C2H4+H(+M)=C2H5(+M) 1.367000E+009 1.463000E+000 1.355000E+003
LOW /2.027000E+039 -6.642000E+000 5.769000E+003/
TROE /1.000000E+000 1.000000E-015 9.500000E+001 2.000000E+002/
H2 /2.000000E+000/ H2O /6.000000E+000/ CH4 /2.000000E+000/ CO /1.500000E+000/ CO2 /2.000000E+000/
C3H3+C3H3=C6H6 3.000000E+012 0.000000E+000 0.000000E+000
C6H6+O=C6H5+OH 6.000000E+013 0.000000E+000 1.106400E+004
C6H5+H(+M)=C6H6(+M) 1.000000E+014 0.000000E+000 0.000000E+000
LOW /6.600000E+075 -1.630000E+001 7.000000E+003/
TROE /1.000000E+000 1.000000E-001 5.849000E+002 6.113000E+003/
H2 /2.000000E+000/ H2O /6.000000E+000/ CH4 /2.000000E+000/ CO /1.500000E+000/ CO2 /2.000000E+000/
HCO+HCO=H2+CO+CO 3.000000E+012 0.000000E+000 0.000000E+000
C6H6O=C5H6+CO 1.000000E+012 0.000000E+000 6.080200E+004
C3H3+C3H3=C6H5+H 1.000000E+013 0.000000E+000 0.000000E+000
CH2CO+H=HCCO+H2 3.000000E+007 2.000000E+000 1.000000E+004
CH2CO+OH=HCCO+H2O 7.500000E+012 0.000000E+000 2.000000E+003
H+CH2CO=CH3+CO 1.110000E+007 2.000000E+000 8.364000E+003
CH2CO+OH=CH2OH+CO 2.000000E+012 0.000000E+000 -1.010000E+003
HCO+CH3=CO+CH4 1.200000E+014 0.000000E+000 0.000000E+000
C2H4+OH=CH2O+CH3 2.000000E+012 0.000000E+000 9.600000E+002
C2H4+O=CH2CHO+H 4.700000E+006 1.880000E+000 1.800000E+002
C2H4+O=CH2CO+H2 6.700000E+005 1.880000E+000 1.800000E+002
C2H4+O=C2H3+OH 1.510000E+007 1.910000E+000 3.790000E+003
C2H5+O=C2H4+OH 2.650000E+013 0.000000E+000 0.000000E+000
C2H5+O=CH2O+CH3 4.238000E+013 0.000000E+000 0.000000E+000
C2H5+H=C2H4+H2 1.810000E+012 0.000000E+000 0.000000E+000
C2H5+OH=C2H4+H2O 2.410000E+013 0.000000E+000 0.000000E+000
C2H5CHO=C2H5+HCO 2.450000E+015 0.000000E+000 7.286400E+004
C2H5CHO=CH3+CH2CHO 7.000000E+015 0.000000E+000 8.170300E+004
CH3CO+H=CH2CO+H2 2.000000E+012 0.000000E+000 0.000000E+000
O2+C2H4O2=>HO2+CO+CH2OH 6.82E+06 2 38109.91
H+C2H4O2=>H2+CO+CH2OH 9.63E+06 2 2387.18
OH+C2H4O2=>H2O+CO+CH2OH 1.60E+06 2 -3343.83
O+C2H4O2=>OH+CO+CH2OH 5.41E+06 2 1094.46
O2+C2H4O2=>HO2+C2H2O2+H 1.70E+06 2 40722.49
H+C2H4O2=>H2+C2H2O2+H 2.41E+06 2 3950.57
OH+C2H4O2=>H2O+C2H2O2+H 3.99E+05 2 -2259.83
O+C2H4O2=>OH+C2H2O2+H 1.35E+06 2 2579.54
O2+C2H2O2=>HO2+CO+HCO 1.36E+07 2 38109.91
H+C2H2O2=>H2+CO+HCO 1.93E+07 2 2387.18

```
OH+C2H2O2=>H2O+CO+HCO 3.20E+06 2 -3343.83
O+C2H2O2=>OH+CO+HCO 1.08E+07 2 1094.46
O2+C6H6O3=>HO2+C5H4O2+CO+H 6.82E+06 2 38109.91
H+C6H6O3=>H2+C5H4O2+CO+H 9.63E+06 2 2387.18
OH+C6H6O3=>H2O+C5H4O2+CO+H 1.60E+06 2 -3343.83
O+C6H6O3=>OH+C5H4O2+CO+H 5.41E+06 2 1094.46
O2+C5H4O2=>HO2+2CO+C3H3 6.82E+06 2 38109.91
H+C5H4O2=>H2+2CO+C3H3 9.63E+06 2 2387.18
OH+C5H4O2=>H2O+2CO+C3H3 1.60E+06 2 -3343.83
O+C5H4O2=>OH+2CO+C3H3 5.41E+06 2 1094.46
O2+C5H8O4=>HO2+OH+H2O+C5H4O2 3.41E+06 2 40722.49
H+C5H8O4=>H2+OH+H2O+C5H4O2 4.81E+06 2 3950.57
OH+C5H8O4=>H2O+OH+H2O+C5H4O2 7.99E+05 2 -2259.83
O+C5H8O4=>OH+OH+H2O+C5H4O2 2.71E+06 2 2579.54
O2+C5H8O4=>HO2+CH2CHO+C2H4O2+CO 3.41E+06 2 40722.49
H+C5H8O4=>H2+CH2CHO+C2H4O2+CO 4.81E+06 2 3950.57
OH+C5H8O4=>H2O+CH2CHO+C2H4O2+CO 7.99E+05 2 -2259.83
O+C5H8O4=>OH+CH2CHO+C2H4O2+CO 2.71E+06 2 2579.54
O2+C6H10O5=>HO2+C6H8O4+OH 8.52E+05 2 40722.49
H+C6H10O5=>H2+C6H8O4+OH 1.20E+06 2 3950.57
OH+C6H10O5=>H2O+C6H8O4+OH 2.00E+05 2 -2259.83
O+C6H10O5=>OH+C6H8O4+OH 6.77E+05 2 2579.54
O2+C6H10O5=>HO2+CO+OH+CH2O+C4H6O2 8.52E+05 2 40722.49
H+C6H10O5=>H2+CO+OH+CH2O+C4H6O2 1.20E+06 2 3950.57
OH+C6H10O5=>H2O+CO+OH+CH2O+C4H6O2 2.00E+05 2 -2259.83
O+C6H10O5=>OH+CO+OH+CH2O+C4H6O2 6.77E+05 2 2579.54
O2+C6H8O4=>HO2+C6H6O3+OH 1.70E+06 2 40722.49
H+C6H8O4=>H2+C6H6O3+OH 2.41E+06 2 3950.57
OH+C6H8O4=>H2O+C6H6O3+OH 3.99E+05 2 -2259.83
O+C6H8O4=>OH+C6H6O3+OH 1.35E+06 2 2579.54
O2+C9H10O2=>HO2+CH2CO+0.5C10H8+CH2CHO 6.82E+06 2 38109.91
H+C9H10O2=>H2+CH2CO+0.5C10H8+CH2CHO 9.63E+06 2 2387.18
OH+C9H10O2=>H2O+CH2CO+0.5C10H8+CH2CHO 1.60E+06 2 -3343.83
O+C9H10O2=>OH+CH2CO+0.5C10H8+CH2CHO 5.41E+06 2 1094.46
O2+C4H6O2=>HO2+CH3CO+CH2CO 1.02E+07 2 45025.57
H+C4H6O2=>H2+CH3CO+CH2CO 1.44E+07 2 6525.57
OH+C4H6O2=>H2O+CH3CO+CH2CO 2.40E+06 2 -474.43
O+C4H6O2=>OH+CH3CO+CH2CO 8.12E+06 2 5025.57
C2H4O2=>2CO+2H2 4.28E+06 0 26000
C2H2O2=>2CO+H2 4.28E+06 0 26000
C3H6O=>0.5CO2+0.5H2+1.25C2H4 4.28E+06 0 26000
C3H4O2=>CO2+C2H4 4.28E+06 0 26000
C6H6O3=>3CO+1.5C2H4 4.28E+06 0 26000
C6H10O5=>2.5CO2+1.5H2+1.75C2H4 4.28E+06 0 26000
C5H8O4=>2CO2+H2+1.5C2H4 4.28E+06 0 26000
C9H10O2=>2CO+1.5C2H4+2C2H2 4.28E+06 0 26000
C6H6O=>0.5CO2+0.25C2H4+2.5C2H2 4.28E+06 0 26000

END
```